Systematic annotation of a complete adult male *Drosophila* nerve cord connectome reveals principles of functional organisation

Elizabeth C. Marin[1], Billy J. Morris[1], Tomke Stuerner[2,1], Andrew S. Champion[1,2], Dominik Krzeminski[1,2], Griffin Badalamente[1], Marina Gkantia[1], Christopher R. Dunne[1], Katharina Eichler[1], Shin-ya Takemura[4], Imaan F. M. Tamimi[1], Siqi Fang[1], Sung Soo Moon[3], Han S. J. Cheong[4], Feng Li[4], Philipp Schlegel[1,2], Stuart Berg[4], FlyEM Project Team, Gwyneth M. Card[4,5], Marta Costa[1], David Shepherd[6], Gregory S.X.E. Jefferis[2,1]

[1]*Drosophila* Connectomics Group, Department of Zoology, University of Cambridge, Downing Street, Cambridge, UK
[2]Neurobiology Division, MRC Laboratory of Molecular Biology, Cambridge, UK
[3]Department of Chemical Engineering and Biotechnology, University of Cambridge, Philippa Fawcett Drive, Cambridge, UK
[4]Janelia Research Campus, Howard Hughes Medical Institute, Ashburn, USA
[5]Zuckerman Institute, Columbia University, New York, USA
[6]School of Biological Sciences, University of Southampton, Southampton, UK

Correspondence: em711@cam.ac.uk, jefferis@mrc-lmb.cam.ac.uk

Summary

Our companion paper (Takemura et al., 2023) introduces the first completely proofread connectome of the nerve cord of an animal that can walk or fly. The base connectome consists of neuronal morphologies and the connections between them. However, in order to efficiently navigate and understand this connectome, it is crucial to have a system of annotations that systematically categorises and names neurons, linking them to the existing literature. In this paper we describe the comprehensive annotation of the VNC connectome, first by a system of hierarchical coarse annotations, then by grouping left-right and serially homologous neurons and eventually by defining systematic cell types for the intrinsic interneurons and sensory neurons of the VNC; descending and motor neurons are typed in (Cheong et al., 2023). We assign a sensory modality to over 5000 sensory neurons, cluster them by connectivity, and identify serially homologous cell types and a layered organisation likely corresponding to peripheral topography. We identify the developmental neuroblast of origin of the large majority of VNC neurons and confirm that (in most cases) all secondary neurons of each hemilineage express a single neurotransmitter. Neuroblast hemilineages are serially repeated along the segments of the nerve cord and generally exhibit consistent hemilineage-to-hemilineage connectivity across neuromeres, supporting the idea that hemilineages are a major organisational feature of the VNC. We also find that more than a third of individual neurons belong to serially homologous cell types, which were crucial for identifying motor neurons and sensory neurons across leg neuropils. Categorising interneurons by their neuropil innervation patterns provides an additional organisation axis. Over half of the intrinsic neurons of the VNC appear dedicated to the legs, with the majority restricted to single leg neuropils; in contrast, inhibitory interneurons connecting different leg neuropils, especially those crossing the midline, appear rarer than anticipated by standard models of locomotor circuitry. Our annotations are being released as part of the neuprint.janelia.org web application and also serve as the basis of programmatic analysis of the connectome through dedicated tools that we describe in this paper.

INTRODUCTION

The ventral nerve cord of insects is analogous to the vertebral spinal cord. In adult flies this means that it contains premotor circuits controlling walking and flight located in the thoracic **neuromeres**, while the abdominal neuromeres regulate and report on the gut and reproductive tracts. As such it represents the final common pathway for the majority of the nervous system's behavioural outputs. Indeed flies without a head are still able to carry out numerous motor actions, suggesting that large parts of the motor control circuitry reside within the VNC. Conversely, key sensory pathways from the legs, wings and viscera project into the VNC. While some sensory neurons ascend straight to the brain, most incoming information is processed locally and only a fraction then ascends.

Anatomically the VNC has both a segmental organisation along the anterior-posterior length of the nerve cord and a layered organisation along the dorso-ventral axis. The segmental organisation is directly analogous to spinal cord segments. It is inherited from the larval nervous system and is most obvious in the three thoracic neuromeres (T1, T2, T3) associated with pairs of legs in the adult. The dorso-ventral axis has two main organisational features. The first is a layered arrangement in which neurons controlling the legs are located more ventrally, while wing-control neurons reside more dorsally; an intermediate layer contains neurons that bridge motor systems or have more complex functions. The second organisational motif is the arrangement of sensory neurons in more ventral regions and motor neurons in more dorsal regions i.e. the opposite arrangement to the mammalian spinal cord. These features are visible in the gross anatomy of the VNC, resulting in the definition of named **neuropil** domains which provide a framework for describing both the regional organisation of the nerve cord and the structure of individual neurons (Court et al., 2020).

Insect central neurons of VNC origin arise from stereotyped arrays of neuroblasts (neural stem cells) each generating a reproducible set of neuronal cell types. These neuroblasts are exactly reflected across the midline and repeat (with variations) in each segment. Each neuroblast produces two distinct populations of progeny called **hemilineages**, which usually differ in gross morphology, gene expression, and neurotransmitter (Lacin et al., 2019; Truman et al., 2010). Members of each hemilineage may mature to function in larval and/or adult life or be eliminated by programmed cell death.

In holometabolous insects such as moths and flies that undergo metamorphosis, the dramatic changes in body plan and behaviour in larvae vs adults necessitate significant expansion and reorganisation of the nervous system during development. New populations of sensory neurons are generated during development of the adult-specific cuticle and appendages such as legs and wings. Meanwhile, the larval CNS is transformed by the death or remodelling of the embryonically produced **primary** neurons and the addition of a much larger population of later born, adult-specific **secondary** neurons (Truman and Riddiford, 2023). In *Drosophila melanogaster*, the targeted activation of each postembryonic hemilineage has been associated with a specific behaviour (Harris et al., 2015), supporting a role for hemilineages as the functional units of the VNC.

Except for a small number of embryonically produced sensory neurons (Tix et al., 1989; Williams and Shepherd, 1999) adult *Drosophila* sensory systems are generated during post embryonic life. In contrast to central neurons, sensory neurons are born peripherally from populations of cells, set aside in the embryo, that are the precursors of the adult appendages and epidermis (Bate and Arias, 1991). As these imaginal tissues grow the

sensory neurons emerge, *in situ*, in precise and reproducible patterns (Nottebohm et al., 1994; Palka et al., 1984). Axons from sensory neurons grow centripetally into the VNC to form synaptic connections with their targets (Jan et al., 1985).

In common with other insects, the sensory projections in the *Drosophila* VNC neuropil are highly organised. Sensory neurons from different classes of sensilla project into different regions of neuropil with axons that serve different sensory modalities terminating in different layers of neuropil (Merritt and Murphey, 1992; Murphey et al., 1989a). Within these modality specific regions there is a further order. Tactile afferents, for example, form a somatotopic map of the body surface (Murphey et al., 1989b), and chordotonal neurons encoding different features of limb movement project to different regions of the proprioceptive layers (Mamiya et al., 2018). This precise ordering of the sensory system makes it possible to identify most sensory neurons based on their afferent projections within the VNC.

In this study, we provide functional and developmental annotation of the first complete synaptic resolution connectome of an adult *Drosophila* male nerve cord. This provides a comprehensive framework to understand the organisational principles of sensory-motor circuits within the VNC. We provide a multi-resolution catalogue of the neuronal constituents of the VNC including incoming sensory neurons, outgoing motor neurons, descending neurons from the brain and ascending neurons connecting to the head. Building on this work, a companion paper (Cheong et al., 2023) reveals detailed principles of the logic of descending control of motor circuits. We place particular emphasis on the ~16,000 VNC neurons organised by individual neuronal hemilineages, thereby linking developmental origin to connectome structure. We also identify examples of serial homology in leg and abdominal neuropils that allow identification of recurring circuit motifs. This work confirms that developmental origins generate natural units of functional organisation and also provide a unified way to define cell types across the dataset.

In the following sections, we will present the atlas of annotations provided in this work. We begin by providing a first account of the neuronal classes and general organisational features of the VNC dataset and how we have conducted cell typing. Then we will explore information flow within the VNC regions and how we predicted neurons with electrical and neurosecretory transmission. We will then examine the general characteristics of hemilineages, birth time, diversity, and serial homology in the VNC, before dissecting each of the 45 hemilineages annotated in this work. Finally we will present the sensory neurons, their inferred modalities and how they connect with the different hemilineages. The paper is structured so that the initial and concluding sections should be useful and accessible for the general reader; the sections describing each secondary hemilineage are intended for those with specific circuit interest and are therefore ordered by hemilineage number for easy reference.

RESULTS

Orientation and broad classes

The adult *Drosophila* central nervous system can be divided into the brain in the head capsule and the ventral nerve cord (VNC) in the thorax, joined by axons running through a narrow neck connective. The MANC connectome provides the first detailed and complete inventory of neurons in the VNC as well as the neck connective.

In more detail the adult VNC can be grossly characterised as consisting of bilaterally symmetrical and often segmentally repeating information processing units, with a limited number of connections to the brain and to each other. It can be divided into three thoracic segments, or neuromeres (T1/T2/T3) and an abdominal neuromere (ANm) consisting of segments A1-A10. T1, T2, and T3 are associated with the front legs, middle legs, and hind legs, respectively, while T2 is also associated with the wing and T3 with a flight-associated balancing structure called the haltere (Figure 1A). The presence or absence of these appendages is expected to drive the number of neurons needed for information processing and motor control in each neuromere.

We assigned every reconstructed neuron in MANC a broad class and corresponding abbreviation (Figure 1B). 1328 descending neurons (DN) relay information from the brain to the VNC via the neck connective; 5937 sensory neurons (SN) relay information through a nerve from the periphery to terminate in the VNC; 539 sensory ascending neurons (SA) ascend to the brain; 13059 intrinsic neurons (IN) are restricted to the VNC; 1866 ascending neurons (AN) originate in the VNC but ascend to the brain, 93 efferent neurons (EN) exit via nerves and 8 efferents (EA) also ascend to the brain; 737 motor neurons (MN) originate in the VNC but exit via nerves to control the muscles. These broad classes are not evenly distributed across neuromeres; for example, significantly more intrinsic neurons originate in T2 than in T1 or T3, but ~twice as many ascending neurons originate in T1 as compared to T2 and T3.

With this basic parts list in place we can make some simple but instructive comparisons between the brain and VNC. The FAFB full adult female brain is reported to contain about 133,000 cells, of which at least 115,000 are neurons (Mu et al., 2021). Recent collaborative work from our group focusing on the central brain (i.e. the brain without the massively expanded optic lobes) finds about 34,000 neurons with cell bodies in the central brain and 5,500 sensory neurons (Schlegel et al., manuscript in prep) compared with 15,763 for MANC. Although the central brain and VNC are roughly equivalent in volume, this means that the central brain includes twice as many neurons, not including the sensory neurons from peripheral tissues (Figure 1A). VNC neurons are therefore larger on average, perhaps reflecting the need for rapid communication near the motor periphery. The central brain has a ratio of 6:1 between intrinsic and sensory neurons and 55:1 between intrinsic and motor neurons. Conversely, the VNC displays a considerably reduced ratio of 2.4:1 for intrinsic to sensory neurons and a substantially smaller ratio of 9:1 for intrinsic to motor neurons. These numbers highlight the VNC's significance for sensory processing and as the principal centre for motor control. Nevertheless, the great majority of VNC neurons (83%) are intrinsic neurons restricted to the nerve cord that define local circuits for sensory-motor processing.

Organisational features and systematic typing

We were motivated to develop a systematic nomenclature for the adult VNC because only a small fraction of its cell types have been identified and named in the light level literature. (The exceptions are the descending neurons and motor neurons, both of which were typed separately as described in our companion manuscript (Cheong et al., 2023). In pursuit of this goal, we sought anatomical features that could be used to subdivide the neurons – particularly the large populations of unnamed intrinsic and sensory neurons – into units with likely relevance for function. We have listed all features in a reference table (Table 1).

The VNC can be divided into a set of major neuropils reflecting neuroanatomical organisation and function (Court et al., 2020) (Figure 2A). In the thorax, the six leg neuropils (LegNp) each consist of two sensory neuropils - the ventral association centre (VAC) and medial ventral association centre (mVAC) - along with the intermediate neuropil (IntNp). The tectulum lies dorsal to the leg neuropils, is specialised for flight, and is composed of the ventralmost lower tectulum (LTct), the intermediate tectulum (IntTct), and finally the dorsalmost upper tectulum, which is further divisible into the neck tectulum (NTct), wing tectulum (WTct), and haltere tectulum (HTct). We assigned every neuron an origin neuropil (or peripheral structure) based on the observed or inferred locations of its postsynapses and a target neuropil (or peripheral structure) based on its presynapses.

The individual neuropils also contribute to segmental units called neuromeres. The anteriormost is the first thoracic neuromere (T1) or prothorax and includes the NTct and prothoracic leg neuropils, LegNp(T1). The second thoracic neuromere (T2) or mesothorax includes the specialised wing and notum sensory neuropil called the accessory mesothorax (AMNp) or ovoid (Ov), along with the WTct and the mesothoracic leg neuropils, LegNp(T2). The third thoracic neuromere (T3) or metathorax includes the HTct and the metathoracic leg neuropils, LegNp(T3). The abdominal neuromeres (ANm) are treated as one neuropil consisting of fused neuromeres A1-A10. For every neuron originating in the VNC, we annotated the **soma position** or (**tosoma_position** if missing the soma), **soma neuromere** (e.g., T1, T2, etc) and the **soma side** (RHS, LHS, or midline); we annotated the **root side** (axon entry side) for neurons originating in the brain or periphery. Neurons matched across the midline by morphology and connectivity were assigned the same **group** number, while neurons matched across neuromeres were assigned the same **serial** number.

We assigned **systematic type** names to all descending neurons (DN) and motor neurons (MN) based on their target neuropils and muscles, respectively (Figure 3A,B). Descending neurons that could be matched with confidence to light level images were assigned canonical **type** names (e.g., DNp50) and **synonyms** (e.g., Moonwalker) if applicable and otherwise received the systematic type name as their type name (as described in our companion manuscript (Cheong et al., 2023). Similarly, motor neurons matched to light level images were assigned canonical type names (e.g., hg1 MN) and synonyms (e.g., vMS2) if applicable and otherwise received the systematic type name as their type name (Cheong et al., 2023). Many of the leg motor neurons are serially repeating, so we used “lg” (leg) as the neuropil abbreviation for all of them and have given them the same systematic type. Each neuron was also assigned an **instance** based on its position in the volume: the hemineuromere (soma neuromere and side) of origin was used for MNs, and the root side was used for DNs.

Axons enter and exit the VNC via a defined set of peripheral nerves (Court et al., 2020). The anteriormost is the cervical connective (CvC), which connects the VNC to the brain. The small cervical nerve (CvN) connects laterally to the CvC. The dorsal prothoracic nerve (DProN), prosternal nerve (PrN), prothoracic chordotonal nerve (ProCN), prothoracic accessory nerve (ProAN), ventral prothoracic nerve (VProN), and prothoracic leg nerve (ProLN) directly innervate the prothoracic neuromere (T1). The anterior dorsal mesothoracic nerve (ADMN), posterior dorsal mesothoracic nerve (PDMN), mesothoracic accessory nerve (MesoAN), and mesothoracic leg nerve (MesoLN) innervate the mesothoracic neuromere (T2). The dorsal metathoracic nerve (DMetaN) and metathoracic leg nerve (MetaLN) innervate the metathoracic neuromere (T3). Finally, the abdominal neuromeres are innervated by the bilaterally paired first, second, third, and fourth abdominal nerves (AbN1, AbN2, AbN3, AbN4) and by the fused abdominal nerve trunk (AbNT). We assigned an **entry nerve** and/or **exit nerve** to all neurons with axons entering or leaving the VNC - that is, SNs and ANs vs MNs, EN, and EAs, respectively.

The entry nerve was used as the instance of sensory neurons (SA if ascending to the brain, SN if not), but systematic typing was based on inferred modality (Figure 3C). We used weighted nearest neighbour clustering to assign the systematic types (Figures 51-52 and Methods) and annotated any names from light level matching in the synonyms field. Many leg sensory neurons are serially repeating, so we assigned the same systematic type to all neurons that could be matched across sides and neuromeres.

Most of the remaining ~15,000 neurons have only been described previously at light level as part of large populations deriving from the same postembryonic neuroblast (Shepherd et al., 2019) or labelled by a driver (Harris et al., 2015). 30 paired and one unpaired VNC neuroblast in each neuromere divide embryonically to generate an initial set of **primary** neurons (Schmid et al., 1999), but at most 25 + 1 divide post-embryonically to generate adult-specific **secondary** neurons (Booker and Truman, 1987; Prokop and Technau, 1991; Truman and Bate, 1988). Each neuroblast typically buds off a series of transient ganglion mother cells that divide once to generate a pair of post-mitotic cells (Bate, 1976; Doe and Goodman, 1985). Through lateral inhibition, one daughter cell acquires a $Notch^{ON}$ (A) fate while the other acquires a $Notch^{OFF}$ (B) fate, resulting in two distinct hemilineages as progeny accumulate over time (Truman et al., 2010). In most cases, the embryonic and postembryonic neuroblasts had already been mapped onto each other (Birkholz et al., 2015; Lacin and Truman, 2016), but we found evidence for two new neuroblast matches (Figure 49J,K) and one novel hemilineage from a known neuroblast (Figure 40).

Secondary neurons from the same hemilineage are expected to share similar gross morphology (Shepherd et al., 2019; Truman et al., 2004) and express the same neurotransmitter (Allen et al., 2020; Lacin et al., 2019), making hemilineages strong candidates as units of functional organisation in the VNC. We assigned >90% of VNC neurons to a **hemilineage**, relying primarily on soma tract entry position and gross morphology but also on several clustering methods and serially homologous cell types (Methods). This allowed systematic typing of the interneurons ascending to the brain (AN), intrinsic neurons restricted to the VNC (IN), neurosecretory efferent neurons exiting one or more nerves (EN), and neurosecretory efferent neurons exiting one or more nerves and ascending to the brain (EA). Within each hemilineage, matching groups and serial sets (Figure 11) and predicted neurotransmitter (**predicted nt**, Figure 7D) were used to inform the clustering used to assign systematic type names and type names (Figure 3D-E and Methods). The hemineuromere (**soma neuromere** and **side**) of origin was used for the

instance. Any names from matching to light-level literature were annotated in the synonyms field.

Neurons of VNC Origin

Information Flow

We employed laterality and neuropil innervation as criteria to classify ANs and INs into distinct subclasses. The subclass nomenclature is based on these two indicators. The first letter reflects whether a neuron shows bilateral (B), ipsilateral (I), or contralateral (C) innervation of the VNC (Figure 4 Supplemental A,B). The second letter indicates whether the neuron ascends to the brain (A), is restricted to a single neuropil (R), or interconnects multiple neuropils (I) (refer to Figure 4A and the Materials and Methods section for more details). Furthermore, we identified a subset of 30 ANs with fewer than 5 synapses in the VNC, which we designated as subclass XA (see Figure 4C for a corresponding image).
The most abundant subclass among the classified neurons in IR, comprising intrinsic neurons that solely innervate a single neuropil ipsilateral to their soma location. The majority of these IR neurons target individual leg neuropils, similarly seen for the subclass CR (see Figure 4B, white arrows pointing to IR neurons that have all their input and output from the front left leg neuropil). The second largest subclass is BI, consisting of intrinsic neurons that bilaterally interconnect multiple neuropils. Upon closer examination of their neuropil innervation, this subclass could be further divided into two groups: those interconnecting the upper tectulum (a combination of NTct, WTct and HTct) and those interconnecting the leg neuropils (LegNpT1-T3) (Figure 4B).

We assigned every neuron an origin neuropil (or peripheral structure) based on the observed or inferred locations of its postsynapses and a target neuropil (or peripheral structure) based on its presynapses (see materials and methods for details). This allows us to characterise the main input and output neuropils for each individual neuron to produce a general model of information flow for ANs and INs (Figure 5A). For both ANs and INs we see that many neurons receive input and give output to the same neuropil (diagonal along the top panels in Figure 5A). Many ANs primarily innervate the front legs while the INs have a roughly even number of neurons innervating all six legs neuropils and the abdominal neuropil. When removing neurons that have the same top input and top output neuropil, we see interesting connections between the neuropils (lower panels in Figure 5A). There are four groups of connections that stand out for the ANs: bilateral connections between the NTct, HTct and LegNpT1 neuropils as well as a small group of HTct to NTct connecting ANs (Figure 5B). INs also have a high number of neurons that bilaterally connect the haltere neuropils (Figure 5C, first example). However, they also show a high number of neurons projecting from the Halteres to the Wing neuropils, a combination that was not seen for ANs (Figure 5C, second example). All leg neuropils show groups of IN neurons that project between the two sides, however, the largest number is seen in the hind leg neuropils (Figure 5C, third example). The abdomen neuropil mesh (ANm) is not split by hemisphere, if one compares neurons with the ANm as their top input and output neuropil, the majority are projecting across the midline (Figure 5C, fourth example).

We use the origin and target neuropils to see how many of the IR and CR subclass were innervating the leg versus other neuropils (Figure 5D). We find that 95% of IR and CR

neurons are restricted to one of the leg neuropil and only a few neurons are restricted to one of the upper tectulum neuropil, abdomen or inter tectulum neuropil. Next we looked into the numbers of the BR subclass and how many of these neurons connect between the same neuropil on the two hemispheres (Figure 5E). Here as expected from Figure 5A we saw an increased bilateral connection between BR neurons of the T3 leg neuropils and the halteres. The largest connection between them was, however, in most cases not directed but with approximately the same amount of input and output on both sides. For neurons connecting the ANm however, the majority of the connections were directed, meaning with more than 60% input on one hemisphere and more than 60% on the other hemisphere. Finally we looked at neurons connecting the upper tectulum or leg neuropils within one hemisphere (II and CR subclass). The number of neurons connecting are few in number apart from the connection between the WTct and HTct, which have over 100 neurons that connect the two undirected (Figure 5F).

Electrical and neurosecretory transmission

There are several important caveats regarding the preceding subdivision of VNC neurons by synapse location. Some neurons are missing synapses due to poor segmentation (typically an artefact of darkly stained profiles) or truncation (because they leave the volume or because segments could not be joined through a damaged area). Motor neurons and sensory neurons were especially difficult to reconstruct in this dataset, and many neurons that exit or enter the leg nerves are incomplete.

In addition, our synapse prediction models were only trained to recognise chemical synapses, which in *Drosophila* can be manually identified by the presence of T-bars, vesicles, and postsynaptic densities. However, some neurons are known to be activated by electrical coupling via gap junctions, for example targets of the Giant Fiber descending neurons (Kennedy and Broadie, 2018). Innexin gap junction proteins such as ShakB are widely expressed in the VNC (Ammer et al., 2022) but were not included in MANC segmentation or annotation.

To address these issues, we manually reviewed neurons with unusually low presynaptic density by volume (excluding sensory and motor neurons) (Figure 6A). We noted matches to electrical neurons in the literature such as the peripherally synapsing interneuron or PSI (Figure 6C) and annotated 189 morphologically similar neurons with low presynaptic density and thick, smooth axons as having putative electrical transmission (Figure 6D). Many of these have been investigated in more detail with respect to flight circuits in our companion manuscript (Cheong et al., 2023).

We also noted matches to neurosecretory neurons from the literature such as the octopaminergic neurons from the medial neuroblast (Pop et al., 2020) (Figure 6E). We annotated other, unidentified efferent neurons as having putative neurosecretory transmission (Figure 6F). We also noted a number of primary neurons that broadly innervate the neuropil surface, with unpolarised synaptic swellings resembling beads on a string and annotated these as putative neurosecretory (Figure 6F).

These minority transmission populations were not uniformly distributed in the dataset but rather belonged to a small number of specific hemilineages (Figure 6B). Indeed, we were able to match one primary-only hemilineage to its neuroblast of origin based largely on the presence of putative neurosecretory cells (Figure 49K).

Introduction to hemilineage-based organisation

Embryonic divisions by segmentally repeating rows and columns of neuroblasts produce serially homologous primary neurons throughout the VNC. However, only segment-specific subsets of neuroblasts generate postembryonic progeny (Truman and Bate, 1988), facilitating an expansion of neuronal types in the thorax and distal abdomen for complex sensorimotor functions. In late larva, secondary hemilineages restricted to the leg neuropils are present in all three thoracic neuromeres, while those associated with dorsal (flight) neuropils (e.g., 3B, 11A, 11B, 12A, 18B) are absent or greatly reduced in at least one (Marin et al., 2012; Truman et al., 2004).

Because hemilineages represent developmental and likely functional units in the VNC, we wanted them to play a central role in any systematic typing scheme. However, assignment of individual neurons to specific hemilineages based on light-level images of postembryonic neuroblast clones (Shepherd et al., 2019) proved a complex and multifaceted process. The relative position of midline crossing is very useful for distinguishing hemilineages that project contralaterally (Shepherd et al., 2016); however, many hemilineages are confined to ipsilateral leg neuropil or flight neuropil. The locations of primary neurite bundles are also key characters, but these typically remain tightly bundled only if all neurons target a similar area; in hemilineages with diverse cell types, they can be pulled apart during development.

Typically only the most common cell types are bright enough to be distinguished in neuroblast clone light-level images, and if both secondary hemilineages survive, it can be quite difficult to distinguish between their respective projections (Figure 7A, B). We originally seeded secondary soma tract bundles with hemilineage annotations, then mined for nearby soma tracts using a form of NBLAST. Neurotransmitter predictions helped to confirm or distinguish between identifications based on morphology. Left-right matching and serial set identification by cosine clustering also helped with hemilineage assignment, particularly when the primary neurite was displaced. Motor neurons were especially challenging to assign as many are primary neurons that have not been associated with a hemilineage in the light level literature; please see (Cheong et al., 2023) for more details on motor neuron identification and Methods (this paper) for identification of individual hemilineages.

Secondary neurons belonging to the same hemilineage are expected to express the same neurotransmitter (Lacin et al., 2019). We generated a neurotransmitter prediction for every neuron in MANC (see Takemura et al for details), which matched the expected neurotransmitter for the large majority of neurons assigned to each hemilineage (Figure 7D). There were numerous exceptions, most of which can be explained by a paucity of chemical presynapses in the MANC volume because of class (e.g., ascending or motor neuron), transmission mode (e.g., putative electrical), or incomplete reconstruction. However, we also identified consistent secondary subpopulations within hemilineages, notably 00A (Figure 15C) and 09B (Figure 7C, Figure 29C), that we believe could represent genuine biological diversity (perhaps previously undetected due to incomplete coverage from genetic driver lines). In addition, several hemilineages featured serially homologous early born neurons expressing a distinct neurotransmitter, e.g., 14A (Figure 11A) and 19A (Figure 43C).

For reference, we have plotted all postsynapses vs presynapses for each annotated hemilineage by projecting the contents of all T2 neuropils onto a transverse section (Figure 8). It should be noted that we have not carried out axon/dendrite splits, and these synapses could engage in any of the four types of connections: dendro-dendritic, dendro-axonic, and axo-axonic in addition to the canonical axo-dendritic. This likely explains the high degree of

intra-hemilineage connectivity that we observe for many hemilineages (Figure 7 supplement 1).

For the most part, we found very similar connectivity patterns between pairs of hemilineages across the thoracic neuromeres, particularly for the hemilineages that innervate leg neuropils (Figure 7E). Many secondary hemilineages that innervate flight neuropils survive in T2 but are missing in T1 and/or T3. But there were some interesting differences suggesting segment-specific specialisation even among flight hemilineages that survive in multiple neuromeres, particularly 06B and 19B.

Birthtime

VNC neuroblasts divide embryonically to generate an initial set of primary neurons and post-embryonically to generate adult-specific secondary neurons (Booker and Truman, 1987; Prokop and Technau, 1991; Truman and Bate, 1988). Primary neurons typically mature towards the end of embryogenesis and function in the larval nervous system, although there are exceptions (Schmid et al., 1999). In response to steroidal signalling before and during metamorphosis, some primary neurons die, while survivors mature or reorganise their arbours to innervate adult targets (reviewed in (Tissot and Stocker, 2000)). These are expected to comprise <10% of the neurons in thoracic neuromeres in *Drosophila*, with the remainder being secondary neurons that mature during metamorphosis (Truman and Bate, 1988). Secondary neurons belonging to the same hemilineage are expected to share similar gross morphology (Shepherd et al., 2019; Truman et al., 2004) and to express the same neurotransmitter (Allen et al., 2020; Lacin et al., 2019).

Birth order influences cell fate via a series of temporal factors expressed by neuroblasts and inherited by ganglion mother cells and their progeny (Isshiki et al., 2001; Kambadur et al., 1998). Both primary and early secondary neurons in the adult fly brain are typically larger and elaborate more extensively than late born secondary neurons from the same lineage (Lee et al., 2020). In the ventral nerve cord, several neuroblasts have been reported to generate distinct cell types in a stereotyped sequence during embryogenesis (reviewed in (Doe, 2017)), but the effect of birth order on adult cell fate has not yet been examined.

We annotated all neurons originating in the VNC as primary, early secondary, or (late) secondary based on position within the soma tract, soma size, and primary neurite diameter (see Methods). Primary neurons tend to be more exuberant and are more likely to connect distinct neuropils contralaterally and bilaterally (Figure 9C). Despite there being far fewer primary neurons than secondary neurons, they are much more centrally positioned within the VNC network (Figure 9D'). An important measure of network centrality is the load centrality, which is the fraction of shortest paths between each pair of nodes that passes through a given node (Newman, 2001). Conversely, primary neurons are less insular than their secondary counterparts, connecting more abundantly and evenly with other hemilineages across the VNC (Figure 9D''). Their centrality in the network is reflected in their overrepresentation in the rich-club relative to their population (Figure 9E). In a network, a rich-club is a set of high-centrality nodes, here measured by load centrality, that are more strongly interconnected than other neurons. Secondary neurons also tend to be further from input and output neurons (Figure 9F), and signals received by them take longer to leave their originating neuropil (Figure 9G). Overall, earlier born neurons seem to play more central and global roles than their secondary counterparts.

Hemilineage Diversity

The VNC circuit is responsible for a large assortment of functions, and hemilineages might serve as the basic units of those functions. In order for a relatively small number of hemilineages to be responsible for such a wide variety of functions, there must be considerable variety across the hemilineages. Secondary neurons show considerable morphological variety across most hemilineages (Figure 10A), and other network properties have high diversity. Occurrence of different subclasses varies amongst hemilineages, with some being exclusively motor neurons, a few with a strong majority of IR neurons (restricted to the ipsilateral neuromere), and some more evenly distributed between the subclasses (Figure 10B). Hemilineages with a higher proportion of IR neurons tend to retain received signals in their local neuropils for longer than those with lower proportion of IR neurons (Figure 10C). On average, signals sent to IR and CR neurons tend to stay within the originating neuropil for 3 more hops than BI or II neurons (data not shown). Hemilineages with more distributed occurrences of subclasses may have more bimodal distributions of intra-neuropil depth (e.g. 09A) while others with more concentrated subclass occurrences are more unimodal (e.g. 20A/22A).

There is also significant variety in the position that hemilineages take within the global structure of the VNC network, even amongst just secondary neurons (Figure 10D). Hemilineages closer to the edges of the graph (e.g. 05B) tend to have higher load centrality values (Figure 10E). These hemilineages also tend to have lower intra-neuropil depths, but this trend does not always hold (e.g. 16B, 04B). The position that individual hemilineages take in global and local circuits can vary across neuromeres. Hemilineage 10B, for instance, has a flat distribution amongst subclasses, and its neurons split evenly into two locations in the network, one closer to outputs and one closer to inputs (Fig 10D). The neurons of 09A have a relatively unimodal location in the global network, but are split into two different locations within the neuropil, with about half the neurons retaining signals for 2 to 3 more synapses than the other half. The network position of individual hemilineages across neuromeres is not entirely consistent either. In T1, signals received by hemilineage 17A tend to stay in the local neuropil 3 hops deeper than in T2 or T3 (Figure 10C). For hemilineage 07B, the global location varies significantly within T1, but is more limited in other neuromeres, with T2 being closer to VNC inputs and T3 closer to outputs (data not shown). These network differences are often reflected morphologically. For example, 07B is quite morphologically uniform in T3, very disparate in T2, and in T1 about half the neurons are in one large group of similar neurons while the rest are relatively dissimilar (data not shown). In summary, across the VNC, hemilineages show high levels of diversity in both morphology and circuit role and function.

Serial homology and motifs

The majority of hemilineage populations were expected to repeat across neuromeres in a general sense, owing to their origins in a repeating neuroblast array and similar gross morphology in the late larva (Truman et al., 2004). However, we discovered that numerous individual neurons could also be identified across multiple neuromeres. This was especially evident in large primary neurons with discordant neurotransmitter predictions, such as the gabaergic 14A primary neurons (Figure 11A). We annotated these initial serial sets and used them as seeds for an iterative graph matching process that predicted candidate sets of neurons with homologous connectivity in adjacent neuromeres (Figure 11B). These

candidates were manually reviewed and annotated, generating additional seeds for the next run. Later on, we leveraged serial annotations to identify more candidates using serial cosine clustering (Figure 11C).

We were able to assign 5663 neurons with similar appearance, connectivity, hemilineage, and/or predicted neurotransmitter across neuromeres to 760 serial sets. The largest population (and the easiest to identify) were “independent leg” neurons that were largely restricted to the leg neuropils and did not appear to interact with homologues in other neuromeres. These were typically very similar in topology and connectivity across neuromeres, albeit with differences in morphology attributable to segment-specific neuropil rotation and expansion (Figure 12A). This category was dominated by gabaergic and glutamatergic neurons, suggesting a large role for serially homologous inhibitory circuits. Most leg motor neurons were also serially homologous, allowing us to propagate light level matches across thoracic neuromeres (please see (Cheong et al., 2023) for details).

However, we also identified numerous more complex serial motifs. We assigned those that primarily innervated non-leg neuropils to a “dorsal” category (Figure 12B) and those exclusively composed of neurons ascending via the neck connective to an “ascending” category (Figure 12C). A small but especially interesting category were the “sequential” sets in which neurons featured dendrites in one neuromere but sent their axons up to the next anterior neuromere or down to the next posterior neuromere (Figure 12D); for a discussion of their likely role in intersegmental leg coordination, please see our accompanying manuscript.

We identified numerous cases of “convergence” of axons of presumed serially homologous neurons, including a few that included neurons descending from the brain (Figure 12E). We assigned those with peripheral dendrites in leg neuropils and axons converging centrally in non-leg neuropils to a special “centripetal” category (Figure 12F). Conversely, we found a very small number of “centrifugal” neurons with central, partially overlapping dendrites and axons projecting out to one or more leg neuropils (Figure 12G). The remaining serial sets with more complicated patterns of connectivity were lumped together as “complex” (Figure 12H) and form the largest motif category apart from the “independent leg” (Figure 12I).

While these serial sets were interesting in their own right as examples of segment-specific reuse and diversification of repeated elements during nervous system development, they also proved to be extremely useful in the systematic typing of the VNC, particularly of sensory neurons in the leg neuropils (see below) and leg motor neurons (as described in our accompanying manuscript (Cheong et al., 2023)). They also informed our annotation of abdominal soma neuromeres, and sets bridging the thoracic and abdominal neuromeres aided in abdominal hemilineage assignments (Figure 12H). We might also expect them to aid in assigning hemilineage to serially homologous descending neurons in the brain once a complete CNS dataset has been obtained.

Cell typing

We partitioned the population of intrinsic, ascending, and efferent neurons into systematic types on the basis of their synaptic connectivity, using the lateral and serial homologues we have identified. The purpose of this typing is fourfold: first, to identify granular sets of neurons that are likely to be mutually identifiable between multiple VNCs; second, to provide units for exploratory and functional analysis, which may be broader than lateral homologues; third, to identify seriality or other symmetries that might not be captured by the previously

described approaches; and fourth, to assign a systematic nomenclature consistent with those developed for the sensory, descending, and motor neuron populations.

Types are determined by a clustering of synaptic connectivity, which uses our annotations of laterality and seriality to inform and constrain the process at several stages. The connectivity adjacency is symmetrized by either or both of lateral and serial homology (Figure 13A), then each annotated hemilineage is independently clustered. Terminal type clusters for each hemilineage are selected on the basis of consistency between independent clusterings of each lateral side (without lateral symmetrization), attempting to select clustering parameters coinciding with a peak in consistency nearest the most granular typing (Figure 13B). Selecting parameters consistent across lateral variability is intended to make types robust to noise and error in the reconstruction and exploit lateral variability as a proxy for inter-individual variability in connectivity (Schneider-Mizell et al., 2016). These parameters are then applied to the whole laterally and serially aggregated hemilineage, constrained to place each serial set in at most one type cluster (see Methods).

The resulting types most often consist of single pairs of laterally grouped neurons, and types containing a serial set most often contain only one (Figure 13C). Consequently mean homogeneity of birthtime and subclass within each type is high (Figure 13D), though some hemilineages with overly broad type clusters result in types with highly inhomogeneous birthtime and subclass (e.g., 03A, Figure 19 supplement 1). Because they are based on the neuromere-serialised network symmetry whose orbits are identified by the annotated serial homologue sets, types are highly serial, frequently containing neurons from multiple neuromeres (Figure 13E). As with other serial annotations, types are broadly structured into three block communities: the thoracic neuromeres, A1 through A7, and A8 through A10. Of these, the A8 through A10 community has the least serial frequency between its neuromeres, though it has the most seriality with neuromeres outside the block, namely A8 and A9 with T3 and the rest of the abdominal neuromeres. As expected, A1 shares many types with T3 and the other thoracic neuromeres.

The structure of connectivity similarity within hemilineages and thus the similarity structure of types varies between hemilineages. For example, hemilineage 19A has a highly block-structured connectivity cosine distance (Figure 13G), resulting in types containing lateral groups strongly similar within the type but dissimilar between types (Figure 13F). In contrast, hemilineage 13B has broad, but structured connectivity similarity, which results in types that only form segments of a larger similarity structure. This larger structure is not defined by neuromere-specific communities, but is anchored by primary neurons.

To characterise this inter-hemilineage variability of intra-hemilineage connectivity similarity, the spectral radius of the hemilineage connectivity cosine distance matrix (its largest absolute value eigenvalue, equivalently the 2-norm in this case) measures how strongly diagonal similarity is distributed (Figure 19H). Hemilineages like 19A containing small type clusters with low intra-cluster variance and high inter-cluster variance have a high normalised spectral radius, while those with less distinct clusters, more inter-cluster similarity, are lower. However, this single measure does not characterise hemilineages with large clusters but low intra-cluster variance or those composed of distinct populations with inhomogeneous similarity structure.

Secondary Hemilineages

Embryonic divisions by segmentally repeating rows and columns of neuroblasts produce serially homologous primary neurons throughout the VNC. However, only segment-specific

subsets of neuroblasts generate postembryonic progeny (Truman and Bate, 1988), facilitating an expansion of neuronal types in the thorax and distal abdomen for complex sensorimotor functions. In late larva, secondary hemilineages restricted to the leg neuropils are present in all three thoracic neuromeres, while those associated with dorsal (flight) neuropils (e.g., 3B, 11A, 11B, 12A, 18B) are absent or greatly reduced in at least one (Marin et al., 2012; Truman et al., 2004). Only three neuroblasts produce secondary neurons in abdominal segments A2-A7 (Birkholz et al., 2015; Truman and Bate, 1988), but 13 neuroblasts divide postembryonically in A1, 31 in A8, 23 in A9, and 11 in A10 (Birkholz et al., 2013).

We were able to attribute 97% of neurons in the thorax and 38% of neurons in the abdomen (mainly in A1) to a specific hemilineage. We find that in the adult thorax, leg hemilineages are relatively consistent in neuron number and connectivity, while flight hemilineages tend to be much more variable (Figure 7D,E). In the abdomen, the middle segments contain the fewest neurons and the highest proportion of primary neurons and serial homologues, as compared with the most anterior and posterior neuromeres (Figure 50).

Each secondary hemilineage has been reported to exhibit a characteristic broad morphology (e.g., ipsilateral leg neuropil, bilateral flight neuropils, etc) (Shepherd et al., 2019). We have summarised the locations of postsynapses and presynapses for every T2 secondary hemilineage in our dataset for reference (Figure 14).

Below we describe in more depth every hemilineage that produces more than one or two secondary neurons. For each of these 36 hemilineages, we show (A) the overall morphology of the secondary population, (B) individual representatives (as estimated by highest average NBLAST score to other members of the hemilineage), and (C) specific notable examples (which in some cases may be primary). We then report (D) the locations of their connectors (postsynapses and presynapses), (E) their upstream and downstream partners by class, and (F) their upstream and downstream partners by finer subdivisions corresponding to their systematic types (secondary hemilineage, target, or sensory modality).

Hemilineage 00A

Secondary 00A neurons survive in T1-A1, with comparable numbers of neurons in neuromeres T1 and T2 (77) but a smaller number (39) in T3. They enter the neuropil at the ventral midline at the posterior edge of each neuromere, project dorsally, and exhibit bilaterally symmetrical dendrites and axons innervating the mVAC and nearby neuropils (Figure 15A,B,D). Soma tracts of the larger primary neurons from lineage 00 run adjacent to the 00A secondary neurons, although a few diverge early on to innervate leg neuropil (not shown). Most secondary neurons are predicted to be gabaergic, consistent with previous predictions, but a small subpopulation is predicted to be glutamatergic (Figure 15C bottom). They receive substantial input from descending neurons in T1 and T2 but more input from proprioceptive sensory neurons in T3 and A1 (Figure 15E,F). Otherwise, their strongest upstream partners are from hemilineages 09A and 10B, while they inhibit target neurons of 08B, 11A, and 12A from T1-T2, 23B from T3, and 12B from A1 (Figure 15F). No functional studies have been published for secondary 00A neurons.

Hemilineage 01A

Secondary 01A neurons survive in T1-T3 with comparable numbers of neurons in all three neuromeres. They enter the neuropil from the anterior edge of each neuromere and project

their axons across the ventral surface to curve around the contralateral leg neuropil in a characteristic “crook” (Figure 16A,B). A subset is intersegmental, with dendrites innervating a leg neuropil in the neuromere of origin and axons projecting to a more posterior neuropil (Figure 16C). We also identified serially homologous cholinergic neurons that enter the neuropil more medially to cross the midline in the aV (not shown).

01A neurons receive much of their input from descending neurons, particularly those innervating multiple leg neuropils. They are predicted to be cholinergic and activate target neurons from many leg hemilineages, notably 03A, 14A, 16B, and 20A/22A in T1-T3, 13A in T1, 08A in T2, 04B in T3 (Figure 16F), and leg MNs in T1 and T3. Activation of 01A secondary neurons bilaterally results in erratic forward locomotion interrupted by bouts of grooming (Harris et al., 2015).

Hemilineage 01B

Secondary 01B neurons survive in T2-A1 but solely innervate the next anterior neuromere; to facilitate connectivity analyses, we have opted to assign the neuromere of innervation (T1-T3) rather than of true developmental origin. There are comparable numbers of neurons in all three neuromeres. Their primary neurites only converge as they enter the ventral leg neuropil and their dendrites are largely restricted to the sensory association neuropils (Figure 17A), where they receive input from chemosensory, proprioceptive, and tactile sensory neurons (Figure 17F). However, they also receive input from leg hemilineages 12B, 13B, 14A, 20A/22A, and 23B and inhibit the same hemilineages plus 04B and especially 03A (Figure 17F). No functional studies have been published for secondary 01B neurons.

Hemilineage 02A

Secondary 02A neurons survive in T1-T3 with comparable numbers of neurons in all three neuromeres. They enter the neuropil at the anterior margin of each neuromere and close to the midline and project dorsally into the tectulum, arborising primarily ipsilaterally with some having a small contralateral projection in dorsal neuropil (Figure 18A). In this data set, 02A in T2 exhibited a striking developmental defect: the majority of the RHS neurons were shifted laterally but still projected dorsally in parallel with their LHS counterparts, then turned laterally to innervate the RHS dorsal neuropil (Figure 18A). A few RHS neurons crossed the midline to project dorsally with the LHS neurons before splitting off and turning in the opposite direction to exhibit their expected, RHS-appropriate, morphology. We identified serial pairs of intersegmental early born neurons that either converge in an anterior neuromere or ascend sequentially to the next anterior neuromere (Figure 18C). We also identified a serially homologous set of neurons that follow the 02A soma tracts but cross the midline near the dorsal surface to elaborate contralaterally and are predicted to be cholinergic (not shown).

02A secondary neurons receive inputs mostly from descending neurons innervating the tectulum as well as from hemilineages 06A (T2 and T3) and 07B (T3) and proprioceptive sensory neurons (Figure 18E,F). They are predicted to be glutamatergic and synapse onto hemilineages 06A and 07B (Figure 18F), and T1 02A neurons target primary motor neurons (Figure 18E). Activation of 02A secondary neurons bilaterally drives high frequency wing flapping, occasionally interrupted by a bout of wing grooming (Harris et al., 2015).

Hemilineage 03A

Secondary 03A neurons survive in T1-T3 with consistent neuron numbers in all three neuromeres. They enter the neuropil at the posterior margin of the neuropil, projecting

ventrally to arborise extensively in the ipsilateral leg neuropil with a subset in T1 and T2 projecting posteriorly into the adjacent neuropil (Figure 19A). They receive inputs mostly from leg hemilineages 1B, 4B, 8A, 12B, 13B, 14A, 16B, 20/22A, and 23B and from descending neurons, particularly those innervating multiple leg neuropils (Figure 19F). They are predicted to be cholinergic and input primarily onto hemilineage 13A and leg motor neurons, with lesser inputs onto the leg hemilineages 04B, 08A,19A and 20A/22A (Figure 19F). No functional studies have been published for secondary 03A neurons.

Hemilineage 03B

Secondary 03B neurons survive in T1- A1. The number of neurons in each neuromere varies, with T2 having the largest number and a dramatic reduction in T3 (Figure 20E). They enter the neuropil at the posterior margin of the neuropil with 03A and project dorsally to the tectulum with arborisation from T1 and T3 tending to converge onto the ipsilateral T2 neuropil (Figure 20A). We found that 03B primary neurites overlapped with those of 12A in T1, making it more difficult to distinguish them. The A1 neurons project anteriorly to arborise in the ipsilateral wing tectulum in T2.

03B secondary neurons receive inputs from proprioceptive sensory neurons in T1 and T2, but in T3 the major input is from tactile sensory neurons. Their inputs are broadly similar in T1, T2 and A1: from proprioceptive sensory neurons, hemilineages 06A, 07B and 19B, and descending neurons innervating the upper tectulum (Figure 20F). They are predicted to be gabaergic and output primarily onto motor neurons (Figure 20E), proprioceptive sensory neurons, and hemilineages 06A and 06B, 07B, 17A and especially 19B (Figure 20F). In contrast, the neurons in T3 receive inputs from tactile sensory neurons and output onto hemilineage 19A (Figure 20F), suggesting a specialised role. Also, a substantial number of 03B neurons in T1 and T2 were predicted to be electrical (Figures 6B and 20C bottom). Bilateral activation of 03B secondary neurons results in repetitive, poorly coordinated leg movements, occasional grooming bouts, wing flicking, and wing scissoring movements (Harris et al., 2015).

Hemilineage 04B

Secondary 04B neurons survive in T1 - T3 with comparable numbers of neurons in all thoracic neuromeres. The neurons do not form a coherent neurite bundle entering the neuropil and arborise extensively in the ipsilateral leg neuropil (Figure 21A). They receive inputs from descending neurons that innervate multiple leg neuromers and from tactile and proprioceptive sensory neurons (Figure 21F). They are predicted to be cholinergic and output onto leg motor neurons and leg hemilineages 03A, 08A, 13B, and 19A (Figure 21F). No functional studies have been published for secondary 04B neurons.

Hemilineage 05B

Secondary 05B neurons survive in T1-T3 with comparable neuron numbers in T1 and T2 and slightly fewer in T3 (Figure 22E). They enter the neuropil in the posterior neuromere close to the midline, crossing almost immediately and arborising extensively on both sides of the midline as well as contralateral to the side of entry in adjacent thoracic neuropils (Figure 22A). Their inputs are primarily from descending interneurons that innervate multiple neuropils, with lesser inputs from proprioceptive and tactile sensory neurons. They are predicted to be gabaergic and output onto a range of hemilineages in all thoracic neuromeres (00A, 08B, 11A,12A and 23B) as well as 03A and 19B in T1 and 18B and 19B and primary motor neurons in T3 (Figure 22E,F). Bilateral activation of 05B secondary

neurons results in limb repositioning/splaying that brings the fly closer to the ground (Harris et al., 2015).

Hemilineage 06A

Secondary 06A neurons survive in T1-A1 with comparable neuron numbers in T1-T3 and slightly fewer in A1. They enter the neuropil in the posterior of the neuromere and project dorsally to arborise in ipsilateral tectulum in the neuromere of origin, i.e. T1 in neck tectulum, T2 in wing tectulum and T3 in haltere tectulum. The neurons also cross the midline and extend neuromere-specific processes into adjacent neuromeres, with T2 being a region of convergence. In T1 the projections ascend through the cervical connective and descend into T2. T2 projections remain largely within T2, and T3 projections converge on T2. The A1 neurons converge on the haltere tectulum in T3 ipsilaterally and contralaterally ascend into T1 (Figure 23A). We identified a single motor neuron in T2 - A5 that shared the primary neurite tract of 06A (not shown). Many 06A neurons in T2 were predicted to be glutamatergic, some but not all of which featured thick, simple axons with an unusually low density of presynapses, suggesting that they might be electrically coupled to partners via gap junctions (Cheong et al., 2023).

Secondary 06A inputs are consistent for all neuromeres: from descending neurons in the tectulum, proprioceptive sensory neurons, and hemilineage 7B (Figure 23F). They are predicted to be gabaergic and output onto hemilineages 03B, 07B and 19B (Figure 23F) and onto primary motor neurons, particularly in T2 (Figure 23E). Bilateral activation of 06A secondary neurons results in erratic leg movements with occasional wing flicking and high frequency flapping in a partially spread position (Harris et al., 2015).

Hemilineage 06B

Secondary 06B neurons survive in all thoracic neuromeres but with many more neurons in T2 than T1 or T3. They enter the neuropil in the posterior of the neuromere and project dorso-medially to cross the midline and arborise extensively both sides of the midline in the ventral tectulum. The mass of the arborisation from all three neuromeres is concentrated on T2, with T1 neurons tending to project posteriorly and T3 neurons extending anteriorly (Figure 24A). We found that the intersegmental neurons forming varicose projections in lateral leg neuropils (Shepherd et al., 2019) likely belong to 06B rather than 06A (e.g., bodyid 28229, not shown).

Their inputs come from descending neurons, tactile and proprioceptive sensory neurons and hemilineages 08B, 17A, 19B and 07B (Figure 24F). There are some segmental variations in the balance of these inputs. They are predicted to be gabaergic and output onto primary motor neurons (particularly in T3) (Figure 24E), proprioceptive sensory neurons, and hemilineages 19B, 17A, 12A, 07B, 06A and 03B, with some small segment-specific variations (Figure 24F). Bilateral activation of 06B neurons elicits leg-related movements without substantial forward locomotion along with occasional wing grooming bouts (Harris et al., 2015); perhaps 06B inhibition of flight circuits tends to disinhibit leg movement.

Hemilineage 07B

Secondary 07B neurons survive in T1-A1, with T2 having the largest population. They enter the neuropil in the anterior of the neuromeres, projecting dorsomedially to cross the midline and arborise in the tectulum on both sides of the midline but more profusely ipsilaterally. The T1, T3 and A1 hemilineages ascend into the contralateral cervical connective. The T2 hemilineage likewise extends contralateral axons anteriorly into the connective but also

posteriorly into T3 (Figure 25A). 07B inputs come from descending neurons, proprioceptive sensory neurons, and flight-related hemilineages 06A, 06B, 02A and 19B. They are predicted to be cholinergic and output onto hemilineages 06A, 03B and 19B (Figure 25F) and onto primary motor neurons (Figure 25E). Bilateral activation of 07B secondary neurons results in spontaneous grooming with occasional wing flicking, ending in a characteristic takeoff sequence (wings raised, mesothoracic legs extended in a jump, wing depression and flapping) (Harris et al., 2015).

Hemilineage 08A

Secondary 08A neurons survive in T1-T3 with comparable neuron numbers in all neuromeres but T2 having the largest population. They enter the neuropil in the anterior of the neuromeres and arborise in the ipsilateral leg neuropil (Figure 26A). Their inputs come from descending neurons that innervate multiple leg neuropils, proprioceptive and tactile sensory neurons, and hemilineages 04B, 08A, 08B, 16B and 17A. They are predicted to be glutamatergic and output onto leg motor neurons in their respective neuromeres, also onto hemilineage 03A and less so onto 13A and16B with some segmental variation (Figure 26F). Bilateral activation of 08A secondary neurons does not drive any noticeable change in behaviour aside from leg repositioning (Harris et al., 2015).

Hemilineage 08B

Secondary 08B neurons survive in T1-T3 with comparable neuron numbers in all neuromeres but T3 having a smaller population. They enter the neuropil in the anterior of the neuromeres and project dorsomedially to cross the midline and arborise both sides of the midline in the tectulum (Figure 26A). Their inputs come from descending neurons that innervate multiple neuropils, proprioceptive sensory neurons, and hemilineages 05B and 07B, with some neuromere-specific variation. They are predicted to be cholinergic, and their outputs vary by neuromere: in T1 to hemilineage 05B and 12A, in T2 mostly to 06B and motor neurons, and in T3 to 06A and 07B and motor neurons (Figure 26E,F). No functional studies have been published for secondary 08B neurons.

Hemilineage 09A

Secondary 09A neurons survive in the three thoracic neuromeres in ~identical numbers (Figure 28E). Their primary neurites enter the anterior neuromere with 09B and project posteriorly with a characteristic curve towards the midline and then away again, and they mainly innervate the ipsilateral leg neuropil and especially the mVAC. There is a small subset that ascend to the next neuromere (e.g., Figure 28C top). 09A secondary neurons receive much of their input from proprioceptive sensory neurons, from descending neurons targeting the front legs or multiple legs, and from hemilineages 03A, 10B, and especially 20A/22A. They are predicted to be gabaergic and primarily inhibit 10B and 20A/22A (Figure 28F). Bilateral activation of 09A neurons results in a subtle repositioning/splaying out of legs with occasional bouts of spontaneous grooming (Harris et al., 2015).

Hemilineage 09B

Secondary neurons from hemilineage 09B were predicted to be glutamatergic (Lacin et al., 2019), but we find that a subset, particularly those in abdominal segments, are cholinergic (Figure 29C). They enter the anterior neuromere with 09A, cross near the anterior ventral surface, and project to the brain and/or other neuromeres (Figure 29A). In T1-T3, they primarily receive inputs from hemilineages 01B and especially 23B but also from tactile

sensory neurons and descending neurons to multiple legs and neuromeres. In A1, they also receive inputs from chemosensory and proprioceptive sensory neurons and from hemilineage 03A. They target numerous other hemilineages but particularly 00A, 04B, 11A, 17A, and 23B in T1-T3, and the A1 secondary neurons also target hemilineages 01B, 12B, and 14A, 20A/22A and descending neurons to multiple neuromeres (Figure 29F). No functional studies have been published for secondary 09B neurons.

Hemilineage 10B

Secondary neurons from hemilineage 10B are predicted to be cholinergic, found in comparable numbers in the three thoracic neuromeres and, unusually uniform in morphology and connectivity. They enter the anterior neuromere and innervate the ipsilateral mVAC and leg neuropil before crossing the midline and projecting to the brain and/or other neuromeres (Figure 30A). They receive inputs primarily from proprioceptive sensory neurons and from hemilineages 00A and 09A, and they primarily activate 00A, 09A, and especially other 10B neurons (Figure 30F). These features support a role in coordinating leg movements across neuromeres. Indeed, bilateral activation of 10B secondary neurons results in somewhat erratic leg movements, with occasional pivoting or backwards walking (sometimes accompanied by wing flicking and wing buzzing) (Harris et al., 2015).

Hemilineage 11A

Hemilineage 11A secondary neurons only survive in T1 and T2. They enter the posterior neuromere with 19B and 23B and generally exhibit dendrites in the flight neuropils but send axons into the leg neuropils (Figure 31A,D). They include electrical neurons shown to be coupled to the Giant Fiber (Figure 31C) (Kennedy and Broadie, 2018). Unusually, they receive significant input from chemosensory neurons in both neuromeres as well as from proprioceptive and tactile sensory neurons; they also receive it from numerous flight hemilineages including 00A, 06A, 06B, and 07B and from descending neurons targeting the upper or lower tectulum or multiple legs or neuropils (Figure 31F). They are predicted to be cholinergic and primarily activate 00A, 08B, and 17A in T1 and 00A, 05B, 06B, and 07B in T2 (Figure 3F) as well as primary motor neurons (Figure 31E). Bilateral activation of both 11A and 11B secondary neurons evokes takeoff behaviour but with wing flapping prior to the jump (Harris et al., 2015).

Hemilineage 11B

Hemilineage 11B is the most extreme of the segment-specific dorsal hemilineages, with secondary neurons surviving only in T2. Their primary neurites enter the neuromere dorsally near 11A but turn sharply to project to dorsal neuropils (Figure 32A). Notably, they produce a subpopulation of putative electrical neurons (e.g., Figure 32C). They receive most inputs from hemilineages 07B, 08B, 17A, 19B, and especially 06A as well as from descending neurons to the upper tectulum and to multiple neuropils and from proprioceptive sensory neurons (Figure 32F). They are predicted to be gabaergic and inhibit primary motor neurons (Figure 32E) as well as hemilineages 03B, 06B, 12A, 17A, 19B, and especially 06A (Figure 32F). Bilateral activation of both 11A and 11B secondary neurons evokes takeoff behaviour but with wing flapping prior to the jump (Harris et al., 2015).

Hemilineage 12A

Hemilineage 12A secondary neurons exhibit a segment-specific pattern of survival consistent with a role in wing control, with populations in T1 and T2 but not in T3 (Figure

33A,E). They enter the posterior of the neuromere before projecting to the tectulum and are difficult to separate from 03A and 03B in T1. Much of their input is from descending neurons to the upper tectulum, to multiple legs, or to multiple neuropils, but they also receive input from proprioceptive sensory neurons and from flight hemilineages 00A, 06B, and 08B in T1-T2 and additionally from 05B in T1 and from 07B and especially 06A in T2. They are predicted to be cholinergic and activate primary motor neurons (Figure 33E) and flight hemilineages 00A, 06B, and 08B in T1-T2 and additionally 03B, 06A, and 11B in T2. Bilateral activation of 12A secondary neurons results in a sequence of behaviours: walking, wing flicking, and lateral extension and vibration of one wing (akin to male courtship song) (Harris et al., 2015).

Hemilineage 12B

Hemilineage 12B secondary neurons survive in comparable numbers in T1-T3, with an additional small population in A1 (Figure 34E). They generally enter the posterior of the neuromere and cross the midline in the posterior intermediate commissure to innervate the contralateral leg neuropil. However we also identified a minority intersegmental population that innervates the mVACs (e.g., Figure 34C). 12B secondary neurons in T1-T3 receive inputs from descending neurons to multiple legs, tactile sensory neurons, and from hemilineages 01B, 14A, 20A/22A, and 23B; in A1 they receive distinct inputs, from 00A, 10B, and proprioceptive sensory neurons. They are predicted to be gabaergic and in T1-T3 inhibit leg motor neurons and hemilineages 19A and 20A/22A, and to a lesser extent 03A and 04B, but in A1 inhibit 10B and proprioceptive sensory neurons (Figure 34F). Bilateral activation of 12B secondary neurons sometimes results in variable movements of T1 legs with extreme extension of the T2 and T3 legs (Harris et al., 2015).

Hemilineage 13A

Hemilineage 13A secondary neurons survive in roughly comparable numbers across the thoracic neuromeres (Figure 35E). Their primary neurites converge upon neuropil entry and their processes are largely restricted to the ipsilateral leg neuropil of origin (Figure 35A). They receive input predominantly from hemilineage 03A as well as from 04B and 16B and from descending neurons targeting the front leg or all leg neuropils and from proprioceptive and tactile sensory neurons (Figure 35F). They are predicted to be gabaergic and provide outputs mainly to 16B and 20A/22A in T1 and to 03A, 04B, and 19A in T2-T3. They also inhibit front and hind leg motor neurons and to a lesser extent middle leg motor neurons. No functional studies have been published for secondary 13A neurons.

Hemilineage 13B

Hemilineage 13B secondary neurons survive in ~identical numbers across the thoracic neuromeres and cross the midline very ventrally to innervate the contralateral leg neuropils (Figure 36A,E). They receive significant inputs from proprioceptive and tactile sensory neurons and descending neurons targeting the front legs or multiple leg neuropils, as well as from numerous leg hemilineages, especially 01B, 03A, 12B, 14A, 20A/22A, and 23B (Figure 37F). They are predicted to be gabaergic and provide output primarily to 20A/22A and to a lesser extent to 01B, 03A, 09A, and 23B. Bilateral activation of 13B secondary neurons results in a tonic postural change with progressive sideways leg extension (Harris et al., 2015).

Hemilineage 14A

Hemilineage 14A secondary neurons survive in ~identical numbers across the thoracic neuromeres and cross the midline very ventrally to innervate the contralateral leg neuropils (Figure 37A,E). They receive significant inputs from proprioceptive and tactile sensory neurons and descending neurons targeting multiple leg neuropils, as well as from numerous leg hemilineages, especially 01A, 01B, 09A, and 20A/22A (Figure 37F). They are predicted to be glutamatergic and provide output to hemilineages 03A and 12B and to a lesser extent to 01B, 09A, 10B, 19A, and 23B. No functional studies have been published for secondary 14A neurons.

Hemilineage 15B

Hemilineage 15B produces secondary leg motor neurons in all three thoracic neuromeres (Figure 38A). These receive most inputs from leg hemilineages 03A, 04B, 09A, 12B, and especially 20A/22A and also from descending neurons to multiple legs and proprioceptive sensory neurons (Figure 38F). Their axons have been reported to target muscles in the femur and tibia (Baek and Mann, 2009; Brierley et al., 2012).

Hemilineage 16B

Hemilineage 16B secondary neurons enter each thoracic neuromere anterolaterally and are largely restricted to the ipsilateral leg neuropil, although in T1 an additional population projects across the midline (Figure 39A), serving as a critical feature to distinguish this hemilineage from 08A. 16B neurons receive strong input from the descending neurons targeting the front leg neuropils and from DNs targeting multiple leg neuropils, as well as from proprioceptive and tactile sensory neurons and numerous leg hemilineages. They are predicted to be glutamatergic and mainly target hemilineages 03A, 08A, 13A in thoracic neuromeres and in T1 08B and motor neurons (Figure 39E,F). No functional studies have been published for secondary 16B neurons.

Hemilineage 16X

Hemilineage 16B secondary neurons project to the future ipsilateral leg neuropil in late larva (Truman et al., 2004) but have previously appeared in light-level neuroblast clones in adults accompanied by a distinct, unnamed dorsal population (Shepherd et al., 2019). We identified a glutamatergic population that projected straight dorsally to innervate ipsilateral flight neuropil in all three thoracic neuromeres (Figure 40A). In T3, it closely resembles the dorsal population in published images (Figure 40C top). It also appears to be closely associated with earlier born motor neurons to the neck, wings, and halteres (Figure 40C bottom). As this dorsal population has been observed in lineage 16 clones but no Notch data is available, we have annotated it as “16X” but believe it is likely to be 16A. 16X secondary neurons receive much of their input from proprioceptive sensory neurons but also from dorsal hemilineages 06A, 06B, and 07B. It targets those same hemilineages as well as 12A and 17A in T2 and 19B in T3, and primary motor neurons in T1 and T2 (Figure 40E,F). No functional studies have been published for secondary 16X neurons.

Hemilineage 17A

17A secondary neurons are found from T1-A1, but their numbers vary widely, with a dramatic expansion in T2, suggesting segment-specific specialisations for flight (Figure 41A,E). They enter the anterior neuromere near 18B and are likewise cholinergic but remain largely restricted to ipsilateral neuropils except for some T2 types that spread into the upper tectulum (Figure 41A). They receive diverse inputs, notably from tactile sensory neurons in

T1, proprioceptive sensory neurons in T2 and A1, and chemosensory neurons in A1; their postsynaptic partners include 03A in T1 and A1, 06B in T2 and T3, and leg motor neurons in all three thoracic neuromeres (Figure 41E,F). No functional studies have been published for secondary 17A neurons.

Hemilineage 18B

18B is a small, cholinergic secondary hemilineage that survives in T2-A1. 18B neurons enter the anterior neuromere near 17A and cross the midline in an anterior intermediate commissure to innervate the tectulum and dorsolateral leg neuropils (Figure 42A). They include two known electrical cell types (Figure 42C) but are otherwise cholinergic. Their inputs vary from neuromere to neuromere but include 07B in T2, 17A and 19B in A1, and descending neurons throughout. Their postsynaptic partners also vary but are predominantly primary motor neurons in T2-A1 and 07B in T1, 08A in T2, and 03B, 06B, and 17A in T3 (Figure 42F). Bilateral activation of 18B secondary neurons initiates walking, sometimes accompanied by partially folded wing movements, eventually followed by a jump and wing flapping (Harris et al., 2015).

Hemilineage 19A

Hemilineage 19A secondary neurons are typically gabaergic and found in similar numbers in all three thoracic neuromeres. They enter the posterior of each neuromere quite dorsally and mainly innervate the ipsilateral leg neuropil, although a subpopulation crosses the midline just anterior to the leg sensory neuropils (Figure 43A), and we identified an early born cholinergic population that descend or ascend to adjacent neuromeres (e.g., Figure 43C top). They receive considerable input from 03A, 04B, 12B, and both proprioceptive and tactile sensory neurons; unusually, they also inhibit sensory neurons, particularly proprioceptive neurons (Figure 43F). Bilateral activation of 19A results in incessant waving of T2 legs without movement of T1 or T3 legs (Harris et al., 2015).

Hemilineage 19B

Hemilineage 19B secondary neurons are predicted to be cholinergic and are found in T1-A1, but their numbers and connectivity vary dramatically, likely reflecting segment-specific specialisations for flight (Figure 44A,E,F). They enter the neuropil with 11A and 23B near the posterior edge of the neuromere and generally cross the midline in an intermediate commissure to innervate the contralateral tectulum (Figure 44A). We also ascribed a small cholinergic population of cells to 19B that cross much more dorsally (Figure 44C bottom). In T1 and T2, 19B secondary neurons receive input mainly from 03B and from descending neurons, while in T3 they form connections mainly with 06A and 07B (Figure 44F). The A1 neurons have distinct upstream and downstream partners but were identified by serial minority subtypes (e.g., Figure 44C top). 19B neurons also activate primary motor neurons in all neuromeres although to a lesser extent in T3 (Figure 44E). No functional studies have been published for secondary 19B neurons.

Hemilineage 20A/22A

Hemilineages 20A and 22A produce cholinergic secondary neurons that enter the posterior and dorsal neuropil near 21A and can be distinguished in late larva but not in the adult (Lacin et al., 2019; Shepherd et al., 2019; Truman et al., 2004). We identified two largely separable but overlapping cholinergic populations in T1-T3 that we annotated collectively as “20A.22A” (Figure 45A). Serial sets sometimes contained two morphologically identical

neurons entering the leg neuropil in distinct soma tracts (Figure 46C), suggesting that some cell types have been preserved in both hemilineages since the ancestral duplication of their neuroblast. The 20A/22A neurons receive input mainly from hemilineages 09A, 12B, 13B, and 14A as well as descending neurons targeting multiple legs and proprioceptive sensory neurons (Figure 46F). They appear to activate 09A, 12B, and leg motor neurons. Bilateral activation of 20A/22A neurons results in extension/splaying of the legs with occasional grooming bouts (Harris et al., 2015).

Hemilineage 21A

Secondary 21A neurons are found in similar numbers in all thoracic neuromeres. They enter the neuropil in a posterior lateral position and are mainly restricted to the ipsilateral leg neuropils but also project to the tectulum (Figure 46A). They can be difficult to distinguish from the 20A and 22A neurons that enter nearby but include a diagnostic subpopulation that splits to diverge orthogonally to the primary neurite (Figure 46C top). While most 21A neurons were predicted to be glutamatergic as expected, a subset were predicted to be cholinergic, and we cannot be sure that these were correctly assigned. They receive input mainly from 20A/22A and from descending neurons that target the legs or the VNC more broadly, and they primarily target 20A/22A and leg motor neurons in all neuromeres and also 19A in T3 (Figure 46F). Bilateral activation of 21A secondary neurons evokes incessant, uncoordinated leg movements without locomotion (Harris et al., 2015).

Hemilineage 23B

Secondary 23B neurons are cholinergic and survive in T1-A1, although the number in A1 is much reduced (Figure 47E). They enter the neuropil with 19B and 11A in a posterior and dorsal soma tract, innervate the ipsilateral leg sensory neuropil, then project across the midline and almost immediately ascend or descend, creating a characteristic hourglass curve when viewed in transverse section (Figure 47A). Perhaps unsurprisingly, most of their input in T1-T3 is from tactile sensory neurons, while they activate multiple hemilineages including 01B, 03A, 04B, 09B, and especially 12B. The A1 neurons are quite distinct in morphology and connectivity, mainly synapsing onto 05B and 08B, but were validated using several serial minority subtypes (e.g., Figure 47C bottom). Bilateral activation of 23B secondary neurons results in intersegmental limb movements (Harris et al., 2015).

Hemilineages 24B and 25B

Hemilineages 24B and 25B are both small leg motor neuron secondary hemilineages that have not been clearly distinguished at light level (Brown and Truman, 2009; Lacin and Truman, 2016). We identified 8-9 motor neurons in each thoracic hemineuromere resembling those reported from lineage 24 (Brierley et al., 2012) but exiting via two different prothoracic nerves, suggesting that they arise from distinct neuroblasts. The 24B.25B secondary neurons receive input mainly from 03A and 08A and 13A as well as from descending neurons targeting leg neuropils (Figure 48F). They have been reported to target muscles in the coxa, trochanter, and femur (Baek and Mann, 2009; Brierley et al., 2012). Bilateral stimulation of 24B neurons produces repetitive leg movements (Harris et al., 2015).

Primarily primary hemilineages

Several hemilineages do not include a significant secondary population, either because the parent neuroblast is eliminated by programmed cell death after generating neurons in the

embryo or because all/most of the secondary neurons are eliminated soon after birth (Truman et al., 2010). We have tentatively assigned a neuroblast of origin to 11 populations of early-born neurons that are not associated with, or appear significantly distinct from, an identifiable secondary hemilineage (Figure 49). In most cases, light-level data regarding Notch expression was unavailable, so we could not confidently assign as “A” vs “B” and instead opted for “X”.

Based on light-level developmental studies (Pop et al., 2020; Truman et al., 2010), we had expected to identify the octopaminergic 00B primary neurons from the medial neuroblast in all neuromeres (Figure 49A), a secondary neuron from 04A crossing in an intermediate commissure in T1-T3 (Figure 49B), the dorsally projecting 14B hemilineage in T1-T3 (Figure 49D), the primary motor neurons produced by lineage 17 and 18 in T1-T3 (Figure 49G), the two efferent neurons from lineage 21 in T1 (Figure 49H), and the one or two secondary motor neurons reported from hemilineages 20B, 21B, and/or 22B in T1-T3 (Figure 49I). In addition to these, we associated several cell populations with specific neuroblasts based on reports from the late embryo (Schmid et al., 1999). We annotated a small population of early born cholinergic neurons with very similar morphology to 05B in T1-T3 (Figure 49C), a small number of leg neuropil-restricted intrinsic neurons that may correspond to hemilineage 15A in T1-T3 (Figure 49E), a population of gabaergic neurons in T2-A1 that we have ascribed to 17B (Figure 49F), a small number of gabaergic neurons innervating the contralateral leg neuropil in T1-T3 that we attribute to NB5-1/lineage 26 (Figure 49J), and a distinctive population of putative neurosecretory cells in T1-A1 that we attribute to NB5-5/lineage 27 (Figure 49K). Please see the Methods section for more details regarding the identification of these hemilineages. For reference, we have plotted the postsynapses and presynapses for all primary neurons in T2 neuropils by annotated hemilineage (Figure 49 - supplemental 1).

Organisation of abdominal ganglia

The thoracic ganglia undergo tremendous expansion in preparation for their roles in adult locomotion, and contributing secondary neurons have been documented extensively at light level. In contrast, little has been reported regarding the morphology or expected connectivity of neurons in the adult abdominal ganglia.

Posterior to A1, only a small number of neuroblasts survive to produce postembryonic progeny, so the abdominal neuromeres are expected to consist of a relatively high proportion of primary neurons that have persisted and reorganised their processes during metamorphosis. Only three neuroblasts - NB3-5 (lin 09), NB5-2 (lin 06), and NB3-5 (lin 05) - produce secondary neurons in abdominal segments A3-A7, plus NB6-2 (lin 19) in A2 (Birkholz et al., 2015; Truman and Bate, 1988). In contrast, 13 neuroblasts divide postembryonically in A1, 31 in A8, 23 in A9, and 11 in A10 (Birkholz et al., 2013).

This expansion of the secondary neuron population at either end of the abdomen would be expected to reflect more complex functions associated with thoracic appendages or genitalia. Notably, nearly half of abdominal neurons innervate the thoracic neuropils instead of, or in addition to, the abdominal neuropils (Figure 50A), indicating that they have indeed been co-opted for adult-specific appendages and locomotion. This is especially conspicuous in A1, which almost appears to operate as an auxiliary thoracic neuropil (Figure 50B).

Most abdominal neurons look so different from those in the thoracic ganglia that they are very difficult to assign to a hemilineage (or sometimes even to the correct soma

neuromere). However, we were able to assign over two-thirds of neurons in A1, and in some cases in more posterior neuromeres, based on serial homology and predicted neurotransmitter expression (Figure 50C). We also assigned over 88% of abdominal neurons to a serial set, compared with fewer than 34% of thoracic neurons (reflecting the segment-specific expansion and specialisation of postembryonic neuron populations in the thorax). Most of the unassigned abdominal neurons originated in A1 or A8-A10 as small secondary populations with no obvious matches.

Sensory Neurons

Together with descending control from the brain, the VNC receives a significant amount of sensory input. Within the VNC, sensory neurons target specific regions of neuropil depending upon the modality of the information that they convey (Tsubouchi et al., 2017)(Merritt and Murphey, 1992; Murphey et al., 1989a); (Tsubouchi et al., 2017). Utilising this, we classified neurons into **chemosensory** (responsive to chemical stimuli), **tactile** (responsive to touch), and **proprioceptive** (providing information as to the location and movement of the body). These broad categories have distinctive patterns of connectivity to hemilineages within the VNC (Figure 51D).

Chemosensory neurons provide strong input to 09B and 05B; however, despite the relatively lower total number of synaptic connections, hemilineage 01B has the highest number of neurons that receive direct information from chemosensory neurons (Figure 51D,E). As information is propagated deeper into the network, much of the information is retained within 01B, 09B and 05B; however, additional hemilineages are recruited, notably 23B and 12B (Figure 51F).

The strongest downstream hemilineage partner of tactile neurons is 23B, which also has the greatest number of neurons receiving information directly (Figure 51D,E). Hemilineages that also have large populations of neurons receiving information in this layer are 14A and 01B. At the third level of the network 23B retains a large number of active neurons, with large active populations also evident in 03A and 04B (Figure 51F).

Proprioceptive neurons have a broader connectivity profile, possibly relating to the multiple functionally distinct subtypes within this modality (Figure 51D). At the third layer within the network, several hemilineages have high numbers of activated neurons: 07B, 06A, 10B and 03B (Figure 51F).

In addition to modality, we provide fine scale categorisation for the 6478 sensory neurons reconstructed in the MANC dataset. Coarsely, these neurons can be separated into three regions: those originating from the legs, dorsal nerves and the abdomen. We classify each of these regions independently, see Methods.

We categorise the leg-originating sensory neurons into 25 clusters. We identify 8 clusters which correspond to chemosensory populations (Figure 52B, 1-8), 8 clusters which convey tactile stimuli (Figure 52B, 9-16), 6 which are composed of proprioceptive neurons (Figure 52B, 19- 24), 2 clusters of mixed modality (Figure 52B, 17-18), and a final cluster of neurons of unknown function (Figure 52B, 25). We observe significant variance in the synaptic connectivity of these clusters. Broadly, clusters of the same modality share similar outputs, however this is not always the case (Figure 52C). The hemilineages that receive the most input from the leg sensory clusters are 05B and 23B. Chemosensory clusters notably provide a large proportion of their outputs to hemilineage 05B. Strikingly, this is not the case for cluster 6, which corresponds to sweet-sensitive chemosensory neurons that instead preferentially target 01B. Cluster 3, which is composed solely of neurons from the forelegs,

also has a different pattern of connectivity, with 09B receiving the largest proportion of its outputs.

Tactile clusters have a broader pattern of connectivity. The majority of these target 23B as the strongest downstream hemilineage. Proprioceptive clusters have a diverse range of connectivity profiles, broadly separating into two groups; clusters 19,20, and 24, and clusters 21-23. Several of these clusters are identifiable as known types. Cluster 19 are FeCO (**fe**moral **c**hordotonal **o**rgan) claw neurons, responsive to the angle of the leg. These neurons connect strongly with hemlineages 13A and 19A. Cluster 20 can be identified as FeCO hook neurons, which fire in response to changes in the extension or flexion of the leg. This population has a broader pattern of connectivity, principally targeting hemilineage 09A. The last FeCO population, FeCO clubs, are recognisable in clusters 21 and 22. These clusters differ in their connectivity to hemilineage 12B, which is the top downstream hemi lineage from cluster 22 but receives negligible input from cluster 21, which instead targets 10B and 09A. These distinct patterns of connectivity are maintained as the information is propagated deeper into the network (Figure 51D).

We identify 45 sensory neuron clusters across the dorsal nerves (Figure 53B). The majority of these clusters were identified to be proprioceptive (28/45), however we also identify 3 chemosensory clusters and 11 tactile clusters. The 3 chemosensory clusters show distinct, yet overlapping hemilineage connectivity profiles. All have strong outputs onto hemilineage 05B, but also each have unique, strong targets: cluster 1 targeting 23B, cluster 2 targeting 03B, and cluster 3 targeting 11A. The dorsal proprioceptive clusters can be separated into two broad categories based on their connectivity to hemilineages. The first has broad connectivity spanning hemilineages 03B, 16X, 06A, 07B and 19B. The majority of this group is composed of neurons entering the VNC through the DMeta nerve, carrying information from the haltere. This is not exclusive however, with cluster 27 entering from through the prothoracic nerves. The second group displays connectivity to hemilineages 23B, 17A, and 06B, and these neurons primarily enter through the ADMN, conveying information from the wings.

The sensory neurons that enter through the abdomen have been divided into 20 clusters (Figure 54B). We are unable to identify the modality of the majority of these, with the exception of clusters 4 and 5 which are composed of proprioceptive neurons. Several of these clusters are strikingly specific in the hemilineages which they connect to, though it should be noted that the majority of neurons in the abdomen have not yet been assigned a hemilineage. Clusters 7 and 10 almost exclusively target hemilineage 01A, clusters 13 and 19 connect strongly to hemilineage 09B, and cluster 20 provides a majority of its hemilineage-identified outputs to 27X.

We report the reconstruction of 539 sensory ascending neurons that presumably relay peripheral stimuli directly to the brain. However, the degree to which local sensory neurons contribute to information ascending to the brain was previously unknown. We have discovered a subset of ascending neurons that receive strong, direct input from local sensory neurons (Figure 55A). These neurons show clear divisions in the modality of sensory information that they receive, strikingly with low degrees of intermixing between modality signals (Figure 55B). This group is dominated by primary neurons (Figure 55C), suggesting that modality specific pathways are created at an early stage within the developing nervous system. The ratio of ascending neurons specific to each modality is strikingly similar to that of all sensory populations (Figure 55D,E), which may reflect a uniform convergence ratio from sensory input to ascending information channels.

DISCUSSION

In this first fully reconstructed ventral nerve cord connectome, we have reconstructed and classified 13,059 intrinsic neurons, 1866 ascending neurons, 1328 descending neurons, 737 motor neurons, ~100 other efferent neurons, and nearly 6500 sensory neurons (Figure 1). But our extensive annotation (Figures 2-4, Table 1) allows us to go far beyond mere cell counts.

We have assigned a developmental hemilineage to 88% of the 15762 VNC neurons (97% of the 13429 originating in thoracic neuromeres) and a soma side and neuromere to each one. We also found that over a third of neurons had recognisable serial homologues in other neuromeres, suggesting that when describing circuit organisation and function, consideration should be given to the segmentally repeated nature of the VNC and the possibility of inter-neuromere connectivity. These annotations formed the basis of our systematic typing and nomenclature that should prove highly useful in leveraging this connectome for light-level developmental and functional studies.

Annotating the estimated birthtime of each neuron based on soma tract morphology and location inspired analysis of the role of each cohort in the VNC network (Figure 9). It also allows us to revisit the predicted secondary neuron network first posited on the basis of immature neuron morphology in the late larva (Truman et al., 2004). A direct comparison of the predicted and observed T2 secondary network (Figure 56B) largely validates these predictions while revealing many more strong connections between members of different hemilineages than could have been anticipated - a testament to the power of whole-volume connectomics. In particular, we added 23B, the 24B/25B motor neurons, and our newly identified glutamatergic dorsal hemilineage 16X to this network. We also have predicted neurotransmitters for every secondary hemilineage, refining our understanding of how they might function in such a network. Notably, we observe a high level of intra-hemilineage communication for specific hemilineages, particularly 03A, 04B, 07B, 08B, 17A, 19B, 20A/22A, and 23B (Figure 56A) - all cholinergic - suggesting the potential for a local feedforward mechanism.

We also show that not all hemilineages can be considered to be morphological and functional units to the same degree. A few, such as 13B, 14A, and 20A/22A appear to be nearly homogeneous with respect to morphology, connectivity, and position within the VNC network, including across neuromeres (Figures 10, 36 supplemental 1, 37 supplemental 1, 45 supplemental 1). However, many hemilineages are much more diverse. Positions in both local and global circuits differ across neuromeres for several hemilineages, suggesting different functions in different local circuits, as well as distinct functions in the global circuit of the VNC. Even when not identifiable by intra-hemilineage morphological disparity, these local circuit distinctions are identifiable in typing assignments (see supplemental materials for Figures 15-49). Hemilineages that have greater differences in network positions across neuromeres generally have less equal distributions of neuromeres in each type (i.e. they have lower Shannon Entropy in their distributions of counts of neuromere identity per type) (data not shown).

Many minority cell types could not be distinguished in light-level postembryonic neuroblast clones (Shepherd et al., 2019) and so have not yet been captured in driver lines or tested for function (Harris et al., 2015). Moreover, primary neurons tend to be much more diverse, form many more connections, and likely play unique roles in the adult VNC network

(Figure 9), yet very few have been previously characterised; we are the first to report their morphologies and connectivity (Figure 49, Figure 49 supplemental 1).

Drosophila possess intricate leg circuits that enable them to navigate their environment with remarkable agility. While studies have successfully mapped the proprioceptive sensory input and motor output to individual leg neuropils (Azevedo et al., 2020; Brierley et al., 2012; Kuan et al., 2020; Tuthill and Wilson, 2016), the INs that integrate these functions remain largely unknown. In our research, we have undertaken a significant effort to reconstruct and identify leg sensory neurons, and in a companion paper (Cheong et al., 2023) the leg motor neurons of the MANC dataset. Additionally we have conducted a thorough annotation effort for the INs, encompassing cell typing, hemilineage annotation, birthtime, and innervation patterns, which enabled a comprehensive description of this neuron class.

This detailed understanding has provided us with the first complete grasp of the number of neurons involved in the leg circuits, both upstream of SNs and downstream of MNs (Figure 57). Notably, we have discovered that over 950 INs are concentrated within each of the six leg neuropils, accounting for 40% of all INs in the VNC (see also Figure 4 and 5). It is not surprising that the intrinsic leg circuits exhibit such complexity, considering their role in coordinating various behaviours like turning during walking (more details in (Cheong et al., 2023)). For coordination between the leg neuropils specifically, we find an additional 930 neurons, with the largest subgroup connecting the T3 leg neuropils to each other. One might have expected a comparable number of neurons within other single neuropils of the VNC. However, the maximum number of neurons dedicated to any other single neuropil is 60 neurons, found within each of the wing neuropils (Figure 5D). The INs and ANs in the upper tectulum have a different organisation, with a relatively large amount of diagonal connections between the haltere and wing neuropils or the halteres and neck neuropil, respectively (Figure 4). We assume that because the wings of the fly act to offset haltere movement and slight asymmetries during flight can cause large effects (Deora et al., 2015), this behaviour requires a strong diagonal coordination between them, a type of connection which is rarely found in the leg neuropils.

We also examined general patterns of connectivity in the abdominal neuromeres. While 888 abdominal neurons are restricted to the boundaries of the ANm, the majority of these project across the midline, joining the two hemispheres (Figure 5E). We additionally identify 571 neurons that strongly link the abdomen with the thorax and an additional 245 that solely innervate the thorax (Figure 50). Most originate in A1, suggesting that many secondary neuron populations there survive because they have been co-opted for the complex processing required for behaviours such as walking or flying. In more posterior neuromeres, we find that most neurons are segmentally repeated primary neurons that participate in local circuits.

Our extensive annotation of sensory neuron modality enables a comprehensive view of sensory modality and hemilineage association across the thoracic segments. We show that there are robust relationships between specific hemilineages and sensory modalities, eg. 23B and tactile sensory neurons, and 05B and chemosensory neurons (Figure 51D). Whilst these associations are clear, we also demonstrate variance within modalities, with clusters of the same modality often having an individual association to one or more unique hemilineages (Figure 52C, 53C). It remains to be examined whether finer grain analyses would uncover additional diversity within our defined clusters. Several of our clusters correspond to sensory neuron types with known subtypes, e.g. leg cluster 20 are FeCO hook neurons, which have been shown to have extension and flexion subtypes (Chen et al.,

2021). Additional analysis may not only provide supporting evidence for existing types, but with the single cell resolution of our dataset, establish the existence of novel subtypes within previously characterised populations. We are currently examining sensory neuron connectivity with respect to specific cell types within selected hemilineages in more detail as well as characterising sensory neuron subtypes not previously discerned at light level. These analyses will help elucidate the complex circuits that underlie sensory processing in the VNC.

METHODS

Cell typing and nomenclature

We have given **systematic type** names to all neurons using a prefix based on their broad class (intrinsic neuron, IN; ascending neuron, AN; efferent non-ascending, EN; efferent ascending, EA; motor neuron, MN; descending neuron, DN). Motor neurons and descending neurons were typed separately as described in our companion manuscript (Cheong et al., 2023). Reconstructed bodies that entered the volume via a nerve were classified as sensory neurons, assigned to an entry nerve, and clustered within that nerve (details below). The remaining neurons were assigned to a developmental hemilineage where possible (details below) and clustered within that hemilineage. Serially repeating cell types generally have identical systematic type names; in a few cases, ascending neurons and intrinsic neurons were judged to be the same type and so have the same hemilineage and number but differing class prefixes.

Subclass of ANs and INs

ANs and INs were given a two letter **subclass** defined by their innervation pattern in the VNC. The first letter represents the laterality of their dendritic and axonic arbour in the dataset. To this end the total number of pre and post synapses was scored in both hemispheres of the VNC for all ANs and INs. If a neuron had more than 5 synapses in total on both sides it was classified as a neuron with bilateral innervation and given the first letter B. If it has less than 5 synapses on one of the two hemispheres of the VNC the neuron either receives the letter I for ipsilateral innervation or C for contralateral innervation in respect to its soma location. The second letter of the subclass defines if a neuron is ascending, A, restricted to a single neuropil, R, or interconnecting neuropils, I. Restricted to a given neuropil was defined by having no less than 5 synapses outside of a neuropil mesh. In cases where different subclasses were given to neurons of the same group, the average across the group was used to make the assignment. There were 30 ANs that had less than 5 synapses in the entire VNC, so we gave them the subclass XA.

Sensory neuron reconstruction and classification

In general, reconstructed bodies that 1) appeared to enter the volume via a nerve and 2) lacked a soma were classified as sensory neurons; those that also appeared to leave via the CvC were classified as ascending sensory neurons. However, many neurons highly similar in morphology and connectivity could not be followed all the way to the nerve due to staining artefacts and possible degeneration, particularly in the leg neuropils, and these were also

classified as sensory neurons. Also, a small number of sensory neuron somas located at the base of the nerves were preserved in the volume.

Initially bodies with no class assignment were compared to previously reconstructed sensory neurons using NBLAST (Costa et al., 2016). The resultant score matrix was then rearranged to produce a ranked spreadsheet of candidates, progressing from high score to low score, which were manually reviewed and either extended into sensory neurons or discarded. Secondarily, we selected classless bodies that were presynaptic to neurons downstream of previously annotated sensory neurons. These classless bodies were similarly manually reviewed and processed.

Once reconstruction had been completed, we compared the morphologies of sensory neurons to light level data to classify them to known types. However, due to limitations in the segmentation quality, reconstruction status, and underlying light level data we were unable to assign the majority of sensory neurons to known types. We then proceeded to cluster the neurons using Weighted Nearest Neighbour clustering (Hao et al., 2021). For this analysis we used a range of synaptic connectivity, morphological and network traversal features, including synaptic outputs to single neurons, synaptic inputs from single neurons, synaptic outputs to neurons aggregated by hemilineage, synaptic inputs from neurons aggregated by hemilineage, NBLAST scores between sensory neurons, and mean graph traversal distances from sensory neurons to all neurons within the VNC. Individual nerve clusterings were then detected using HDBSCAN from a UMAP representation of the WNN output (Campello et al., 2013). In order to detect serial SN types in the leg originating nerves and abdominal nerves, these groups were independently aggregated using the cosine distance of their outputs to serial groups. These distances were used to generate a dendrogram, from which clusters were determined to be below an optimal cut height, taken as that which maximised the adjusted mutual information across the component independent clusterings. All final clusters were manually reviewed by an expert annotator.

The sensory afferent projections in the VNC are highly ordered and organised according to peripheral location of the receptor, receptor type and physiological properties (reviewed in (Tuthill and Wilson, 2016). We used this precise and structured order to assign the sensory neurons to the major sensory modalities of the VNC: proprioceptive, tactile and chemosensory. Annotations were manually assigned to clusters generated for each of the nerves. In the case of the leg nerves, clusters were annotated based on a single nerve, MesoLN_R, and then propagated to the other leg-associated nerves using serialised cosine clustering. The combination of sensory modality and assigned cluster were used to generate systematic types for the sensory neurons.

Sensory Neuron Annotation

Using detailed knowledge of the sensory afferent arrays we used key diagnostic features such as entry nerve, neuropils innervated and morphology to further assign sensory neurons into subclasses that reflect the sensory structures from which each neuron originates.

Proprioceptive Neurons

Proprioceptive neurons in *Drosophila* do not fall into a single morphological class and are derived from a mix of external receptor types (Campaniform Sensilla and Hair plates) and internal stretch receptors (e.g femoral chordotonal organ) (Merritt and Murphey, 1992). Each

receptor type produces a characteristic afferent projection, and it is possible to identify each sensory neuron type from its projections within the VNC.

Leg Proprioceptive neurons

FeCO

The FeCO has a complex sensory afferent projection reflecting the diverse functional properties of its neurons. All FeCO afferents enter the VNC via their respective leg nerve but segregate into 3 functionally distinct projections known as the “Club”, “Claw” and “Hook” (Mamiya et al., 2018). The club neurons form a coherent medially projecting club shaped projection restricted to ipsilateral mVAC. The claw has a characteristic three-pointed projection in ipsilateral LegNp. The hook is the smallest of the FeCO classes and forms a projection similar to the club but with a single bifurcating process close to the entry point to the leg neuropil.

Hair plates

Hair plates are small, tightly packed clusters of short hairs, with each hair innervated by a single neuron. They are positioned at cuticular articulations and are deflected by joint movement. Afferents from HPs enter the VNC via the respective leg neuropil and bifurcate on entry to project around the anterior and posterior margins of the ipsilateral leg neuropil (Merritt and Murphey, 1992). There is anatomical similarity between hair plate sensory afferents and afferents from some leg campaniform sensilla (Merritt and Murphey, 1992), and it is not possible to fully distinguish these.

Campaniform Sensilla

Campaniform sensilla are small cuticular domes which detect tension in the surrounding cuticle and are typically grouped in fields in regions of high strain (Dinges et al., 2021). The projections of afferents from leg campaniform sensilla are diverse, and some are uniquely identifiable (Merritt and Murphey, 1992). Not all leg campaniform sensilla afferents have been described, and it was not possible to annotate them all reliably. Moreover, these sensory populations suffered most severely from degradation and therefore are underrepresented in our dataset.

Dorsal Proprioceptive neurons

Prothorax

Prosternal organ/Hair plates

The prosternal organ is a hair plate located on the anterior wall of the thorax immediately under the neck (Power, 1948). Sensory afferents from the hair plates enter the VNC via the prosternal nerve, a thin nerve that enters the VNC just medial to the dorsal prothoracic nerve (Court et al., 2020). On entry to the prothoracic neuromere, the hair plate afferents project medially around the anterior margin of the ipsilateral leg neuropil before turning dorsally to arborise in ipsilateral NTct and then extending posteriorly to arborise further in the ipsilateral HTct (Smith and Shepherd, 1996).

Prothoracic Chordotonal Nerve (ProCN)

The prothoracic chordotonal organ is located at the anterior/lateral margin of the VNC and connects to the VNC via the ProCN which is a short, thick connection between each prothoracic chordotonal (pCO) sense organ and the first thoracic neuromere (Power, 1948). The pCO afferents project posterior-medially from their entry to arborise in the dorsal most

part of the ipsilateral ovoid and lower tectulum before projecting further posteriorly to arborise in the anteriormost region of the MetaLNp (Smith and Shepherd, 1996); (Stölting et al., 2007).

Mesothorax

Wing blade campaniform sensilla

The Drosophila wing has 8 Campaniform Sensilla found at specific locations on the anterior wing blade (Dickinson and Palka, 1987; Smith and Shepherd, 1996). The sensory afferent from these sensilla enter the VNC via the ADMN and arborise in the lateral regions of the ipsilateral ovoid. The axons then project posteriorly following either a medial or a lateral tract that run just ventral to the LTct to terminate with arborisations in the MetaLNp and the anterior ANm (Dickinson and Palka, 1987; Smith and Shepherd, 1996).

Proximal wing hinge campaniform sensilla

The proximal wing blade has three clusters of campaniform sensilla (Smith and Shepherd, 1996). The sensory afferents from these sensilla enter the VNC via the ipsilateral ADMN and form a complex but characteristic projection that extends anteriorly through the CvC to the brain and posteriorly to produce terminal arborisations in ipsilateral HTct. The largest arborisations are, however, in the ipsilateral WTct (Smith and Shepherd, 1996).

Metathorax

Halteres

The halteres have a large number of campaniform sensilla, organised into fields at the base of each haltere. The sensory afferents from the campaniform fields enter the VNC via the ipsilateral DMetaN and form a robust anterior-directed projection that ascends through the CvC to the SEZ and brain (Smith and Shepherd, 1996). The major arborisation in the VNC is within ipsilateral HTct with minor arborisations in the ipsilateral WTct and NTct. Afferents from different fields have different projection profiles within this major projection and have been described in detail at light level (Chan and Dickinson, 1996).

Tactile Neurons

The body surface of the fly is covered with bristles, each innervated by a single neuron that is activated by mechanical deflection. In *Drosophila* there are two types of tactile bristles, the larger macrochaetes and the smaller, more numerous microchaetes.

Leg Tactile Neurons

Leg bristles are all microchaetes, and their associated sensory neurons enter the VNC via their respective LegN to form a dense topographic projection in the ipsilateral, ventral legNp. These projections have two components, an anterior-lateral group projection from bristles on anterior leg and a posterior-medial projection from bristles on posterior leg (Murphey et al., 1989b).

Wing and Notum Tactile neurons

Wing bristles are all microchaetes distributed across the wing blade and anterior margin. The neurons from these bristles enter the VNC via the ipsilateral ADMN and terminate in ipsilateral ovoid with a small number projecting anteriorly into the ProNm. The tactile

afferents enter the VNC in close association with wing chemosensory afferents loosely enveloping the more densely packed chemosensory neurons (Tsubouchi et al., 2017).

The notum features both micro- and macrochaetes, the microchaetes being far more numerous and evenly distributed. The macrochaetes are fewer in number, lie at highly conserved positions, and can be uniquely identified by position and sensory projections ((Ghysen, 1980; Usui-Ishihara and Simpson, 2005). The sensory neuron associated with each macrochaete has a unique projection in the VNC, and these have been described in detail (Ghysen, 1980) and are readily identified. The macrochaete sensory axons have large diameter axons and enter the VNC by the PDMN and run to the ventral most ovoid before projecting anteriorly into the ProNm and posteriorly, with a small number extending as far as the MesoNm and MetaNm. Macrochaete axons project across the midline in the posterior ovoid to produce a small contralateral projection that mirrors the ipsilateral projection.

Microchaete neurons are not individually identifiable and form a coherent and recognisable projection within the CNS. The microchaete neurons are smaller in diameter but share features with macrochaete projections, entering the VNC via the PDMN to run to the ventral most ovoid where they project anteriorly into the ProNm and cross the midline in posterior ovoid to form a short contralateral projection. Unlike the macrochaetes, none of the microchaetes have a posterior projection(Usui-Ishihara and Simpson, 2005).

Chemosensory Neurons

Leg Chemosensory Neurons

Leg chemosensory sensory neurons are associated with sensilla on the tarsus and tibia (Ling et al., 2014). Each sensillum is innervated by four chemosensory neurons, each with a different sensitivity (Sweet, high salt, low salt and water)(Kwon et al., 2014). Leg chemosensory afferents enter the VNC via the respective leg nerve and project medially to terminate ipsilaterally in the ventral most LegNp adjacent to the midline (Murphey et al, 1989b). Within this projection there are nine projection types, six of which also project anteriorly to the SEZ (Kwon et al., 2014). There is also a single mechanosensory neuron associated with each chemosensory bristle; the projections of these neurons are indistinguishable from the tactile bristle afferents(Murphey et al., 1989a)**.**

Wing chemosensory Neurons

The wing of *Drosophila* has approximately 40 chemosensory sensilla running along its anterior margin(He et al., 2019). The afferents from these bristles enter the VNC via the relevant ADMN to terminate in ipsilateral ovoid. The chemosensory afferents project in close association with the wing tactile afferents, but form a more densely packed projection and terminate more medially than the tactile afferents (Kallman et al., 2015).

Hemilineage assignments

Each hemilineage is generated by a specific neuroblast during development; in most cases the primary neurites of the secondary neurons converge to enter the neuropil at the same point and/or bundle together before branching. Secondary neurons were assigned to hemilineages by comparison with light microscopy images of neuroblast clones (Shepherd et al., 2019) and sparse driver lines (Harris et al., 2015; Shepherd et al., 2016). Key diagnostic features included the relative positions of soma tract entry points and backbones, particularly at midline crossing, as well as neuropils innervated and gross morphology. We describe these features in more detail for each hemilineage below.

Initially, expert annotators seeded the thoracic soma tract bundles of manually identified secondary neurons and ported those hemilineage and soma neuromere annotations to Clio Neuroglancer. Later we used computational methods to assign morphologically similar bodies with somas to the appropriate hemilineage.

We calculated NBLAST on cell body fibres to assign scores of similarity between the neurons (Costa et al., 2016). Next, hierarchical Ward clustering was performed on all-by-all NBLAST scores transformed to a distance space. 12 major clusters were selected arbitrarily, after analysing a clustering dendrogram structure. Next, for each of the 12 clusters, a subsequent clustering procedure was done with a cut-off point resulting in k_{opt} subclusters. In each of the resulting subclusters, a candidate hemilineage assignment was proposed based on the existing preannotated neurons for a given list of hemilineages. If a subcluster did not contain any previously annotated neurons, or the neurons within the cluster did not have consistent labels (at least 50%), the subcluster was left without any candidate assignement.
The number of subclusters k_{opt} for each of 12 clusters was selected automatically based on the following criterion:
k_opt = RI_k - NL_k/N_sc
where *RI_K* is a Rand Index of previously annotated labels and generated candidates, and *NL_k* is a number of unlabelled subclusters as a result of a split *k*; and *N_sc* is a total number of neurons within a subcluster. The resulting candidates for hemilineage labels were manually verified by expert annotators. The procedure was repeated iteratively with confirmed candidates used as priors.

Several hemilineages proved challenging to differentiate from proximal hemilineages due to similar soma tract entry points to the neuropil and overlapping neuron morphologies. To assist in hemilineage assignment, neurons from these hemilineages were clustered using the Weighted Nearest Neighbour (WNN) workflow from the Seurat package. Briefly, WNN is a form of multimodality integration developed for single-cell genomics workflows, whereby each modality is integrated with a weighting calculated for each individual cell based on its ability to predict similarity of to its nearest neighbours across each separate modality. The modalities utilised for this analysis were single cell synaptic connectivity, hemilineage aggregated synaptic connectivity, whole neuron NBLAST scores, and cell body fibre NBLAST scores. Community detection was performed on the integrated data using the Louvain algorithm. These communities were then used to assist in hemilineage assignment, alongside UMAP visualisations of the integrated data.

Hemilineages 00A and 00B

00A and 00B derive from the ventral unpaired median neuroblast (VUM or MNB) (Truman et al., 2004), which produces 3 bilaterally exiting neurosecretory cells, 6 intersegmental interneurons, and 2-6 dorsally projecting interneurons per segment in the embryo (Schmid et al., 1999).

00A secondary neurons survive in T1-A1 (Truman et al., 2010); these are mainly gabaergic (Lacin et al., 2019), enter the neuropil at a landmark midline position at the posterior edge of each neuromere in both larva and adult, and project dorsally in a coherent bundle before branching, generally exhibiting bilaterally symmetric morphologies.

00B neurons are octopaminergic efferents, with small clusters of primary neurons found in each segment in adults (Monastirioti et al., 1995; Pop et al., 2020). Each neuron has bilaterally symmetric dendrites and exits the VNC in homologous nerves on both sides.

Hemilineages 01A and 01B

Hemilineages 01A and 01B derive from NB1-2 at the anterior edge of each neuromere (Truman et al., 2004) that generates 2-4 MNs in T2, 1 MN in T3, 3-4 intersegmental neurons, and 10-15 local interneurons in the embryo (Schmid et al., 1999). Both secondary hemilineages *innervate* all three adult thoracic segments, but they separate during metamorphosis, with 1B ascending to innervate the leg neuropil of the next anterior neuromere (Shepherd et al., 2019); we have opted to use the hemineuromere of innervation rather than the hemineuromere of origin as the 1B instance.

01A is mainly cholinergic (Lacin et al., 2019) and the most anterior and lateral of the hemilineages that run along the ventral surface and cross the midline to innervate the contralateral leg neuropil, with a characteristic "crook" that curves around the leg neuropil (Truman et al., 2004) before forming the terminal axon branches (Shepherd et al., 2019, 2016).

01B is mainly gabaergic (Lacin et al., 2019), and its primary neurites converge to innervate the ipsilateral ventral leg neuropil of the next anterior neuromere (Shepherd et al., 2019). 01B neurites overlap with those of 04B but generally enter more laterally, while 01B dendrites are largely restricted to the VAC (Shepherd et al., 2019). There were several primary neurons, particularly in T3, that we found difficult to ascribe to 01B vs 04B.

Hemilineage 02A

02A is the only surviving secondary hemilineage of anterior neuroblast NB2-1 (Truman et al., 2004), which produces 15 local interneurons in the embryo (Schmid et al., 1999). 02A is mainly glutamatergic (Lacin et al., 2019) and projects dorsally in a coherent bundle near the anterior edge of each thoracic neuromere, just lateral to the midline. Secondary neurons then turn laterally to innervate the dorsal neuropil, sometimes projecting into adjacent neuromeres, although a small number project contralaterally (Shepherd et al., 2019).

Hemilineages 03A and 03B

Hemilineages 03A and 03B derive from posterior neuroblast NB7-1 (Truman et al., 2004), which generates 4-6 "U" MNs and ~30 local interneurons in the embryo (Schmid et al., 1999). The "U" MNs survive metamorphosis to become the MN1-MN5 flight neurons in the adult (Consoulas et al., 2002). Both secondary hemilineages are present in all three thoracic neuromeres, but 03B is reduced in T3 (Shepherd et al., 2019) and present in A1 (Marin et al., 2012).

03A is one of several posterior cholinergic secondary hemilineages that innervate the ipsilateral leg neuropil (Lacin et al., 2019). It was distinguished from 20A and 22A by two key features. First, 03A somas are interspersed with 03B somas and their primary neurites run in the same tract before 03B diverge to project to dorsal neuropil. Second, 03A neurites wrap around the surface of the ipsilateral leg neuropil, with minimal innervation of the interior (Shepherd et al., 2019).

03B is mainly gabaergic (Lacin et al., 2019). Its primary neurites run in the same tract as 03A before diverging to project dorsolaterally in a coherent bundle and innervate the ipsilateral tectulum (Shepherd et al., 2019). We found that 03B primary neurites overlapped with those of 12A in T1, making it more difficult to distinguish them. Also, a surprising number of 03B neurons in T2 were predicted to be glutamatergic, some but not all of which featured thick, simple axons with an unusually low density of presynapses, suggesting they may be electrically coupled to partners via gap junctions.

Hemilineages 04A and 04B

04B is the main secondary hemilineage (Truman et al., 2010) from medial neuroblast NB3-1 (Truman et al., 2004), which generates 4 contralateral MNs, 3-6 intersegmental interneurons, and a variable number of local interneurons in the embryo (Schmid et al., 1999). 04B is mainly cholinergic (Lacin et al., 2019) and found in all three thoracic segments (Truman et al., 2004). Its medial primary neurites wrap around the surface of the ipsilateral leg neuropil in several separate bundles before elaborating. Most 04B secondary neurons innervate the ipsilateral leg neuropil diffusely, especially the surface, but a small subset exhibit intersegmental projections (Shepherd et al., 2019). Nothing has been published regarding activation of 04B neurons.

There are also one or two contralaterally projecting 04A secondary neurons (Truman et al., 2010) which we identified as cholinergic bilateral intersegmental neurons closely associated with 04B neurons in the adult.

Hemilineages 05A and 05B

05B is mainly gabaergic (Lacin et al., 2019) and is the only surviving secondary hemilineage (Truman et al., 2010) from posterior neuroblast NB5-3 (Birkholz et al., 2015; Lacin and Truman, 2016), which generates a single ipsilateral MN in T1 as well as 12-15 intersegmental interneurons and 12-15 local interneurons per segment in the embryo (Schmid et al., 1999). In the adult, the primary neurites of 05B secondary neurons enter the neuropil near the posterior edge of each neuromere, cross the midline in the posterior commissure (ventral to 06B in T1-T2) (Shepherd et al., 2016), and run anteriorly and/or posteriorly in a ventral tract to innervate the primary sensory neuropil of up to all six leg neuropils and the ovoid (Shepherd et al., 2019).

We identified a small population of early born cholinergic neurons with similar morphology to 05B that we have tentatively annotated as 05A but may also belong to 05B. We did not identify any local 05A or 05B or interneurons in the adult.

Hemilineages 06A and 06B

Hemilineages 06A and 06B derive from posterior medial neuroblast NB5-2 (Birkholz et al., 2015; Lacin and Truman, 2016), which generates one contralateral MN, 4-8 intersegmental neurons, and ~30 local interneurons in the embryo (Schmid et al., 1999). Both secondary hemilineages are mainly gabaergic (Lacin et al., 2019) and survive in all three thoracic segments, although the number of 06B neurons is reduced in T3 (Shepherd et al., 2019) and 06A secondary neurons are also found in A1 (Marin et al., 2012). Their somas separate into two distinct hemilineages during metamorphosis (Harris et al., 2015).

06A secondary neurons project dorsally to elaborate in the ipsilateral tectulum before crossing the midline in the posterior dorsal commissure and then projecting anteriorly and posteriorly (Shepherd et al., 2019).

06B secondary neurons are medial to the 06A neurons in adult thoracic segments and cross the midline in the posterior intermediate commissure anterior to the 12B neurons (Shepherd et al., 2016). 06B neurites are especially prominent in the ovoid, the wing sensory neuropil between T1 and T2 (Shepherd et al., 2019).

Hemilineages 07A and 07B

Hemilineage 07B is believed to derive from NB3-2 (Lacin and Truman, 2016) (but see also (Birkholz et al., 2015; Truman et al., 2004)), which generates 6 ipsilateral MNs and 10-16 contralateral interneurons in the embryo (Schmid et al., 1999). 07B secondary neurons are found in T1-A1 in the adult (Truman et al., 2010, 2004) and cholinergic (Lacin et

al., 2019). Their primary neurites converge to form a coherent tract, elaborate in the ipsilateral tectulum, and then cross the midline posterior to 08B (Shepherd et al., 2019, 2016).

We were not able to distinguish primary 07A cells from the rest of the leg motor neurons. We found that 07B primary neurites enter the neuropil lateral to those of 08B in T1 but medial to 8B in T2-T3 (although with some overlap in T3, where they fan out over the ventral surface of the leg neuropils). A subset of secondary neurons in T2 cross the midline before terminating in all three contralateral leg neuropils (Shepherd et al., 2019).

We have designated two pairs of 07B neurons in A1 with mitochondria-rich terminals as putative electrical. Whilst the majority of 07B neurons in our dataset are predicted to be cholinergic, we also identified a small population of neurons that enter the neuropil with 07B but cross the midline more dorsally and are predicted to be gabaergic; these were assigned to the 14B hemilineage (below). In addition, some early born intersegmental neurons associated with 07B are consistently predicted to be glutamatergic.

Hemilineages 08A and 08B

Hemilineages 08A and 08B are believed to derive from NB3-3 (Lacin and Truman, 2016) (but see also (Birkholz et al., 2015)), which produces 1 MN in abdominal segments plus 3 intersegmental neurons and 4-10 local interneurons in the embryo (Schmid et al., 1999). This lineage also appears to produce one thoracic motor neuron postembryonically (Truman et al., 2004).

08A secondary neurons are mainly glutamatergic (Lacin et al., 2019) and largely restricted to the ipsilateral leg neuropil (Shepherd et al., 2019). In the larva, lineage 16 is medial to lineage 08 in all three thoracic segments (Truman et al., 2004), but as metamorphosis progresses, 08A and 16B are pulled laterally towards the developing leg neuropil, while 08B is pulled medially by its contralateral projections. In the adult, 08A and 16B primary neurites enter the neuropil close together (Shepherd et al., 2016).

We had difficulty distinguishing between 08A and 16B in MANC because they are both glutamatergic and the 16B primary neurites diverge (and merge across hemilineages) depending on innervation targets. The dorsal projections of 08A in T2 were identified from Fru+ neuroblast clones (Cachero et al., 2010) and used to assign the rest of the neurons sharing the soma tract.

08B secondary neurons are mainly cholinergic (Lacin et al., 2019) and feature several major contralaterally projecting morphological subtypes (Shepherd et al., 2019). Their primary neurites enter the neuropil medial to those of 08A in all three thoracic neuromeres (Shepherd et al., 2016). Nothing has been published regarding activation of 08B neurons.

We found that 08B primary neurites enter the neuropil medial to those of 07B in T1 but lateral to 07B in T2-T3 (although with some overlap in T3, where they fan out over the ventral surface of the leg neuropils).

Hemilineages 09A and 09B

Hemilineages 09A and 09B derive from anterior dorsal neuroblast NB3-5 (Lacin and Truman, 2016), which generates an MN in T1 only as well as 12-15 intersegmental neurons and 12-15 local interneurons in the embryo (Schmid et al., 1999). Both are preserved in T1-T3 as well as (at reduced numbers) in abdominal segments (Truman et al., 2004).

09A secondary neuron projections are largely restricted to the ipsilateral leg neuropil (Shepherd et al., 2019). The distinctive “curl” of its axons observed in the larva (Truman et

al., 2004) is preserved as a landmark feature of many secondary neurons in the adult, but there is another population that projects medially and ventrally to invade the ipsilateral mVAC (Shepherd et al., 2019). 09A secondary neurons are mainly gabaergic (Lacin et al., 2019).

09B is a small hemilineage that enters the neuropil with 09A; its neurons cross the midline near the ventral surface, generally between 01A and 14A, and elaborate in the leg sensory neuropil on either side (Shepherd et al., 2019). 09B is reportedly glutamatergic (Lacin et al., 2019), but we identified two subpopulations of 09B neurons in thoracic neuromeres, one predicted to be glutamatergic and the other cholinergic, confirmed by gene expression studies (S Cachero and E Dona, personal communication).

Hemilineage 10B

10B is the only surviving secondary hemilineage (Truman et al., 2010) of anterior medial neuroblast NB2-2 (Birkholz et al., 2015; Lacin and Truman, 2016), which generates 2-3 MNs, 2-4 intersegmental interneurons, and 15 local interneurons in the embryo (Schmid et al., 1999). In the adult, 10B secondary neurons are restricted to thoracic segments (Truman et al., 2004), are mainly cholinergic (Lacin et al., 2019) and innervate the ipsilateral mVAC (Shepherd et al., 2019) before crossing the midline quite ventrally in the anterior intermediate commissure, just anterior to the orthogonally projecting 2A primary neurites (Shepherd et al., 2016).

Hemilineages 11A and 11B

Hemilineages 11A and 11B are believed to derive from posterior dorsal neuroblast 7-2 (Lacin and Truman, 2016) (but see also (Birkholz et al., 2015)), which produces ~10 intersegmental interneurons and 5 local interneurons in thoracic segments of the embryo (Schmid et al., 1999). 11A secondary neurons are found in T1 and T2, while 11B secondary neurons survive in T2 only (Marin et al., 2012). We note here that the morphological descriptions of 11A vs 11B have been reversed in the adult lineages atlas (Shepherd et al., 2019) when compared to neuroblast clones in the late larva (Truman et al., 2010).

11A secondary neurons project ventrally and medially, curving around the tectulum to innervate the dorsal leg neuropil, ventral tectulum, and mechanosensory neuropil of the ovoid (Shepherd et al., 2019). They are mainly cholinergic (Lacin et al., 2019), but we identified a subset of predicted glutamatergic neurons with unusually low presynaptic density which we suggest are electrically coupled to partners via gap junctions.

11B secondary neurons feature a sharp bend in their primary neurites as they turn to innervate the dorsal tectulum (Shepherd et al., 2019). They are mainly gabaergic (Lacin et al., 2019), but we identified a subset of predicted glutamatergic neurons with unusually thick axons and low presynaptic density which we suggest are electrically coupled to partners via gap junctions.

Hemilineages 12A and 12B

Hemilineages 12A and 12B derive from posterior ventral neuroblast NB6-1 (Truman et al., 2004), which generates 1 MN (in T1 only), 3-5 intersegmental interneurons, and ~20 local interneurons in the embryo (Schmid et al., 1999). 12A secondary neurons survive in T1, T2, and A1, while 12B neurons survive in all three thoracic segments (Marin et al., 2012; Truman et al., 2004).

The primary neurites of 12A secondary neurons enter the neuropil lateral to those of 12B (Shepherd et al., 2016). In T1, their arborisations create a characteristic

“A-Frame”-shaped projection when viewed from dorsal, while in T2, they diverge in three major bundles to innervate the tectulum (Shepherd et al., 2019). 12A secondary neurons are mainly cholinergic (Lacin et al., 2019).

The 12B secondary neurons appear to be superficially similar in appearance across all thoracic segments, crossing the midline in the posterior intermediate commissure (posterior to 6B) and innervating the ventral tectulum and contralateral leg neuropil (Shepherd et al., 2019). They are mainly gabaergic (Lacin et al., 2019).

Hemilineages 13A and 13B

Hemilineages 13A and 13B are believed to derive from neuroblast NB4-2 (Lacin and Truman, 2016) (but see also (Birkholz et al., 2015; Truman et al., 2004)), which produces 4 MNs and ~20 local interneurons in the embryo (Schmid et al., 1999). Both secondary hemilineages survive in all thoracic segments (Truman et al., 2004) and are predicted to be gabaergic (Lacin et al., 2019). Their somas separate into two distinct hemilineages during metamorphosis (Harris et al., 2015).

The primary neurites of 13A secondary neurons spread over the VNC surface and only converge as they enter the neuropil. We distinguished them from other anterior ipsilateral leg neuropil hemilineages by their characteristic subpopulation of neurons projecting medially and dorsally (Shepherd et al., 2019).

The primary neurites of 13B secondary neurons cross the midline near the ventral surface of the neuropil, just posterior to those of 14A (Truman et al., 2004). 13B secondary neurons innervate the contralateral leg neuropil, and their somas are sometimes pulled across the midline (Shepherd et al., 2019). We have opted to use the soma side of origin (as inferred by morphology) for the instance.

Hemilineages 14A and 14B

Hemilineages 14A and 14B derive from medial neuroblast NB4-1 (Birkholz et al., 2015; Lacin and Truman, 2016), which generates the motor neuron of the transverse nerve, ~8 intersegmental interneurons, and 20-24 local interneurons in the embryo (Schmid et al., 1999). Their secondary neurons are found only in thoracic neuromeres (Truman et al., 2004), and only one or two 14B neurons survive in each hemisegment (Truman et al., 2010).

The primary neurites of 14A secondary neurons cross the midline near the ventral surface of the neuropil, just anterior to those of 13B (Truman et al., 2004).

14A secondary neurons innervate the contralateral leg neuropil, and their somas are sometimes pulled across the midline (Shepherd et al., 2019). We have opted to use the soma side of origin (as inferred by morphology) for the instance. 14A secondary neurons are glutamatergic (Lacin et al., 2019), but we have also identified a serially homologous set of gabaergic primary neurons.

14B secondary neurons project dorsally to cross the midline in the anterior dorsal commissure (Truman et al., 2010) and innervate both ipsilateral and contralateral leg neuropil (Shepherd et al., 2019). We have identified a serially homologous set of glutamatergic secondary neurons matching these characteristics as 14B. They share a primary neurite tract with additional gabaergic and/or glutamatergic neurons that we have also tentatively assigned to 14B.

Hemilineages 15A and 15B

Hemilineage 15B is believed to derive from anterior neuroblast NB2-3 (Lacin and Truman, 2016) (but see also (Birkholz et al., 2015)), which produces 3 putative leg MNs and 3-5 local

interneurons in the embryo (Schmid et al., 1999). 15B secondary neurons are glutamatergic (Lacin et al., 2019). They are found only in T1-T3 and assumed to be motor neurons (Truman et al., 2004). Their dendrites are confined to ipsilateral leg neuropil, while their axons target muscles in the femur and tibia (Baek and Mann, 2009; Brierley et al., 2012).

Many leg motor neurons in the MANC dataset are poorly reconstructed due to nerve damage and/or staining artefacts, and several hemilineages producing leg motor neurons appear to enter the neuropil in the same location, making them very difficult to differentiate. Fortunately, 15B (aka LinA) leg motor neurons have been mapped to their target muscles (Baek and Mann, 2009; Brierley et al., 2012). As described in detail in our companion manuscript (Cheong et al., 2023), we matched motor neurons in T1 by morphology to cells annotated in the FANC dataset (Lesser et al., 2023) and then identified their serial homologues in T2 and T3 using morphology and connectivity. We then annotated hemilineage 15B neurons based on their inferred target muscles.

We also identified four cholinergic, serially homologous early born neurons per hemineuromere that enter the neuropil incoherently near 08A and are restricted to ipsilateral leg neuropil. We believe these to be the 15A primaries, although 16A and 24A are also possible.

Hemilineages 16B and 16X

Hemilineage 16B derives from anterior neuroblast NB1-1 (Birkholz et al., 2015; Lacin et al., 2019), which generates 1 or 2 motor neurons, 1 thoracic intersegmental interneuron, and 6-10 local interneurons in the embryo (Schmid et al., 1999). 16B secondary neurons are glutamatergic (Lacin et al., 2019) and largely confined to their ipsilateral leg neuropil (Shepherd et al., 2019). Nothing has been published regarding activation of 16B secondary neurons.

In the larva, lineage 16 is medial to lineage 08 in all three thoracic segments (Truman et al., 2004), but as metamorphosis progresses, 08A and 16B are pulled laterally towards the developing leg neuropil, while 08B is pulled medially by its contralateral projections. In the adult, 08A and 16B primary neurites enter the neuropil close together (Shepherd et al., 2016). We had difficulty distinguishing between 08A and 16B in MANC but assigned glutamatergic hemilineages with prominent T1 ventral dendrites crossing the midline to 16B, based on light-level neuroblast clones (Shepherd et al., 2019).

We have also identified a novel glutamatergic population entering the neuropil near 08A and 16B and containing ascending neurons (T1 only), intrinsic neurons, and motor neurons that innervate ipsilateral dorsal neuropil and exit via DProN, ADMN, and AbN1 in T1, T2, and T3 respectively. Most of the T2 motor neurons linked to courtship song and flight (O'Sullivan et al., 2018) belong to this hemilineage, but previous studies did not investigate their developmental origin. The secondary, intrinsic population is visible in lineage 16 neuroblast clones (Shepherd et al., 2019) and may correspond to 16A, but as we do not know whether they express Notch, we have annotated them as 16X.

Hemilineages 17A and 17B

Hemilineage 17A derives from anterior dorsal neuroblast NB2-5 (Birkholz et al., 2015; Lacin and Truman, 2016), which generates one motor neuron, 4-6 intersegmental interneurons, and 6-8 local interneurons in the embryo (Schmid et al., 1999). 17A secondary neurons have been reported in T2-A1 (Truman et al., 2004) and T1 (Birkholz et al., 2015). We identified serially homologous 17A neurons in all three thoracic segments, although the number of surviving neurons in T1 was reduced. 17A projections are quite diverse, particularly in T2,

but unlike those of 18B, they generally remain ipsilateral except where they cross the midline in the dorsalmost tectulum.

17A secondary neurons are mainly cholinergic (Lacin et al., 2019), but we also identified one subset consistently predicted to be glutamatergic, with low presynaptic density, which may be electrically coupled to partners via gap junctions. We also identified two serially homologous sets of motor neurons with anterior soma tracts that we have tentatively annotated as 17X.18X (since we do not know whether they express activated Notch during development).

Furthermore, we identified a set of neurons that entered the neuropil with the 09/17/18 anterodorsal triad but were predicted to be gabaergic and had a characteristic morphology, with the primary neurite turning dorsally upon entry then projecting straight ventrally before ascending. These neurons are quite distinct from 09A (the only gabaergic secondary hemilineage in the vicinity) in both morphology and connectivity and so could only belong to 17B or 18A. We have tentatively assigned them to 17B because NB2-5 (but not NB2-4) has been reported to generate intersegmental neurons in the embryo.

Hemilineage 18B

Hemilineage 18B is believed to derive from anterior dorsal neuroblast NB2-4 (Lacin and Truman, 2016) (but see also (Birkholz et al., 2015)), which generates one motor neuron and 7-10 local interneurons in the embryo (Schmid et al., 1999).

18B secondary neurons survive in T2-A1 only and cross the midline in the anterior intermediate commissure (Truman et al., 2004) to innervate the tectulum and dorsolateral leg neuropils (Harris et al., 2015). 18B secondary neurons are mainly cholinergic (Lacin et al., 2019), but we also identified a small subset predicted glutamatergic that we matched to neurons reported to be electrically coupled to the Giant Fiber descending neurons (Kennedy and Broadie, 2018).

We also identified two serially homologous sets of motor neurons with anterior soma tracts that we have tentatively annotated as 17X.18X (since we do not know whether they express activated Notch during development).

Hemilineages 19A and 19B

Hemilineages 19A and 19B derive from posterior dorsal neuroblast NB6-2 (Birkholz et al., 2015; Lacin and Truman, 2016), which generates 3-4 intersegmental interneurons and ~20 local interneurons in the embryo (Schmid et al., 1999). Both secondary hemilineages survive in all thoracic neuromeres, but the number of 19B in T1 is greatly reduced (Truman et al., 2004).

The 19A secondary hemilineage is mainly restricted to ipsilateral leg neuropil (Harris et al., 2015) but also includes subtypes that cross the midline in a small anterior and ventral tract to wrap around the contralateral leg neuropil. Bilateral activation of 19A results in incessant waving of T2 legs without movement of T1 or T3 legs (Harris et al., 2015). 19A is mainly gabaergic (Lacin et al., 2019), but we also identified a population of closely associated, cholinergic, ipsilateral intersegmental neurons that we believe to be primary or early secondary 19A.

19B secondary neurons are cholinergic (Lacin et al., 2019), share a large, complex primary neurite tract with 11A and 23B (Shepherd et al., 2016), and generally project contralaterally in the posterior intermediate commissure (Truman et al., 2004) to elaborate in contralateral dorsal tectulum.

We also identified a small number of cholinergic neurons that project contralaterally in the dorsalmost tectulum or cross very ventrally and are closely associated with the 19B soma tract in T1.

Lineages 20, 21, and 22

Hemilineages 20A, 21A, and 22A are posterior lateral hemilineages that innervate the six ipsilateral leg neuropils, with all three entering the neuropil in approximately the same location. 21A is mainly glutamatergic (Lacin et al., 2019) and includes a distinctive neuronal subtype with a "T-junction" morphology that innervates the mVAC (Shepherd et al., 2019). 20A and 22A have proved very difficult to distinguish in the adult at light level, but are both predicted to be cholinergic (Lacin et al., 2019).

Hemilineages 21A and 21B derive from neuroblast NB4-3 (Birkholz et al., 2015; Lacin and Truman, 2016), which generates 2-3 neurosecretory cells and 10-12 local interneurons in the embryo (Schmid et al., 1999). 21B normally produces one secondary ipsilateral leg MN (Truman et al., 2010)., but it has not been distinguished at light level from those of 20B or 22B in the adult (Brierley et al., 2012). Lineage 20 was reported to include two secondary motor neurons while lineage 22 included a single secondary motor neuron, all of which are thought to originate with the "B" hemilineage (Truman et al., 2010). These MNs have not been distinguished at light level from those of 21B or each other in the adult (Brierley et al., 2012). In MANC, all of these MNs enter the neuropil together and exit via the ProAN in T1, the MesoLN in T2, and the MetaLN in T3, so differential origins cannot be inferred. We therefore opted to designate all of these posterior MNs as "20B.21B.22B." We have also annotated a pair of bilateral efferent neurons associated with 21A primary neurites as 21X, believing them to be the NB4-3 NSCs.

Secondary hemilineages 20A and 22A are only present in thoracic neuromeres and innervate the ipsilateral leg neuropil, and in late larva they can be distinguished by separate primary neurite bundles (Truman et al., 2004). Both have been ascribed to NB5-4 (Birkholz et al., 2015), which generates 2-4 efferent cells in the embryo and 2-4 local interneurons in the abdomen (Schmid et al., 1999). However, more recently 20A was associated with a novel neuroblast, NB5-7, which does not produce any embryonic progeny (Lacin and Truman, 2016).

The dispersal of the 20A and 22A primary neurites in MANC made it impossible to assign all neurons to one or the other with confidence. Indeed, we observed numerous cases in which the best contralateral homologue for a given neuron clearly belonged to a different primary neurite cluster (presumed other hemilineage). This is consistent with the hypothesised evolutionary duplication of an ancestral 20A/22A neuroblast (Lacin and Truman, 2016), with many neuronal types persisting in both hemilineages. We therefore opted to annotate both ipsilateral hemilineages as "20A.22A."

We identified distinct clusters of cells with the morphology expected for 21A in all six hemineuromeres, most of which were predicted to be glutamatergic. However, we predicted a surprising number of these "21A" neurons to be cholinergic and cannot be completely confident that they have been assigned to the correct hemilineage, although morphologically they look more typical for 21A neurons and can be clustered separately by soma tract plus connectivity.

Hemilineage 23B

Hemilineage 23B derives from posterior dorsal neuroblast NB7-4 (Birkholz et al., 2015; Lacin and Truman, 2016), which generates 8-15 thoracic interneurons and 5-6 glia in the embryo

(Schmid et al., 1999). 23B secondary neurons are mainly cholinergic (Lacin et al., 2019) and share a large, complex primary neurite tract with 11A and 19B (Shepherd et al., 2016). The 23B primary neurites bend towards the midline as they project ventrally to innervate the ipsilateral sensory neuropil, resulting in a characteristic “hourglass” morphology when viewed in a transverse section (Shepherd et al., 2019).

Hemilineages 24B and 25B

Hemilineage 24B is believed to derive from NB4-4 (Birkholz et al., 2015; Lacin and Truman, 2016), which generates 1 MN, two intersegmental interneurons, and 8-5 local interneurons in the embryo (Schmid et al., 1999). 24B is present in thoracic neuromeres, produces only leg motor neurons postembryonically (Brown and Truman, 2009), and has been reported to be glutamatergic (Lacin et al., 2019). The dendrites of its 6 secondary motor neurons are confined to lateral ipsilateral leg neuropil, and their axons target muscles in the coxa, trochanter, and femur (Baek and Mann, 2009; Brierley et al., 2012). However, NB4-4 is virtually indistinguishable from adjacent NB3-4, which is believed to correspond to lineage 25 (Lacin and Truman, 2016) (but see also (Birkholz et al., 2015)). And 25 is also a small thoracic postembryonic lineage predicted to generate leg motor neurons (Lacin and Truman, 2016).

As described in detail in our companion manuscript (Cheong et al., 2023), we matched motor neurons in T1 by morphology to cells annotated in the FANC dataset (Lesser et al., 2023) and then identified their serial homologues in T2 and T3 using morphology and connectivity. We then annotated 24B MNs based on their inferred target muscles. Given that 25 had not yet been identified/reported at the time that leg motor neurons were mapped to their target muscles, we strongly suspect that some of the MNs previously ascribed to 24B actually belong to 25. This would account for our observation that “24B” MN types consistently exit either the ProLN or DProN in T1 (and their serial homologues also segregate into two distinct populations in the MesoLN and MetaLN), while all “15B” MNs exit the ProLN. But as we have no way to distinguish between 24B and 25, we have opted to annotate all members of both putative hemilineages as “24B.25B.”

Hemilineage 26X

We have identified a population of gabaergic primary neurons that seem likely to derive from the same neuroblast but do not align with any previously reported secondary hemilineage. The neurons appear to originate at a posterior and medial position but target the contralateral leg neuropil, often resulting in T1 somas being dragged across the midline. Based on this soma position and neurotransmitter prediction, we suggest that 26X neurons might originate from embryonic NB5-1.

Lineage 27X

We have identified a population of primary neurons that appear to originate from the same neuroblast but do not align with any previously reported secondary hemilineage. The neurons enter the neuropil near 5B and 6B but project very dorsally and nearly converge with their contralateral homologues before crossing the midline. As this primary population is enriched in putative neurosecretory cells, we suggest that it might originate from embryonic NB5-5, which is located at approximately the same anteroposterior position as NB5-2 (6B) and NB5-3 (5B). It is predicted to be lateral, but like 13B neurons, NB5-5 progeny might be pulled towards the midline by their targets during development.

Birthtime assignment and analysis

We sought to classify the VNC neurons into the three birthtime categories: “primary”, “early secondary” and “secondary”. For this, we used the following morphological features estimated from neurons segmentation after the skeletonization procedure: soma size, average spine radius, average total radius, spine length, total arbours length, the proportion of pre- to post-synaptic connections, and relative cell-body fibre radius within hemilineage. To simplify the problem, we considered only binary labels of “primary”, and “secondary” neurons. In total, we used 946 examples as our training set, spanning across the whole VNC. Our final classification combined predictions from 40 independently trained support vector machine classifiers with radial-basis kernel and cost factor $C = 10$. Next, we used a permutation-based variable importance measure to assess what features have the biggest discriminatory power (Biecek, 2018). Our analysis suggested that 5 corresponded to 80% of variance, and these were subsequently used to train an ensemble of classifiers. We performed a 10-fold cross-validation to verify the robustness of our classification and achieved an F1 score of 58%. The final classification with a measure of confidence (normalised length of margin vectors) was manually inspected by annotators.

We calculated total connection counts by summing the total number of upstream or downstream synapses, respectively, that are associated with each upstream or downstream partner per neuron. To remove possible false synapse predictions, we used only partners that have more than one upstream or downstream synapse with the target neuron, respectively. We calculated morphological exuberancy by counting the number of neuropils in which each neuron has upstream or downstream connections. For each neuropil in which a neuron had more than 1% of their total upstream or downstream connections, we added one to the respective upstream or downstream exuberancy counts. We also added one to a neuron if it was a motor neuron or ascending. We calculated relative proportions of neuron types by determining the proportion of each birthtime population that starts with each applicable two-letter prefix (see Naming Scheme section for more details??). We subtracted the proportion of each prefix for secondary neurons from that of the primary neurons, which gives a comparative proportion for neuronal types in each birthtime.

For the functional comparisons, we restricted all hemilineage partners to just those partners that are upstream or downstream of a specific thoracic segment (T1, T2, T3) and of only one birthtime per hemilineage per segment (each partner may connect with several neurons of one birthtime). We then calculated the percent of total upstream or downstream connections that each partner had in each neuropil.

Origin and target

Neurons belonging to the classes DN,IN,AN,SN and MN were ascribed an origin and target in accordance with the neuropils they innervate within the VNC. The percentage of post-synapses or pre-synapses in each neuropil was scored for origin and target respectively. Neurons with over 80% of their post-synapses or pre-synapses concentrated in a single neuropil were considered to have that particular neuropil as their origin or target. In instances where a neuropil is divided into left or right hemispheres, an underscore L or R

denoted the respective hemisphere (i.e. *LegNpT1_L*). If the cumulative percentage of two neuropils surpassed the 80% threshold and both neuropils contributed at least 5%, both neuropils were included with a full stop (.) between them. Thus, a neuron receiving input from the front leg neuropil and the neck tectulum on the left hemisphere of the VNC would have *LegNpT1_L.NTct_L* as its origin. A substantial proportion of neurons innervate a combination of leg neuropils (LegNpT1-T3) or upper tectulum neuropils (NTct, WTct, HTct). Consequently, we also assessed neurons based on their innervation within these two combined neuropil groups, assigning them the origin or target LegNp or UTct, respectively. Anything that did not fall into one of these three categories was given *multi* as origin or target, which corresponds to 16% of the VNC neurons.

Exceptions were made for different classes of neurons, as their origin or target lie outside of the VNC. DNs were systematically assigned the brain as their origin, MNs were designated their respective identified muscle as target, and SNs were assigned their appendage as origin. ANs target the brain; however, the majority possess axons with numerous synapses in the VNC. Consequently, we decided to represent the target within the VNC for this neuron class. ANs of the XA subclass have both their origin and target annotated as brain, as they have less than 5 synapses within the VNC.

Primary origin or target, used in Figure 5 for ANs and INs, is defined as the neuropil with the highest percentage of post-synapses or pre-synapses, respectively. For all neurons that do not have multi as an origin or target this top neuropil upstream or downstream is the first neuropil in origin and target.

Serial homology assignment

For the identification of serially homologous neurons, we used a semi-automated iterative procedure. We started with a small pool of homologous neurons defined by expert curation based on manual assessment of morphological and connection similarity. We then obtained connectivity information for upstream and downstream partners of this initial set, where the neurons from specific VNC segments were first matched based on their connectivity patterns. We employed a “seeded” version of the Fast Approximate Quadratic Assignment algorithm (Fishkind et al., 2019), which aims to minimise the number of edge disagreements between the two graphs. The “candidates” generated in the process were manually revised, and the procedure kept repeating with confirmed matches as the new seeds. We also used serial cosine clustering to identify more candidates with similar connectivity within each annotated hemilineage. Our approaches allowed us to identify serially homologous groups across both thoracic and abdominal segments.

For INs restricted to the 6 leg neuropils (subclass IR, CR and BR) we took an additional approach with hemilineage connectivity vectors. To construct a connectivity vector for a given target neuron, we group connections by available hemilineage labels divided into ipsilateral and contralateral (with respect to the target), further split with regard to incoming and outgoing edges from the target. We normalise the in- and out- contributions separately, so that the in- and out-vectors both sum to 1. The connectivity to hemilineages allows us to distinguish and cluster neurons of the same serial set. We perform hierarchical clustering of these vectors using the Euclidean metric and weighted linkage method in the scipy.cluster.hierarchy.linkage implementation. The resulting dendrogram provides a hierarchical structure of the clustering that can be extracted. We consider all possible clusters and evaluate them using a metric that rewards clusters that are evenly distributed across the leg neuropils. The clusters are then ranked and filtered to produce the proposed

serial groups for proofreading. Below we give the details of the filtering procedure. Firstly, we implement a 'balance' score B to measure how balanced the number of neurons in each of the leg neuropils is for a given cluster. This score B is Shannon's entropy normalised by the maximum possible entropy value:

$$B = \frac{-\sum_{i=1}^{n} p_i \ln(p_i)}{\ln(N)}. \qquad (1)$$

To calculate the leg neuropil balance for a given cluster, n is the number of leg neuropils represented in the cluster, and pi gives the proportion of neurons in each leg neuropil. N is total number of leg neuropils so ln(6) is the largest entropy value when the cluster is most balanced - in this case, pi = 1/6 for all i gives the score B = 1. The same formula above can be used to measure the balance of other indicators such as the proportion of neurons with somas on the left or right sides. The left-right balance score is useful for ensuring that clusters are symmetric without penalising them for missing neurons in some leg neuropils.

Initially, all clusters are sorted by the leg neuropil balance score. We then discard a cluster if it overlaps (i.e. has common neurons) with a more balanced cluster. This procedure will retain the most balanced clusters across the leg neuropils but discards the clusters that do not span all regions but are still useful components of serial homologues. The simple filtering did well to find balanced clusters of multiples of six in the leg interneurons. For the bilateral neurons, there were few clusters that were perfectly balanced and the clusters that were highly balanced were too large to meaningfully extract serial homologues. To search for useful groupings of size four or multiples of two, we implement a ranking based on clustered height in the dendrogram (priority to tighter clusters), left-right balance score, size (priority to larger clusters), and leg neuropil balance score. These ranks are aggregated by taking the mean to give an overall ranking, which we go through and discard any cluster that has overlaps with a higher-ranked cluster. By performing the above procedures for the leg interneurons and bilateral neurons, we can retrieve clusters of multiples of six, as well as those with four-fold symmetry across two neuromeres. This method proposed clusters which when proofread was able to assign or correct 103 serial sets.

Systematic cell typing and nomenclature

Intrinsic, ascending, and efferent neurons were clustered into systematic types on the basis of their synaptic connectivity, considering both lateral and serial symmetries. Connectivity adjacency between all neurons with an annotated class was considered.

To aggregate connectivity across lateral symmetry, the columns of adjacency matrix blocks corresponding to right-hand soma side neurons for neurons in annotated lateral groups were permuted to match their left-hand homologues (Figure 13A). Rows and columns for each group were then aggregated as sums (as cosine similarity is used, mean aggregation is equivalent). Midline and ungrouped adjacency blocks were unaffected. To aggregate connectivity across serial symmetry, the columns of the adjacency matrix corresponding to each serial set were sum aggregated. Columns not in an annotated serial set were unaffected. Distances for clustering were computed as cosine distance for this whole-network adjacency matrix with either or both aggregations applied, as described below.

Type clusterings of the cosine distance matrix were then performed with Ward's method independently for each hemilineage. Serial sets were constrained to be in a leaf when initialising the cluster linkage. The distance threshold for flat type clusterings was chosen for each hemilineage by evaluating the consensus of independent clusterings of each, unsymmetrised lateral set of neurons (Figure 13B). For each distance in the symmetrized clustering linkage where an agglomeration was made, consensus was measured as the adjusted mutual information (Vinh et al., 2009) (within the intersection set of annotated lateral groups) between both independent lateral clusterings thresholded at that distance. The symmetrized clustering threshold chosen as the distance corresponding to the peak consensus metric nearest the dendrogram leaves. To improve robustness to reconstruction noise, annotation error, and intrinsic variability, as well as smooth the consensus metric, this threshold was chosen by cross-validation randomly omitting single lateral groups from each iteration. Cross-validation was performed either 20 fold or the number of lateral groups in the hemilineage, whichever was less.

In the special cases of the midline hemilineages 00A and 00B, for lateral consensus soma side annotations were augmented with a bootstrapped side assignment based on connectivity. At each iteration, unassigned neurons were assigned a side preference based on their total synaptic connectivity to all neurons with a side assignment (either annotated or already bootstrapped). Then the ratio of left- to right-side maximal presynaptic preference for each yet-to-be-assigned group was considered, and for those within 10% of balanced preference (meaning groups with a nearly equal number of member neurons preferring each side) the preferences were taken as side assignments. This process was repeated until no further groups were assigned, resulting in the assignment of 81 neurons, sufficient for lateral consistency analysis. These assignments were only for lateral consistency analysis and no side annotations were made.

For per-hemilineage type nomenclature, flat type clusters resulting from this process were assigned serial identifiers. Serial identifiers are the descending ordering of hemilineages' type clusters by mean neuron size. Preliminary work showed this ordering to be highly reliable between sides, and it depends only on neuron segmentation, not annotation or synapse or other predictions. Motor neurons were included in the lateral consistency and symmetrized clustering process, as they may be important to hemilineage connectivity similarity structure, but were not assigned a type based on the result.

Programmatic Tools Analysis

The neuprint website (neuprint.janelia.org) provides a graphical front end to explore the VNC connectome by selecting the VNC dataset from the main dropdown menu (Plaza et al., 2022). Authentication via is required but this is available to anyone with a Google account. Most connectome scale analysis was carried out using the natverse suite of tools (Bates et al., 2020) (see natverse.org) written in the R statistical programming language (www.r-project.org). Connectome data was queried via the neuprint API (Plaza et al., 2022) using the neuprintr package (natverse.org/neuprintr) (Schlegel et al., 2021). A specialised open source natverse package, malevnc (documented at natverse.org/malevnc and downloadable from github.com/natverse/malevnc) was written to facilitate connectome annotations and analysis. Annotations were initially written programmatically using the clio API or interactively via the clio front end (clio.janelia.org, select **annotate** from the first drop down menu and then the **VNC** dataset) (Takemura et al., 2023) and then synchronised with neuprint where they can now be queried.

ACKNOWLEDGEMENTS

We would like to thank Joseph Hsu for assistance with proofreading, Sebastian Cachero and Erika Dona for LM-EM matching that elucidated the 08A vs 16B hemilineage assignments, and James W. Truman for discussions on nomenclature and access to unpublished light level data. This work was principally funded by Wellcome Trust collaborative awards (220343/Z/20/Z and 221300/Z/20/Z to GSXEJ with GMC, GM Rubin, S Waddell and M Landgraf) for proofreading, annotation and analysis of MANC neurons. Additional funding came from the Howard Hughes Medical Institute at Janelia to GMC and SB; Neuronex2 (NSF 2014862, MRC MC_EX_MR/T046279/1) award and core support from the MRC (MC-U105188491) to GSXEJ; a Walter Benjamin DFG fellowship to TS.

FIGURE LEGENDS

Figure 1. Overview of the male adult nerve cord (MANC). A. Orientation schematic showing a ventral view of the adult male *Drosophila* central nervous system. The ventral nerve cord (VNC) can be roughly divided into three thoracic neuromeres (T1, T2, T3) and the abdominal neuromeres (ANm). The thoracic neuromeres contain serial repeating units controlling the three pairs of legs. T2 has additional circuitry dedicated to flight. Number of neurons in the central brain are current estimates from FlyWire-FAFB (Schlegel et al., manuscript in prep). Cartoon legs and wings are not to scale. **B.** Cartoon overview of the broad classes of neurons in the VNC including their overall and neuromere specific neuron counts in this dataset.

Figure 2. Overview of key features in MANC. A. Overview of the neuropils in the ventral nerve cord. The right side neuropils are removed in the lateral view. **B.** Overview of the nerves in the ventral nerve cord. **C.** Cross section of half of the second thoracic neuromere (T2) showing the array of neuroblasts that divide to produce hemilineages in the embryo and post embryonically. An “X” indicates that neuroblast does not survive into adulthood. **D.** Overview of neuroblast (NB) division into ganglion mother cells (GMC) prior to differentiation into two hemilineages. Primary neurons are born in the embryo followed by early secondary and finally secondary neurons. Cartoon Icons by DBCLS. **E.** Neurotransmitter predictions were made for every neuron in the dataset, see Scheffer et al., 2022 for details. Most neurons in a hemilineage share the same neurotransmitter prediction. **F.** Hemilineages are serially repeated along the segments of the nerve cord. This provides a basis for identifying serially homologous neurons, which are concentrated in the six leg neuropils.

Figure 3. Summary of systematic cell typing scheme for broad cell classes. A. Descending neurons are assigned a systematic type composed of the prefix “DN” followed by an abbreviation for the target VNC neuropil and a number consistent for members of their cell type. Their root side is used to denote the instance. **B.** Motor neurons are assigned a systematic type composed of the prefix “MN” followed by an abbreviation for the target muscle and a number consistent for members of their cell type. Their soma neuromere and side are used to denote the instance. **C.** Sensory neurons are assigned a systematic type composed of the prefix “SN” (if not ascending) or “SA” (if ascending) followed by an abbreviation for their assigned modality and a number consistent for members of their connectivity cluster. Their entry nerve is used to denote the instance. **D.**

Intrinsic neurons and ascending neurons are assigned a systematic type composed of the prefix “IN” or “AN” followed by their assigned hemilineage and a number consistent for members of their connectivity cluster. Their soma neuromere and side are used to denote the instance. **E.** Efferent neurons are assigned a systematic type composed of the prefix “EN” (if not ascending) or “EA” (if ascending) followed by their assigned hemilineage and a number consistent for members of their connectivity cluster. Their soma neuromere and side are used to denote the instance.

Figure 4. Subclasses of ANs and INs. VNC innervation of ascending neurons and intrinsic neurons. **A.** First letter of the subclass reflects if the neuronal arbour is Ipsilateral, Contralateral, Bilateral or not eXisting in the VNC. The second letter indicates if it is Ascending to the brain, Restricted to one neuropil in the VNC or Interconnecting different neuropils in the VNC. **B.** Single neuron inputs and outputs to VNC neuropils separated by subclass. Arrows pointing to a group of IR subclass neurons that receive all their input and give all their output to the front left leg neuropil. **C.** Example images for neurons of different subclasses.

Figure 4 - Supplemental 1: **Subclass defined by ipsi and contralateral innervation of the VNC. A.** Total number of synapses ipsilateral and contralateral for each neuron of a given subclass. Colours correspond to bilateral (magenta), no synapses (yellow), ipsilateral (green), contralateral (blue). **B.** description of the two-letter code of the subclass. The first letter refers to the laterality and the second if a neuron is ascending, restricted to one neuropil or interconnecting VNC neuropils.

Figure 5. Information flow. Neurons within and projecting between neuropils. **A.** Primary origin and target of ascending (left) and intrinsic neurons (right). Top panels show all neurons and lower panels show all that do not have the same primary origin and target fields (shown in grey). **B.** Example images of ANs projecting between neuropils. **C.** Example images of INs projecting between neuropils. **D.** Illustration of the number of intrinsic neurons restricted to one neuropil, numbers showing ipsilateral in green and contralateral numbers in blue, neurons with origin and target in the same leg neuropil shown in the right top panel in A. **E.** Illustration of the number of neurons bilaterally restricted to one neuropil (in magenta). Numbers within the dotted neuropil schematic have 80% of their input and output in that area. Arrows indicate neurons that are projecting, having > 60% input in a different neuropil than > 60% of their output. Double arrows show neurons that connect neuropils almost evenly. **F.** Number of neurons interconnecting leg or upper tectulum neuropils on just one hemisphere. Numbers showing ipsilateral in green and contralateral numbers in blue.

Figure 6. Neurons with suspected electrical or neurosecretory transmission. A. Unusually low presynaptic density by volume is predictive of electrical or neurosecretory transmission. **B.** Candidate electrical and neurosecretory neurons are produced by specific hemilineages. **C.** Example of an electrical neuron, PSI (group 11446). **D.** Examples of putative electrical neurons (groups 20924 and 12943). **E.** Examples of a neurosecretory neuron (serial 11170). **F.** Examples of putative neurosecretory neurons (group 10985 and serial 10083).

Figure 7. Hemilineage overview. A. 09A and 09B secondary neurons in postembryonic neuroblast clone generated in T2 RHS. **B.** Secondary 09A and 09B neurons in T2 RHS

identified in MANC from light-level images, coloured by predicted neurotransmitter. **C.** All 09A and 09B neurons in T2 RHS identified in MANC, coloured by predicted neurotransmitter. **D.** Predicted neurotransmitters for all VNC neurons by hemilineage and neuromere (neurons of unknown hemilineage have been omitted and all abdominal neuromeres have been combined). **E.** Intra-neuromere hemilineage synaptic connectivity for the three thoracic neuromeres (T1, T2, T3).

Figure 7 - Supplemental 1. Intra-neuromere hemilineage synaptic connectivity across all three thoracic neuromeres (T1, T2, T3).

Figure 8. Summary of the anatomical organisation of synapses for each hemilineage originating in T2 RHS. A. Side and ventral views illustrating the neuropils surveyed: T2 Leg Neuropil (LNP), medial ventral association center (mVAC), ovoid (Ov), wing tectulum (WTct), lower tectulum (LTct), and Intermediate tectulum (IntTct). The orange dashed line shows the approximate location of the transverse section onto which their synapses have been projected. **B.** Template transverse section with major neuropils labelled and axes for orientation. **C.** Projected synapses for T2 RHS neurons of each hemilineage. Top (blue): postsynapses, connections to upstream neurons. Bottom (orange): presynapses, connections to downstream neurons. 21X is only observed in T1.

Figure 9. Roles in the VNC network differ by birthtime. A. Cartoon of birthtime development. Primary neurons are born during embryogenesis while secondaries are born during the larval phase of development. Metamorphosis prunes and remodels primary neurons while secondary neurons continue to elaborate. **B.** Counts of primary, early secondary, and secondary annotations for all VNC origin neurons with annotated hemilineage. *Primary only hemilineages. Inset is frequency of birthtime amongst all annotated neurons. **C-G**. Data is shown only for neurons in T1, T2 and T3. **C.** Comparative representation of each subclass between primary and secondary neurons within each hemilineage. Pink values have a higher percentage representation in the primary population than secondary, and vice-versa for blue, while black represents equal percentage abundance. White boxes have no neurons with that subclass in that hemilineage. *Primary only hemilineages. **D.** Key measures of centrality and insularity within the network, compared between primary and secondary neurons in the full graph, as well as in a network excluding primary intrinsic neurons. Here, one community is all neurons of a hemilineage with a soma in a hemineuromere (e.g. all neurons identified as hemilineage 19A that have somas in the left side of T2 would be one community). **D'.** Load centrality is a measure of centrality, defined as the fraction of all shortest paths between all pairs of nodes that pass through a given node (as introduced in (Newman, 2001)). **D''.** Diversity coefficient is a measure of insularity, calculated as the Shannon Entropy of the distribution of a node's connections to all communities divided by the log of the number of communities (inspired by (Eagle et al., 2010), except with weights to communities instead of individual nodes). The diversity coefficient is 1 minus the sum of the squares of the fraction of a node's total degree that is associated with each community (introduced in (Guimerà and Nunes Amaral, 2005)). Non-redundant community promiscuity is the count of the total number of communities that are connected to a node's community solely because of a node. A node *X* has a score of *n* if, by removing *X* from the graph, the community *X* is a member of is directly connected to *n* less communities. **E.** Normalised weighted rich-club coefficient across birthtimes. Rich-club coefficient was calculated along load coefficient instead of degree. Using $\log_{10}$ of the load

coefficient, we made 1000 bins, from minimum to maximum value in the network. At each bin, we removed all nodes with lower $\log_{10}$ load centrality than the bin and recorded the full weight of the network. Normalised rich-club coefficient (as in (Alstott et al., 2014)) shown was achieved by dividing the normal graph weights at each bin by the mean at each bin of 1,000 graphs with shuffled edge weights. Inset shows the percentage occurrence of the three birthtimes in the rich-club. **F.** Contour plot of depth from and to input neurons (all SNs and DNs) and output neurons (all MNs and ANs), respectively. MNs and ANs were included, and distance to themselves excluded. **G.** Distribution of mean depth where a received signal leaves the neuropil at which it originated. Traversal was done by randomly selecting amongst all synapses that have the query neuron as downstream partner. Then a random synapse was chosen from all the synapses with the query neuron as the upstream partner. Traversal followed the downstream partner of that synapse, randomly choosing a synapse that has that neuron as the upstream partner. Traversal ended when the signal left the neuropil, or encountered a neuron with no downstream partners, or else reaches a motor or ascending neuron, and was repeated 10,000 times per neuron. Data shown here were measured via iGraph (Csardi et al., 2006) and NetworkX (Hagberg et al., 2008) graph implementations of the VNC, based on either the full dataset or a subset of the dataset without primary intrinsic neurons (referred to as “secondary only graph” in the figure).

Figure 10. Diversity levels by hemilineage. Data is shown for secondary neurons in T1, T2, and T3 with a hemilineage assignment. **A.** Morphologic similarity between hemilineages (only considering secondary neurons). NBLAST (Costa et al., 2016) score was calculated as the mean of all distance scores (from 0 to 2) between each neuron in the query target and its most similar match in the target hemilineage. **B.** Percentage of neurons in each hemilineage annotated with each respective subclass. White cell indicates no neurons annotated with respective prefix within hemilineage. Hemilineages 15B and and 24B.25B are motor neuron only hemilineages. **C.** Depth at which a signal leaves the originating neuropil, or else reaches a motor or ascending neuron. Traversal implemented the same as in Figure 9G. **D.** Mean global shortest path distance to and from all output and input neurons, respectively. **E.** Load centrality (Newman, 2001) distributions of all secondary neurons in each hemilineage, subdivided by neuromere. **F.** Diversity coefficient (inspired by (Eagle et al., 2010), except with weights to hemilineage-in-a-hemineuromere communities instead of individual nodes) distributions for all secondary neurons in each hemilineage, subdivided by neuromere. Data shown here were measured via iGraph (Csárdi and Nepusz, 2006) and NetworkX (Hagberg et al., 2008) graph implementations of the VNC.

Figure 11. Identification of serially homologous neurons. A. Example of a manually identified serial set, serial 10424. **B.** Iterative serial homologue prediction and annotation procedure. Briefly, identified serial homologues were used as seeds for graph matching by **F**ast **A**pproximate **Q**uadratic **A**ssignment **P**roblem solver (graspologic). Predicted matches were subjected to automated validation for consistency across sides and neuromeres, producing candidate serial matches which were manually reviewed for shared features including class, hemilineage, morphology, and predicted neurotransmitter. Those confirmed were annotated and used as seeds for the next round of predictions. Please see Methods for further details. **C.** Selected sub-heatmap from serial cosine clustering of 14A. **D.** Heat maps showing consistency of connectivity across neuromeres and hemispheres for thoracic serial homologues.

Figure 12. Classification of serial sets into motifs. A. Independent leg example. **B.** Dorsal example. **C.** Ascending example. **D.** Sequential (ascending or descending to the next neuromere) examples. **E.** Convergent example. **F.** Centripetal example. **G.** Centrifugal example. **H.** Complex example. **I.** Number of neurons assigned to each serial motif, coloured by predicted neurotransmitter.

Figure 13. Typing of intrinsic neurons by connectivity. A. Schematic of aggregation of the connectivity adjacency matrix by lateral symmetry and neuromere seriality. **B.** Example of consistency of independent connectivity clustering of each side of a hemilineage, 09B. The adjusted mutual information (AMI) between sides' increasingly granular clusters is shown between the corresponding dendrograms for each side. Peak consistency chosen to select clusters for systematic types is indicated by a yellow cross. Lines between the heatmaps of serially aggregated connectivity cosine distance indicate neurons whose terminal position in each side's cluster dendrogram differs, shaded by the distance of this difference. **C.** Density histogram of the number of neurons and serial sets per clustered type in all hemilineages' intrinsic, non-motor popular. See E for colour scale. **D.** Density histogram of the birthtime and subclass homogeneity of all types in C. See E for colour scale. **E.** Type seriality, as a histogram of number of types containing any neuron in each pair of neuromeres. Values are normalised by rows, to show relative distributions when population size differs. **F.** Example comparison of the inter-hemilineage variability of intra-hemilineage connectivity similarity structure. Each panel is a UMAP embedding the hemilineage's symmetrized, serially aggregated connectivity cosine similarity, with each point representing a lateral group. Panels are coloured by neuromere, birthtime, and class as in all other figures. Types are coloured arbitrarily for visualisation. **G.** Heatmaps of symmetrized, serially aggregated connectivity cosine distance for the hemilineages in F. **H.** Normalised spectral radius versus number of neurons for all hemilineages. Hemilineages from F and G are labelled.

Figure 14. Synaptic organisation by secondary hemilineage. Summary of the anatomical organisation of synapses for secondary neurons in each hemilineage originating in T2 RHS. **A.** Side and ventral views illustrating the neuropils surveyed: T2 Leg Neuropil (LNP), medial ventral association center (mVAC), ovoid (Ov), wing tectulum (WTct), lower tectulum (LTct), and Intermediate tectulum (IntTct). The orange dashed line shows the approximate location of the transverse section onto which their synapses have been projected. **B.** Template transverse section with major neuropils labelled and axes for orientation. **C.** Projected synapses for T2 RHS neurons of each hemilineage. Top (blue): postsynapses, connections to upstream neurons. Bottom (orange): presynapses, connections to downstream neurons. 21X is only observed in T1.

Figure 15. Hemilineage 00A. A. Secondary neurons plotted in neuromere-specific colours. **B.** Selected secondary neurons plotted in neuromere-specific colours. The neurons were selected by choosing the skeleton with the top accumulated NBLAST score among all neurons from the hemilineage. **C.** Selected neurons. Top: serial 13701 innervating mVAC. Bottom: glutamatergic subcluster 21723. **D.** Synapses of secondary neurons. Blue: postsynapses; dark orange: presynapses. **E.** Proportions of connections from secondary neurons to upstream or downstream partners, normalised by neuromere and coloured by broad class. Numbers indicate the total number of synapse **F.** Ratios of connections from secondary neurons originating in each neuromere to upstream or downstream partners,

normalised by row. Excepting descending and sensory neurons, only secondary partners are included.

Figure 15 - Supplemental 1. Systematic typing of hemilineage 00A. A. Hierarchical clustering dendrogram of hemilineage groups by laterally and serially aggregated connectivity cosine clustering. **B.** Categorical annotations of each hemilineage group, each column corresponding to the aligned leaf in A. Colours for type, serial set, and group are arbitrary for visualisation. Colours for neuromere, birthtime, neurotransmitter, subclass, and class are as in all other figures. **C.** Similarity distance heatmap for hemilineage. Cosine distance is in the upper triangle, while laterally symmetrised NBLAST distance is in the lower triangle. Systematic type names of some types are labelled. **D.** Morphologically representative groups from dendrogram subtrees. Each group, indicated by colour and line connecting to its column in B and C, is the most morphologically representative group (medoid of NBLAST distance) from a subtree of A. The subtrees (flat clusters) are equal height cuts of A determined to yield the number of groups per plot and plots in D.

Figure 16. Hemilineage 01A. A. RHS secondary neurons plotted in neuromere-specific colours. **B.** Representative secondary neurons plotted in neuromere-specific colours. **C.** Selected neurons. Top: sequential serial 10039. Bottom: convergent serial 10789. **D.** Synapses of secondary neurons. Blue: postsynapses; dark orange: presynapses. **E.** Proportions of connections from secondary neurons to upstream or downstream partners, normalised by neuromere and coloured by broad class. Numbers indicate the total number of synapses. **F.** Ratios of connections from secondary neurons originating in each neuromere to upstream or downstream partners, normalised by row. Excepting descending and sensory neurons, only secondary partners are included.

Figure 16 - Supplemental 1. Systematic typing of hemilineage 01A. A. Hierarchical clustering dendrogram of hemilineage groups by laterally and serially aggregated connectivity cosine clustering. **B.** Categorical annotations of each hemilineage group, each column corresponding to the aligned leaf in A. Colours for type, serial set, and group are arbitrary for visualisation. Colours for neuromere, birthtime, neurotransmitter, subclass, and class are as in all other figures. **C.** Similarity distance heatmap for hemilineage. Cosine distance is in the upper triangle, while laterally symmetrised NBLAST distance is in the lower triangle. Systematic type names of some types are labelled. **D.** Morphologically representative groups from dendrogram subtrees. Each group, indicated by colour and line connecting to its column in B and C, is the most morphologically representative group (medoid of NBLAST distance) from a subtree of A. The subtrees (flat clusters) are equal height cuts of A determined to yield the number of groups per plot and plots in D.

Figure 17. Hemilineage 01B. A. RHS secondary neurons plotted in neuromere-specific colours. **B.** Representative secondary neurons plotted in neuromere-specific colours. **C.** Selected neurons. Top: independent leg serial 12532. Bottom:ascending serial 14128. **D.** Synapses of secondary neurons. Blue: postsynapses; dark orange: presynapses. **E.** Proportions of connections from secondary neurons to upstream or downstream partners, normalised by neuromere and coloured by broad class. Numbers indicate the total number of synapses. **F.** Ratios of connections from secondary neurons originating in each neuromere to upstream or downstream partners, normalised by row. Excepting descending and sensory neurons, only secondary partners are included.

Figure 17 - Supplemental 1. Systematic typing of hemilineage 01B. A. Hierarchical clustering dendrogram of hemilineage groups by laterally and serially aggregated connectivity cosine clustering. **B.** Categorical annotations of each hemilineage group, each column corresponding to the aligned leaf in A. Colours for type, serial set, and group are arbitrary for visualisation. Colours for neuromere, birthtime, neurotransmitter, subclass, and class are as in all other figures. **C.** Similarity distance heatmap for hemilineage. Cosine distance is in the upper triangle, while laterally symmetrised NBLAST distance is in the lower triangle. Systematic type names of some types are labelled. **D.** Morphologically representative groups from dendrogram subtrees. Each group, indicated by colour and line connecting to its column in B and C, is the most morphologically representative group (medoid of NBLAST distance) from a subtree of A. The subtrees (flat clusters) are equal height cuts of A determined to yield the number of groups per plot and plots in D.

Figure 18. Hemilineage 02A. A. RHS secondary neurons plotted in neuromere-specific colours. **B.** Representative secondary neurons plotted in neuromere-specific colours. **C.** Selected neurons. Top: convergent serial 12420. Bottom: sequential serial 10193. **D.** Synapses of secondary neurons. Blue: postsynapses; dark orange: presynapses. **E.** Proportions of connections from secondary neurons to upstream or downstream partners, normalised by neuromere and coloured by broad class. Numbers indicate the total number of synapses. **F.** Ratios of connections from secondary neurons originating in each neuromere to upstream or downstream partners, normalised by row. Excepting descending and sensory neurons, only secondary partners are included.

Figure 18 - Supplemental 1. Systematic typing of hemilineage 02A. A. Hierarchical clustering dendrogram of hemilineage groups by laterally and serially aggregated connectivity cosine clustering. **B.** Categorical annotations of each hemilineage group, each column corresponding to the aligned leaf in A. Colours for type, serial set, and group are arbitrary for visualisation. Colours for neuromere, birthtime, neurotransmitter, subclass, and class are as in all other figures. **C.** Similarity distance heatmap for hemilineage. Cosine distance is in the upper triangle, while laterally symmetrised NBLAST distance is in the lower triangle. Systematic type names of some types are labelled. **D.** Morphologically representative groups from dendrogram subtrees. Each group, indicated by colour and line connecting to its column in B and C, is the most morphologically representative group (medoid of NBLAST distance) from a subtree of A. The subtrees (flat clusters) are equal height cuts of A determined to yield the number of groups per plot and plots in D.

Figure 19. Hemilineage 03A. A. RHS secondary neurons plotted in neuromere-specific colours. **B.** Representative secondary neurons plotted in neuromere-specific colours. **C.** Selected neurons. Top: sequential serial 10262. Bottom: sequential subcluster 15430. **D.** Synapses of secondary neurons. Blue: postsynapses; dark orange: presynapses**. E.** Proportions of connections from secondary neurons to upstream or downstream partners, normalised by neuromere and coloured by broad class. Numbers indicate the total number of synapses. **F.** Ratios of connections from secondary neurons originating in each neuromere to upstream or downstream partners, normalised by row. Excepting descending and sensory neurons, only secondary partners are included.

Figure 19 - Supplemental 1. Systematic typing of hemilineage 03A. A. Hierarchical clustering dendrogram of hemilineage groups by laterally and serially aggregated connectivity cosine clustering. **B.** Categorical annotations of each hemilineage group, each column corresponding to the aligned leaf in A. Colours for type, serial set, and group are arbitrary for visualisation. Colours for neuromere, birthtime, neurotransmitter, subclass, and class are as in all other figures. **C.** Similarity distance heatmap for hemilineage. Cosine distance is in the upper triangle, while laterally symmetrised NBLAST distance is in the lower triangle. Systematic type names of some types are labelled. **D.** Morphologically representative groups from dendrogram subtrees. Each group, indicated by colour and line connecting to its column in B and C, is the most morphologically representative group (medoid of NBLAST distance) from a subtree of A. The subtrees (flat clusters) are equal height cuts of A determined to yield the number of groups per plot and plots in D.

Figure 20. Hemilineage 03B. A. RHS secondary neurons plotted in neuromere-specific colours. **B.** Representative secondary neurons plotted in neuromere-specific colours. **C.** Selected neurons. Top: motor neuron serial 11663 (DVMn). Bottom: putative electrical subcluster 10042. **D.** Synapses of secondary neurons. Blue: postsynapses; dark orange: presynapses. **E.** Proportions of connections from secondary neurons to upstream or downstream partners, normalised by neuromere and coloured by broad class. Numbers indicate the total number of synapses. **F.** Ratios of connections from secondary neurons originating in each neuromere to upstream or downstream partners, normalised by row. Excepting descending and sensory neurons, only secondary partners are included.

Figure 20 - Supplemental 1. Systematic typing of hemilineage 03B. Types for motor neurons were assigned separately as outlined in our accompanying manuscript (Cheong et al., 2023)**. A.** Hierarchical clustering dendrogram of hemilineage groups by laterally and serially aggregated connectivity cosine clustering. **B.** Categorical annotations of each hemilineage group, each column corresponding to the aligned leaf in A. Colours for type, serial set, and group are arbitrary for visualisation. Colours for neuromere, birthtime, neurotransmitter, subclass, and class are as in all other figures. **C.** Similarity distance heatmap for hemilineage. Cosine distance is in the upper triangle, while laterally symmetrised NBLAST distance is in the lower triangle. Systematic type names of some types are labelled. **D.** Morphologically representative groups from dendrogram subtrees. Each group, indicated by colour and line connecting to its column in B and C, is the most morphologically representative group (medoid of NBLAST distance) from a subtree of A. The subtrees (flat clusters) are equal height cuts of A determined to yield the number of groups per plot and plots in D.

Figure 21. Hemilineage 04B. A. RHS secondary neurons plotted in neuromere-specific colours. **B.** Representative secondary neurons plotted in neuromere-specific colours. **C.** Selected neurons. Top: ascending serial 10394. Bottom: independent leg serial 11945. **D.** Synapses of secondary neurons. Blue: postsynapses; dark orange: presynapses. **E.** Proportions of connections from secondary neurons to upstream or downstream partners, normalised by neuromere and coloured by broad class. Numbers indicate the total number of synapses. **F.** Ratios of connections from secondary neurons originating in each neuromere to upstream or downstream partners, normalised by row. Excepting descending and sensory neurons, only secondary partners are included.

Figure 21 - Supplemental 1. Systematic typing of hemilineage 04B. A. Hierarchical clustering dendrogram of hemilineage groups by laterally and serially aggregated connectivity cosine clustering. **B.** Categorical annotations of each hemilineage group, each column corresponding to the aligned leaf in A. Colours for type, serial set, and group are arbitrary for visualisation. Colours for neuromere, birthtime, neurotransmitter, subclass, and class are as in all other figures. **C.** Similarity distance heatmap for hemilineage. Cosine distance is in the upper triangle, while laterally symmetrised NBLAST distance is in the lower triangle. Systematic type names of some types are labelled. **D.** Morphologically representative groups from dendrogram subtrees. Each group, indicated by colour and line connecting to its column in B and C, is the most morphologically representative group (medoid of NBLAST distance) from a subtree of A. The subtrees (flat clusters) are equal height cuts of A determined to yield the number of groups per plot and plots in D.

Figure 22. Hemilineage 05B. A. RHS secondary neurons plotted in neuromere-specific colours. **B.** Representative secondary neurons plotted in neuromere-specific colours. **C.** Selected neurons. Top: complex serial 10142. Bottom: complex serial 11757. **D.** Synapses of secondary neurons. Blue: postsynapses; dark orange: presynapses. **E.** Proportions of connections from secondary neurons to upstream or downstream partners, normalised by neuromere and coloured by broad class. Numbers indicate the total number of synapses. **F.** Ratios of connections from secondary neurons originating in each neuromere to upstream or downstream partners, normalised by row. Excepting descending and sensory neurons, only secondary partners are included.

Figure 22 - Supplemental 1. Systematic typing of hemilineage 05B. A. Hierarchical clustering dendrogram of hemilineage groups by laterally and serially aggregated connectivity cosine clustering. **B.** Categorical annotations of each hemilineage group, each column corresponding to the aligned leaf in A. Colours for type, serial set, and group are arbitrary for visualisation. Colours for neuromere, birthtime, neurotransmitter, subclass, and class are as in all other figures. **C.** Similarity distance heatmap for hemilineage. Cosine distance is in the upper triangle, while laterally symmetrised NBLAST distance is in the lower triangle. Systematic type names of some types are labelled. **D.** Morphologically representative groups from dendrogram subtrees. Each group, indicated by colour and line connecting to its column in B and C, is the most morphologically representative group (medoid of NBLAST distance) from a subtree of A. The subtrees (flat clusters) are equal height cuts of A determined to yield the number of groups per plot and plots in D.

Figure 23. Hemilineage 06A. A. RHS secondary neurons plotted in neuromere-specific colours. **B.** Representative secondary neurons plotted in neuromere-specific colours. **C.** Selected neurons. Top: putative electrical subcluster 12112. Bottom: putative electrical serial 11138. **D.** Synapses of secondary neurons. Blue: postsynapses; dark orange: presynapses. **E.** Proportions of connections from secondary neurons to upstream or downstream partners, normalised by neuromere and coloured by broad class. Numbers indicate the total number of synapses. **F.** Ratios of connections from secondary neurons originating in each neuromere to upstream or downstream partners, normalised by row. Excepting descending and sensory neurons, only secondary partners are included.

Figure 23 - Supplemental 1. Systematic typing of hemilineage 06A. Types for motor neurons were assigned separately as outlined in our accompanying manuscript (Cheong et

al., 2023)**. A.** Hierarchical clustering dendrogram of hemilineage groups by laterally and serially aggregated connectivity cosine clustering. **B.** Categorical annotations of each hemilineage group, each column corresponding to the aligned leaf in A. Colours for type, serial set, and group are arbitrary for visualisation. Colours for neuromere, birthtime, neurotransmitter, subclass, and class are as in all other figures. **C.** Similarity distance heatmap for hemilineage. Cosine distance is in the upper triangle, while laterally symmetrised NBLAST distance is in the lower triangle. Systematic type names of some types are labelled. **D.** Morphologically representative groups from dendrogram subtrees. Each group, indicated by colour and line connecting to its column in B and C, is the most morphologically representative group (medoid of NBLAST distance) from a subtree of A. The subtrees (flat clusters) are equal height cuts of A determined to yield the number of groups per plot and plots in D.

Figure 24. Hemilineage 06B. A. RHS secondary neurons plotted in neuromere-specific colours. **B.** Representative secondary neurons plotted in neuromere-specific colours. **C.** Selected neurons. Top: subcluster 18188. Bottom: centrifugal serial 11261. **D.** Synapses of secondary neurons. Blue: postsynapses; dark orange: presynapses. **E.** Proportions of connections from secondary neurons to upstream or downstream partners, normalised by neuromere and coloured by broad class. Numbers indicate the total number of synapses. **F.** Ratios of connections from secondary neurons originating in each neuromere to upstream or downstream partners, normalised by row. Excepting descending and sensory neurons, only secondary partners are included.

Figure 24 - Supplemental 1. Systematic typing of hemilineage 06B. A. Hierarchical clustering dendrogram of hemilineage groups by laterally and serially aggregated connectivity cosine clustering. **B.** Categorical annotations of each hemilineage group, each column corresponding to the aligned leaf in A. Colours for type, serial set, and group are arbitrary for visualisation. Colours for neuromere, birthtime, neurotransmitter, subclass, and class are as in all other figures. **C.** Similarity distance heatmap for hemilineage. Cosine distance is in the upper triangle, while laterally symmetrised NBLAST distance is in the lower triangle. Systematic type names of some types are labelled. **D.** Morphologically representative groups from dendrogram subtrees. Each group, indicated by colour and line connecting to its column in B and C, is the most morphologically representative group (medoid of NBLAST distance) from a subtree of A. The subtrees (flat clusters) are equal height cuts of A determined to yield the number of groups per plot and plots in D.

Figure 25. Hemilineage 07B. A. RHS secondary neurons plotted in neuromere-specific colours. **B.** Representative secondary neurons plotted in neuromere-specific colours. **C.** Selected neurons. Top: centrifugal subcluster 14004. Bottom: convergent serial 10090. **D.** Synapses of secondary neurons. Blue: postsynapses; dark orange: presynapses. **E.** Proportions of connections from secondary neurons to upstream or downstream partners, normalised by neuromere and coloured by broad class. Numbers indicate the total number of synapses. **F.** Ratios of connections from secondary neurons originating in each neuromere to upstream or downstream partners, normalised by row. Excepting descending and sensory neurons, only secondary partners are included.

Figure 25 - Supplemental 1. Systematic typing of hemilineage 07B. A. Hierarchical clustering dendrogram of hemilineage groups by laterally and serially aggregated

connectivity cosine clustering. **B.** Categorical annotations of each hemilineage group, each column corresponding to the aligned leaf in A. Colours for type, serial set, and group are arbitrary for visualisation. Colours for neuromere, birthtime, neurotransmitter, subclass, and class are as in all other figures. **C.** Similarity distance heatmap for hemilineage. Cosine distance is in the upper triangle, while laterally symmetrised NBLAST distance is in the lower triangle. Systematic type names of some types are labelled. **D.** Morphologically representative groups from dendrogram subtrees. Each group, indicated by colour and line connecting to its column in B and C, is the most morphologically representative group (medoid of NBLAST distance) from a subtree of A. The subtrees (flat clusters) are equal height cuts of A determined to yield the number of groups per plot and plots in D.

Figure 26. Hemilineage 08A. A. RHS secondary neurons plotted in neuromere-specific colours. **B.** Representative secondary neurons plotted in neuromere-specific colours. **C.** Selected neurons. Top: independent leg serial 10198. Bottom: diagnostic dorsal population, subcluster 16785. **D.** Synapses of secondary neurons. Blue: postsynapses; dark orange: presynapses. **E.** Proportions of connections from secondary neurons to upstream or downstream partners, normalised by neuromere and coloured by broad class. Numbers indicate the total number of synapses. **F.** Ratios of connections from secondary neurons originating in each neuromere to upstream or downstream partners, normalised by row. Excepting descending and sensory neurons, only secondary partners are included.

Figure 26 - Supplemental 1. Systematic typing of hemilineage 08A. Types for motor neurons were assigned separately as outlined in our accompanying manuscript (Cheong et al., 2023)**. A.** Hierarchical clustering dendrogram of hemilineage groups by laterally and serially aggregated connectivity cosine clustering. **B.** Categorical annotations of each hemilineage group, each column corresponding to the aligned leaf in A. Colours for type, serial set, and group are arbitrary for visualisation. Colours for neuromere, birthtime, neurotransmitter, subclass, and class are as in all other figures. **C.** Similarity distance heatmap for hemilineage. Cosine distance is in the upper triangle, while laterally symmetrised NBLAST distance is in the lower triangle. Systematic type names of some types are labelled. **D.** Morphologically representative groups from dendrogram subtrees. Each group, indicated by colour and line connecting to its column in B and C, is the most morphologically representative group (medoid of NBLAST distance) from a subtree of A. The subtrees (flat clusters) are equal height cuts of A determined to yield the number of groups per plot and plots in D.

Figure 27. Hemilineage 08B. A. RHS secondary neurons plotted in neuromere-specific colours. **B.** Representative secondary neurons plotted in neuromere-specific colours. **C.** Selected neurons. Top: intersegmental mVAC population, subcluster 10997. Bottom: electrical n-CHINs and putative electrical cHINs, subcluster 10598. **D.** Synapses of secondary neurons. Blue: postsynapses; dark orange: presynapses. **E.** Proportions of connections from secondary neurons to upstream or downstream partners, normalised by neuromere and coloured by broad class. Numbers indicate the total number of synapses. **F.** Ratios of connections from secondary neurons originating in each neuromere to upstream or downstream partners, normalised by row. Excepting descending and sensory neurons, only secondary partners are included.

Figure 27 - Supplemental 1. Systematic typing of hemilineage 08B. A. Hierarchical clustering dendrogram of hemilineage groups by laterally and serially aggregated connectivity cosine clustering. **B.** Categorical annotations of each hemilineage group, each column corresponding to the aligned leaf in A. Colours for type, serial set, and group are arbitrary for visualisation. Colours for neuromere, birthtime, neurotransmitter, subclass, and class are as in all other figures. **C.** Similarity distance heatmap for hemilineage. Cosine distance is in the upper triangle, while laterally symmetrised NBLAST distance is in the lower triangle. Systematic type names of some types are labelled. **D.** Morphologically representative groups from dendrogram subtrees. Each group, indicated by colour and line connecting to its column in B and C, is the most morphologically representative group (medoid of NBLAST distance) from a subtree of A. The subtrees (flat clusters) are equal height cuts of A determined to yield the number of groups per plot and plots in D.

Figure 28. Hemilineage 09A. A. RHS secondary neurons plotted in neuromere-specific colours. **B.** Representative secondary neurons plotted in neuromere-specific colours. **C.** Selected neurons. Top: sequential serial 11194. Bottom: mVAC-restricted independent leg serial 14731. **D.** Synapses of secondary neurons. Blue: postsynapses; dark orange: presynapses. **E.** Proportions of connections from secondary neurons to upstream or downstream partners, normalised by neuromere and coloured by broad class. Numbers indicate the total number of synapses. **F.** Ratios of connections from secondary neurons originating in each neuromere to upstream or downstream partners, normalised by row. Excepting descending and sensory neurons, only secondary partners are included.

Figure 28 - Supplemental 1. Systematic typing of hemilineage 09A. A. Hierarchical clustering dendrogram of hemilineage groups by laterally and serially aggregated connectivity cosine clustering. **B.** Categorical annotations of each hemilineage group, each column corresponding to the aligned leaf in A. Colours for type, serial set, and group are arbitrary for visualisation. Colours for neuromere, birthtime, neurotransmitter, subclass, and class are as in all other figures. **C.** Similarity distance heatmap for hemilineage. Cosine distance is in the upper triangle, while laterally symmetrised NBLAST distance is in the lower triangle. Systematic type names of some types are labelled. **D.** Morphologically representative groups from dendrogram subtrees. Each group, indicated by colour and line connecting to its column in B and C, is the most morphologically representative group (medoid of NBLAST distance) from a subtree of A. The subtrees (flat clusters) are equal height cuts of A determined to yield the number of groups per plot and plots in D.

Figure 29. Hemilineage 09B. A. RHS secondary neurons plotted in neuromere-specific colours. **B.** Representative secondary neurons plotted in neuromere-specific colours. **C.** Selected neurons. Top: cholinergic population. Bottom: glutamatergic population. **D.** Synapses of secondary neurons. Blue: postsynapses; dark orange: presynapses. **E.** Proportions of connections from secondary neurons to upstream or downstream partners, normalised by neuromere and coloured by broad class. Numbers indicate the total number of synapses. **F.** Ratios of connections from secondary neurons originating in each neuromere to upstream or downstream partners, normalised by row. Excepting descending and sensory neurons, only secondary partners are included.

Figure 29 - Supplemental 1. Systematic typing of hemilineage 09B. A. Hierarchical clustering dendrogram of hemilineage groups by laterally and serially aggregated connectivity cosine clustering. **B.** Categorical annotations of each hemilineage group, each

column corresponding to the aligned leaf in A. Colours for type, serial set, and group are arbitrary for visualisation. Colours for neuromere, birthtime, neurotransmitter, subclass, and class are as in all other figures. **C.** Similarity distance heatmap for hemilineage. Cosine distance is in the upper triangle, while laterally symmetrised NBLAST distance is in the lower triangle. Systematic type names of some types are labelled. **D.** Morphologically representative groups from dendrogram subtrees. Each group, indicated by colour and line connecting to its column in B and C, is the most morphologically representative group (medoid of NBLAST distance) from a subtree of A. The subtrees (flat clusters) are equal height cuts of A determined to yield the number of groups per plot and plots in D.

Figure 30. Hemilineage 10B. A. RHS secondary neurons plotted in neuromere-specific colours. **B.** Representative secondary neurons plotted in neuromere-specific colours. **C.** Selected neurons. Top: ascending serial 15289. Bottom: centripetal serial 12404. **D.** Synapses of secondary neurons. Blue: postsynapses; dark orange: presynapses. **E.** Proportions of connections from secondary neurons to upstream or downstream partners, normalised by neuromere and coloured by broad class. Numbers indicate the total number of synapses. **F.** Ratios of connections from secondary neurons originating in each neuromere to upstream or downstream partners, normalised by row. Excepting descending and sensory neurons, only secondary partners are included.

Figure 30 - Supplemental 1. Systematic typing of hemilineage 10B. A. Hierarchical clustering dendrogram of hemilineage groups by laterally and serially aggregated connectivity cosine clustering. **B.** Categorical annotations of each hemilineage group, each column corresponding to the aligned leaf in A. Colours for type, serial set, and group are arbitrary for visualisation. Colours for neuromere, birthtime, neurotransmitter, subclass, and class are as in all other figures. **C.** Similarity distance heatmap for hemilineage. Cosine distance is in the upper triangle, while laterally symmetrised NBLAST distance is in the lower triangle. Systematic type names of some types are labelled. **D.** Morphologically representative groups from dendrogram subtrees. Each group, indicated by colour and line connecting to its column in B and C, is the most morphologically representative group (medoid of NBLAST distance) from a subtree of A. The subtrees (flat clusters) are equal height cuts of A determined to yield the number of groups per plot and plots in D.

Figure 31. Hemilineage 11A. A. RHS secondary neurons plotted in neuromere-specific colours. **B.** Representative secondary neurons plotted in neuromere-specific colours. **C.** Selected neurons. Top: electrical GFC4, subcluster 23460. Bottom: electrical GFC3, subcluster 17383. **D.** Synapses of secondary neurons. Blue: postsynapses; dark orange: presynapses. **E.** Proportions of connections from secondary neurons to upstream or downstream partners, normalised by neuromere and coloured by broad class. Numbers indicate the total number of synapses. **F.** Ratios of connections from secondary neurons originating in each neuromere to upstream or downstream partners, normalised by row. Excepting descending and sensory neurons, only secondary partners are included.

Figure 31 - Supplemental 1. Systematic typing of hemilineage 11A. A. Hierarchical clustering dendrogram of hemilineage groups by laterally and serially aggregated connectivity cosine clustering. **B.** Categorical annotations of each hemilineage group, each column corresponding to the aligned leaf in A. Colours for type, serial set, and group are arbitrary for visualisation. Colours for neuromere, birthtime, neurotransmitter, subclass, and

class are as in all other figures. **C.** Similarity distance heatmap for hemilineage. Cosine distance is in the upper triangle, while laterally symmetrised NBLAST distance is in the lower triangle. Systematic type names of some types are labelled. **D.** Morphologically representative groups from dendrogram subtrees. Each group, indicated by colour and line connecting to its column in B and C, is the most morphologically representative group (medoid of NBLAST distance) from a subtree of A. The subtrees (flat clusters) are equal height cuts of A determined to yield the number of groups per plot and plots in D.

Figure 32. Hemilineage 11B. A. RHS secondary neurons plotted in neuromere-specific colours. **B.** Representative secondary neurons plotted in neuromere-specific colours. **C.** Selected neurons. Top: putative electrical subcluster 10326. Bottom: putative electrical group 15495. **D.** Synapses of secondary neurons. Blue: postsynapses; dark orange: presynapses. **E.** Proportions of connections from secondary neurons to upstream or downstream partners, normalised by neuromere and coloured by broad class. Numbers indicate the total number of synapses. **F.** Ratios of connections from secondary neurons originating in each neuromere to upstream or downstream partners, normalised by row. Excepting descending and sensory neurons, only secondary partners are included.

Figure 32 - Supplemental 1. Systematic typing of hemilineage 11B. A. Hierarchical clustering dendrogram of hemilineage groups by laterally and serially aggregated connectivity cosine clustering. **B.** Categorical annotations of each hemilineage group, each column corresponding to the aligned leaf in A. Colours for type, serial set, and group are arbitrary for visualisation. Colours for neuromere, birthtime, neurotransmitter, subclass, and class are as in all other figures. **C.** Similarity distance heatmap for hemilineage. Cosine distance is in the upper triangle, while laterally symmetrised NBLAST distance is in the lower triangle. Systematic type names of some types are labelled. **D.** Morphologically representative groups from dendrogram subtrees. Each group, indicated by colour and line connecting to its column in B and C, is the most morphologically representative group (medoid of NBLAST distance) from a subtree of A. The subtrees (flat clusters) are equal height cuts of A determined to yield the number of groups per plot and plots in D.

Figure 33. Hemilineage 12A. A. RHS secondary neurons plotted in neuromere-specific colours. **B.** Representative secondary neurons plotted in neuromere-specific colours. **C.** Selected neurons. Top: subcluster 13602. Bottom: subcluster 13377. **D.** Synapses of secondary neurons. Blue: postsynapses; dark orange: presynapses. **E.** Proportions of connections from secondary neurons to upstream or downstream partners, normalised by neuromere and coloured by broad class. Numbers indicate the total number of synapses. **F.** Ratios of connections from secondary neurons originating in each neuromere to upstream or downstream partners, normalised by row. Excepting descending and sensory neurons, only secondary partners are included.

Figure 33 - Supplemental 1. Systematic typing of hemilineage 12A. A. Hierarchical clustering dendrogram of hemilineage groups by laterally and serially aggregated connectivity cosine clustering. **B.** Categorical annotations of each hemilineage group, each column corresponding to the aligned leaf in A. Colours for type, serial set, and group are arbitrary for visualisation. Colours for neuromere, birthtime, neurotransmitter, subclass, and class are as in all other figures. **C.** Similarity distance heatmap for hemilineage. Cosine distance is in the upper triangle, while laterally symmetrised NBLAST distance is in the lower triangle. Systematic type names of some types are labelled. **D.** Morphologically

representative groups from dendrogram subtrees. Each group, indicated by colour and line connecting to its column in B and C, is the most morphologically representative group (medoid of NBLAST distance) from a subtree of A. The subtrees (flat clusters) are equal height cuts of A determined to yield the number of groups per plot and plots in D.

Figure 34. Hemilineage 12B. A. RHS secondary neurons plotted in neuromere-specific colours. **B.** Representative secondary neurons plotted in neuromere-specific colours. **C.** Selected neurons. Top: independent leg serial 10370. Bottom: ascending mVAC serial 10208. **D.** Synapses of secondary neurons. Blue: postsynapses; dark orange: presynapses. **E.** Proportions of connections from secondary neurons to upstream or downstream partners, normalised by neuromere and coloured by broad class. Numbers indicate the total number of synapses. **F.** Ratios of connections from secondary neurons originating in each neuromere to upstream or downstream partners, normalised by row. Excepting descending and sensory neurons, only secondary partners are included.

Figure 34 - Supplemental 1. Systematic typing of hemilineage 12B. A. Hierarchical clustering dendrogram of hemilineage groups by laterally and serially aggregated connectivity cosine clustering. **B.** Categorical annotations of each hemilineage group, each column corresponding to the aligned leaf in A. Colours for type, serial set, and group are arbitrary for visualisation. Colours for neuromere, birthtime, neurotransmitter, subclass, and class are as in all other figures. **C.** Similarity distance heatmap for hemilineage. Cosine distance is in the upper triangle, while laterally symmetrised NBLAST distance is in the lower triangle. Systematic type names of some types are labelled. **D.** Morphologically representative groups from dendrogram subtrees. Each group, indicated by colour and line connecting to its column in B and C, is the most morphologically representative group (medoid of NBLAST distance) from a subtree of A. The subtrees (flat clusters) are equal height cuts of A determined to yield the number of groups per plot and plots in D.

Figure 35. Hemilineage 13A. A. RHS secondary neurons plotted in neuromere-specific colours. **B.** Representative secondary neurons plotted in neuromere-specific colours. **C.** Selected neurons. Top: independent leg serial 11077. Bottom: independent leg serial 10711. **D.** Synapses of secondary neurons. Blue: postsynapses; dark orange: presynapses. **E.** Proportions of connections from secondary neurons to upstream or downstream partners, normalised by neuromere and coloured by broad class. Numbers indicate the total number of synapses. **F.** Ratios of connections from secondary neurons originating in each neuromere to upstream or downstream partners, normalised by row. Excepting descending and sensory neurons, only secondary partners are included.

Figure 35 - Supplemental 1. Systematic typing of hemilineage 13A. A. Hierarchical clustering dendrogram of hemilineage groups by laterally and serially aggregated connectivity cosine clustering. **B.** Categorical annotations of each hemilineage group, each column corresponding to the aligned leaf in A. Colours for type, serial set, and group are arbitrary for visualisation. Colours for neuromere, birthtime, neurotransmitter, subclass, and class are as in all other figures. **C.** Similarity distance heatmap for hemilineage. Cosine distance is in the upper triangle, while laterally symmetrised NBLAST distance is in the lower triangle. Systematic type names of some types are labelled. **D.** Morphologically representative groups from dendrogram subtrees. Each group, indicated by colour and line connecting to its column in B and C, is the most morphologically representative group

(medoid of NBLAST distance) from a subtree of A. The subtrees (flat clusters) are equal height cuts of A determined to yield the number of groups per plot and plots in D.

Figure 36. Hemilineage 13B. A. RHS secondary neurons plotted in neuromere-specific colours. **B.** Representative secondary neurons plotted in neuromere-specific colours. **C.** Selected neurons. Top: independent leg serial 13871. Bottom: independent leg serial 10116. **D.** Synapses of secondary neurons. Blue: postsynapses; dark orange: presynapses. **E.** Proportions of connections from secondary neurons to upstream or downstream partners, normalised by neuromere and coloured by broad class. Numbers indicate the total number of synapses. **F.** Ratios of connections from secondary neurons originating in each neuromere to upstream or downstream partners, normalised by row. Excepting descending and sensory neurons, only secondary partners are included.

Figure 36 - Supplemental 1. Systematic typing of hemilineage 13B. A. Hierarchical clustering dendrogram of hemilineage groups by laterally and serially aggregated connectivity cosine clustering. **B.** Categorical annotations of each hemilineage group, each column corresponding to the aligned leaf in A. Colours for type, serial set, and group are arbitrary for visualisation. Colours for neuromere, birthtime, neurotransmitter, subclass, and class are as in all other figures. **C.** Similarity distance heatmap for hemilineage. Cosine distance is in the upper triangle, while laterally symmetrised NBLAST distance is in the lower triangle. Systematic type names of some types are labelled. **D.** Morphologically representative groups from dendrogram subtrees. Each group, indicated by colour and line connecting to its column in B and C, is the most morphologically representative group (medoid of NBLAST distance) from a subtree of A. The subtrees (flat clusters) are equal height cuts of A determined to yield the number of groups per plot and plots in D.

Figure 37. Hemilineage 14A. A. RHS secondary neurons plotted in neuromere-specific colours. **B.** Representative secondary neurons plotted in neuromere-specific colours. **C.** Selected neurons. Top: independent leg serial 10019. Bottom: independent leg serial 10533. **D.** Synapses of secondary neurons. Blue: postsynapses; dark orange: presynapses. **E.** Proportions of connections from secondary neurons to upstream or downstream partners, normalised by neuromere and coloured by broad class. Numbers indicate the total number of synapses. **F.** Ratios of connections from secondary neurons originating in each neuromere to upstream or downstream partners, normalised by row. Excepting descending and sensory neurons, only secondary partners are included.

Figure 37 - Supplemental 1. Systematic typing of hemilineage 14A. A. Hierarchical clustering dendrogram of hemilineage groups by laterally and serially aggregated connectivity cosine clustering. **B.** Categorical annotations of each hemilineage group, each column corresponding to the aligned leaf in A. Colours for type, serial set, and group are arbitrary for visualisation. Colours for neuromere, birthtime, neurotransmitter, subclass, and class are as in all other figures. **C.** Similarity distance heatmap for hemilineage. Cosine distance is in the upper triangle, while laterally symmetrised NBLAST distance is in the lower triangle. Systematic type names of some types are labelled. **D.** Morphologically representative groups from dendrogram subtrees. Each group, indicated by colour and line connecting to its column in B and C, is the most morphologically representative group (medoid of NBLAST distance) from a subtree of A. The subtrees (flat clusters) are equal height cuts of A determined to yield the number of groups per plot and plots in D.

Figure 38. Hemilineage 15B. A. RHS secondary neurons plotted in neuromere-specific colours. **B.** Representative secondary neurons plotted in neuromere-specific colours. **C.** Selected neurons. Top: ltm1-tibia MN independent leg serial 10811. Bottom: Ti flexor MN independent leg serial 10710. **D.** Synapses of secondary neurons. Blue: postsynapses; dark orange: presynapses. **E.** Proportions of connections from secondary neurons to upstream or downstream partners, normalised by neuromere and coloured by broad class. Numbers indicate the total number of synapses. **F.** Ratios of connections from secondary neurons originating in each neuromere to upstream or downstream partners, normalised by row. Excepting descending and sensory neurons, only secondary partners are included.

Figure 38 - Supplemental 1. Systematic typing of hemilineage 15B. Types for motor neurons were assigned separately as outlined in our accompanying manuscript (Cheong et al., 2023)**. A.** Hierarchical clustering dendrogram of hemilineage groups by laterally and serially aggregated connectivity cosine clustering. **B.** Categorical annotations of each hemilineage group, each column corresponding to the aligned leaf in A. Colours for cluster, serial set, and group are arbitrary for visualisation. Colours for neuromere, birthtime, neurotransmitter, subclass, and class are as in all other figures. **C.** Similarity distance heatmap for hemilineage. Cosine distance is in the upper triangle, while laterally symmetrised NBLAST distance is in the lower triangle. Systematic type names of some types are labelled. **D.** Morphologically representative groups from dendrogram subtrees. Each group, indicated by colour and line connecting to its column in B and C, is the most morphologically representative group (medoid of NBLAST distance) from a subtree of A. The subtrees (flat clusters) are equal height cuts of A determined to yield the number of groups per plot and plots in D.

Figure 39. Hemilineage 16B. A. RHS secondary neurons plotted in neuromere-specific colours. **B.** Representative secondary neurons plotted in neuromere-specific colours. **C.** Selected neurons. Top: motor neuron group 10068 (TTMn). Bottom: independent leg serial 12061. **D.** Synapses of secondary neurons. Blue: postsynapses; dark orange: presynapses. **E.** Proportions of connections from secondary neurons to upstream or downstream partners, normalised by neuromere and coloured by broad class. Numbers indicate the total number of synapses. **F.** Ratios of connections from secondary neurons originating in each neuromere to upstream or downstream partners, normalised by row. Excepting descending and sensory neurons, only secondary partners are included.

Figure 39 - Supplemental 1. Systematic typing of hemilineage 16B. A. Hierarchical clustering dendrogram of hemilineage groups by laterally and serially aggregated connectivity cosine clustering. **B.** Categorical annotations of each hemilineage group, each column corresponding to the aligned leaf in A. Colours for type, serial set, and group are arbitrary for visualisation. Colours for neuromere, birthtime, neurotransmitter, subclass, and class are as in all other figures. **C.** Similarity distance heatmap for hemilineage. Cosine distance is in the upper triangle, while laterally symmetrised NBLAST distance is in the lower triangle. Systematic type names of some types are labelled. **D.** Morphologically representative groups from dendrogram subtrees. Each group, indicated by colour and line connecting to its column in B and C, is the most morphologically representative group (medoid of NBLAST distance) from a subtree of A. The subtrees (flat clusters) are equal height cuts of A determined to yield the number of groups per plot and plots in D.

Figure 40. Hemilineage 16X. A. RHS secondary neurons plotted in neuromere-specific colours. **B.** Representative secondary neurons plotted in neuromere-specific colours. **C.** Selected neurons. Top: diagnostic dorsal subcluster 14132. Bottom: motor neuron serial 10011. **D.** Synapses of secondary neurons. Blue: postsynapses; dark orange: presynapses. **E.** Proportions of connections from secondary neurons to upstream or downstream partners, normalised by neuromere and coloured by broad class. Numbers indicate the total number of synapses. **F.** Ratios of connections from secondary neurons originating in each neuromere to upstream or downstream partners, normalised by row. Excepting descending and sensory neurons, only secondary partners are included.

Figure 40 - Supplemental 1. Systematic typing of hemilineage 16X. Types for motor neurons were assigned separately as outlined in our accompanying manuscript (Cheong et al., 2023)**. A.** Hierarchical clustering dendrogram of hemilineage groups by laterally and serially aggregated connectivity cosine clustering. **B.** Categorical annotations of each hemilineage group, each column corresponding to the aligned leaf in A. Colours for type, serial set, and group are arbitrary for visualisation. Colours for neuromere, birthtime, neurotransmitter, subclass, and class are as in all other figures. **C.** Similarity distance heatmap for hemilineage. Cosine distance is in the upper triangle, while laterally symmetrised NBLAST distance is in the lower triangle. Systematic type names of some types are labelled. **D.** Morphologically representative groups from dendrogram subtrees. Each group, indicated by colour and line connecting to its column in B and C, is the most morphologically representative group (medoid of NBLAST distance) from a subtree of A. The subtrees (flat clusters) are equal height cuts of A determined to yield the number of groups per plot and plots in D.

Figure 41. Hemilineage 17A. A. RHS secondary neurons plotted in neuromere-specific colours. **B.** Representative secondary neurons plotted in neuromere-specific colours. **C.** Selected neurons. Top: ascending serial 10442. Bottom: ascending serial 11222. **D.** Synapses of secondary neurons. Blue: postsynapses; dark orange: presynapses. **E.** Proportions of connections from secondary neurons to upstream or downstream partners, normalised by neuromere and coloured by broad class. Numbers indicate the total number of synapses. **F.** Ratios of connections from secondary neurons originating in each neuromere to upstream or downstream partners, normalised by row. Excepting descending and sensory neurons, only secondary partners are included.

Figure 41 - Supplemental 1. Systematic typing of hemilineage 17A. A. Hierarchical clustering dendrogram of hemilineage groups by laterally and serially aggregated connectivity cosine clustering. **B.** Categorical annotations of each hemilineage group, each column corresponding to the aligned leaf in A. Colours for type, serial set, and group are arbitrary for visualisation. Colours for neuromere, birthtime, neurotransmitter, subclass, and class are as in all other figures. **C.** Similarity distance heatmap for hemilineage. Cosine distance is in the upper triangle, while laterally symmetrised NBLAST distance is in the lower triangle. Systematic type names of some types are labelled. **D.** Morphologically representative groups from dendrogram subtrees. Each group, indicated by colour and line connecting to its column in B and C, is the most morphologically representative group (medoid of NBLAST distance) from a subtree of A. The subtrees (flat clusters) are equal height cuts of A determined to yield the number of groups per plot and plots in D.

Figure 42. Hemilineage 18B. A. RHS secondary neurons plotted in neuromere-specific colours. **B.** Representative secondary neurons plotted in neuromere-specific colours. **C.** Selected neurons. Top: GFC1, electrical group 10228. Bottom: GFC2, electrical subcluster 13645. **D.** Synapses of secondary neurons. Blue: postsynapses; dark orange: presynapses. **E.** Proportions of connections from secondary neurons to upstream or downstream partners, normalised by neuromere and coloured by broad class. Numbers indicate the total number of synapses. **F.** Ratios of connections from secondary neurons originating in each neuromere to upstream or downstream partners, normalised by row. Excepting descending and sensory neurons, only secondary partners are included.

Figure 42 - Supplemental 1. Systematic typing of hemilineage 18B. A. Hierarchical clustering dendrogram of hemilineage groups by laterally and serially aggregated connectivity cosine clustering. **B.** Categorical annotations of each hemilineage group, each column corresponding to the aligned leaf in A. Colours for type, serial set, and group are arbitrary for visualisation. Colours for neuromere, birthtime, neurotransmitter, subclass, and class are as in all other figures. **C.** Similarity distance heatmap for hemilineage. Cosine distance is in the upper triangle, while laterally symmetrised NBLAST distance is in the lower triangle. Systematic type names of some types are labelled. **D.** Morphologically representative groups from dendrogram subtrees. Each group, indicated by colour and line connecting to its column in B and C, is the most morphologically representative group (medoid of NBLAST distance) from a subtree of A. The subtrees (flat clusters) are equal height cuts of A determined to yield the number of groups per plot and plots in D.

Figure 43. Hemilineage 19A. A. RHS secondary neurons plotted in neuromere-specific colours. **B.** Representative secondary neurons plotted in neuromere-specific colours. **C.** Selected neurons. Top: cholinergic sequential serial 10173. Bottom: independent leg serial 14080. **D.** Synapses of secondary neurons. Blue: postsynapses; dark orange: presynapses. **E.** Proportions of connections from secondary neurons to upstream or downstream partners, normalised by neuromere and coloured by broad class. Numbers indicate the total number of synapses. **F.** Ratios of connections from secondary neurons originating in each neuromere to upstream or downstream partners, normalised by row. Excepting descending and sensory neurons, only secondary partners are included.

Figure 43 - Supplemental 1. Systematic typing of hemilineage 19A. Types for motor neurons were assigned separately as outlined in our accompanying manuscript (Cheong et al., 2023)**. A.** Hierarchical clustering dendrogram of hemilineage groups by laterally and serially aggregated connectivity cosine clustering. **B.** Categorical annotations of each hemilineage group, each column corresponding to the aligned leaf in A. Colours for type, serial set, and group are arbitrary for visualisation. Colours for neuromere, birthtime, neurotransmitter, subclass, and class are as in all other figures. **C.** Similarity distance heatmap for hemilineage. Cosine distance is in the upper triangle, while laterally symmetrised NBLAST distance is in the lower triangle. Systematic type names of some types are labelled. **D.** Morphologically representative groups from dendrogram subtrees. Each group, indicated by colour and line connecting to its column in B and C, is the most morphologically representative group (medoid of NBLAST distance) from a subtree of A. The subtrees (flat clusters) are equal height cuts of A determined to yield the number of groups per plot and plots in D.

Figure 44. Hemilineage 19B. A. RHS secondary neurons plotted in neuromere-specific colours. **B.** Representative secondary neurons plotted in neuromere-specific colours. **C.** Selected neurons. Top: dorsal serial 10177. Bottom: independent leg serial 10715. **D.** Synapses of secondary neurons. Blue: postsynapses; dark orange: presynapses. **E.** Proportions of connections from secondary neurons to upstream or downstream partners, normalised by neuromere and coloured by broad class. Numbers indicate the total number of synapses. **F.** Ratios of connections from secondary neurons originating in each neuromere to upstream or downstream partners, normalised by row. Excepting descending and sensory neurons, only secondary partners are included.

Figure 44 - Supplemental 1. Systematic typing of hemilineage 19B. A. Hierarchical clustering dendrogram of hemilineage groups by laterally and serially aggregated connectivity cosine clustering. **B.** Categorical annotations of each hemilineage group, each column corresponding to the aligned leaf in A. Colours for type, serial set, and group are arbitrary for visualisation. Colours for neuromere, birthtime, neurotransmitter, subclass, and class are as in all other figures. **C.** Similarity distance heatmap for hemilineage. Cosine distance is in the upper triangle, while laterally symmetrised NBLAST distance is in the lower triangle. Systematic type names of some types are labelled. **D.** Morphologically representative groups from dendrogram subtrees. Each group, indicated by colour and line connecting to its column in B and C, is the most morphologically representative group (medoid of NBLAST distance) from a subtree of A. The subtrees (flat clusters) are equal height cuts of A determined to yield the number of groups per plot and plots in D.

Figure 45. Hemilineages 20A and 22A. A. RHS secondary neurons plotted in neuromere-specific colours. **B.** Representative secondary neurons plotted in neuromere-specific colours. **C.** Selected neurons. Top: independent leg serial 10894. Bottom: independent leg serial 12511. **D.** Synapses of secondary neurons. Blue: postsynapses; dark orange: presynapses. **E.** Proportions of connections from secondary neurons to upstream or downstream partners, normalised by neuromere and coloured by broad class. Numbers indicate the total number of synapses. **F.** Ratios of connections from secondary neurons originating in each neuromere to upstream or downstream partners, normalised by row. Excepting descending and sensory neurons, only secondary partners are included.

Figure 45 - Supplemental 1. Systematic typing of hemilineage 20A and 22A. A. Hierarchical clustering dendrogram of hemilineage groups by laterally and serially aggregated connectivity cosine clustering. **B.** Categorical annotations of each hemilineage group, each column corresponding to the aligned leaf in A. Colours for type, serial set, and group are arbitrary for visualisation. Colours for neuromere, birthtime, neurotransmitter, subclass, and class are as in all other figures. **C.** Similarity distance heatmap for hemilineage. Cosine distance is in the upper triangle, while laterally symmetrised NBLAST distance is in the lower triangle. Systematic type names of some types are labelled. **D.** Morphologically representative groups from dendrogram subtrees. Each group, indicated by colour and line connecting to its column in B and C, is the most morphologically representative group (medoid of NBLAST distance) from a subtree of A. The subtrees (flat clusters) are equal height cuts of A determined to yield the number of groups per plot and plots in D.

Figure 46. Hemilineage 21A. A. RHS secondary neurons plotted in neuromere-specific colours. **B.** Representative secondary neurons plotted in neuromere-specific colours. **C.** Selected neurons. Top: independent leg subcluster 23565. Bottom: independent leg serial 11348. **D.** Synapses of secondary neurons. Blue: postsynapses; dark orange: presynapses. **E.** Proportions of connections from secondary neurons to upstream or downstream partners, normalised by neuromere and coloured by broad class. Numbers indicate the total number of synapses. **F.** Ratios of connections from secondary neurons originating in each neuromere to upstream or downstream partners, normalised by row. Excepting descending and sensory neurons, only secondary partners are included.

Figure 46 - Supplemental 1. Systematic typing of hemilineage 21A. A. Hierarchical clustering dendrogram of hemilineage groups by laterally and serially aggregated connectivity cosine clustering. **B.** Categorical annotations of each hemilineage group, each column corresponding to the aligned leaf in A. Colours for type, serial set, and group are arbitrary for visualisation. Colours for neuromere, birthtime, neurotransmitter, subclass, and class are as in all other figures. **C.** Similarity distance heatmap for hemilineage. Cosine distance is in the upper triangle, while laterally symmetrised NBLAST distance is in the lower triangle. Systematic type names of some types are labelled. **D.** Morphologically representative groups from dendrogram subtrees. Each group, indicated by colour and line connecting to its column in B and C, is the most morphologically representative group (medoid of NBLAST distance) from a subtree of A. The subtrees (flat clusters) are equal height cuts of A determined to yield the number of groups per plot and plots in D.

Figure 47. Hemilineage 23B. A. RHS secondary neurons plotted in neuromere-specific colours. **B.** Representative secondary neurons plotted in neuromere-specific colours. **C.** Selected neurons. Top: independent leg serial 12339. Bottom: intersegmental complex serial 11371. **D.** Synapses of secondary neurons. Blue: postsynapses; dark orange: presynapses. **E.** Proportions of connections from secondary neurons to upstream or downstream partners, normalised by neuromere and coloured by broad class. Numbers indicate the total number of synapses. **F.** Ratios of connections from secondary neurons originating in each neuromere to upstream or downstream partners, normalised by row. Excepting descending and sensory neurons, only secondary partners are included.

Figure 47 - Supplemental 1. Systematic typing of hemilineage 23B. A. Hierarchical clustering dendrogram of hemilineage groups by laterally and serially aggregated connectivity cosine clustering. **B.** Categorical annotations of each hemilineage group, each column corresponding to the aligned leaf in A. Colours for type, serial set, and group are arbitrary for visualisation. Colours for neuromere, birthtime, neurotransmitter, subclass, and class are as in all other figures. **C.** Similarity distance heatmap for hemilineage. Cosine distance is in the upper triangle, while laterally symmetrised NBLAST distance is in the lower triangle. Systematic type names of some types are labelled. **D.** Morphologically representative groups from dendrogram subtrees. Each group, indicated by colour and line connecting to its column in B and C, is the most morphologically representative group (medoid of NBLAST distance) from a subtree of A. The subtrees (flat clusters) are equal height cuts of A determined to yield the number of groups per plot and plots in D.

Figure 48. Hemilineages 24B and 25B. A. RHS secondary neurons plotted in neuromere-specific colours. **B.** Representative secondary neurons plotted in

neuromere-specific colours. **C.** Selected neurons. Top: Tr flexor MN independent leg serial 21612. Bottom: Tr flexor MN independent leg serial 18440. **D.** Synapses of secondary neurons. Blue: postsynapses; dark orange: presynapses. **E.** Proportions of connections from secondary neurons to upstream or downstream partners, normalised by neuromere and coloured by broad class. Numbers indicate the total number of synapses. **F.** Ratios of connections from secondary neurons originating in each neuromere to upstream or downstream partners, normalised by row. Excepting descending and sensory neurons, only secondary partners are included.

Figure 48 - Supplemental 1. Systematic typing of hemilineage 24B and 25B. Types for motor neurons were assigned separately as outlined in our accompanying manuscript (Cheong et al., 2023)**. A.** Hierarchical clustering dendrogram of hemilineage groups by laterally and serially aggregated connectivity cosine clustering. **B.** Categorical annotations of each hemilineage group, each column corresponding to the aligned leaf in A. Colours for cluster, serial set, and group are arbitrary for visualisation. Colours for neuromere, birthtime, neurotransmitter, subclass, and class are as in all other figures. **C.** Similarity distance heatmap for hemilineage. Cosine distance is in the upper triangle, while laterally symmetrised NBLAST distance is in the lower triangle. Systematic type names of some types are labelled. **D.** Morphologically representative groups from dendrogram subtrees. Each group, indicated by colour and line connecting to its column in B and C, is the most morphologically representative group (medoid of NBLAST distance) from a subtree of A. The subtrees (flat clusters) are equal height cuts of A determined to yield the number of groups per plot and plots in D.

Figure 49. Hemilineages with few or no associated secondary neurons. Neuron meshes are coloured by soma neuromere and side (green: T1 RHS, cyan: T2 RHS, pink: T3 RHS, purple: A1 RHS). **A.** Octopaminergic hemilineage 00B. **B.** Cholinergic hemilineage 04A. **C.** Cholinergic hemilineage “05A”. **D.** Gabaergic/glutamatergic hemilineage 14B. **E.** Cholinergic hemilineage “15A”. **F.** Gabaergic hemilineage “17B”. **G.** Motor neurons from “17X” or “18X”. **H.** Hemilineage “21X”. **I.** Motor neurons from hemilineages 20B, 21B, or 22B. **J.** Gabergic hemilineage “26X”. **K.** Putative neurosecretory hemilineage “27X”. **L.** Estimated birthtime by hemilineage and soma neuromere (neurons of unknown hemilineage have been omitted and all abdominal neuromeres have been combined).

Figure 49 - Supplemental 1. Summary of the anatomical organisation of synapses for primary neurons in each hemilineage originating in T2 RHS. A. Side and ventral views illustrating the neuropils surveyed: T2 Leg Neuropil (LNP), medial ventral association center (mVAC), ovoid (Ov), wing tectulum (WTct), lower tectulum (LTct), and Intermediate tectulum (IntTct). The orange dashed line shows the approximate location of the transverse section onto which their synapses have been projected. **B.** Template transverse section with major neuropils labelled and axes for orientation. **C.** Projected synapses for T2 RHS neurons of each hemilineage. Top (blue): postsynapses, connections to upstream neurons. Bottom (orange): presynapses, connections to downstream neurons. 21X is only observed in T1.

Figure 49 - Supplemental 2. Systematic typing of hemilineage 00B. A. Hierarchical clustering dendrogram of hemilineage groups by laterally and serially aggregated connectivity cosine clustering. **B.** Categorical annotations of each hemilineage group, each column corresponding to the aligned leaf in A. Colours for type, serial set, and group are

arbitrary for visualisation. Colours for neuromere, birthtime, neurotransmitter, subclass, and class are as in all other figures. **C.** Similarity distance heatmap for hemilineage. Cosine distance is in the upper triangle, while laterally symmetrised NBLAST distance is in the lower triangle. Systematic type names of some types are labelled. **D.** Morphologically representative groups from dendrogram subtrees. Each group, indicated by colour and line connecting to its column in B and C, is the most morphologically representative group (medoid of NBLAST distance) from a subtree of A. The subtrees (flat clusters) are equal height cuts of A determined to yield the number of groups per plot and plots in D.

Figure 49 - Supplemental 3. Systematic typing of hemilineage 04A. A. Hierarchical clustering dendrogram of hemilineage groups by laterally and serially aggregated connectivity cosine clustering. **B.** Categorical annotations of each hemilineage group, each column corresponding to the aligned leaf in A. Colours for type, serial set, and group are arbitrary for visualisation. Colours for neuromere, birthtime, neurotransmitter, subclass, and class are as in all other figures. **C.** Similarity distance heatmap for hemilineage. Cosine distance is in the upper triangle, while laterally symmetrised NBLAST distance is in the lower triangle. Systematic type names of some types are labelled. **D.** Morphologically representative groups from dendrogram subtrees. Each group, indicated by colour and line connecting to its column in B and C, is the most morphologically representative group (medoid of NBLAST distance) from a subtree of A. The subtrees (flat clusters) are equal height cuts of A determined to yield the number of groups per plot and plots in D.

Figure 49 - Supplemental 4. Systematic typing of hemilineage 05A. A. Hierarchical clustering dendrogram of hemilineage groups by laterally and serially aggregated connectivity cosine clustering. **B.** Categorical annotations of each hemilineage group, each column corresponding to the aligned leaf in A. Colours for type, serial set, and group are arbitrary for visualisation. Colours for neuromere, birthtime, neurotransmitter, subclass, and class are as in all other figures. **C.** Similarity distance heatmap for hemilineage. Cosine distance is in the upper triangle, while laterally symmetrised NBLAST distance is in the lower triangle. Systematic type names of some types are labelled. **D.** Morphologically representative groups from dendrogram subtrees. Each group, indicated by colour and line connecting to its column in B and C, is the most morphologically representative group (medoid of NBLAST distance) from a subtree of A. The subtrees (flat clusters) are equal height cuts of A determined to yield the number of groups per plot and plots in D.

Figure 49 - Supplemental 5. Systematic typing of hemilineage 14B. A. Hierarchical clustering dendrogram of hemilineage groups by laterally and serially aggregated connectivity cosine clustering. **B.** Categorical annotations of each hemilineage group, each column corresponding to the aligned leaf in A. Colours for type, serial set, and group are arbitrary for visualisation. Colours for neuromere, birthtime, neurotransmitter, subclass, and class are as in all other figures. **C.** Similarity distance heatmap for hemilineage. Cosine distance is in the upper triangle, while laterally symmetrised NBLAST distance is in the lower triangle. Systematic type names of some types are labelled. **D.** Morphologically representative groups from dendrogram subtrees. Each group, indicated by colour and line connecting to its column in B and C, is the most morphologically representative group (medoid of NBLAST distance) from a subtree of A. The subtrees (flat clusters) are equal height cuts of A determined to yield the number of groups per plot and plots in D.

Figure 49 - Supplemental 6. Systematic typing of hemilineage 15A. A. Hierarchical clustering dendrogram of hemilineage groups by laterally and serially aggregated connectivity cosine clustering. **B.** Categorical annotations of each hemilineage group, each column corresponding to the aligned leaf in A. Colours for type, serial set, and group are arbitrary for visualisation. Colours for neuromere, birthtime, neurotransmitter, subclass, and class are as in all other figures. **C.** Similarity distance heatmap for hemilineage. Cosine distance is in the upper triangle, while laterally symmetrised NBLAST distance is in the lower triangle. Systematic type names of some types are labelled. **D.** Morphologically representative groups from dendrogram subtrees. Each group, indicated by colour and line connecting to its column in B and C, is the most morphologically representative group (medoid of NBLAST distance) from a subtree of A. The subtrees (flat clusters) are equal height cuts of A determined to yield the number of groups per plot and plots in D.

Figure 49 - Supplemental 7. Systematic typing of hemilineage 17B. A. Hierarchical clustering dendrogram of hemilineage groups by laterally and serially aggregated connectivity cosine clustering. **B.** Categorical annotations of each hemilineage group, each column corresponding to the aligned leaf in A. Colours for type, serial set, and group are arbitrary for visualisation. Colours for neuromere, birthtime, neurotransmitter, subclass, and class are as in all other figures. **C.** Similarity distance heatmap for hemilineage. Cosine distance is in the upper triangle, while laterally symmetrised NBLAST distance is in the lower triangle. Systematic type names of some types are labelled. **D.** Morphologically representative groups from dendrogram subtrees. Each group, indicated by colour and line connecting to its column in B and C, is the most morphologically representative group (medoid of NBLAST distance) from a subtree of A. The subtrees (flat clusters) are equal height cuts of A determined to yield the number of groups per plot and plots in D.

Figure 49 - Supplemental 8. Systematic typing of hemilineage 17X and 18X. Types for motor neurons were assigned separately as outlined in our accompanying manuscript (Cheong et al., 2023)**. A.** Hierarchical clustering dendrogram of hemilineage groups by laterally and serially aggregated connectivity cosine clustering. **B.** Categorical annotations of each hemilineage group, each column corresponding to the aligned leaf in A. Colours for cluster, serial set, and group are arbitrary for visualisation. Colours for neuromere, birthtime, neurotransmitter, subclass, and class are as in all other figures. **C.** Similarity distance heatmap for hemilineage. Cosine distance is in the upper triangle, while laterally symmetrised NBLAST distance is in the lower triangle. Systematic type names of some types are labelled. **D.** Morphologically representative groups from dendrogram subtrees. Each group, indicated by colour and line connecting to its column in B and C, is the most morphologically representative group (medoid of NBLAST distance) from a subtree of A. The subtrees (flat clusters) are equal height cuts of A determined to yield the number of groups per plot and plots in D.

Figure 49 - Supplemental 9. Systematic typing of hemilineage 20B, 21B and 22B. Types for motor neurons were assigned separately as outlined in our accompanying manuscript (Cheong et al., 2023)**. A.** Hierarchical clustering dendrogram of hemilineage groups by laterally and serially aggregated connectivity cosine clustering. **B.** Categorical annotations of each hemilineage group, each column corresponding to the aligned leaf in A. Colours for cluster, serial set, and group are arbitrary for visualisation. Colours for neuromere, birthtime, neurotransmitter, subclass, and class are as in all other figures. **C.** Similarity distance

heatmap for hemilineage. Cosine distance is in the upper triangle, while laterally symmetrised NBLAST distance is in the lower triangle. Systematic type names of some types are labelled. **D.** Morphologically representative groups from dendrogram subtrees. Each group, indicated by colour and line connecting to its column in B and C, is the most morphologically representative group (medoid of NBLAST distance) from a subtree of A. The subtrees (flat clusters) are equal height cuts of A determined to yield the number of groups per plot and plots in D.

Figure 49 - Supplemental 10. Systematic typing of hemilineage 21X. A. Hierarchical clustering dendrogram of hemilineage groups by laterally and serially aggregated connectivity cosine clustering. **B.** Categorical annotations of each hemilineage group, each column corresponding to the aligned leaf in A. Colours for cluster, serial set, and group are arbitrary for visualisation. Colours for neuromere, birthtime, neurotransmitter, subclass, and class are as in all other figures. **C.** Similarity distance heatmap for hemilineage. Cosine distance is in the upper triangle, while laterally symmetrised NBLAST distance is in the lower triangle. Systematic type names of some types are labelled. **D.** Morphologically representative groups from dendrogram subtrees. Each group, indicated by colour and line connecting to its column in B and C, is the most morphologically representative group (medoid of NBLAST distance) from a subtree of A. The subtrees (flat clusters) are equal height cuts of A determined to yield the number of groups per plot and plots in D.

Figure 49 - Supplemental 11. Systematic typing of hemilineage 26X. A. Hierarchical clustering dendrogram of hemilineage groups by laterally and serially aggregated connectivity cosine clustering. **B.** Categorical annotations of each hemilineage group, each column corresponding to the aligned leaf in A. Colours for cluster, serial set, and group are arbitrary for visualisation. Colours for neuromere, birthtime, neurotransmitter, subclass, and class are as in all other figures. **C.** Similarity distance heatmap for hemilineage. Cosine distance is in the upper triangle, while laterally symmetrised NBLAST distance is in the lower triangle. Systematic type names of some types are labelled. **D.** Morphologically representative groups from dendrogram subtrees. Each group, indicated by colour and line connecting to its column in B and C, is the most morphologically representative group (medoid of NBLAST distance) from a subtree of A. The subtrees (flat clusters) are equal height cuts of A determined to yield the number of groups per plot and plots in D.

Figure 49 - Supplemental 12. Systematic typing of hemilineage 27X. A. Hierarchical clustering dendrogram of hemilineage groups by laterally and serially aggregated connectivity cosine clustering. **B.** Categorical annotations of each hemilineage group, each column corresponding to the aligned leaf in A. Colours for cluster, serial set, and group are arbitrary for visualisation. Colours for neuromere, birthtime, neurotransmitter, subclass, and class are as in all other figures. **C.** Similarity distance heatmap for hemilineage. Cosine distance is in the upper triangle, while laterally symmetrised NBLAST distance is in the lower triangle. Systematic type names of some types are labelled. **D.** Morphologically representative groups from dendrogram subtrees. Each group, indicated by colour and line connecting to its column in B and C, is the most morphologically representative group (medoid of NBLAST distance) from a subtree of A. The subtrees (flat clusters) are equal height cuts of A determined to yield the number of groups per plot and plots in D.

Figure 50. Organisation of abdominal ganglia. A. Cartoon schematic depicting VNC innervation by neurons originating in abdominal neuromeres. Abdominal neurons have no more than 5 synapses outside of the ANm, abdominal & thoracic neurons have at least 5% of synapses in the ANm and more than 5 synapses outside of the ANm, and thoracic neurons have less than 5% of synapses in the ANm. **B.** Quantification of abdominal neuron VNC innervation categories by soma neuromere. **C.** RHS examples of hemilineages without secondary neuron populations in A1. **D.** RHS examples of hemilineages with secondary neuron populations in A1. Neuron meshes are coloured by soma neuromere: purple = A1, red = A2, dark orange = A3, dark yellow = A4, green = A5, cyan = A6, blue = A7, navy = A8, dark purple = A9, magenta = A10.

Figure 51. Sensory neuron modality. A. Neuron meshes of chemosensory neurons, downstream partners, and neurons that receive information from these neurons in the third layer, i-iii respectively. **B.** Neuron meshes of proprioceptive neurons, downstream partners, and neurons that receive information from these neurons in the third layer, i-iii respectively. **C.** Neuron meshes of tactile neurons, downstream partners, and neurons that receive information from these neurons in the third layer, i-iii respectively. **D.** Heatmap showing normalised sensory neuron modality connectivity to hemilineages in the VNC. **E.** Heatmap showing the number of neurons that receive input from sensory modality, normalised by the total number of neurons activated. The number of neurons activated in each hemilineage is labelled on the heatmap. **E.** Heatmap showing the number of second order partner neurons that receive input from sensory modality, normalised by the total number of neurons activated. The number of neurons activated in each hemilineage is labelled on the heatmap.

Figure 52. Leg sensory neuron clustering. A. Schematic displaying anatomical region of sensory origin. **B.** Neurons that compose each identified sensory cluster. **C.** Heatmap showing normalised sensory neuron cluster connectivity to hemilineages in the VNC. Annotation bar displays annotated modality of component sensory neurons within the sensory neuron cluster. **D.** Dice coefficient between sensory cluster signal propagation within the VNC at layers 2-5, i-v respectively.

Figure 53. Dorsal sensory neuron clustering. A. Schematic displaying principal anatomical regions of sensory origin for Dorsal Sensory neurons. **B.** Neurons that compose each identified sensory cluster. **C.** Heatmap showing normalised sensory neuron cluster connectivity to hemilineages in the VNC. Annotation bar displays annotated modality of component sensory neurons within the sensory neuron cluster.

Figure 54. Abdominal sensory neuron clustering. A. Neurons that compose each identified sensory cluster. **B.** Heatmap showing normalised sensory neuron cluster connectivity to hemilineages in the VNC.

Figure 55: Ascending Sensory Information. **A.** UMAP representation of Ascending Neurons input from VNC classes, normalised.. Region of High sensory input indicated by dotted box. **B.** UMAP of modality inputs to high sensory input ascending neurons, coloured by primary modality, taken as any modality that contributes >50% of inputs. **C.** Pie chart showing the relative proportions of birthtime assigned to ascending neurons with high sensory input. **D.** Pie chart showing the relative proportions of primary sensory modality

received by Ascending Neurons with high sensory input. **E.** Pie chart showing the relative proportions of sensory neuron modality within the VNC.

Figure 56. Secondary hemilineage network. A. Bubble plot showing secondary hemilineage to hemilineage connectivity restricted to T2. Colour of bubble is based on the consensus neurotransmitter prediction for the given upstream hemilineage. **B.** Schematic summary of A showing the top upstream partners and hemilineage neurotransmitter prediction in the adult male (Centre, Right) compared against previously reported data from late larva (Left). Within hemilineage connections are excluded from the schematic. **Left:** initial contacts of neurite bundles made in late larva as reported by Truman et. al., 2004. Bundles within the grey circle were hypothesised to terminate in the ventrolateral neuropil while those in blue stripe hypothesised to project in dorsal tracts. **Centre:** modification of Left based on data in A showing only top upstream partners for each hemilineage. Confirmed strong edge: previously reported edges that are in the top 2 upstream partners per hemilineage. Confirmed edge: previously reported edges that are in the 3rd through 6th (inclusive) top upstream partners per hemilineage. Missing/weak edge: previously reported edges that are not in the top 6 upstream partners per hemilineage. New strong edge: previously unidentified edges that contribute over 15% of all synapses to a hemilineage or are that hemilineages top upstream partner. **Right:** Confirmed and new edges shown in Centre, coloured by the upstream hemilinage's consensus predicted neurotransmitter.

Figure 57: Leg circuit schematic. 6960 IN (>50% of all INs) have origin and target specifically in the leg neuropil. Shown are the numbers of connections of these neurons, in the form of an arrow. Arrow is only shown if >10 neurons have the same origin and target. The great majority of intrinsic neurons of the leg have their origin and target within a single leg neuropil, over 950 neurons per leg neuropil. The number of neurons with the same leg connectivity pattern between legs ipsilaterally are all below 50. The most numerous bilateral connections between legs are in the T3 leg neuropils (>100).

Table 1. Glossary of terms.

REFERENCES

Allen AM, Neville MC, Birtles S, Croset V, Treiber CD, Waddell S, Goodwin SF. 2020. A single-cell transcriptomic atlas of the adult ventral nerve cord. *Elife* **9**. doi:10.7554/eLife.54074

Alstott J, Panzarasa P, Rubinov M, Bullmore ET, Vértes PE. 2014. A unifying framework for measuring weighted rich clubs. *Sci Rep* **4**:7258.

Ammer G, Vieira RM, Fendl S, Borst A. 2022. Anatomical distribution and functional roles of electrical synapses in Drosophila. *Curr Biol* **32**:2022–2036.e4.

Azevedo AW, Dickinson ES, Gurung P, Venkatasubramanian L, Mann RS, Tuthill JC. 2020. A size principle for recruitment of leg motor neurons. *Elife* **9**. doi:10.7554/eLife.56754

Baek M, Mann RS. 2009. Lineage and birth date specify motor neuron targeting and dendritic architecture in adult Drosophila. *J Neurosci* **29**:6904–6916.

Bate CM. 1976. Embryogenesis of an insect nervous system I. A map of the thoracic and abdominal neuroblasts in *Locusta migratoria*. *Development*. doi:10.1242/dev.35.1.107

Bate M, Arias AM. 1991. The embryonic origin of imaginal discs in Drosophila. *Development* **112**:755–761.

Bates AS, Manton JD, Jagannathan SR, Costa M, Schlegel P, Rohlfing T, Jefferis GS. 2020.

The natverse, a versatile toolbox for combining and analysing neuroanatomical data. doi:10.7554/eLife.53350
Biecek P. 2018. DALEX: explainers for complex predictive models in R. *J Mach Learn Res* **19**:3245–3249.
Birkholz O, Rickert C, Berger C, Urbach R, Technau GM. 2013. Neuroblast pattern and identity in the Drosophila tail region and role of doublesex in the survival of sex-specific precursors. *Development* **140**:1830–1842.
Birkholz O, Rickert C, Nowak J, Coban IC, Technau GM. 2015. Bridging the gap between postembryonic cell lineages and identified embryonic neuroblasts in the ventral nerve cord of Drosophila melanogaster. *Biol Open* **4**:420–434.
Booker R, Truman JW. 1987. Postembryonic neurogenesis in the CNS of the tobacco hornworm, Manduca sexta. I. Neuroblast arrays and the fate of their progeny during metamorphosis. *J Comp Neurol* **255**:548–559.
Brierley DJ, Rathore K, VijayRaghavan K, Williams DW. 2012. Developmental origins and architecture of Drosophila leg motoneurons. *J Comp Neurol* **520**:1629–1649.
Brown HLD, Truman JW. 2009. Fine-tuning of secondary arbor development: the effects of the ecdysone receptor on the adult neuronal lineages of the Drosophila thoracic CNS. *Development* **136**:3247–3256.
Cachero S, Ostrovsky AD, Yu JY, Dickson BJ, Jefferis GSXE. 2010. Sexual dimorphism in the fly brain. *Curr Biol* **20**:1589–1601.
Campello RJGB, Moulavi D, Sander J. 2013. Density-Based Clustering Based on Hierarchical Density EstimatesAdvances in Knowledge Discovery and Data Mining. Springer Berlin Heidelberg. pp. 160–172.
Chan WP, Dickinson MH. 1996. Position-specific central projections of mechanosensory neurons on the haltere of the blow fly, Calliphora vicina. *J Comp Neurol* **369**:405–418.
Chen C, Agrawal S, Mark B, Mamiya A, Sustar A, Phelps JS, Lee W-CA, Dickson BJ, Card GM, Tuthill JC. 2021. Functional architecture of neural circuits for leg proprioception in Drosophila. *Curr Biol* **31**:5163–5175.e7.
Cheong HSJ*., Eichler K*., Stuerner T*., Asinof S, Champion AS, Marin EC, Oram TB, Namiki S, Siwanowicz I, Costa M, Berg S, Janelia FlyEM Project Team, Jefferis GSXE, Card GM. 2023. Transforming descending input into behavior: The organization of premotor circuits in the Drosophila Male Adult Nerve Cord connectome. *bioRxiv*.
Consoulas C, Restifo LL, Levine RB. 2002. Dendritic remodeling and growth of motoneurons during metamorphosis of Drosophila melanogaster. *J Neurosci* **22**:4906–4917.
Costa M, Manton JD, Ostrovsky AD, Prohaska S, Jefferis GSXE. 2016. NBLAST: Rapid, Sensitive Comparison of Neuronal Structure and Construction of Neuron Family Databases. *Neuron* **91**:293–311.
Court R, Namiki S, Armstrong JD, Börner J, Card G, Costa M, Dickinson M, Duch C, Korff W, Mann R, Merritt D, Murphey RK, Seeds AM, Shirangi T, Simpson JH, Truman JW, Tuthill JC, Williams DW, Shepherd D. 2020. A Systematic Nomenclature for the Drosophila Ventral Nerve Cord. *Neuron* **107**:1071–1079.e2.
Csardi G, Nepusz T, Others. 2006. The igraph software package for complex network research. *InterJournal, complex systems* **1695**:1–9.
Deora T, Singh AK, Sane SP. 2015. Biomechanical basis of wing and haltere coordination in flies. *Proc Natl Acad Sci U S A* **112**:1481–1486.
Dickinson MH, Palka J. 1987. Physiological properties, time of development, and central projection are correlated in the wing mechanoreceptors of Drosophila. *J Neurosci* **7**:4201–4208.
Dinges GF, Chockley AS, Bockemühl T, Ito K, Blanke A, Büschges A. 2021. Location and arrangement of campaniform sensilla in Drosophila melanogaster. *J Comp Neurol* **529**:905–925.
Doe CQ. 2017. Temporal Patterning in the Drosophila CNS. *Annu Rev Cell Dev Biol* **33**:219–240.
Doe CQ, Goodman CS. 1985. Early events in insect neurogenesis. I. Development and segmental differences in the pattern of neuronal precursor cells. *Dev Biol* **111**:193–205.

Eagle N, Macy M, Claxton R. 2010. Network diversity and economic development. *Science* **328**:1029–1031.
Fishkind DE, Adali S, Patsolic HG, Meng L, Singh D, Lyzinski V, Priebe CE. 2019. Seeded graph matching. *Pattern Recognition*. doi:10.1016/j.patcog.2018.09.014
Ghysen A. 1980. The projection of sensory neurons in the central nervous system of Drosophila: choice of the appropriate pathway. *Dev Biol* **78**:521–541.
Guimerà R, Nunes Amaral LA. 2005. Functional cartography of complex metabolic networks. *Nature* **433**:895–900.
Hagberg A, Swart P, S Chult D. 2008. Exploring network structure, dynamics, and function using networkx (No. LA-UR-08-05495; LA-UR-08-5495). Los Alamos National Lab. (LANL), Los Alamos, NM (United States).
Hao Y, Hao S, Andersen-Nissen E, Mauck WM 3rd, Zheng S, Butler A, Lee MJ, Wilk AJ, Darby C, Zager M, Hoffman P, Stoeckius M, Papalexi E, Mimitou EP, Jain J, Srivastava A, Stuart T, Fleming LM, Yeung B, Rogers AJ, McElrath JM, Blish CA, Gottardo R, Smibert P, Satija R. 2021. Integrated analysis of multimodal single-cell data. *Cell* **184**:3573–3587.e29.
Harris RM, Pfeiffer BD, Rubin GM, Truman JW. 2015. Neuron hemilineages provide the functional ground plan for the Drosophila ventral nervous system. *Elife* **4**. doi:10.7554/eLife.04493
He Z, Luo Y, Shang X, Sun JS, Carlson JR. 2019. Chemosensory sensilla of the Drosophila wing express a candidate ionotropic pheromone receptor. *PLoS Biol* **17**:e2006619.
Isshiki T, Pearson B, Holbrook S, Doe CQ. 2001. Drosophila neuroblasts sequentially express transcription factors which specify the temporal identity of their neuronal progeny. *Cell* **106**:511–521.
Jan YN, Ghysen A, Christoph I, Barbel S, Jan LY. 1985. Formation of neuronal pathways in the imaginal discs of Drosophila melanogaster. *J Neurosci* **5**:2453–2464.
Kallman BR, Kim H, Scott K. 2015. Excitation and inhibition onto central courtship neurons biases Drosophila mate choice. *Elife* **4**:e11188.
Kambadur R, Koizumi K, Stivers C, Nagle J, Poole SJ, Odenwald WF. 1998. Regulation of POU genes by castor and hunchback establishes layered compartments in the Drosophila CNS. *Genes Dev* **12**:246–260.
Kennedy T, Broadie K. 2018. Newly Identified Electrically Coupled Neurons Support Development of the Giant Fiber Model Circuit. *eNeuro* **5**. doi:10.1523/ENEURO.0346-18.2018
Kuan AT, Phelps JS, Thomas LA, Nguyen TM, Han J, Chen C-L, Azevedo AW, Tuthill JC, Funke J, Cloetens P, Pacureanu A, Lee W-CA. 2020. Dense neuronal reconstruction through X-ray holographic nano-tomography. *Nat Neurosci* **23**:1637–1643.
Kwon JY, Dahanukar A, Weiss LA, Carlson JR. 2014. A map of taste neuron projections in the Drosophila CNS. *J Biosci* **39**:565–574.
Lacin H, Chen H-M, Long X, Singer RH, Lee T, Truman JW. 2019. Neurotransmitter identity is acquired in a lineage-restricted manner in the CNS. *Elife* **8**. doi:10.7554/eLife.43701
Lacin H, Truman JW. 2016. Lineage mapping identifies molecular and architectural similarities between the larval and adult Drosophila central nervous system. *Elife* **5**:e13399.
Lee Y-J, Yang C-P, Miyares RL, Huang Y-F, He Y, Ren Q, Chen H-M, Kawase T, Ito M, Otsuna H, Sugino K, Aso Y, Ito K, Lee T. 2020. Conservation and divergence of related neuronal lineages in the Drosophila central brain. *eLife*. doi:10.7554/elife.53518
Lesser E, Azevedo AW, Phelps JS, Elabbady L, Cook AP, Mark B, Kuroda S, Sustar A, Moussa AJ, Dallmann CJ, Agrawal S, Lee S-YJ, Pratt BG, Skutt-Kakari K, Gerhard S, Lu R, Kemnitz N, Lee K, Halageri A, Castro M, Ih D, Gager J, Tammam M, Dorkenwald S, Collman FC, Schneider-Mizell CM, Brittain D, Jordan CS, Sebastian Seung H, Macrina T, Dickinson MH, Lee W-CA, Tuthill JC. 2023. Synaptic architecture of leg and wing motor control networks in Drosophila. *bioRxiv*. doi:10.1101/2023.05.30.542725
Ling F, Dahanukar A, Weiss LA, Kwon JY, Carlson JR. 2014. The molecular and cellular basis of taste coding in the legs of Drosophila. *J Neurosci* **34**:7148–7164.

Mamiya A, Gurung P, Tuthill JC. 2018. Neural Coding of Leg Proprioception in Drosophila. *Neuron* **100**:636–650.e6.
Marin EC, Dry KE, Alaimo DR, Rudd KT, Cillo AR, Clenshaw ME, Negre N, White KP, Truman JW. 2012. Ultrabithorax confers spatial identity in a context-specific manner in the Drosophila postembryonic ventral nervous system. *Neural Dev* **7**:31.
Merritt DJ, Murphey RK. 1992. Projections of leg proprioceptors within the CNS of the fly Phormia in relation to the generalized insect ganglion. *J Comp Neurol* **322**:16–34.
Monastirioti M, Gorczyca M, Rapus J, Eckert M, White K, Budnik V. 1995. Octopamine immunoreactivity in the fruit fly Drosophila melanogaster. *J Comp Neurol* **356**:275–287.
Murphey RK, Possidente D, Pollack G, Merritt DJ. 1989a. Modality-specific axonal projections in the CNS of the flies Phormia and Drosophila. *J Comp Neurol* **290**:185–200.
Murphey RK, Possidente DR, Vandervorst P, Ghysen A. 1989b. Compartments and the topography of leg afferent projections in Drosophila. *J Neurosci* **9**:3209–3217.
Mu S, Yu S-C, Turner NL, McKellar CE, Dorkenwald S, Collman F, Koolman S, Moore M, Morejohn S, Silverman B, Willie K, Willie R, Bland D, Burke A, Ashwood Z, Luther K, Castro M, Ogedengbe O, Silversmith W, Wu J, Halageri A, Macrina T, Kemnitz N, Murthy M, Sebastian Seung H. 2021. 3D reconstruction of cell nuclei in a full Drosophila brain. *bioRxiv*. doi:10.1101/2021.11.04.467197
Newman ME. 2001. Scientific collaboration networks. II. Shortest paths, weighted networks, and centrality. *Phys Rev E Stat Nonlin Soft Matter Phys* **64**:016132.
Nottebohm E, Ramaekers A, Dambly-Chaudière C, Ghysen A. 1994. The leg of Drosophila as a model system for the analysis of neuronal diversity. *J Physiol Paris* **88**:141–151.
O'Sullivan A, Lindsay T, Prudnikova A, Erdi B, Dickinson M, von Philipsborn AC. 2018. Multifunctional Wing Motor Control of Song and Flight. *Current Biology*. doi:10.1016/j.cub.2018.06.038
Palka J, Schubiger M, Murray MA. 1984. Peripheral Neurogenesis in "Drosophila." *Bioscience* **34**:318–321.
Plaza SM, Clements J, Dolafi T, Umayam L, Neubarth NN, Scheffer LK, Berg S. 2022. neuPrint: An open access tool for EM connectomics. *Front Neuroinform* **16**. doi:10.3389/fninf.2022.896292
Pop S, Chen C-L, Sproston CJ, Kondo S, Ramdya P, Williams DW. 2020. Extensive and diverse patterns of cell death sculpt neural networks in insects. *Elife* **9**. doi:10.7554/eLife.59566
Power ME. 1948. The thoracico-abdominal nervous system of an adult insect, Drosophila melanogaster. *J Comp Neurol* **88**:347–409.
Prokop A, Technau GM. 1991. The origin of postembryonic neuroblasts in the ventral nerve cord of Drosophila melanogaster. *Development* **111**:79–88.
Schlegel P, Bates AS, Stürner T, Jagannathan SR, Drummond N, Hsu J, Serratosa Capdevila L, Javier A, Marin EC, Barth-Maron A, Tamimi IF, Li F, Rubin GM, Plaza SM, Costa M, Jefferis GSXE. 2021. Information flow, cell types and stereotypy in a full olfactory connectome. *Elife* **10**. doi:10.7554/eLife.66018
Schmid A, Chiba A, Doe CQ. 1999. Clonal analysis of Drosophila embryonic neuroblasts: neural cell types, axon projections and muscle targets. *Development* **126**:4653–4689.
Schneider-Mizell CM, Gerhard S, Longair M, Kazimiers T, Li F, Zwart MF, Champion A, Midgley FM, Fetter RD, Saalfeld S, Cardona A. 2016. Quantitative neuroanatomy for connectomics in Drosophila. *Elife* **5**. doi:10.7554/eLife.12059
Shepherd D, Harris R, Williams DW, Truman JW. 2016. Postembryonic lineages of the Drosophila ventral nervous system: Neuroglian expression reveals the adult hemilineage associated fiber tracts in the adult thoracic neuromeres. *J Comp Neurol* **524**:2677–2695.
Shepherd D, Sahota V, Court R, Williams DW, Truman JW. 2019. Developmental organization of central neurons in the adult Drosophila ventral nervous system. *J Comp Neurol* **527**:2573–2598.
Smith SA, Shepherd D. 1996. Central afferent projections of proprioceptive sensory neurons

in Drosophila revealed with the enhancer-trap technique. *J Comp Neurol* **364**:311–323.
Stölting H, Stumpner A, Lakes-Harlan R. 2007. Morphology and physiology of the prosternal chordotonal organ of the sarcophagid fly Sarcophaga bullata (Parker). *J Insect Physiol* **53**:444–454.
Takemura S-Y, Huang GB, Januszewski M, Lu Z, Marin EC, Preibisch S, Xu CS, Champion A, Cheong HSJ, Costa M, Eichler K, Knecht CJ, Li F, Morris BJ, Schlegel P, Stuerner T, Badalamente G, Bogovic J, Brooks P, Canino BS, Clements J, Cook M, Dunne CR, Fang S, Finley-May S, Funke J, George R, Gkantia M, Harrington K, Hayworth KJ, Hazlett A, Hopkins GP, Hsu J, Hubbard PM, Javier A, Kainmueller D, Katz WT, Korff W, Kovalyak J, Krzeminski D, Lauchie SA, Manley EA, Mooney C, Neace E, Nichols M, Okeoma N, Ordish C, Parekh R, Paterson T, Phillips EM, Plaza SM, Rivlin PK, Saalfeld S, Shepherd D, Smith C, Takemura S, Talebi I, Tamimi I, Tiscareno C, Trautman ET, Umayam L, Walsh JJ, Yang T, Zhao T, Hess HF, Rubin GM, Scheffer LK, Card G, Jefferis GSXE, Berg S. 2023. A Connectome of the Male Drosophila Ventral Nerve Cord. *bioRxiv*.
Tissot M, Stocker RF. 2000. Metamorphosis in drosophila and other insects: the fate of neurons throughout the stages. *Prog Neurobiol* **62**:89–111.
Tix S, Bate M, Technau GM. 1989. Pre-existing neuronal pathways in the leg imaginal discs of Drosophila. *Development* **107**:855–862.
Truman JW, Bate M. 1988. Spatial and temporal patterns of neurogenesis in the central nervous system of Drosophila melanogaster. *Dev Biol* **125**:145–157.
Truman JW, Moats W, Altman J, Marin EC, Williams DW. 2010. Role of Notch signaling in establishing the hemilineages of secondary neurons in Drosophila melanogaster. *Development* **137**:53–61.
Truman JW, Schuppe H, Shepherd D, Williams DW. 2004. Developmental architecture of adult-specific lineages in the ventral CNS of *Drosophila*. *Development*. doi:10.1242/dev.01371
Tsubouchi A, Yano T, Yokoyama TK, Murtin C, Otsuna H, Ito K. 2017. Topological and modality-specific representation of somatosensory information in the fly brain. *Science* **358**:615–623.
Tuthill JC, Wilson RI. 2016. Parallel Transformation of Tactile Signals in Central Circuits of Drosophila. *Cell* **164**:1046–1059.
Usui-Ishihara A, Simpson P. 2005. Differences in sensory projections between macro- and microchaetes in Drosophilid flies. *Dev Biol* **277**:170–183.
Vinh NX, Epps J, Bailey J. 2009. Information theoretic measures for clusterings comparisonProceedings of the 26th Annual International Conference on Machine Learning. Presented at the ICML '09: The 26th Annual International Conference on Machine Learning held in conjunction with the 2007 International Conference on Inductive Logic Programming. New York, NY, USA: ACM. doi:10.1145/1553374.1553511
Williams DW, Shepherd D. 1999. Persistent larval sensory neurons in adult Drosophila melanogaster. *J Neurobiol* **39**:275–286.

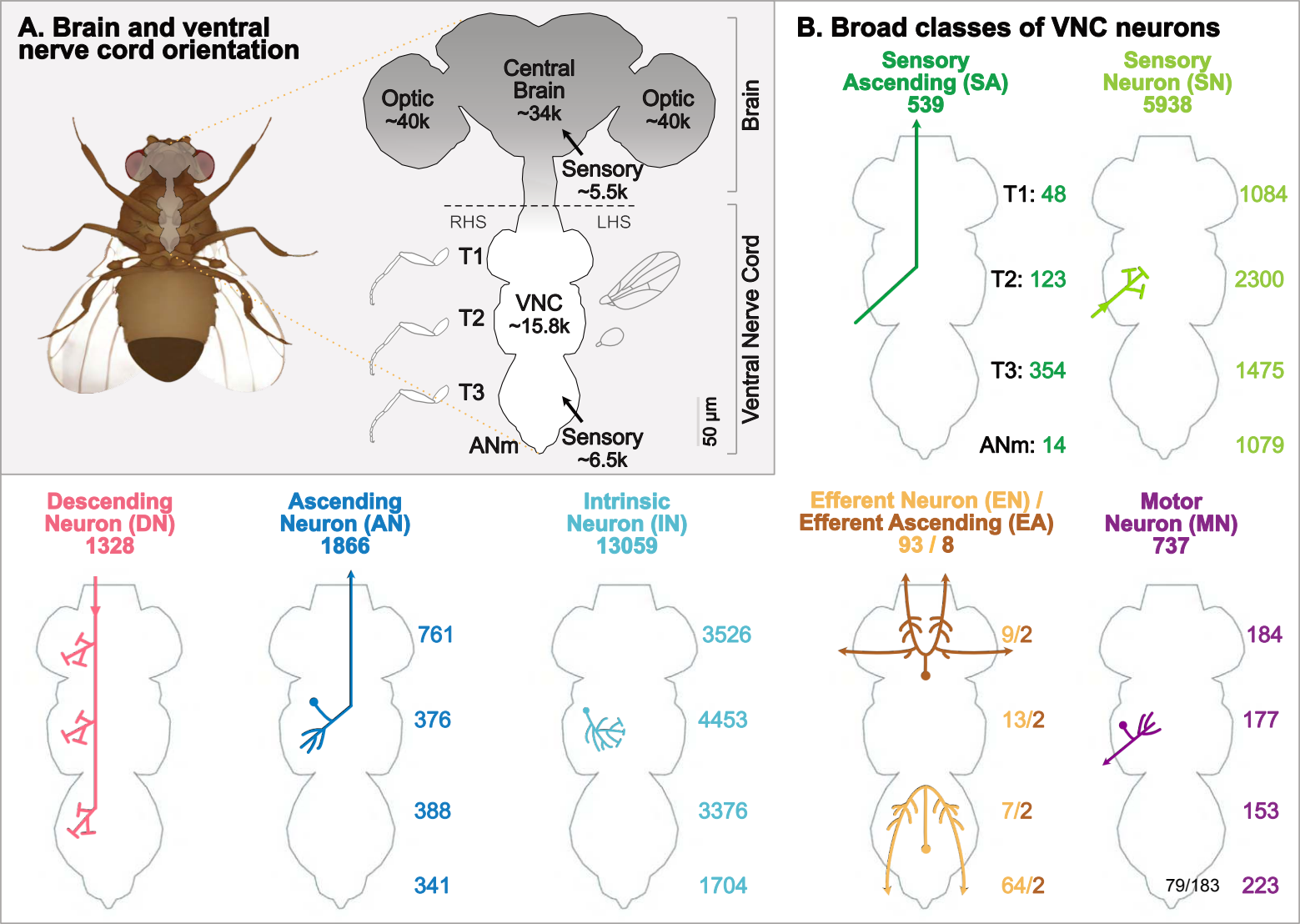
A. Brain and ventral nerve cord orientation
Central Brain ~34k
Optic ~40k
Optic ~40k
Sensory ~5.5k
Brain
RHS
LHS
T1
T2
T3
VNC ~15.8k
ANm
Sensory ~6.5k
50 µm
Ventral Nerve Cord
B. Broad classes of VNC neurons
Sensory Ascending (SA) 539
Sensory Neuron (SN) 5938
T1: 48
T2: 123
T3: 354
ANm: 14
1084
2300
1475
1079
Descending Neuron (DN) 1328
Ascending Neuron (AN) 1866
Intrinsic Neuron (IN) 13059
Efferent Neuron (EN) / Efferent Ascending (EA) 93 / 8
Motor Neuron (MN) 737
761
376
388
341
3526
4453
3376
1704
9/2
13/2
7/2
64/2
184
177
153
223

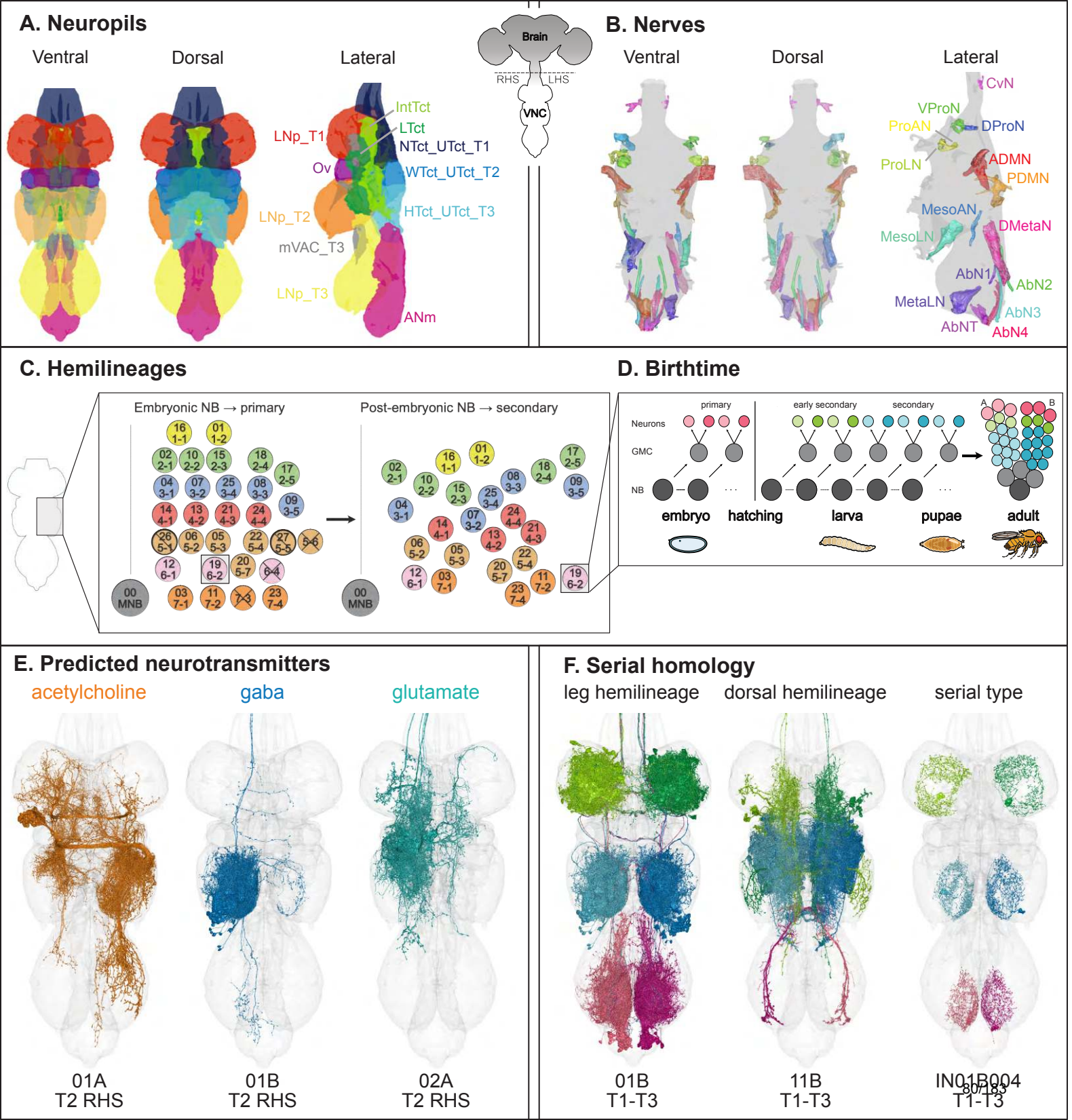
A. Neuropils
Ventral
Dorsal
Lateral
Brain
RHS
LHS
VNC
IntTct
LTct
NTct_UTct_T1
WTct_UTct_T2
HTct_UTct_T3
LNp_T1
Ov
LNp_T2
mVAC_T3
LNp_T3
ANm
B. Nerves
Ventral
Dorsal
Lateral
CvN
VProN
ProAN
DProN
ProLN
ADMN
PDMN
MesoAN
DMetaN
MesoLN
AbN1
AbN2
MetaLN
AbN3
AbNT
AbN4
C. Hemilineages
Embryonic NB → primary
Post-embryonic NB → secondary
00 MNB
D. Birthtime
primary
early secondary
secondary
Neurons
GMC
NB
A
B
embryo
hatching
larva
pupae
adult
E. Predicted neurotransmitters
acetylcholine
gaba
glutamate
01A
T2 RHS
01B
T2 RHS
02A
T2 RHS
F. Serial homology
leg hemilineage
dorsal hemilineage
serial type
01B
T1-T3
11B
T1-T3
IN01B004
T1-T3

Systematic Typing

A Descending Neuron (DN)

DN + target neuropil + # = systematic_type

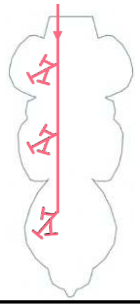

consecutive number consistent between types

DNxl134

-If neuron is matched to light level data, **type** = literature name (e.g., Dna01)

-If it does not have a light level match, **type** = **systematic_type** (e.g., Dnxl134)

-**instance** = type + root_side (e.g.,DNa01_R, Dnxl134_R)

B Motor Neuron (MN)

MN + target muscle + # = systematic_type

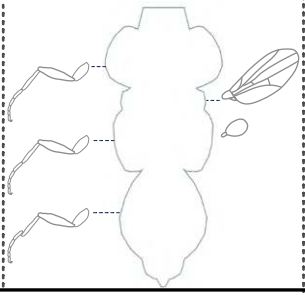

consecutive number consistent between types

MNwm36

-If neuron is matched to light level data, **type** = literature name (e.g., b1 MN)

-If it does not have a light level match, **type** = **systematic_type** (e.g., MNwm36)

-**instance** = type + root_side (e.g., MNwm36_R)

C Sensory Neuron (SN)/Sensory Ascending (SA)

SN or SA + modality + # = systematic_type

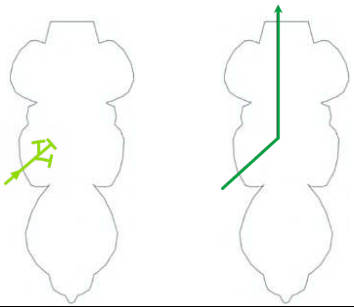

ch	chemosensory
pp	propioceptive
ta	tactile
xx	unknown

consecutive number consistent between types

SNpp41 or SApp04

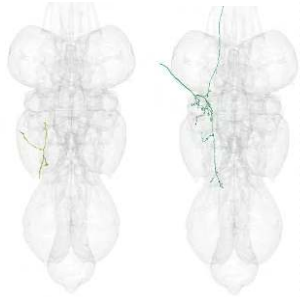

-If neuron is matched to light level data, **synonyms** = literature name (e.g., FeCO, hook, d.Rad.A CS)

-If it does not have a light level match, **type** = **systematic_type** (e.g., Snpp41, SApp04)

-**instance** = type + entry_nerve + root_side (Snpp41_MesoLN_R, Sapp04_ADMN_R)

D Intrinsic Neuron (IN)/Ascending neuron (AN)

IN or AN + hemilineage + # = systematic_type

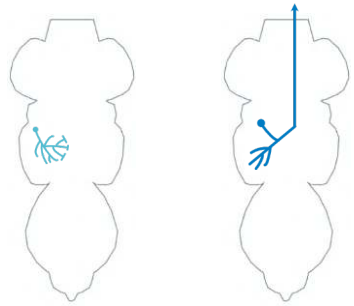

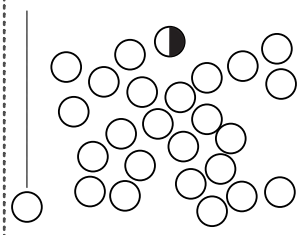

consecutive number consistent between types

IN01B009 or AN04B002

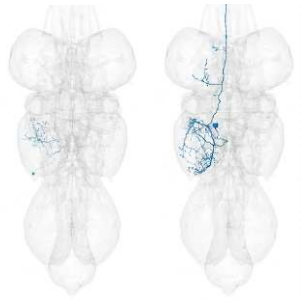

-If neurons not matched to light level data, **type** = **systematic_type** (e.g., AN04B002, IN01B009)

-**instance** = type + soma_neuromere + soma_side (e.g., AN04B002_T2_R, IN01B009_T3_R)

E Efferent neuron (EN)/ Efferent Ascending (EA)

EN or EA + hemilineage + # = systematic_type

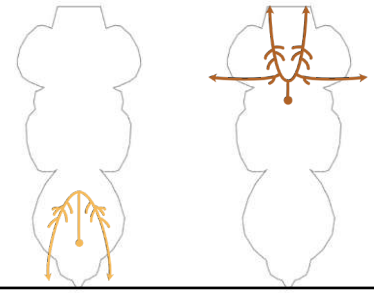

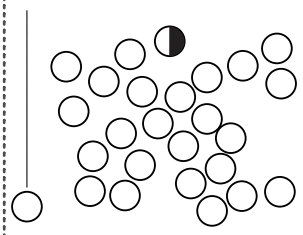

consecutive number consistent between types

EN27X003 or EA06B010

-If neuron is not matched to light level data, **type** = **systematic_type** (e.g., EN27X003, EA06B010)

-**instance** = type + soma_neuromere + soma_side (e.g., EN27X003_T2_R, EA06B010_T2_R)

Glossary

General	
VNC	Ventral nerve cord, a.k.a. ventral nervous system, analogous to vertebrate spinal cord
CvC	Cervical connective, a.ka., neck connective, connecting brain to VNC
root_side	Side of axon entry (from neck connective or nerve)
soma_side	side of soma origin
RHS	Right hand side (from fly's perspective)
LHS	Left hand side (from fly's perspective)
soma_neuromere	neuromere of soma origin
T1	First thoracic segment, i.e., prothorax
T2	Second thoracic segment, i.e., mesothorax
T3	Third thoracic segment, i.e., metathorax
A1,A2…	First abdominal segment, second abdominal segment
soma_ position	coordinates of soma
tosoma_ position	coordinates of presumed tract leading to soma
position	Coordinates that can be used to navigate to a particular neuron
bodyid	unique numerical identifier for a reconstructed body/ neuron
group	matched within neuromere
subcluster	ad hoc notation for neurons sharing common properties (i.e., origin or morphology) but not assignable to a specific hemilineage or serial set
systematic_type	cell type, systematic nomenclature
type	cell type
instance	type and location
synonyms	published name

Broad classes of VNC neurons	
class	broadest cell class (motor, sensory, etc)
ascending neuron(AN)	neuron with soma of VNC origin and axon ascending via neck connective
descending neuron(DN)	neuron with soma of brain origin and axon descending via neck connective
efferent ascending (EA)	neuron with soma of VNC origin and axon ascending via neck connective and leaving the nerve cord
efferent neuron(EN)	neuron with soma of VNC origin and axon leaving the nerve cord
intrinsic neuron(IN)	neuron with soma of VNC origin and processes restricted to the VNC
motor neuron(MN)	neuron with soma of VNC origin and axon exiting the nerve cord via a nerve
sensory ascending(SA)	neuron with soma of peripheral origin and axon entering the VNC via nerve and exiting via neck connective
sensory neuron(SN)	neuron with soma of peripheral origin and axon entering the VNC via nerve
glia	reconstructed body believed to be glia, in most cases not completely traced

Subclasses of VNC neurons	
subclass	general morphology & connectivity
IA	ipsilateral connections ascending
CA	contralateral connections ascending
BA	bilateral connections ascending
XA	no connections ascending
II	ipsilateral interconnecting neuropils
CI	contralateral interconnecting neuropils
BI	bilateral interconnecting neuropils
IR	ipsilateral restricted to one neuropil
CR	contralateral restricted to one neuropil
BR	bilateral restricted to one neuropil

VNC Neuropils/Muscles	
origin	neuropil with > 80% of input
target	neuropil/muscle with > 80% of output
Ntct	neck tectulum neuropil
-nt	neck tectulum
-nm	neck muscle
WTct	wing tectulum neuropil
-wt	wing tectulum
-wm	wing muscle
Htct	haltere tectulum neuropil
-ht	haltere tectulum
-hm	haltere muscle
UTct(ut)	upper tectulum (nt, wt, ht)
IntTc(it)	inter tectulum
Ltct(lt)	lower tectulum
LegNpT1(fl)	front leg neuropil (muscle)
LegNpT2(fl)	middle leg neuropil (muscle)
LegNpT3(fl)	hind leg neuropil (muscle)
LegNp(xl)	multiple leg neuropils
Anm(ad)	abdomen neuropil (muscle)
xn	multiple neuropils
xm	unknown muscle

VNC Nerves	
entry_nerve	nerve by which axon enters VNC
exit_nerve	nerve by which axon exits VNC
DProN	Dorsal Prothoracic Nerve
PrN	Prosternal Nerve
ProCN	Prothoracic Chordotonal Nerve
ProAN	Prothoracic Accessory Nerve
VProN	Ventral Prothoracic Nerve
ProLN	Prothoracic Leg Nerve
ProNTBD	Prothoracic Nerve (to be defined)
ADMN	Anterior Dorsal Mesothoracic Nerve
PDMN	Posterior Dorsal Mesothoracic Nerve
MesoAN	Mesothoracic Accessory Nerve
MesoLN	Mesothoracic Leg Nerve
DMetaN	Dorsal Metathoracic Nerve
MetaLN	Metathoracic Leg Nerve
AbN1	First Abdominal Nerve
AbN2	Second Abdominal Nerve
AbN3	Third Abdominal Nerve
AbN4	Fourth Abdominal Nerve
AbNT	Abdominal Nerve Trunk
AbNX	unnamed abdominal nerve/connective
CvN	Cervical Nerve

VNC lineages	
neuroblast	neural stem cell
lineage	cells produced by the same neuroblast
hemilineage	NotchON or NotchOFF subset of a lineage
birthtime	developmental epoch of origin
primary	born during embryogenesis
early secondary	born in late embryo or early larva
secondary	born during larval life

Predicted Neurotrasmitters	
predicted nt	"winning" neurotransmitter prediction for a neuron
predicted nt prob	measure of confidence of "winning" neurotransmitter prediction

Transmission	
electrical	matched to a neuron reported to be connected to partners by gap junctions
putative electrical	having low presynaptic density and/or morphology typical of electrical neurons
neurosecretory	matched to a neuron reported to be neurosecretory
putative neurosecretory	efferent neuron or unpolarised neuron with beads-on-string morphology suggesting neurosecretory function

Modality	
ch	chemosensory
pp	propioceptive
ta	tactile
xx	unknown

Serial homology	
serial	matched across neuromeres
serial motif	pattern of serial homology
independent leg	serial set with origin and target in same leg neuropil
dorsal	serial set with origin and target in flight neuropils
convergent	serial set with axons converging to common target area(s)
sequential	serial set with axons consistently targeting the next anterior or posterior neuromere
ascending	serial set consisting solely of ascending neurons
centripetal	serial set with distal dendrites (usually leg neuropil) and central axon terminals (usually tectulum)
centrifugal	serial set with central dendrites (usually tectulum) and distal axon terminals (usually leg neuropil)
complex	serial set that does not fall into one of the other categories

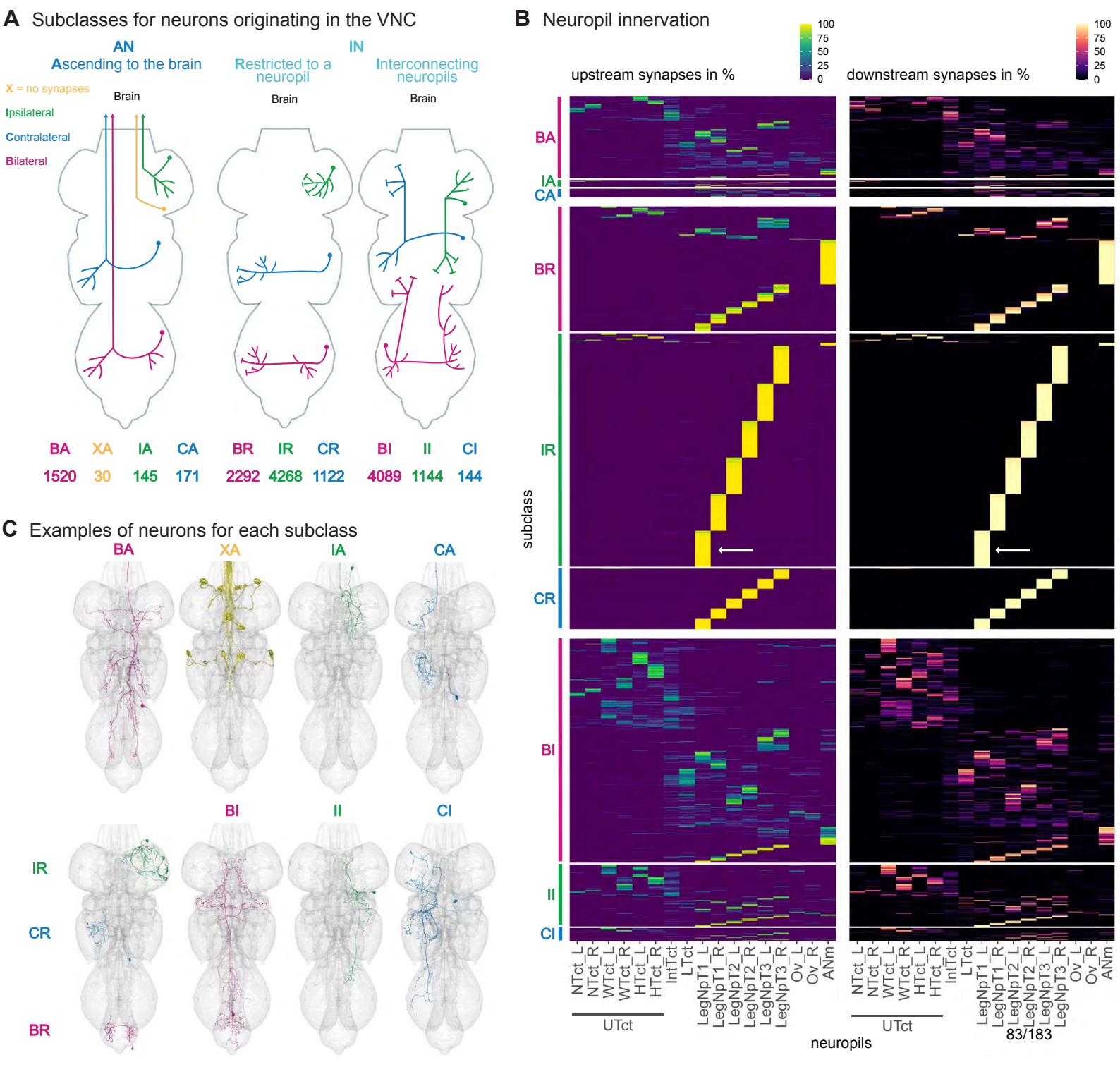
A Subclasses for neurons originating in the VNC
AN
Ascending to the brain
IN
Restricted to a neuropil
Interconnecting neuropils
X = no synapses
Ipsilateral
Contralateral
Bilateral
Brain
Brain
Brain
BA XA IA CA BR IR CR BI II CI
1520 30 145 171 2292 4268 1122 4089 1144 144
B Neuropil innervation
upstream synapses in %
downstream synapses in %
100 75 50 25 0
subclass
BA
IA
CA
BR
IR
CR
BI
II
CI
NTct_L NTct_R WTct_L WTct_R HTct_L HTct_R IntTct LTct LegNpT1_L LegNpT1_R LegNpT2_L LegNpT2_R LegNpT3_L LegNpT3_R Ov_L Ov_R ANm
UTct
83/183
neuropils
C Examples of neurons for each subclass
BA
XA
IA
CA
BI
II
CI
IR
CR
BR

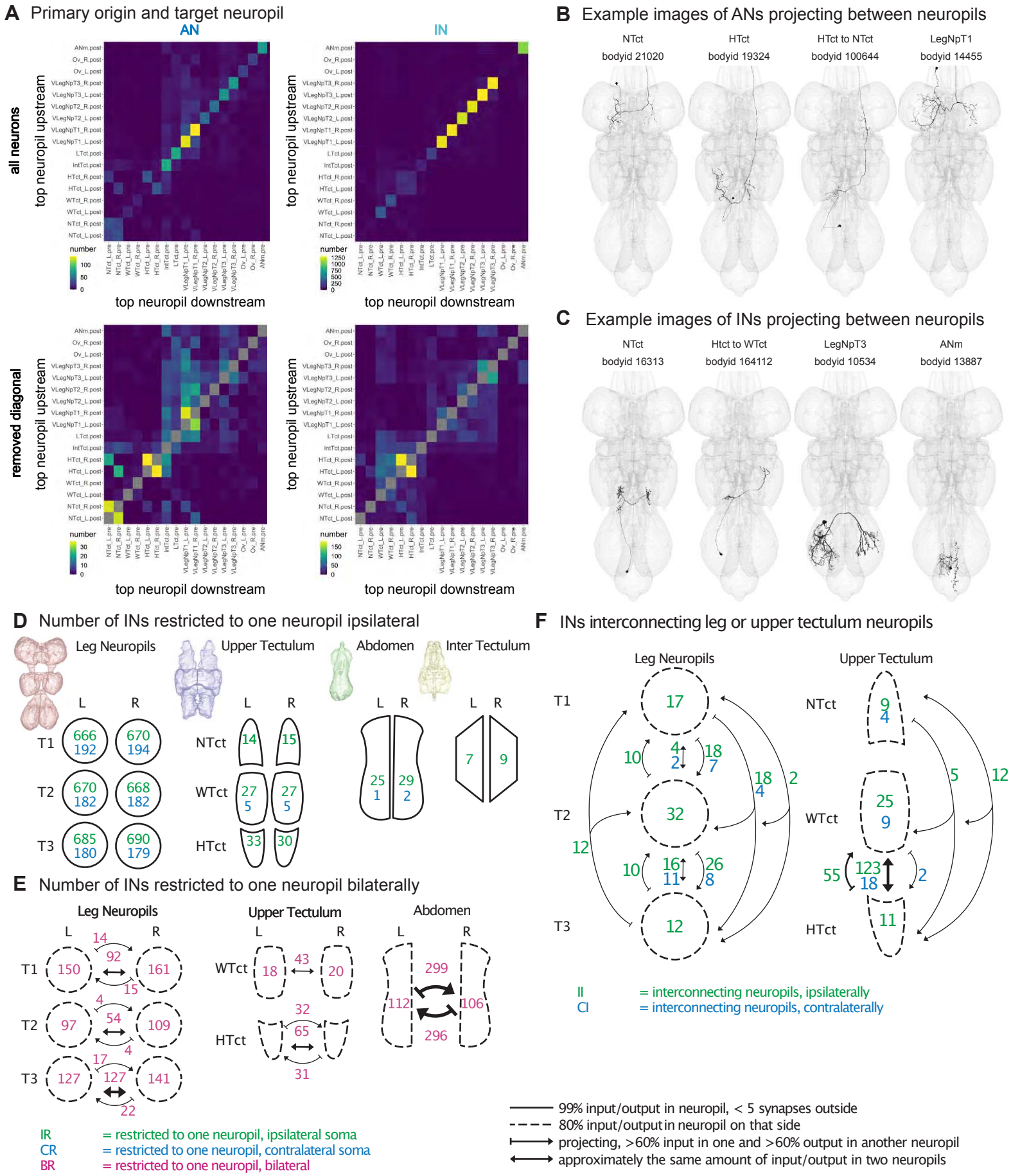
A Primary origin and target neuropil
AN
IN
all neurons
removed diagonal
top neuropil upstream
top neuropil downstream
number
B Example images of ANs projecting between neuropils
NTct bodyid 21020
HTct bodyid 19324
HTct to NTct bodyid 100644
LegNpT1 bodyid 14455
C Example images of INs projecting between neuropils
NTct bodyid 16313
Htct to WTct bodyid 164112
LegNpT3 bodyid 10534
ANm bodyid 13887
D Number of INs restricted to one neuropil ipsilateral
Leg Neuropils
Upper Tectulum
Abdomen
Inter Tectulum
L
R
T1
T2
T3
666 192
670 194
670 182
668 182
685 180
690 179
NTct
WTct
HTct
14
15
27 5
27 5
33
30
25 1
29 2
7
9
E Number of INs restricted to one neuropil bilaterally
Leg Neuropils
Upper Tectulum
Abdomen
150
92
14
15
161
97
54
4
4
109
127
17
127
22
141
WTct
18
43
20
HTct
32
65
31
112
299
296
106
IR = restricted to one neuropil, ipsilateral soma
CR = restricted to one neuropil, contralateral soma
BR = restricted to one neuropil, bilateral
F INs interconnecting leg or upper tectulum neuropils
Leg Neuropils
Upper Tectulum
17
10
4
2
18
7
18
4
2
32
12
10
16
11
26
8
12
NTct
9
4
5
12
WTct
25
9
55
123
18
2
11
HTct
II = interconnecting neuropils, ipsilaterally
CI = interconnecting neuropils, contralaterally
99% input/output in neuropil, < 5 synapses outside
80% input/output in neuropil on that side
projecting, >60% input in one and >60% output in another neuropil
approximately the same amount of input/output in two neuropils

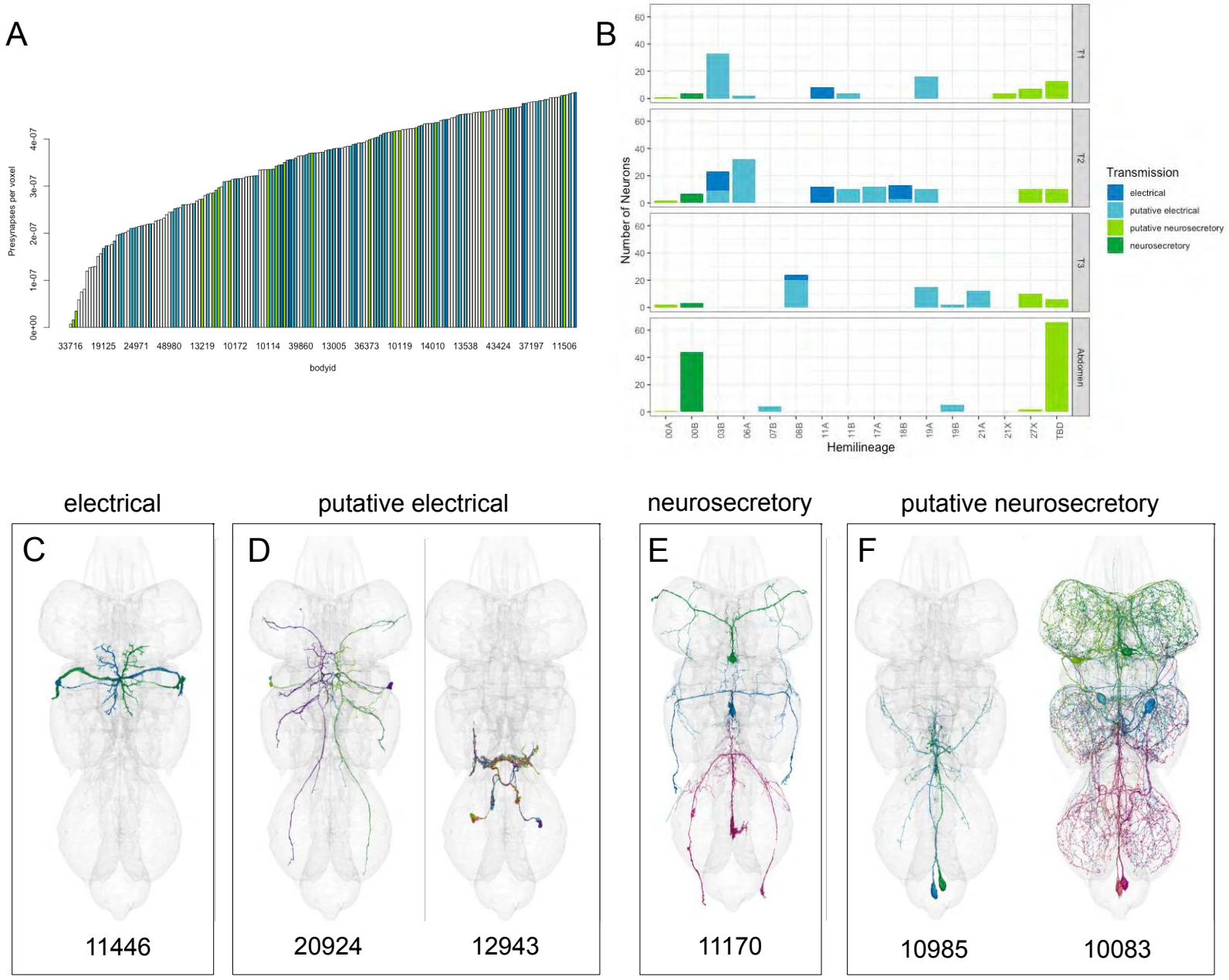
A
Presynapses per voxel
0e+00
1e-07
2e-07
3e-07
4e-07
33716 19125 24971 48980 13219 10172 10114 39860 13005 36373 10119 14010 13538 43424 37197 11506
bodyid
B
Number of Neurons
T1
T2
T3
Abdomen
00A 00B 03B 06A 07B 08B 11A 11B 17A 18B 19A 19B 21A 21X 27X TBD
Hemilineage
Transmission
electrical
putative electrical
putative neurosecretory
neurosecretory
electrical
putative electrical
neurosecretory
putative neurosecretory
C
11446
D
20924
12943
E
11170
F
10985
10083

A

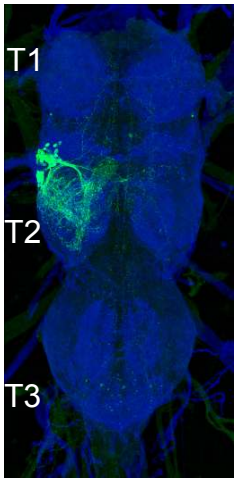

Lin 09 T2 RHS
postembryonic NB clone

B

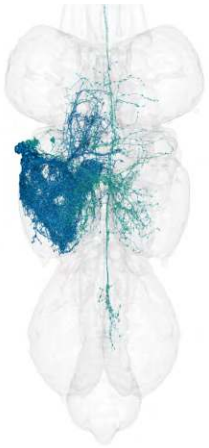

09A 09B

Lin 09 T2 RHS
expected secondary

C

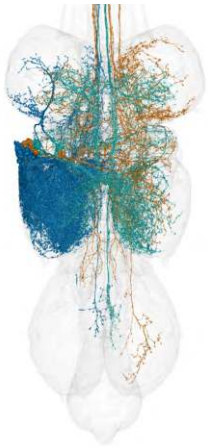

09A 09B 09B

Lin 09 T2 RHS
all neurons

D

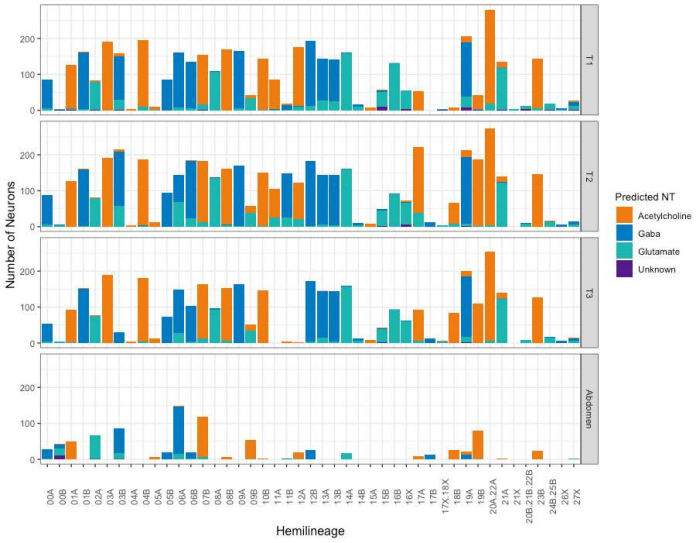

E

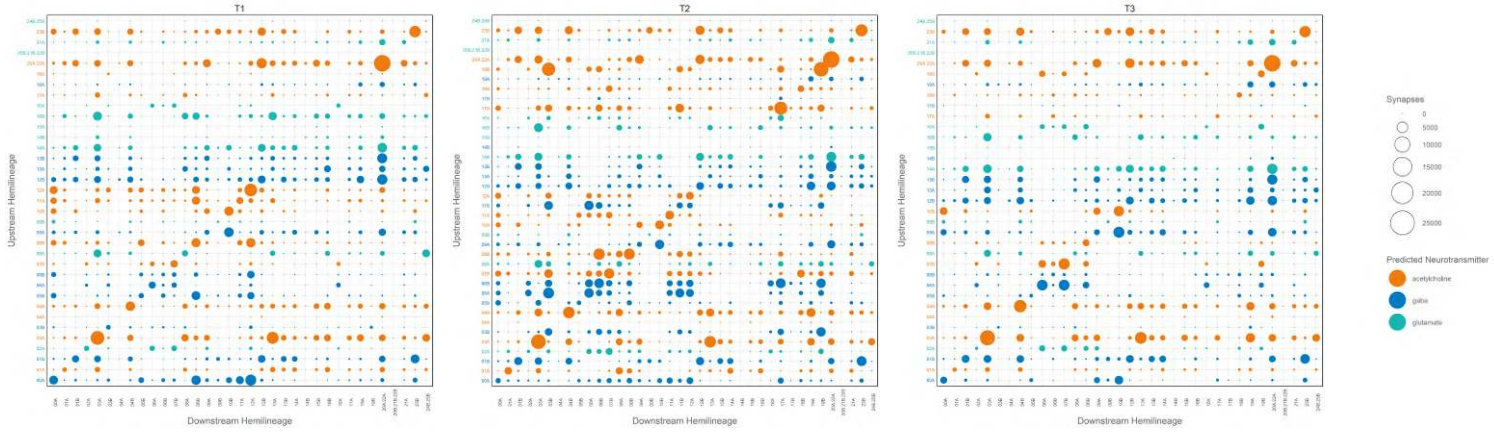

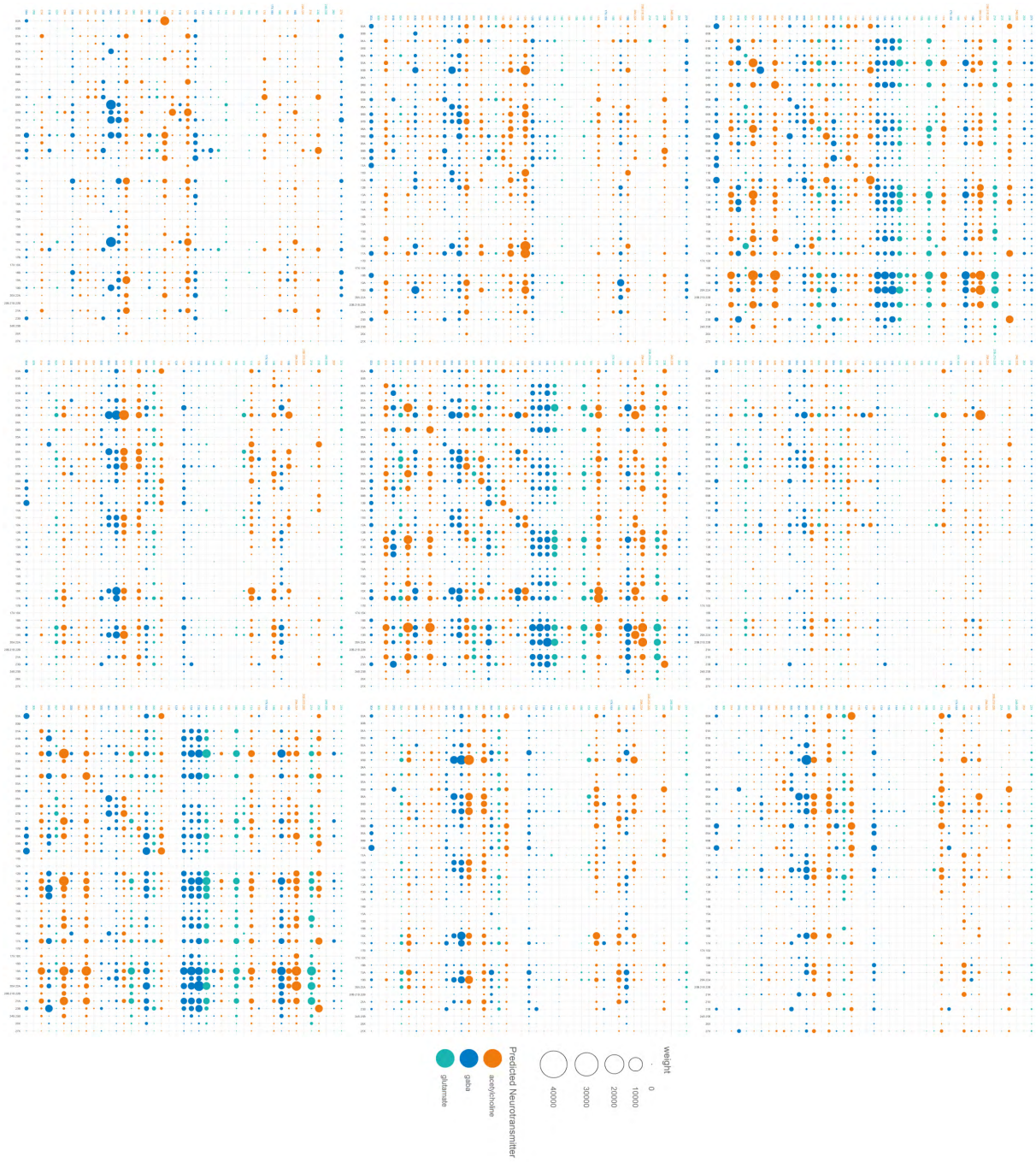
Predicted Neurotransmitter
acetylcholine
gaba
glutamate
weight
40000
30000
20000
10000
0

Synaptic Organisation of T2 Neurons

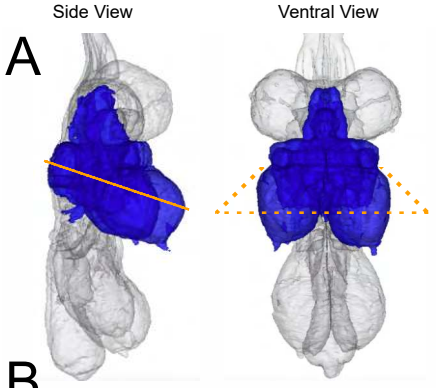

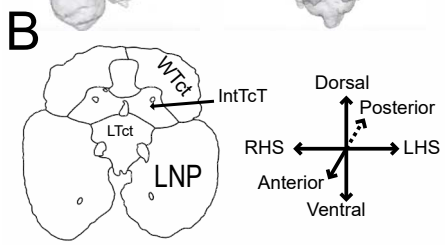

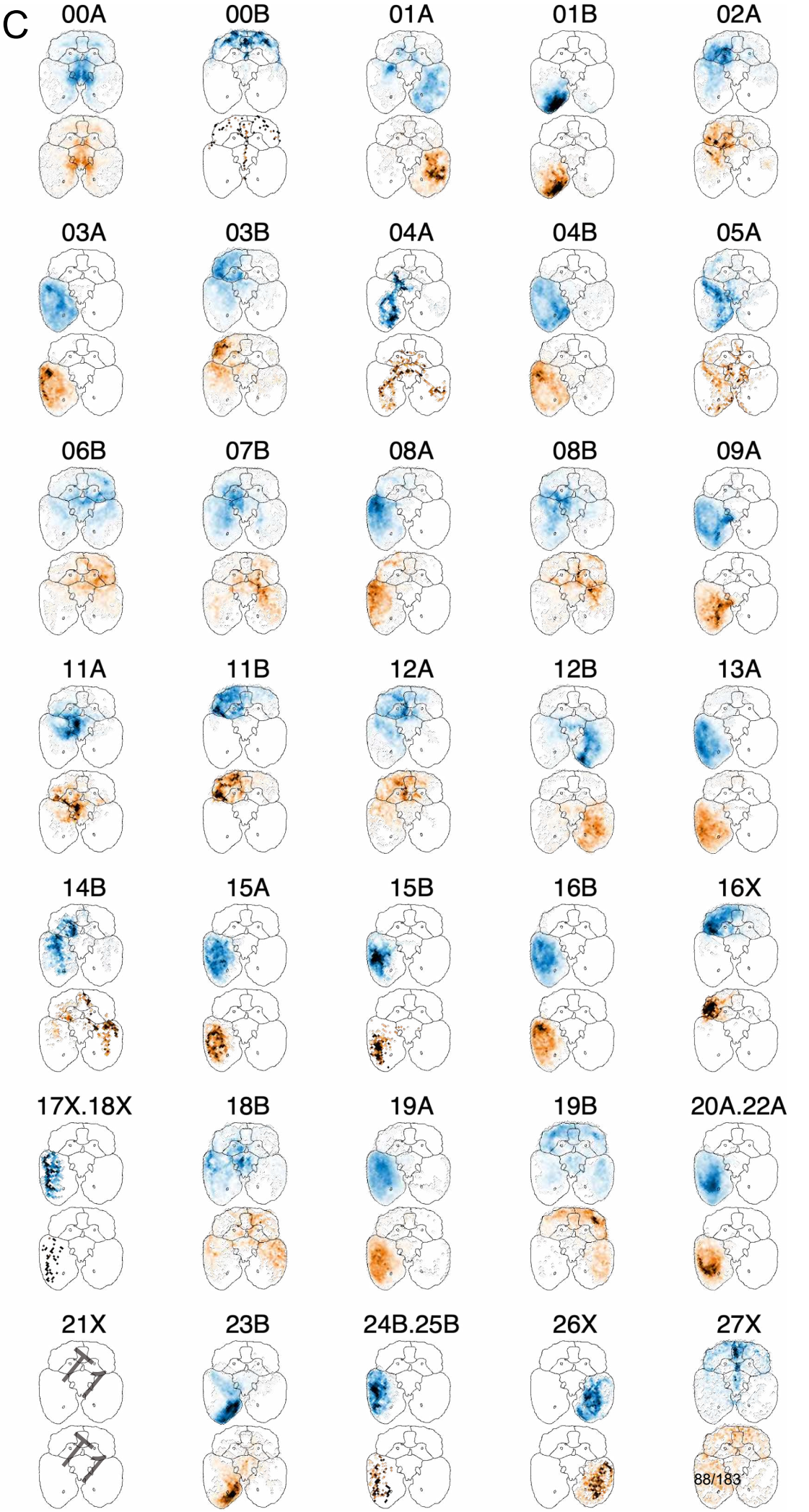

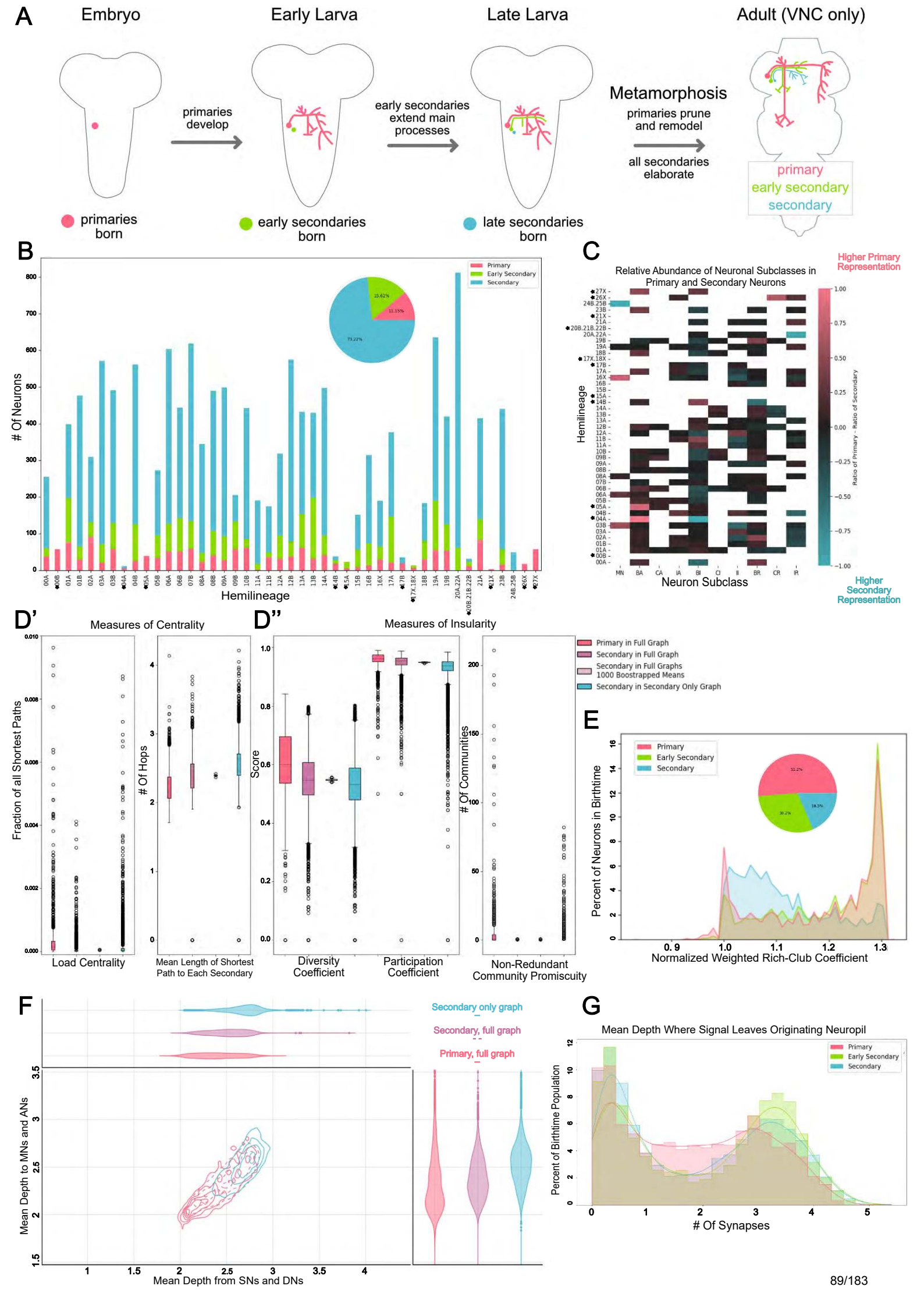
A
Embryo
Early Larva
Late Larva
Adult (VNC only)
primaries develop
early secondaries extend main processes
Metamorphosis
primaries prune and remodel
all secondaries elaborate
primary
early secondary
secondary
primaries born
early secondaries born
late secondaries born
B
Primary
Early Secondary
Secondary
Of Neurons
Hemilineage
C
Relative Abundance of Neuronal Subclasses in Primary and Secondary Neurons
Higher Primary Representation
Higher Secondary Representation
Hemilineage
Neuron Subclass
Ratio of Primary - Ratio of Secondary
D'
Measures of Centrality
Fraction of all Shortest Paths
Of Hops
Load Centrality
Mean Length of Shortest Path to Each Secondary
D''
Measures of Insularity
Score
Of Communities
Diversity Coefficient
Participation Coefficient
Non-Redundant Community Promiscuity
Primary in Full Graph
Secondary in Full Graph
Secondary in Full Graphs 1000 Boostrapped Means
Secondary in Secondary Only Graph
E
Primary
Early Secondary
Secondary
Percent of Neurons in Birthtime
Normalized Weighted Rich-Club Coefficient
F
Secondary only graph
Secondary, full graph
Primary, full graph
Mean Depth to MNs and ANs
Mean Depth from SNs and DNs
G
Mean Depth Where Signal Leaves Originating Neuropil
Primary
Early Secondary
Secondary
Percent of Birthtime Population
Of Synapses

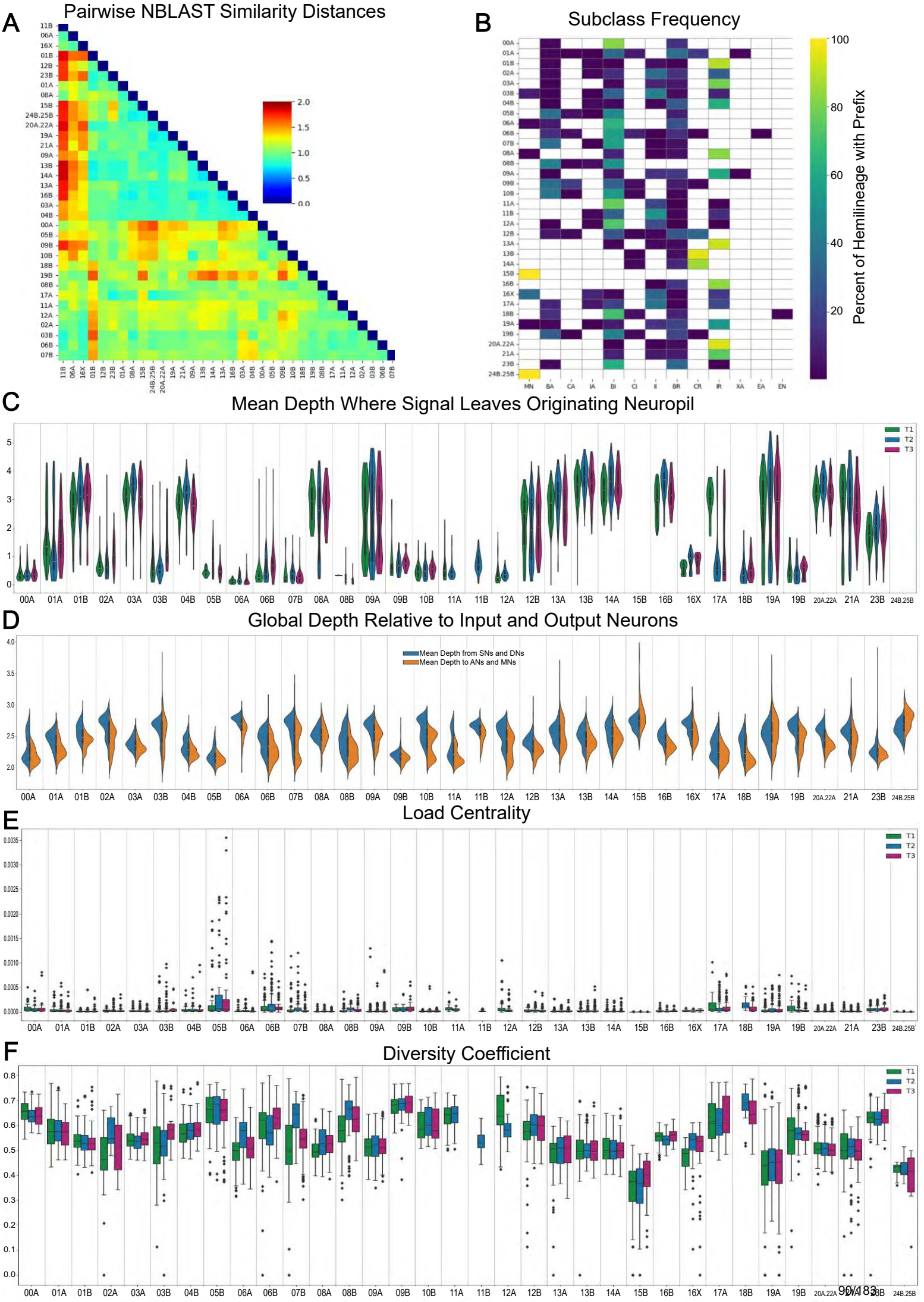
A
Pairwise NBLAST Similarity Distances
B
Subclass Frequency
Percent of Hemilineage with Prefix
C
Mean Depth Where Signal Leaves Originating Neuropil
T1
T2
T3
D
Global Depth Relative to Input and Output Neurons
Mean Depth from SNs and DNs
Mean Depth to ANs and MNs
E
Load Centrality
F
Diversity Coefficient

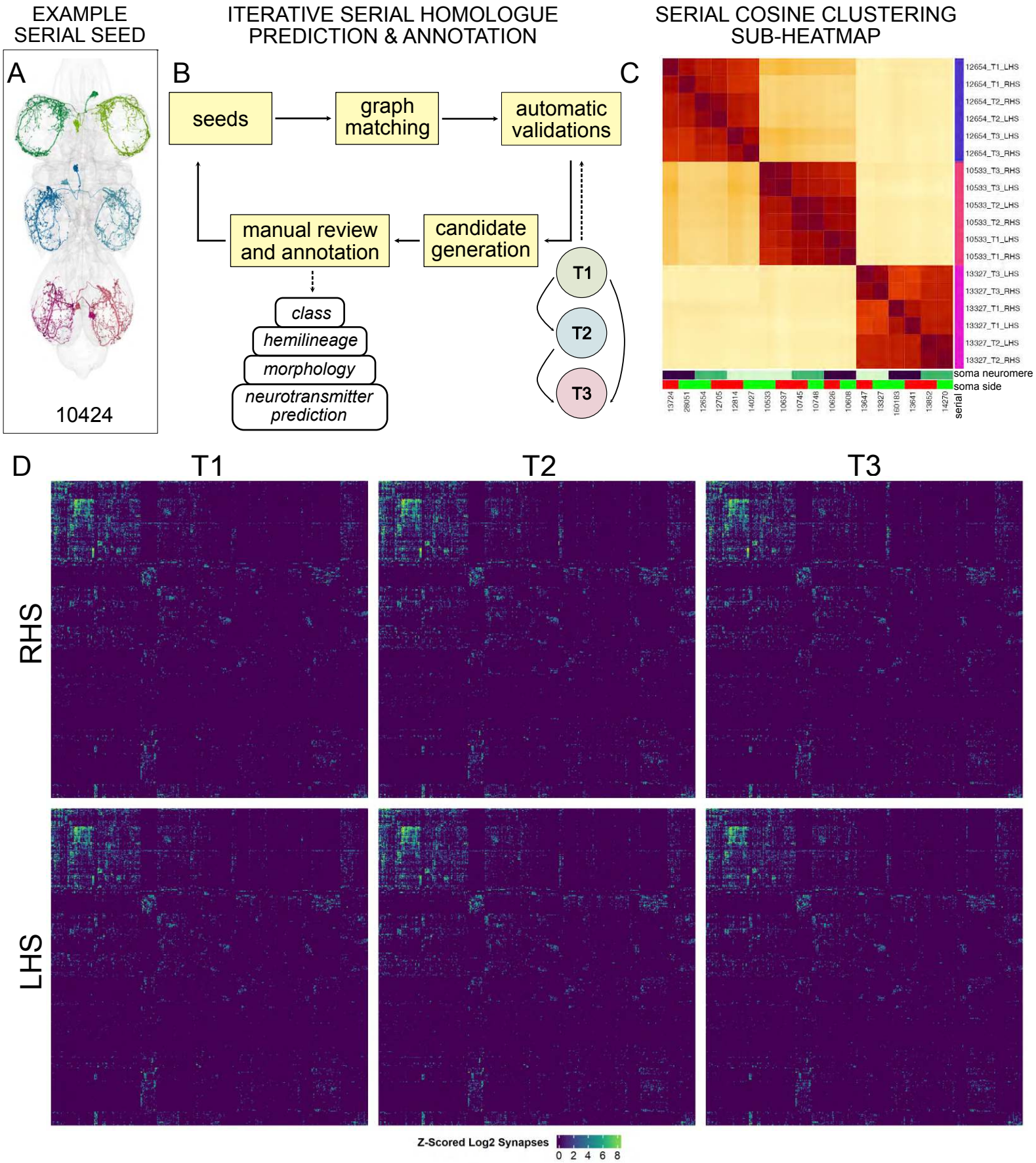
EXAMPLE SERIAL SEED
ITERATIVE SERIAL HOMOLOGUE PREDICTION & ANNOTATION
SERIAL COSINE CLUSTERING SUB-HEATMAP
A
10424
B
seeds
graph matching
automatic validations
manual review and annotation
candidate generation
class
hemilineage
morphology
neurotransmitter prediction
T1
T2
T3
C
12654_T1_LHS
12654_T1_RHS
12654_T2_RHS
12654_T2_LHS
12654_T3_LHS
12654_T3_RHS
10533_T3_RHS
10533_T3_LHS
10533_T2_LHS
10533_T2_RHS
10533_T1_LHS
10533_T1_RHS
13327_T3_LHS
13327_T3_RHS
13327_T1_RHS
13327_T1_LHS
13327_T2_LHS
13327_T2_RHS
soma neuromere
soma side
serial
13724
28051
12654
12705
12814
14027
10533
10637
10745
10748
10626
10608
13647
13327
160183
13641
13852
14270
D
T1
T2
T3
RHS
LHS
Z-Scored Log2 Synapses
0 2 4 6 8

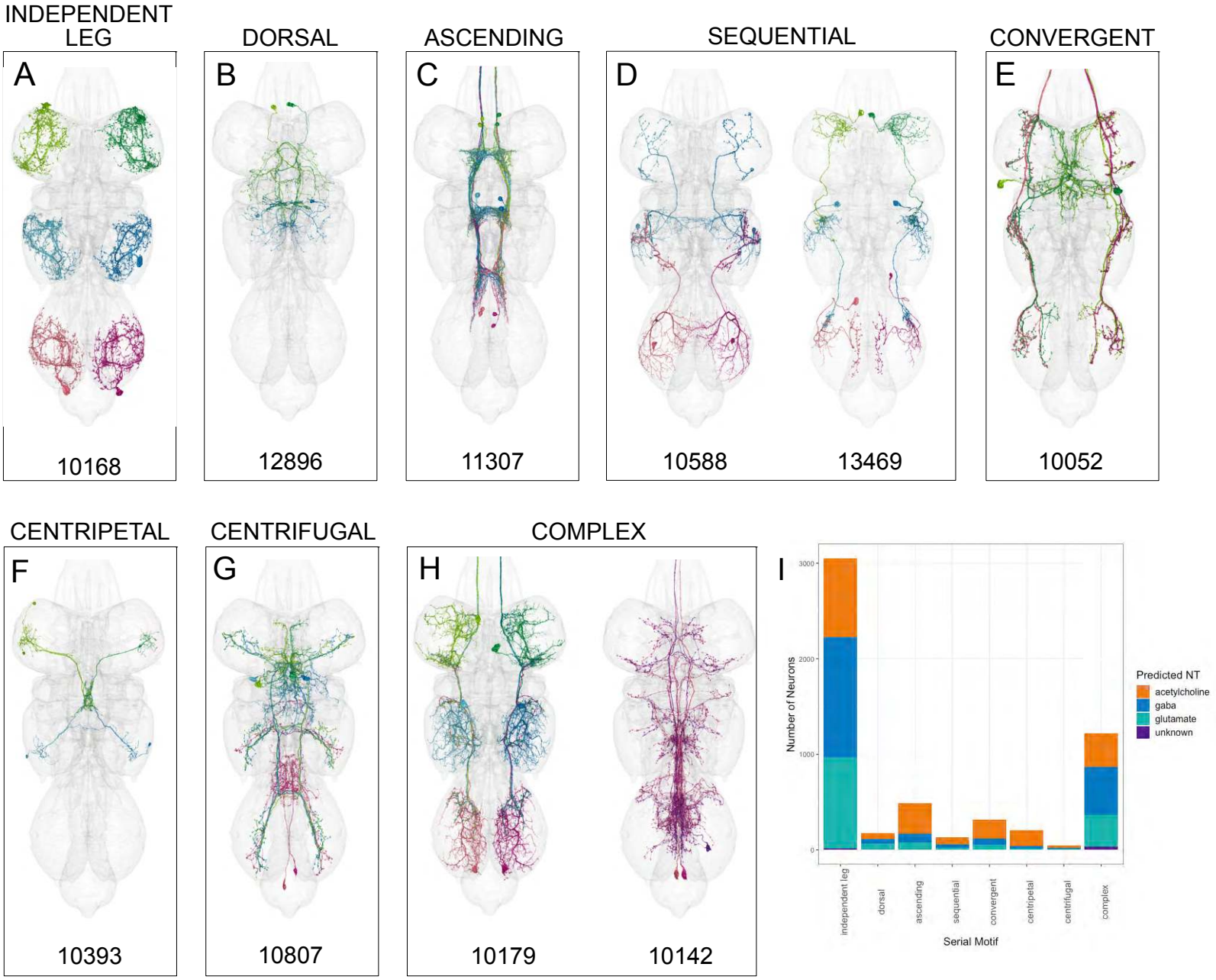
INDEPENDENT LEG
A
10168
DORSAL
B
12896
ASCENDING
C
11307
SEQUENTIAL
D
10588
13469
CONVERGENT
E
10052
CENTRIPETAL
F
10393
CENTRIFUGAL
G
10807
COMPLEX
H
10179
10142
I
Number of Neurons
3000
2000
1000
0
independent leg
dorsal
ascending
sequential
convergent
centripetal
centrifugal
complex
Serial Motif
Predicted NT
acetylcholine
gaba
glutamate
unknown

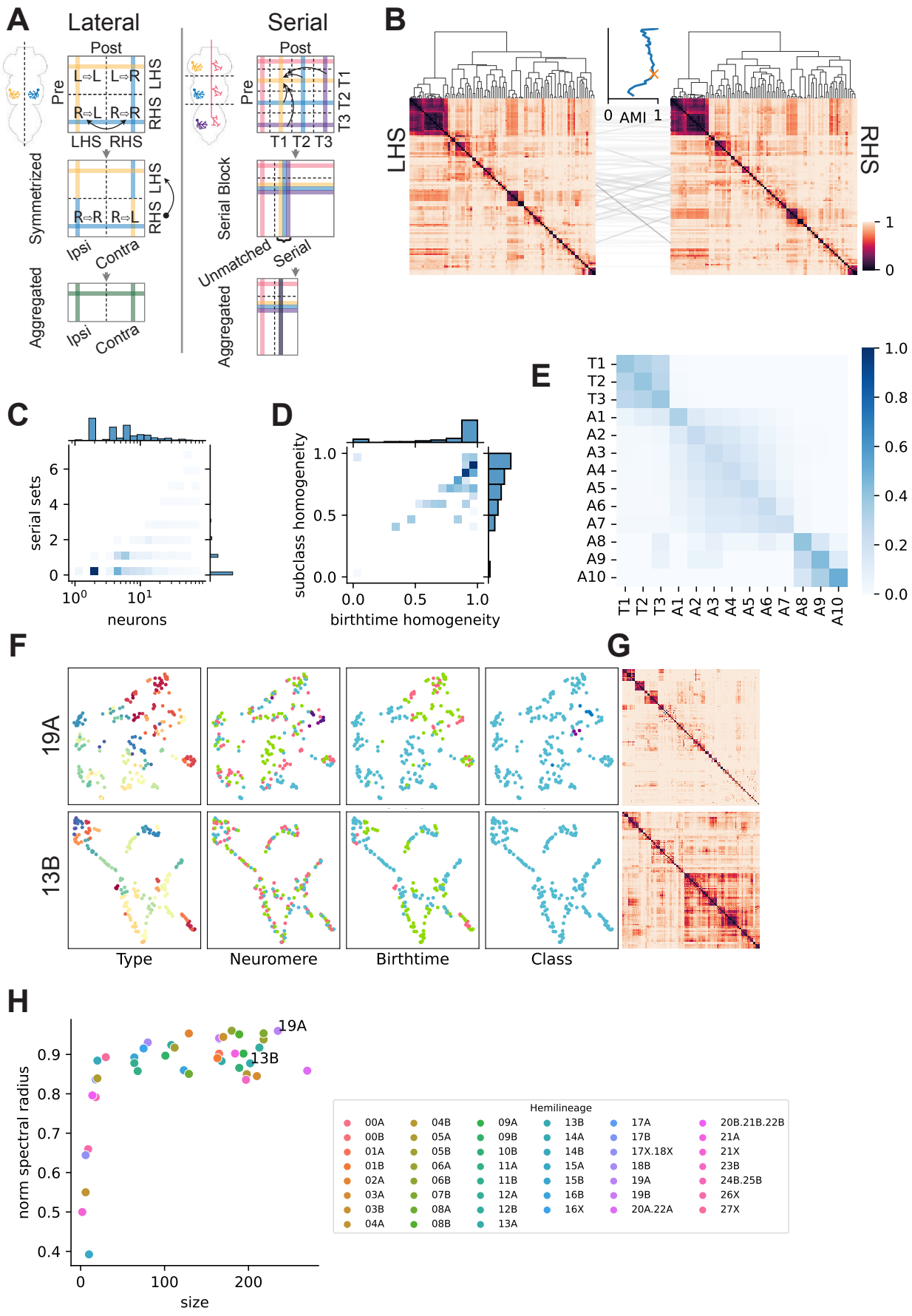
A
Lateral
Serial
Post
Pre
L⇨L
L⇨R
R⇨L
R⇨R
LHS
RHS
Symmetrized
Aggregated
Ipsi
Contra
T1 T2 T3
Serial Block
Unmatched
Serial
B
LHS
RHS
0 AMI 1
C
serial sets
neurons
D
subclass homogeneity
birthtime homogeneity
E
T1
T2
T3
A1
A2
A3
A4
A5
A6
A7
A8
A9
A10
F
G
19A
13B
Type
Neuromere
Birthtime
Class
H
norm spectral radius
size
Hemilineage
00A
00B
01A
01B
02A
03A
03B
04A
04B
05A
05B
06A
06B
07B
08A
08B
09A
09B
10B
11A
11B
12A
12B
13A
13B
14A
14B
15A
15B
16B
16X
17A
17B
17X.18X
18B
19A
19B
20A.22A
20B.21B.22B
21A
21X
23B
24B.25B
26X
27X

Synaptic Organisation of Secondary T2 Neurons

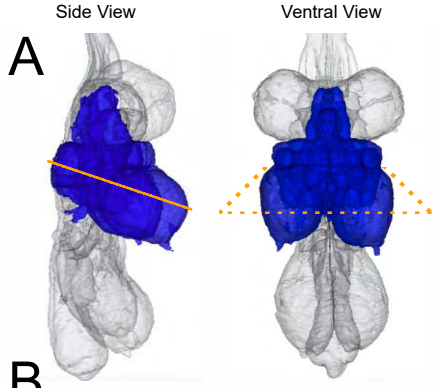

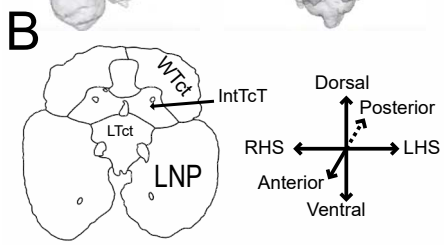

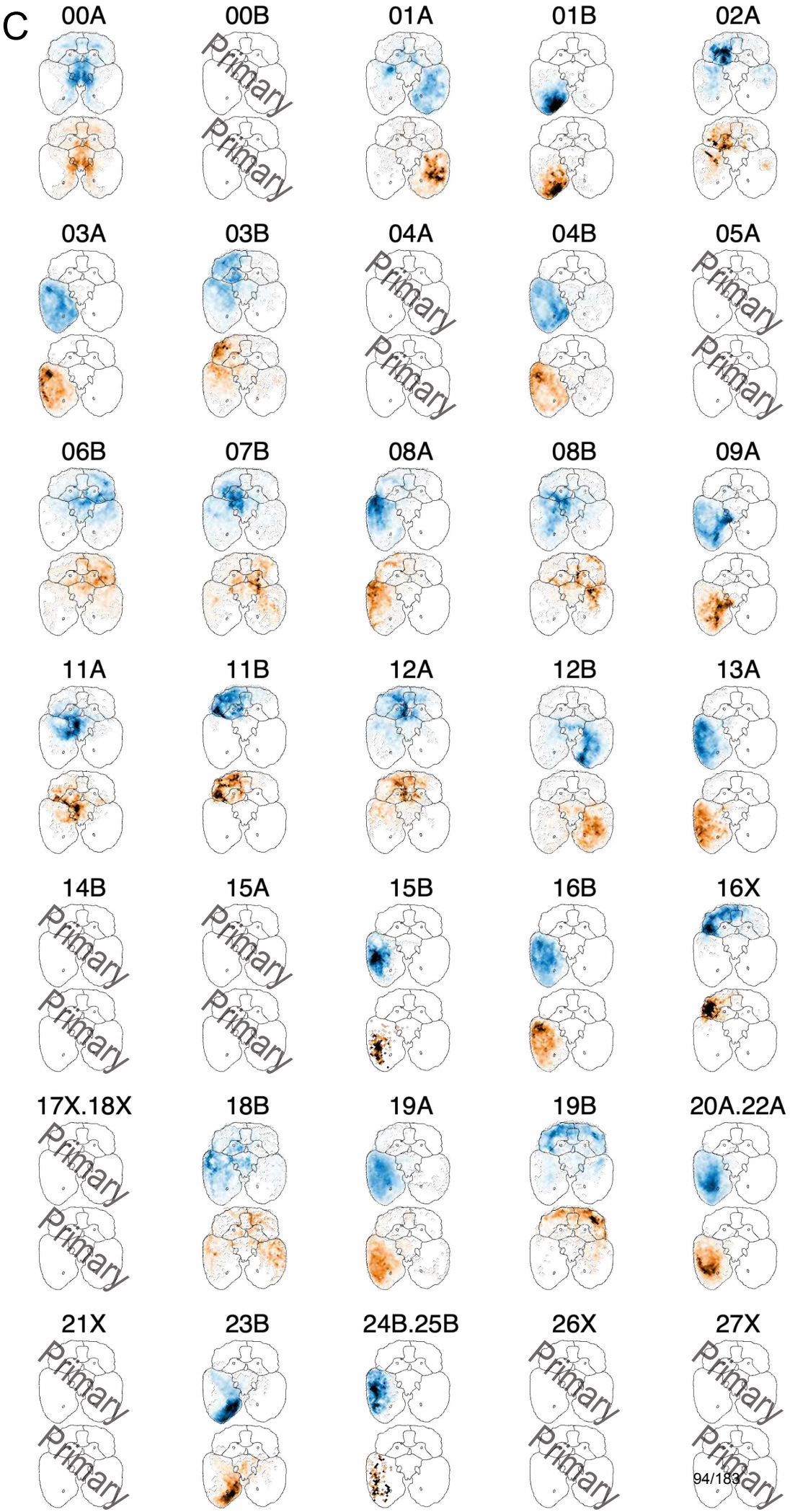

Hemilineage 00A

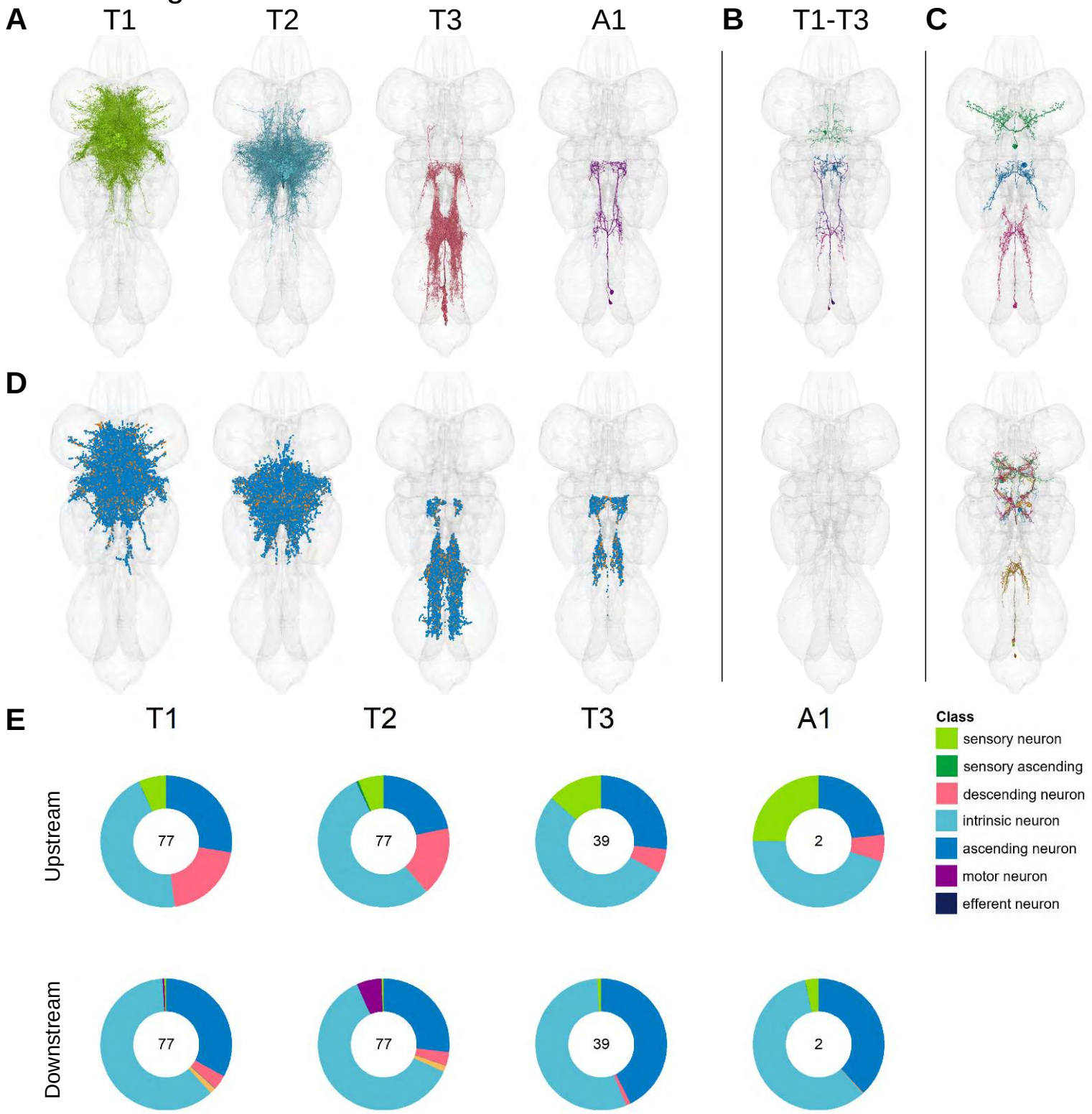

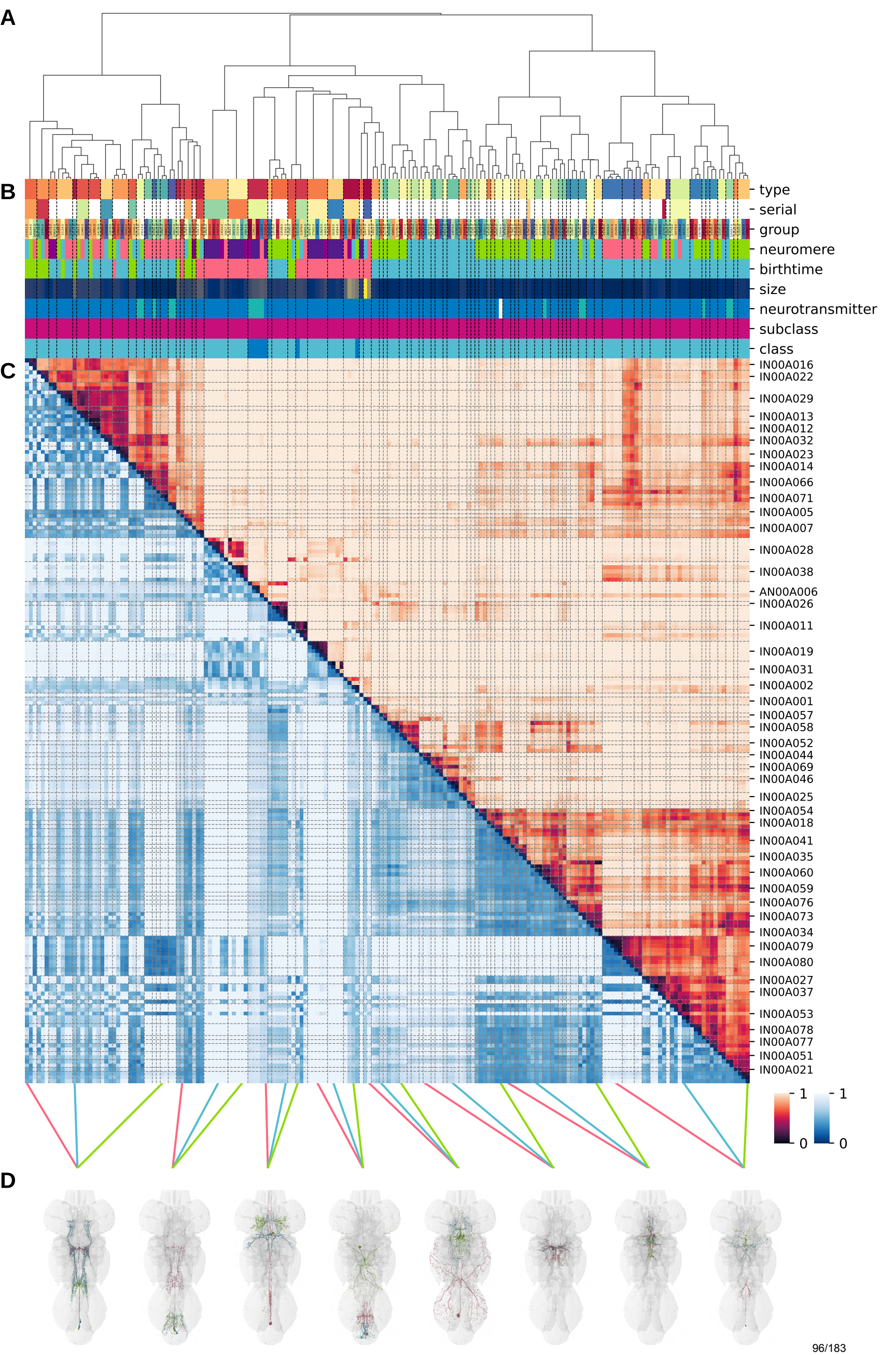
A
B
C
D
type
serial
group
neuromere
birthtime
size
neurotransmitter
subclass
class
IN00A016
IN00A022
IN00A029
IN00A013
IN00A012
IN00A032
IN00A023
IN00A014
IN00A066
IN00A071
IN00A005
IN00A007
IN00A028
IN00A038
AN00A006
IN00A026
IN00A011
IN00A019
IN00A031
IN00A002
IN00A001
IN00A057
IN00A058
IN00A052
IN00A044
IN00A069
IN00A046
IN00A025
IN00A054
IN00A018
IN00A041
IN00A035
IN00A060
IN00A059
IN00A076
IN00A073
IN00A034
IN00A079
IN00A080
IN00A027
IN00A037
IN00A053
IN00A078
IN00A077
IN00A051
IN00A021
1
0
1
0

Hemilineage 01A

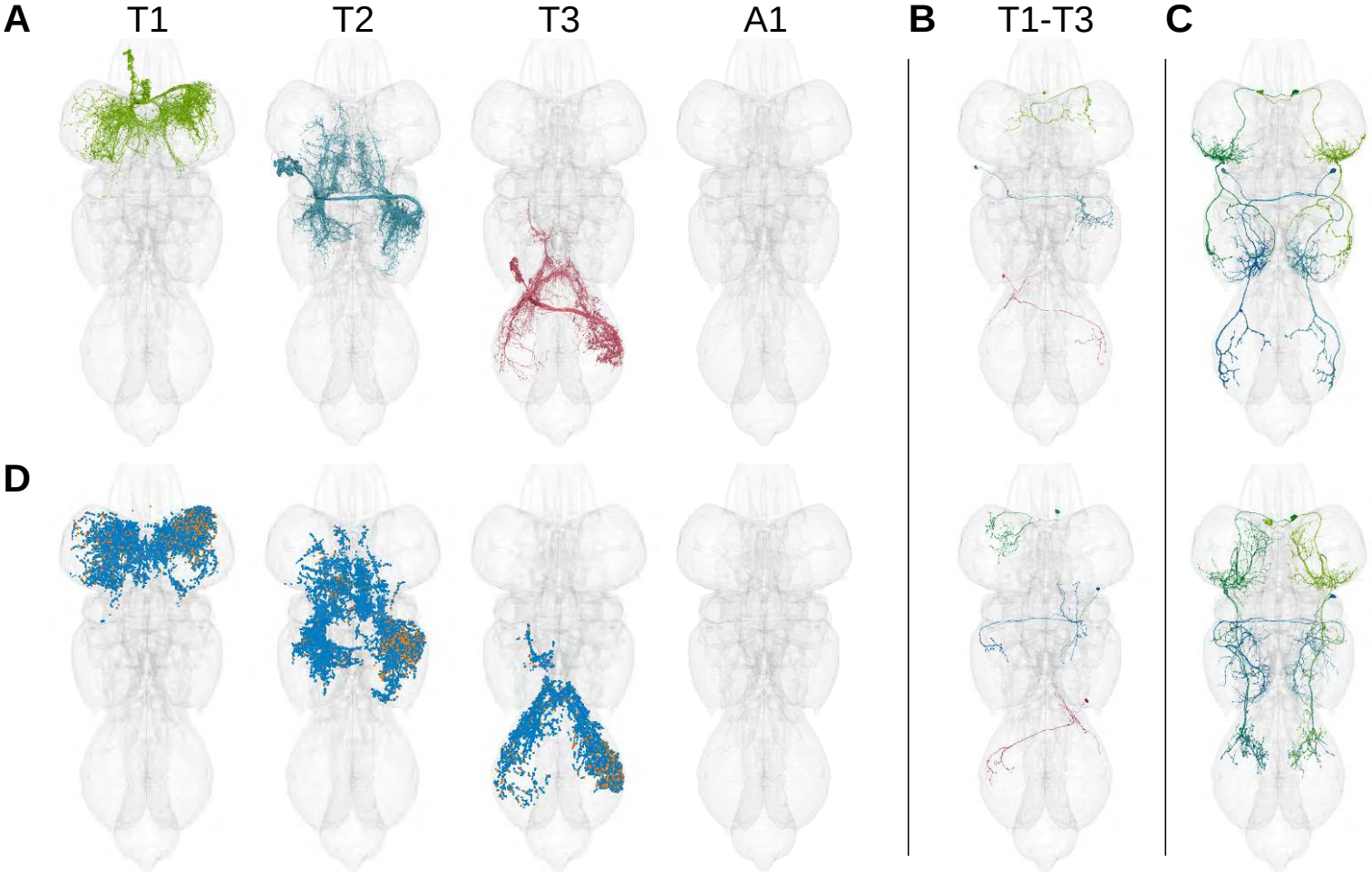

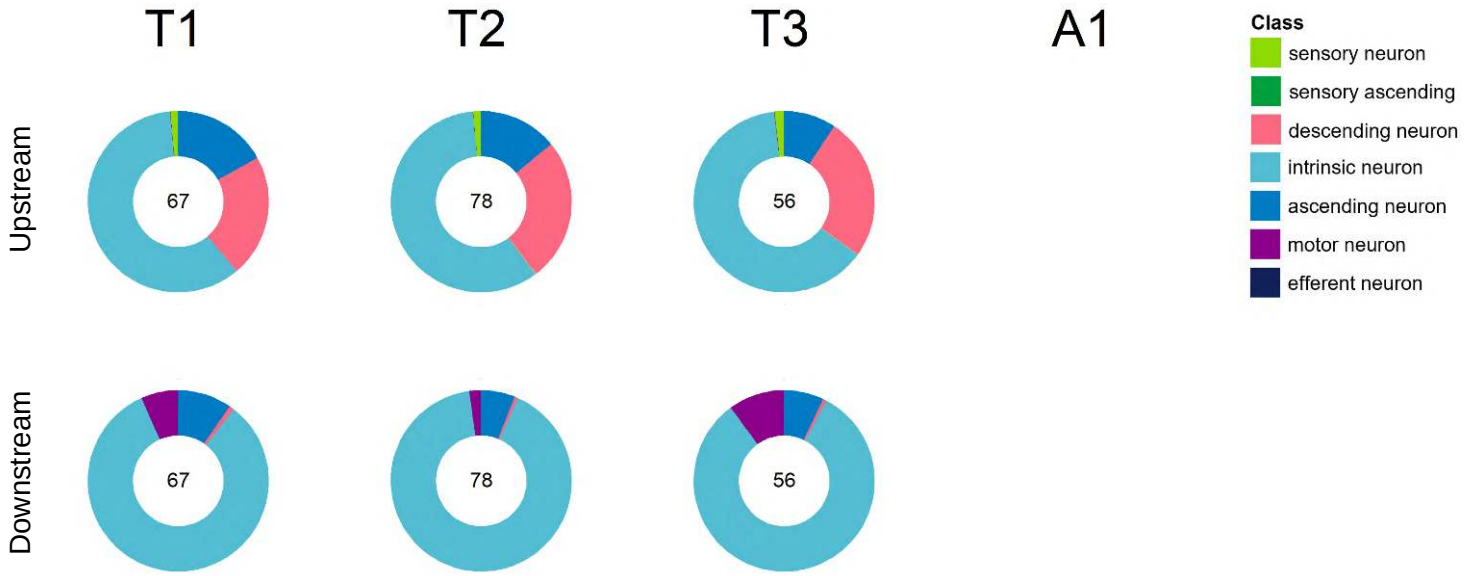

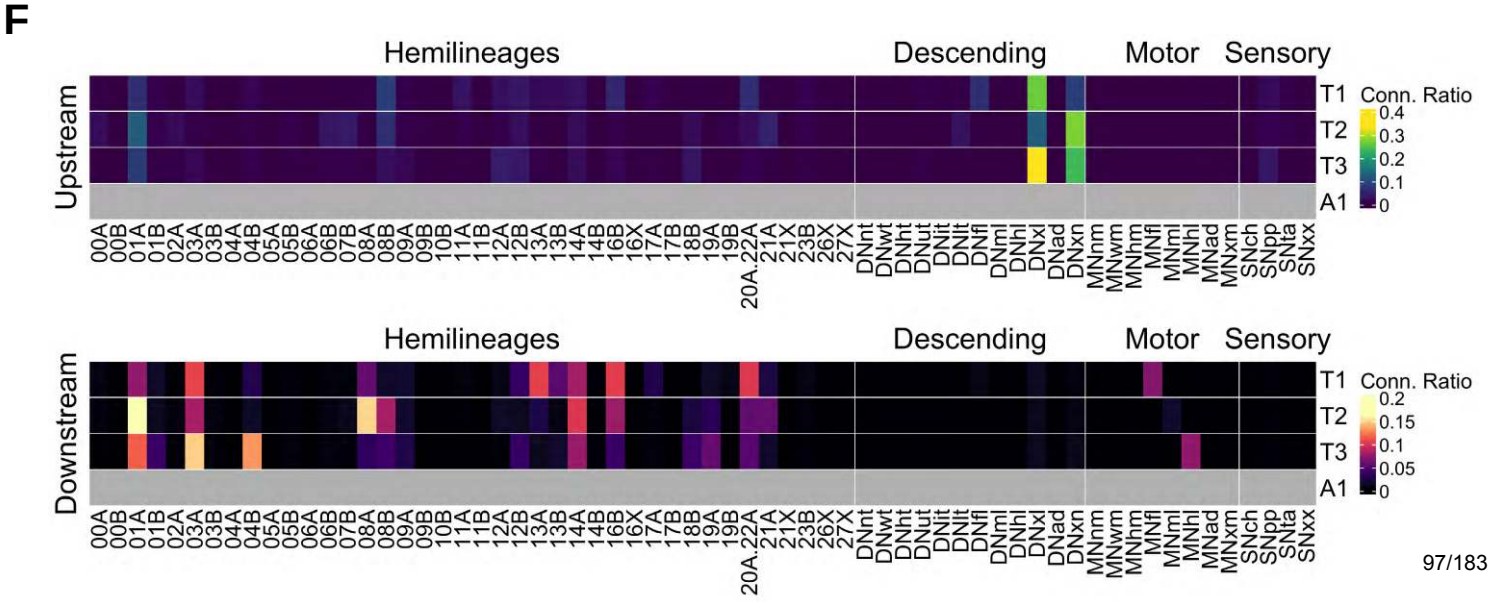

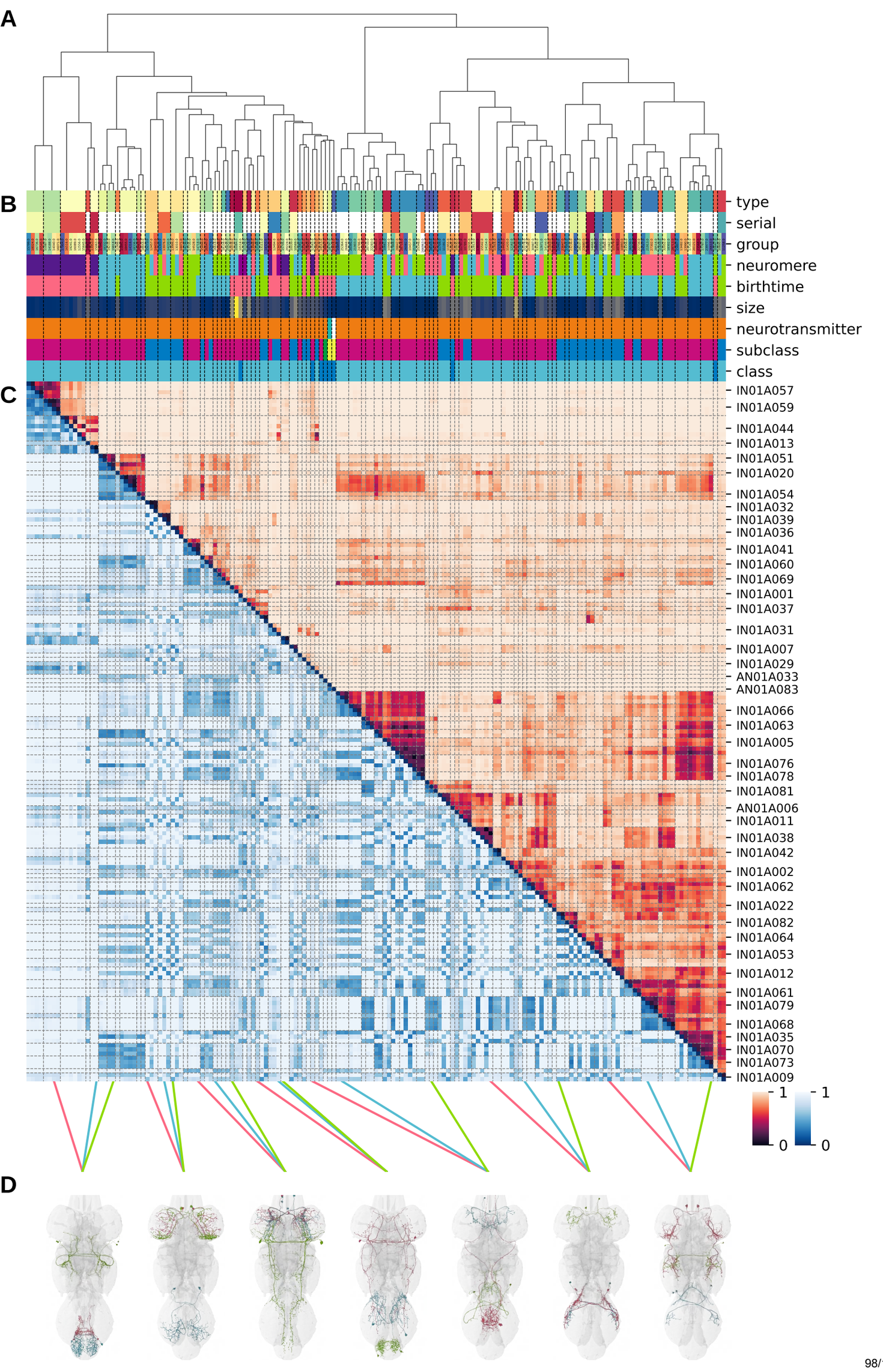
A
B
C
D
type
serial
group
neuromere
birthtime
size
neurotransmitter
subclass
class
IN01A057
IN01A059
IN01A044
IN01A013
IN01A051
IN01A020
IN01A054
IN01A032
IN01A039
IN01A036
IN01A041
IN01A060
IN01A069
IN01A001
IN01A037
IN01A031
IN01A007
IN01A029
AN01A033
AN01A083
IN01A066
IN01A063
IN01A005
IN01A076
IN01A078
IN01A081
AN01A006
IN01A011
IN01A038
IN01A042
IN01A002
IN01A062
IN01A022
IN01A082
IN01A064
IN01A053
IN01A012
IN01A061
IN01A079
IN01A068
IN01A035
IN01A070
IN01A073
IN01A009
1
0
1
0

Hemilineage 01B

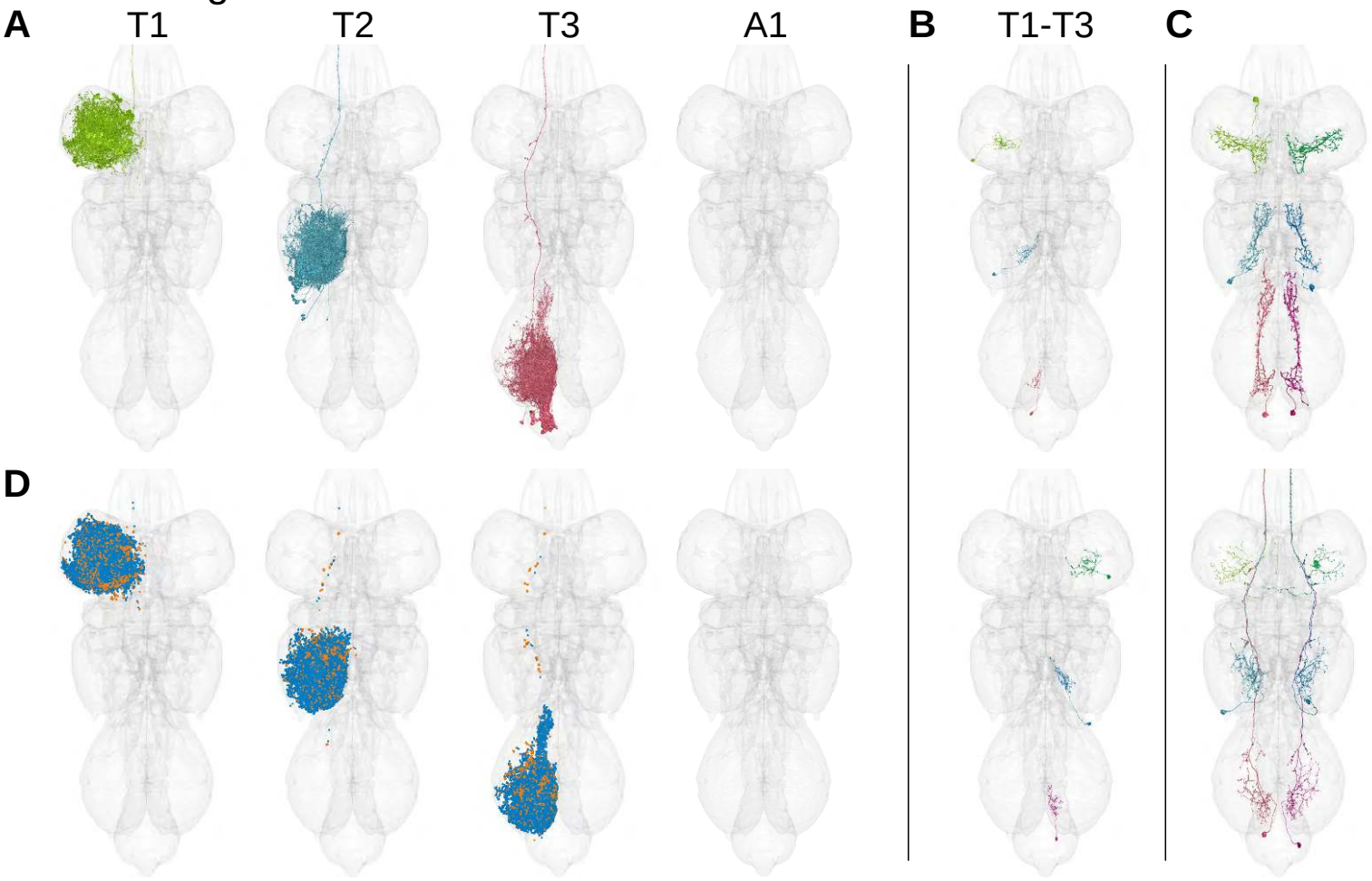

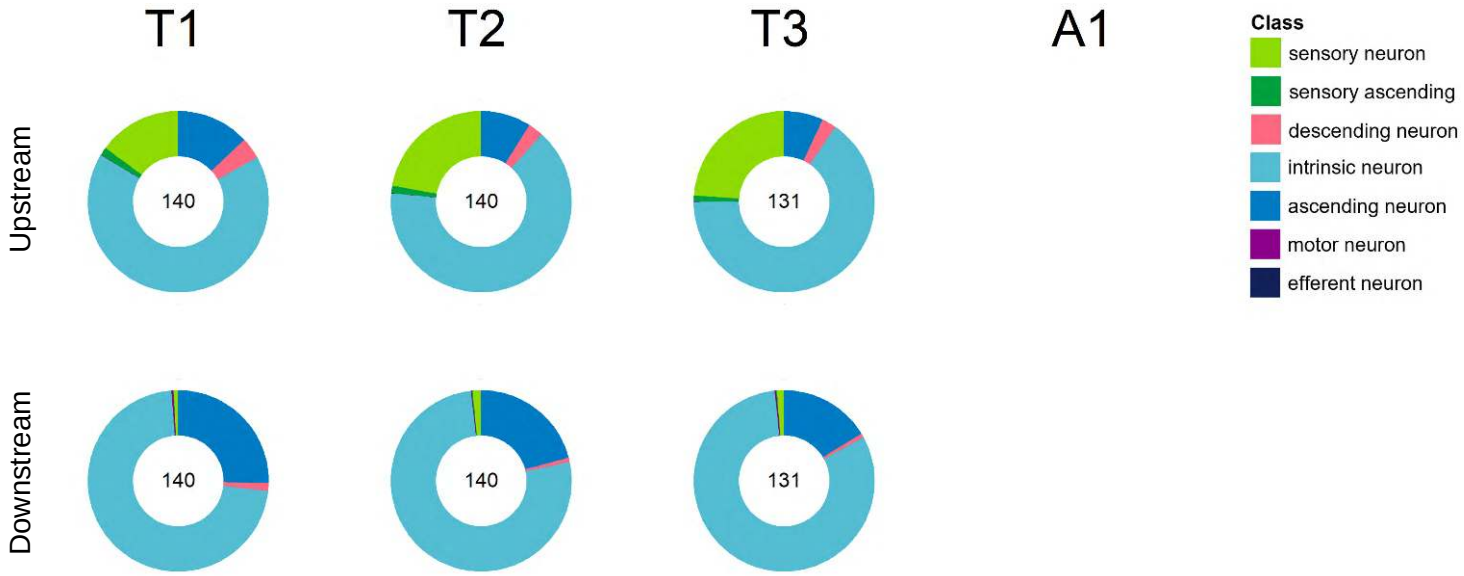

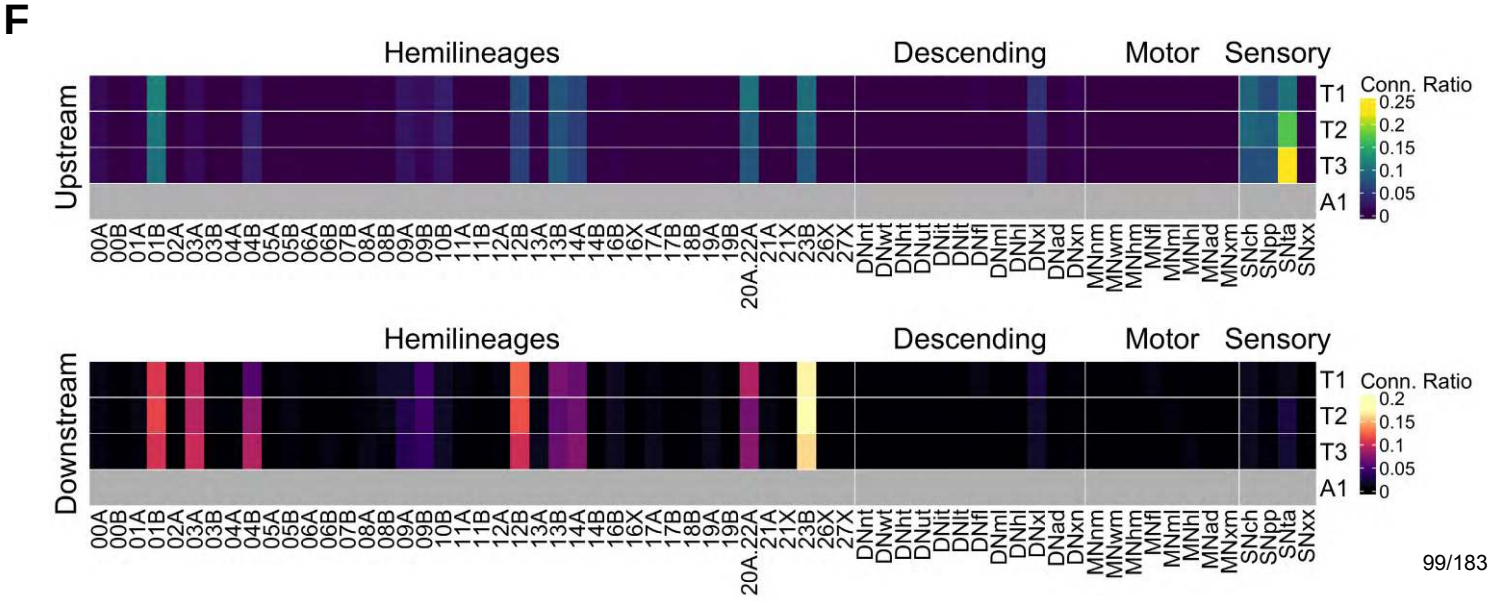

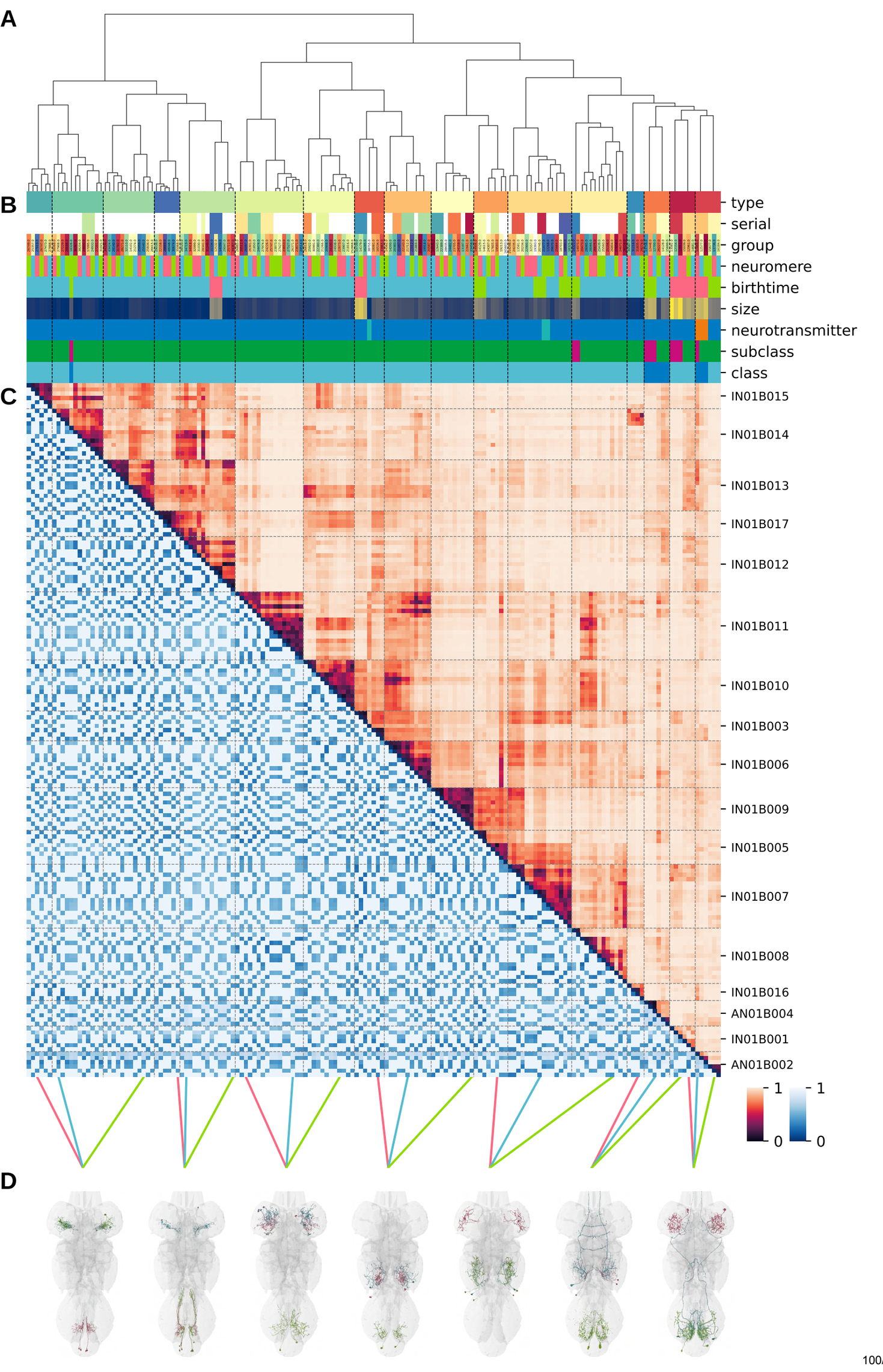
A
B
C
D
type
serial
group
neuromere
birthtime
size
neurotransmitter
subclass
class
IN01B015
IN01B014
IN01B013
IN01B017
IN01B012
IN01B011
IN01B010
IN01B003
IN01B006
IN01B009
IN01B005
IN01B007
IN01B008
IN01B016
AN01B004
IN01B001
AN01B002
1
0
1
0

Hemilineage 02A

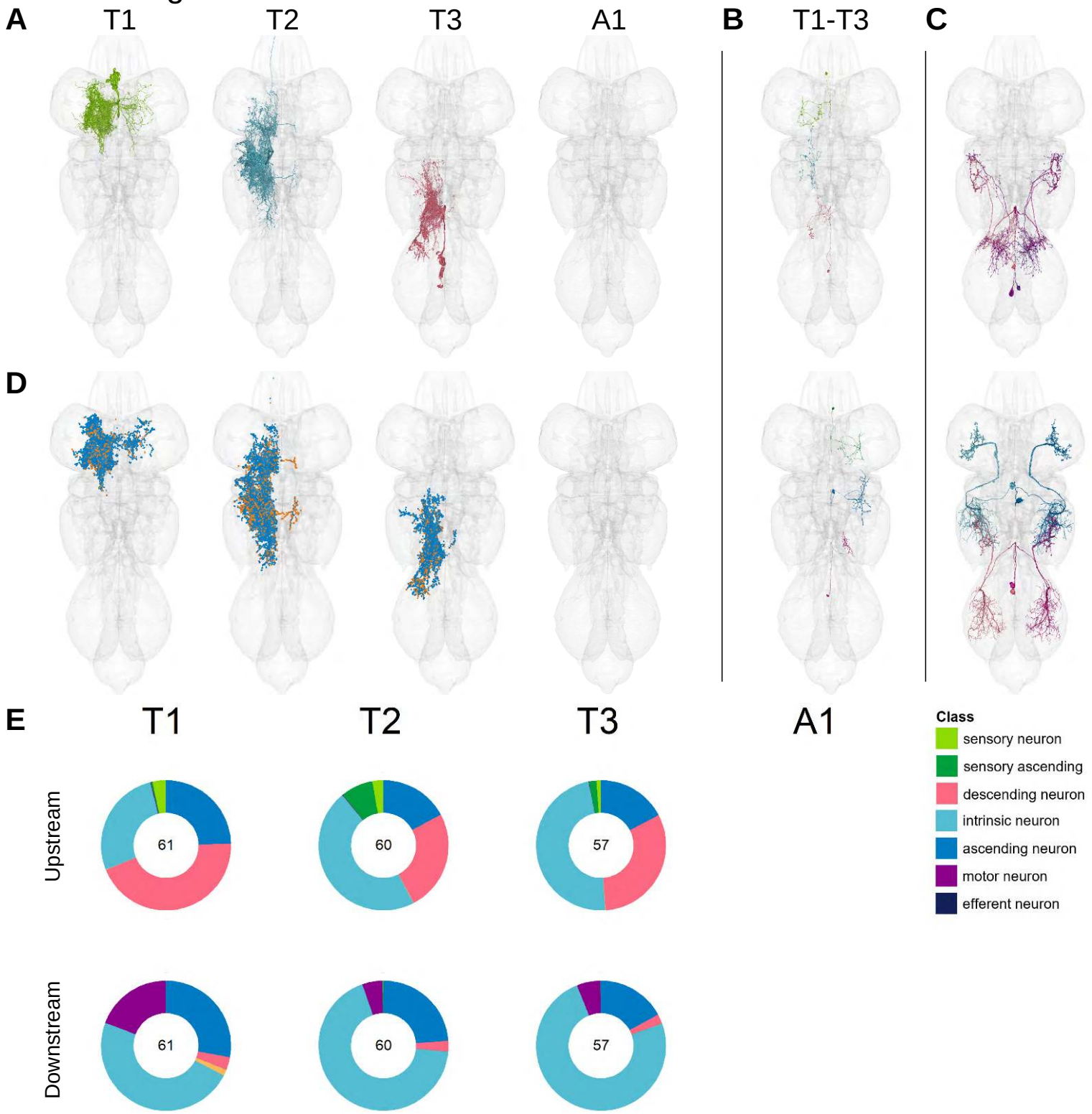

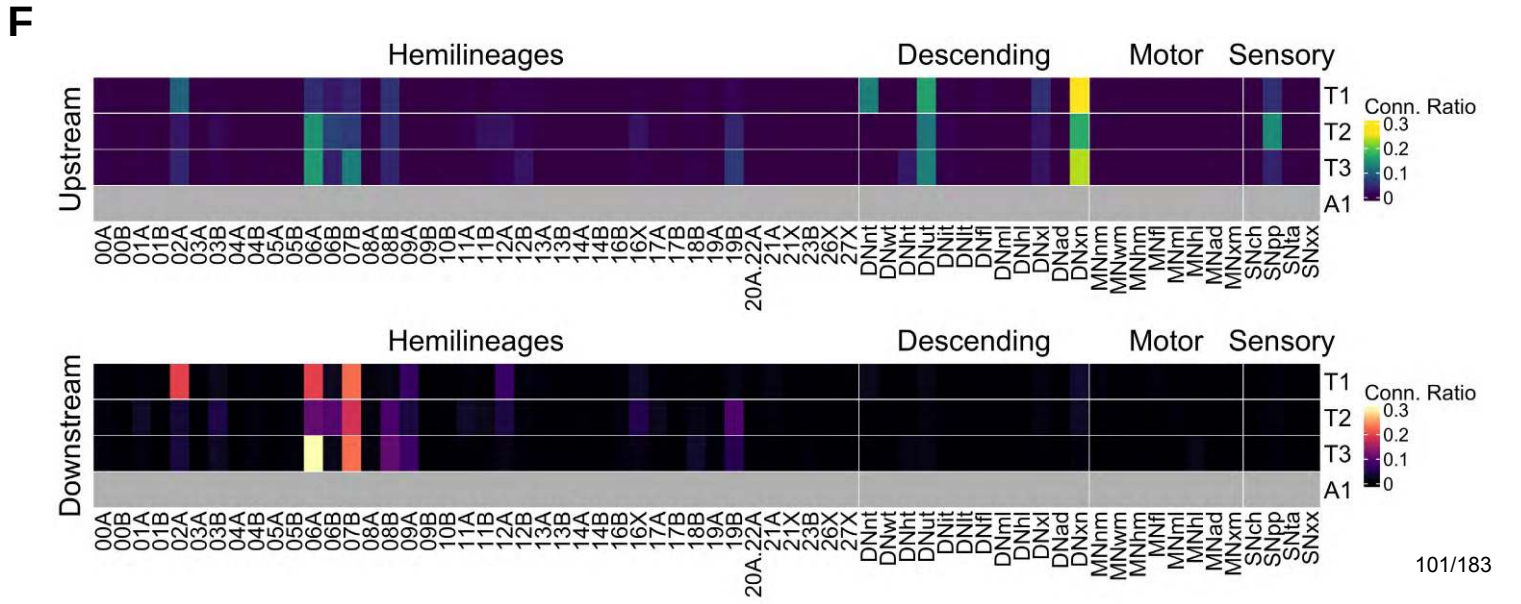

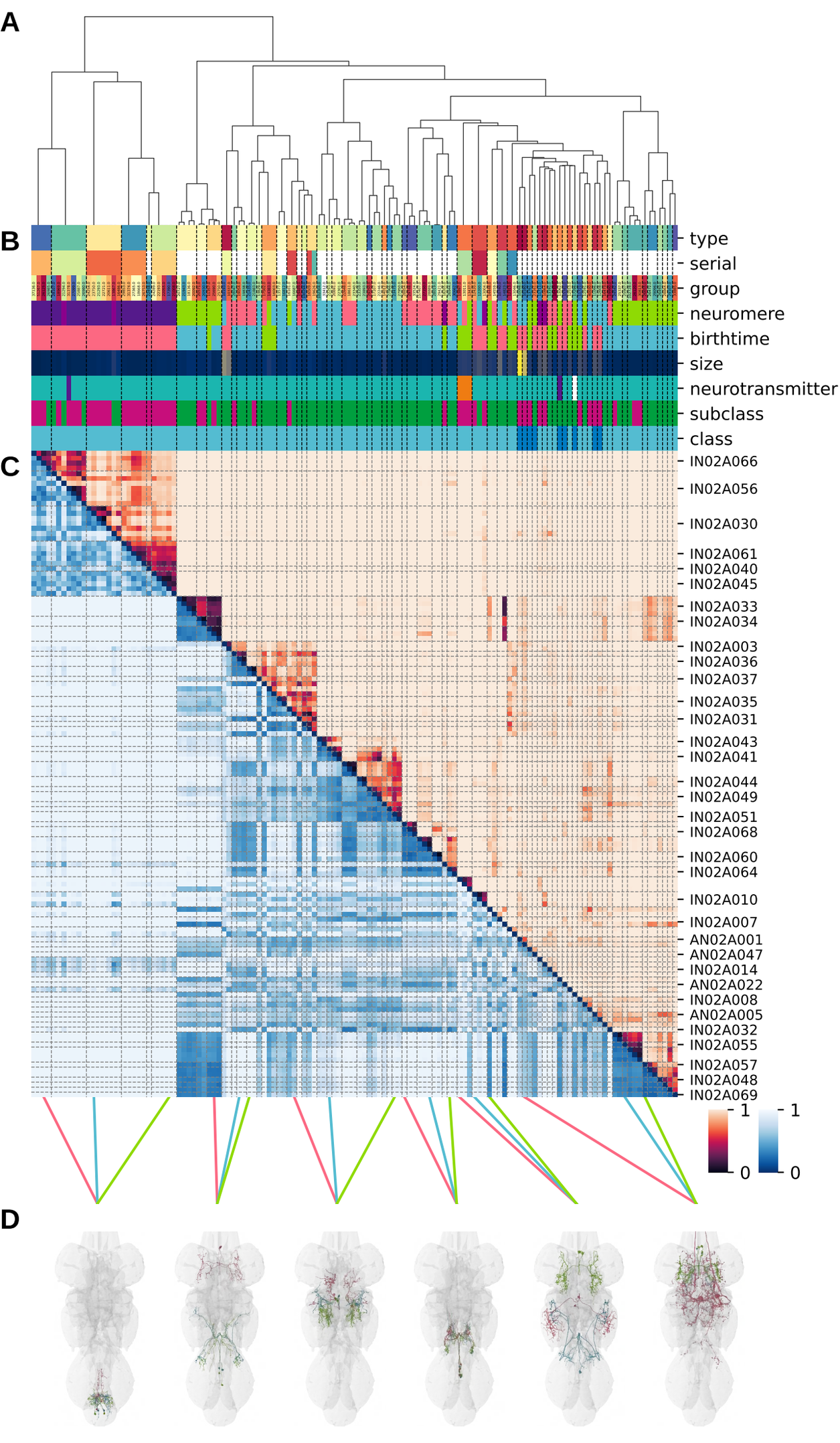
A
B
C
D
type
serial
group
neuromere
birthtime
size
neurotransmitter
subclass
class
IN02A066
IN02A056
IN02A030
IN02A061
IN02A040
IN02A045
IN02A033
IN02A034
IN02A003
IN02A036
IN02A037
IN02A035
IN02A031
IN02A043
IN02A041
IN02A044
IN02A049
IN02A051
IN02A068
IN02A060
IN02A064
IN02A010
IN02A007
AN02A001
AN02A047
IN02A014
AN02A022
IN02A008
AN02A005
IN02A032
IN02A055
IN02A057
IN02A048
IN02A069
1
0
1
0

Hemilineage 03A

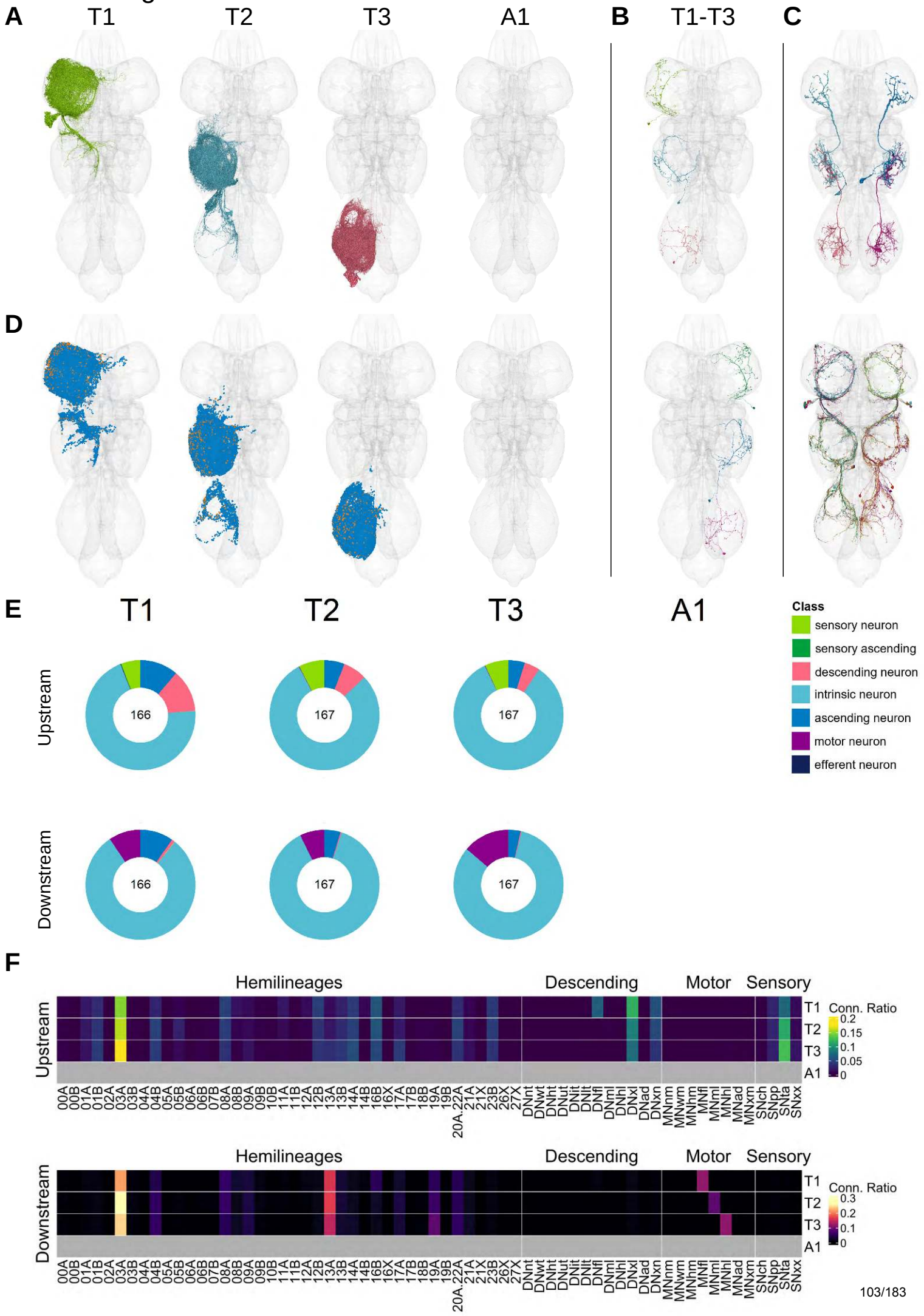

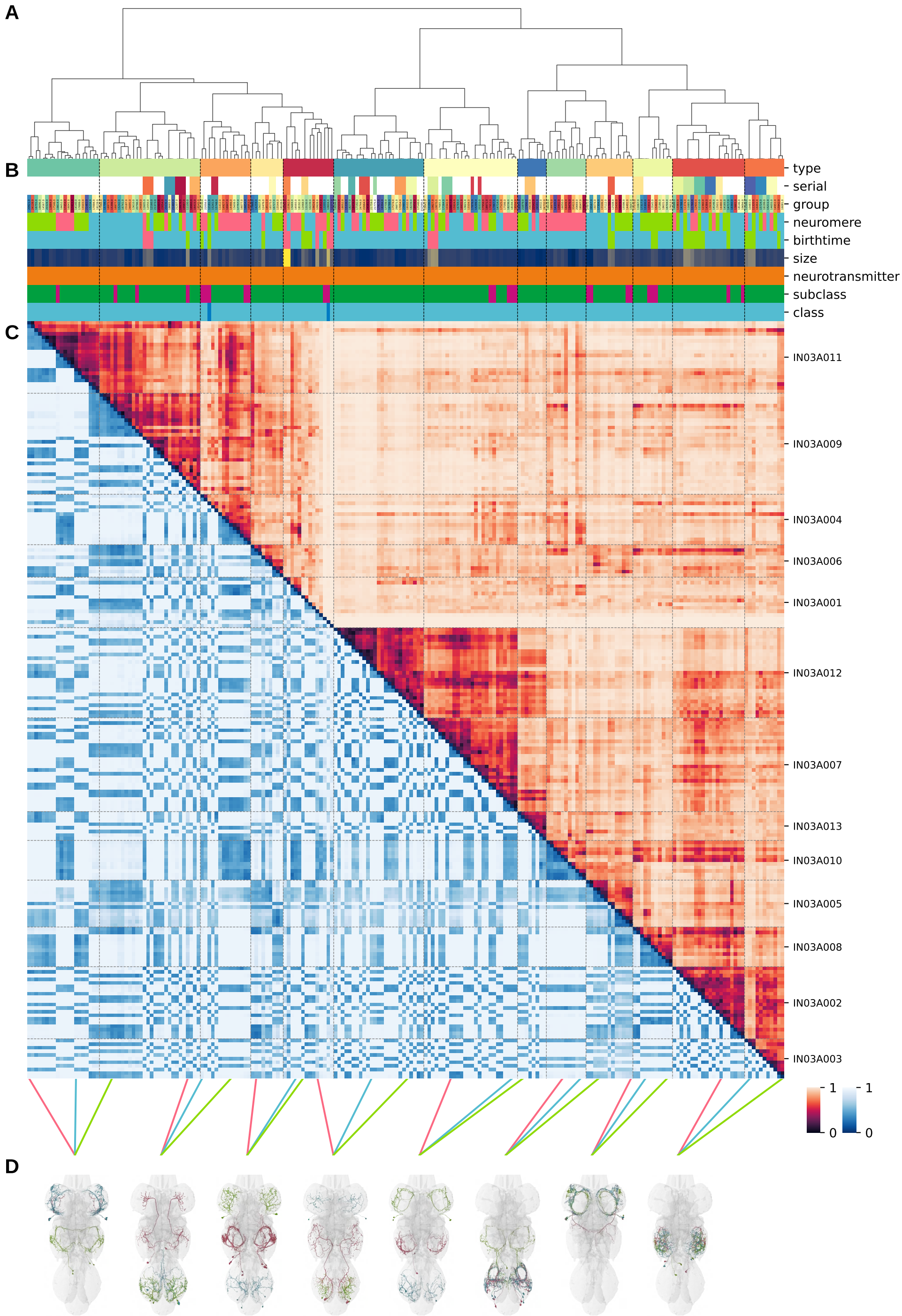
A
B
C
D
type
serial
group
neuromere
birthtime
size
neurotransmitter
subclass
class
IN03A011
IN03A009
IN03A004
IN03A006
IN03A001
IN03A012
IN03A007
IN03A013
IN03A010
IN03A005
IN03A008
IN03A002
IN03A003
1
0
1
0

Hemilineage 03B

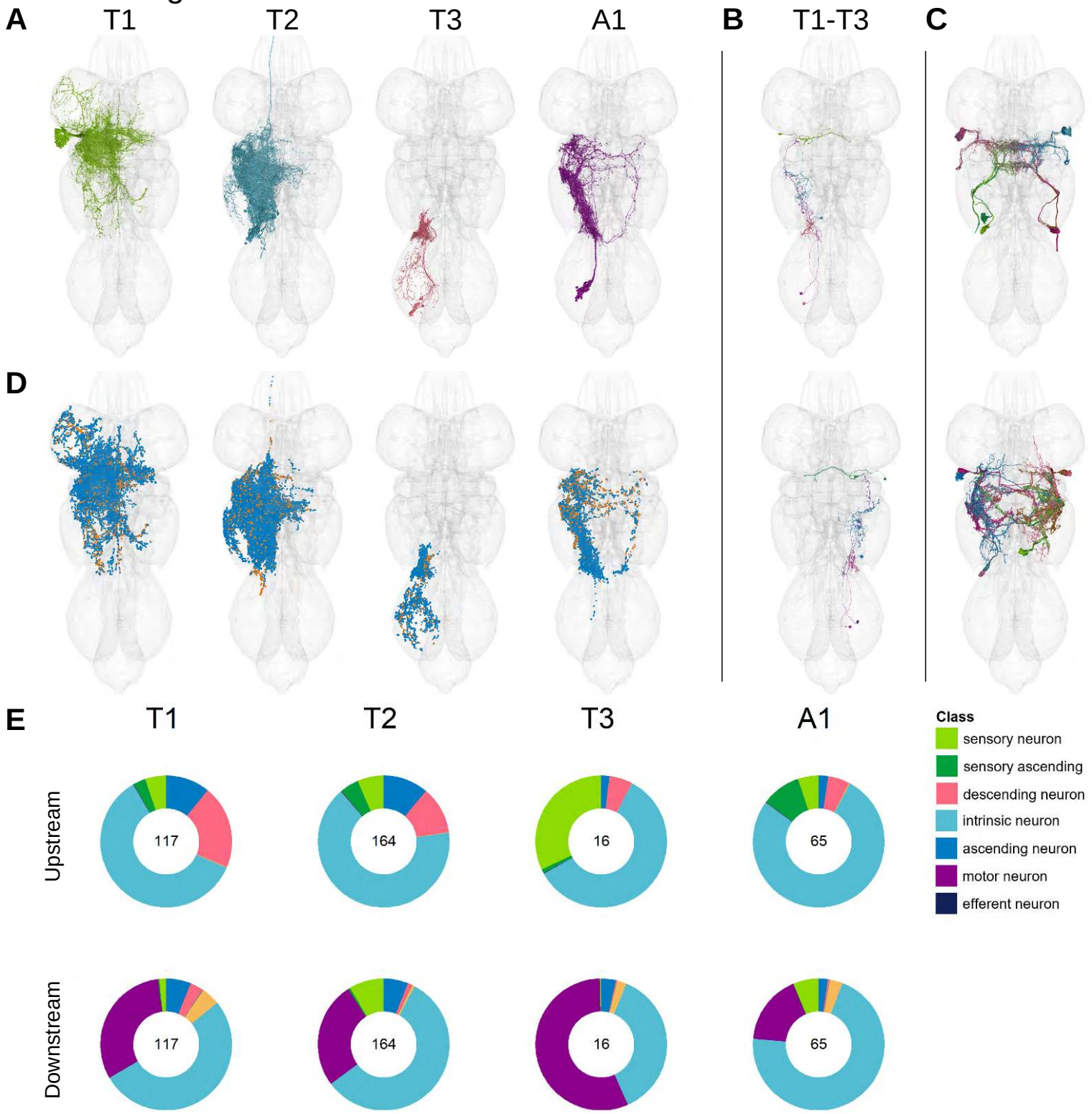

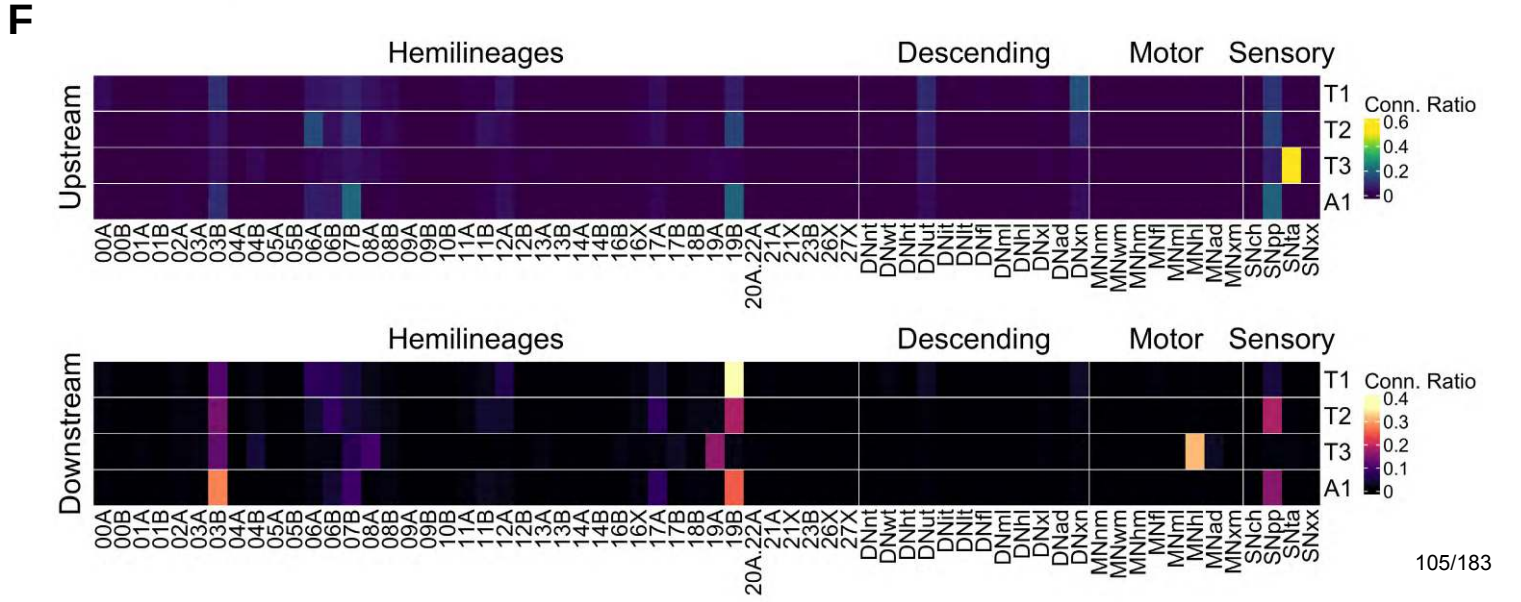

A
B
C
D
type
serial
group
neuromere
birthtime
size
neurotransmitter
subclass
class
IN03B068
IN03B059
IN03B063
IN03B060
IN03B058
IN03B062
IN03B057
IN03B066
IN03B074
IN03B076
IN03B080
IN03B070
IN03B028
IN03B034
IN03B056
IN03B075
IN03B067
IN03B069
IN03B081
IN03B061
IN03B044
IN03B054
IN03B064
IN03B071
IN03B042
IN03B015
IN03B031
IN03B022
IN03B002
IN03B018
IN03B072
IN03B001
IN03B036
IN03B033
AN03B052
IN03B009
1
0
1
0

Hemilineage 04B

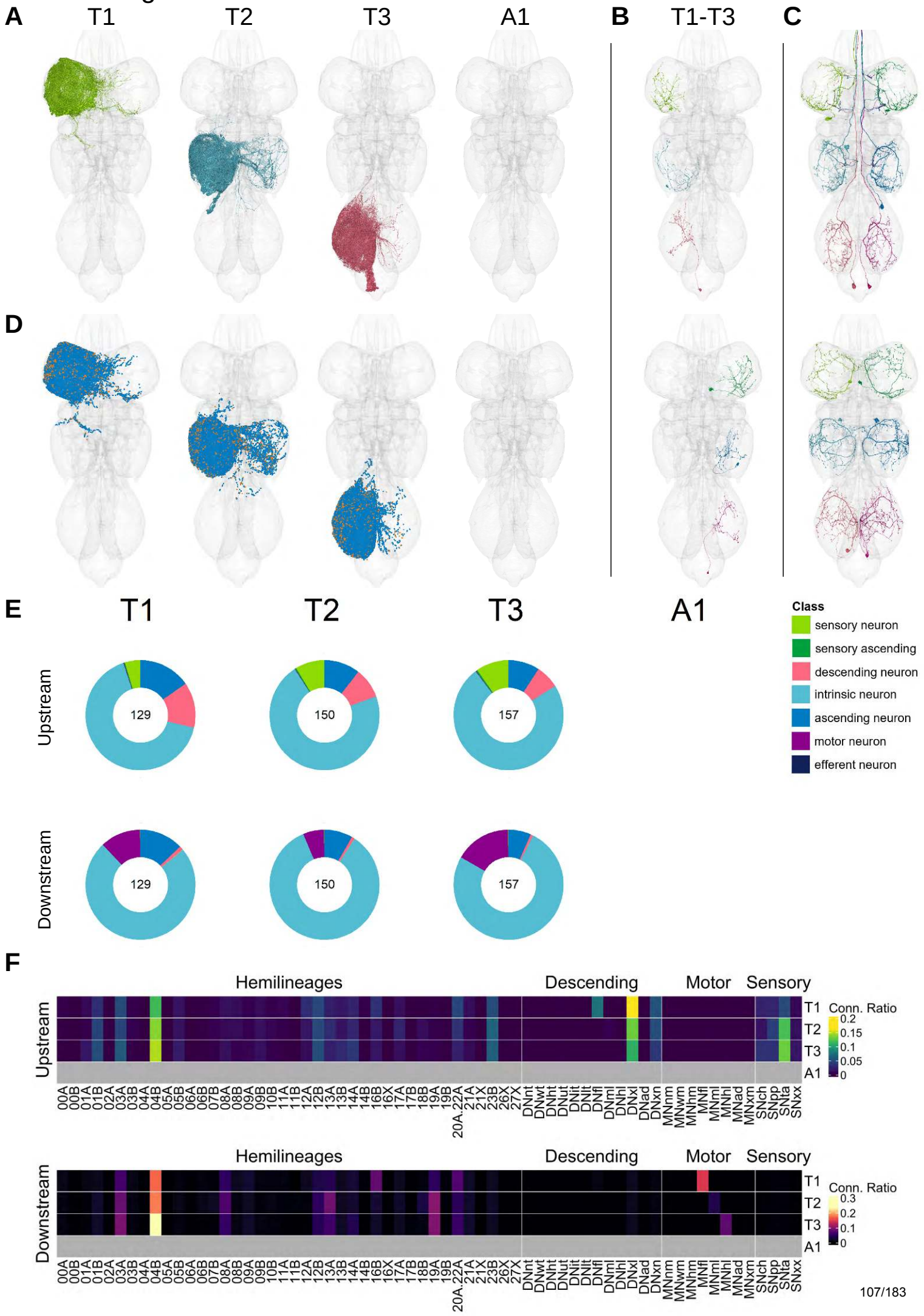

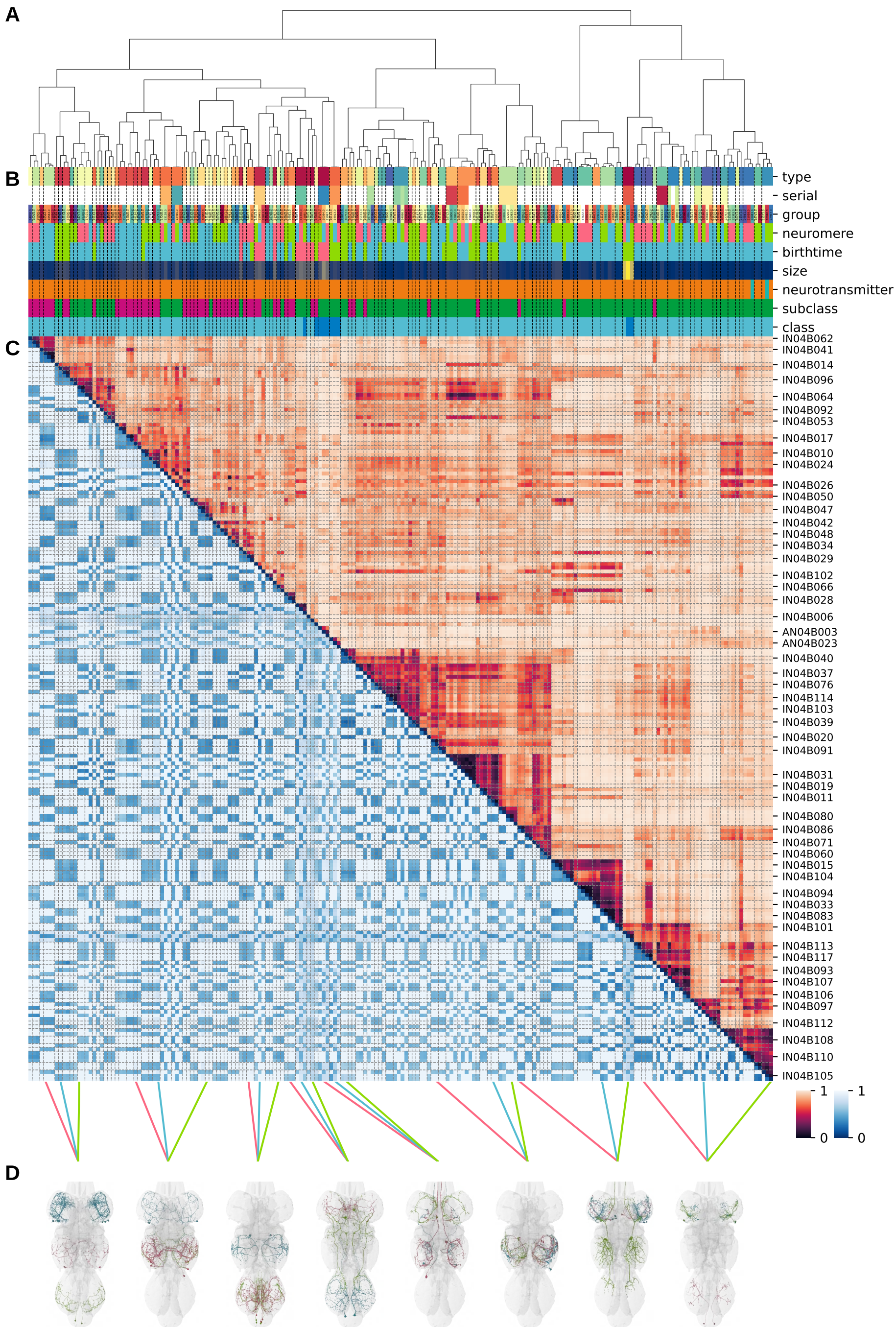
A
B
C
D
type
serial
group
neuromere
birthtime
size
neurotransmitter
subclass
class
IN04B062
IN04B041
IN04B014
IN04B096
IN04B064
IN04B092
IN04B053
IN04B017
IN04B010
IN04B024
IN04B026
IN04B050
IN04B047
IN04B042
IN04B048
IN04B034
IN04B029
IN04B102
IN04B066
IN04B028
IN04B006
AN04B003
AN04B023
IN04B040
IN04B037
IN04B076
IN04B114
IN04B103
IN04B039
IN04B020
IN04B091
IN04B031
IN04B019
IN04B011
IN04B080
IN04B086
IN04B071
IN04B060
IN04B015
IN04B104
IN04B094
IN04B033
IN04B083
IN04B101
IN04B113
IN04B117
IN04B093
IN04B107
IN04B106
IN04B097
IN04B112
IN04B108
IN04B110
IN04B105
1
0
1
0

Hemilineage 05B

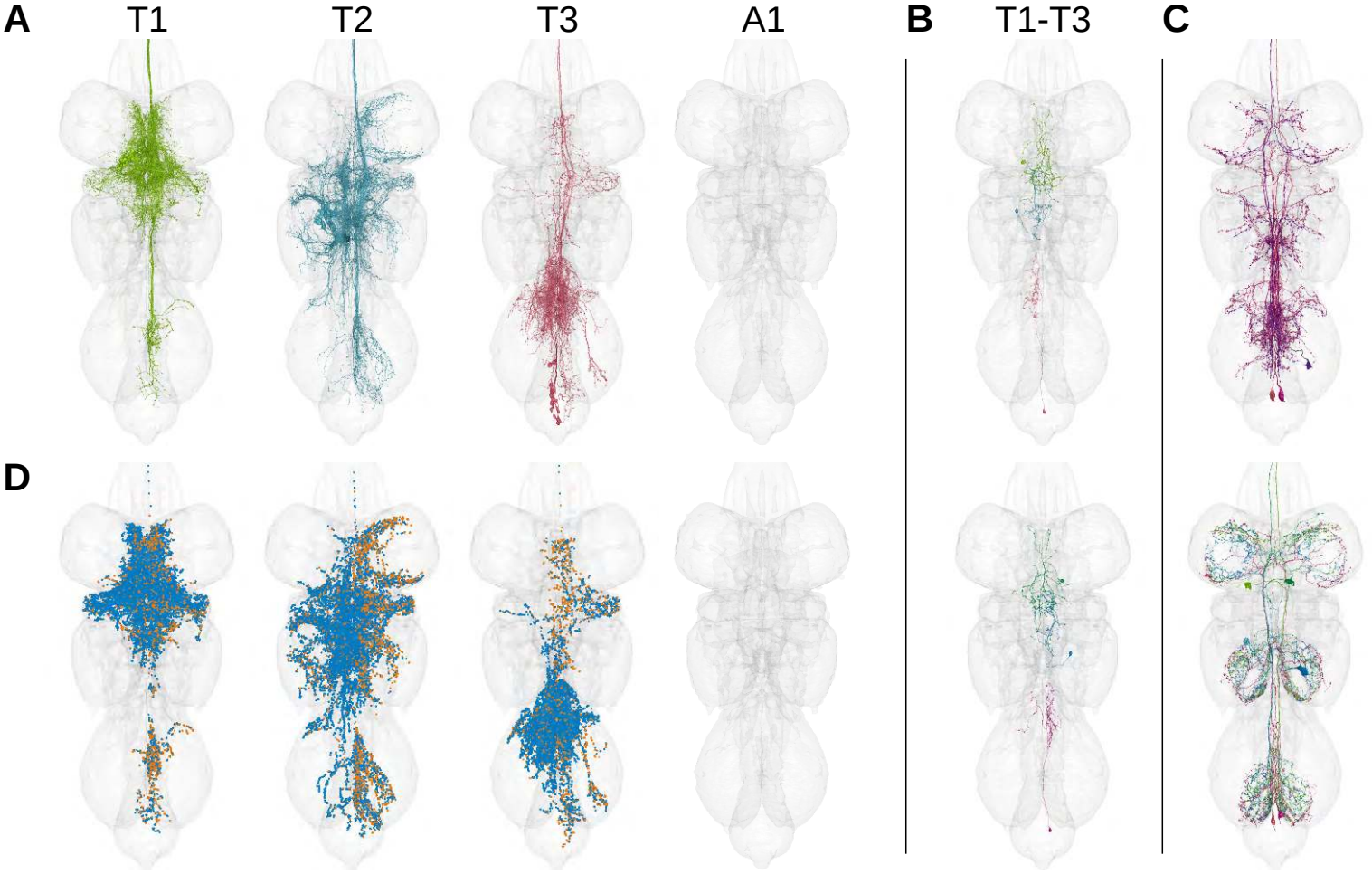

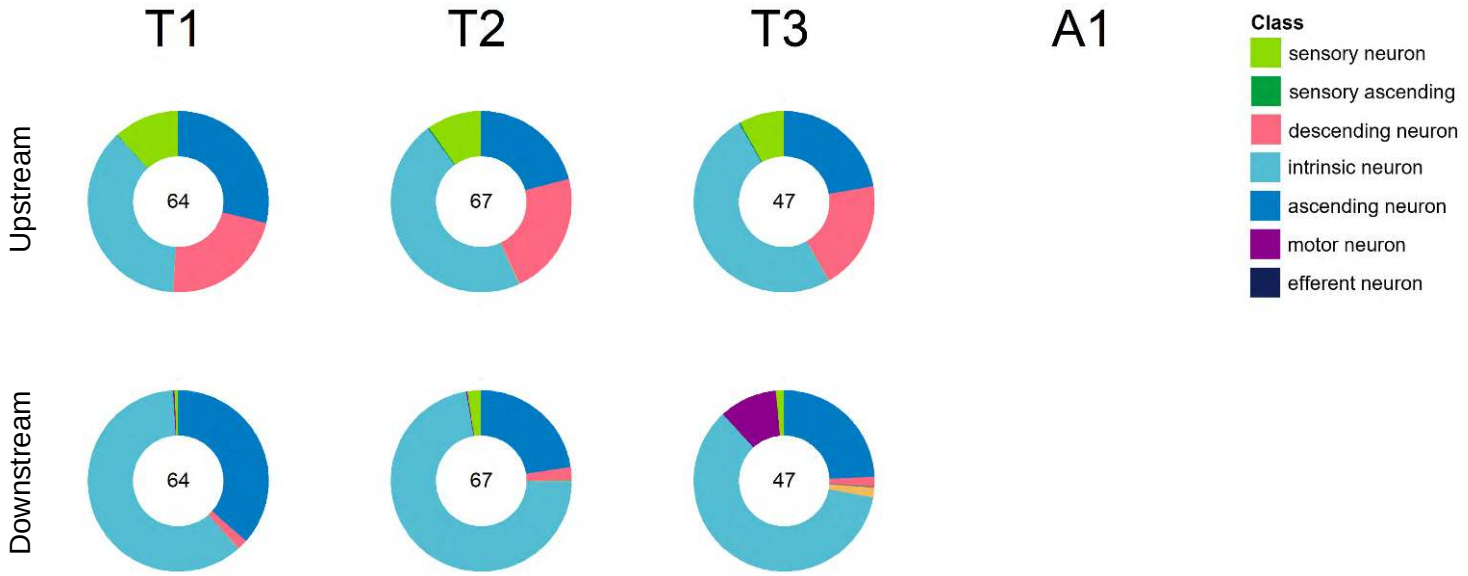

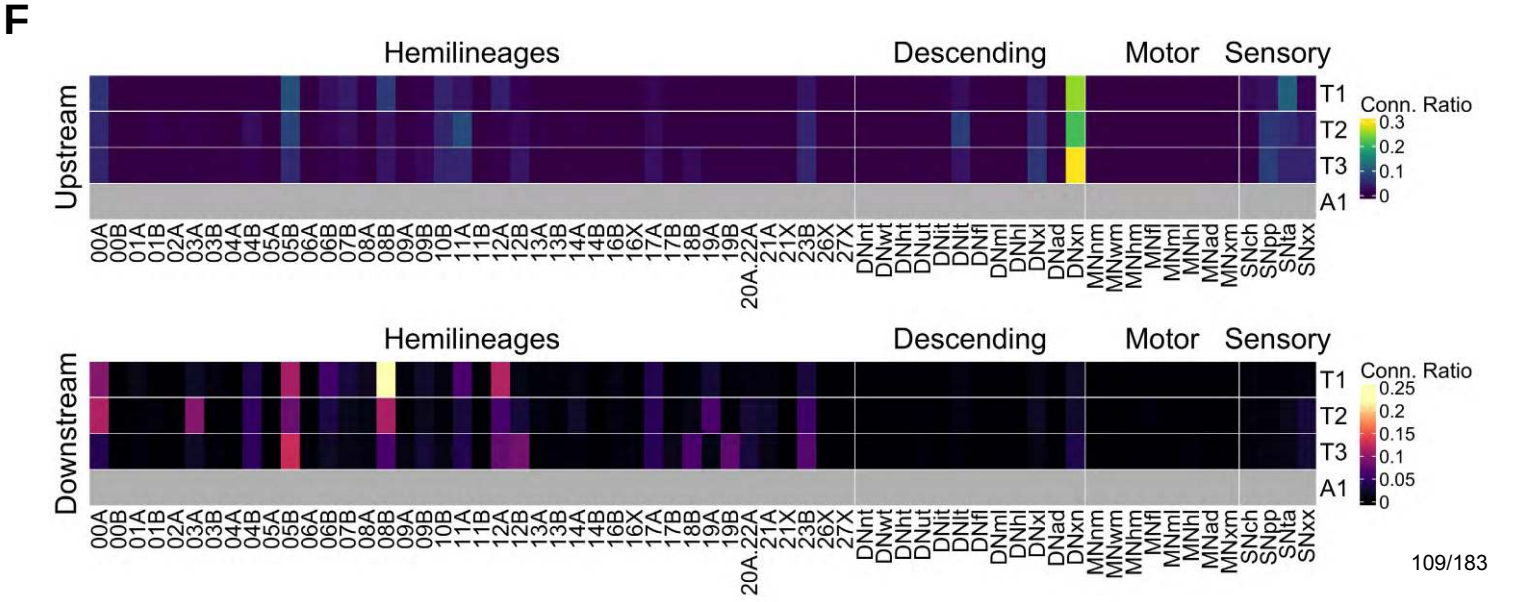

A
B
type
serial
group
neuromere
birthtime
size
neurotransmitter
subclass
class
C
AN05B034
AN05B031
AN05B027
IN05B006
IN05B017
AN05B019
AN05B004
IN05B030
AN05B002
IN05B043
IN05B045
IN05B037
IN05B035
AN05B041
AN05B010
AN05B026
AN05B029
AN05B032
AN05B009
AN05B039
IN05B046
IN05B020
AN05B015
IN05B023
IN05B007
AN05B016
AN05B001
1
0
1
0
D

Hemilineage 06A

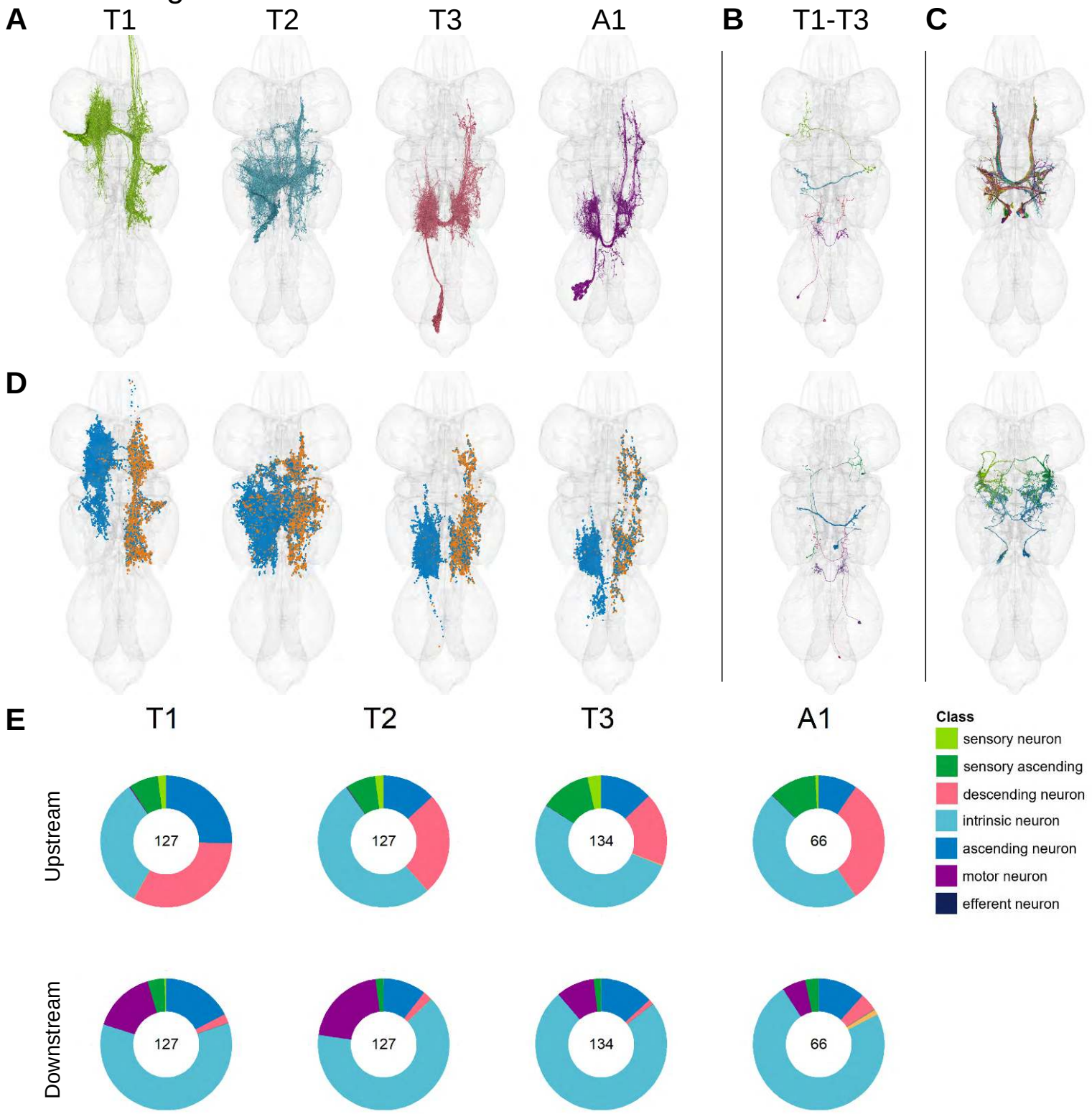

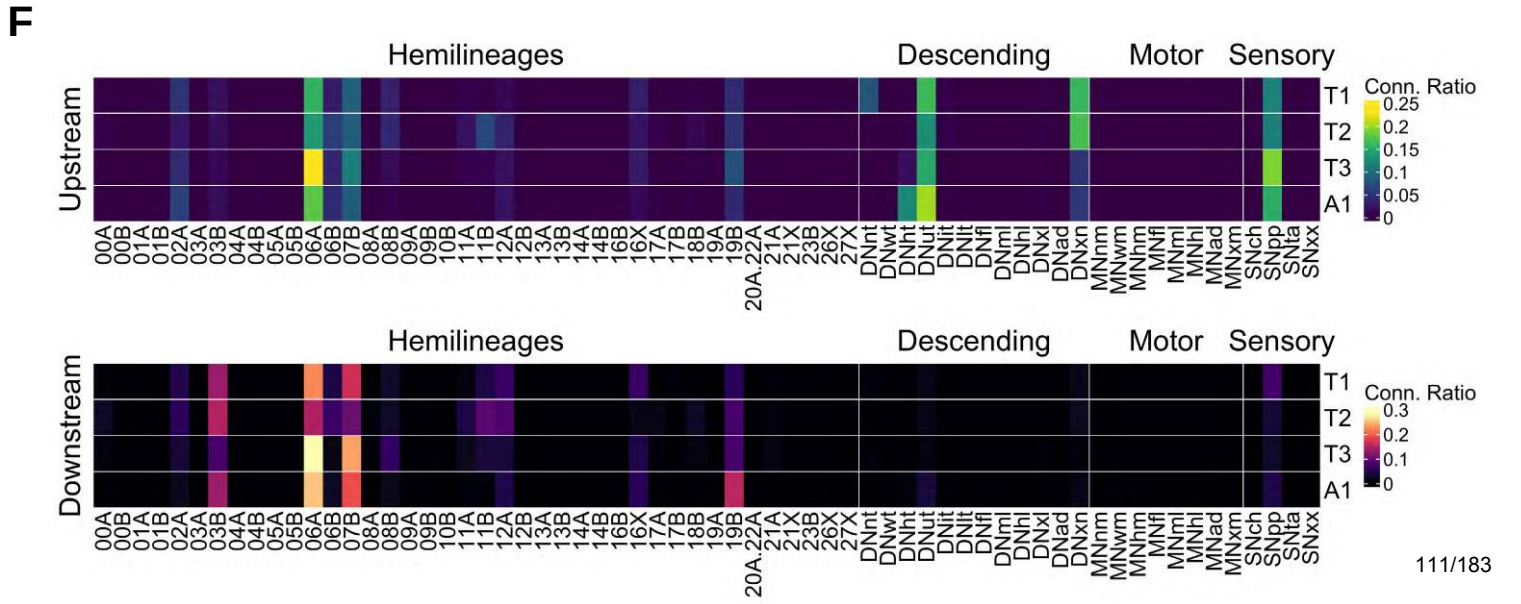

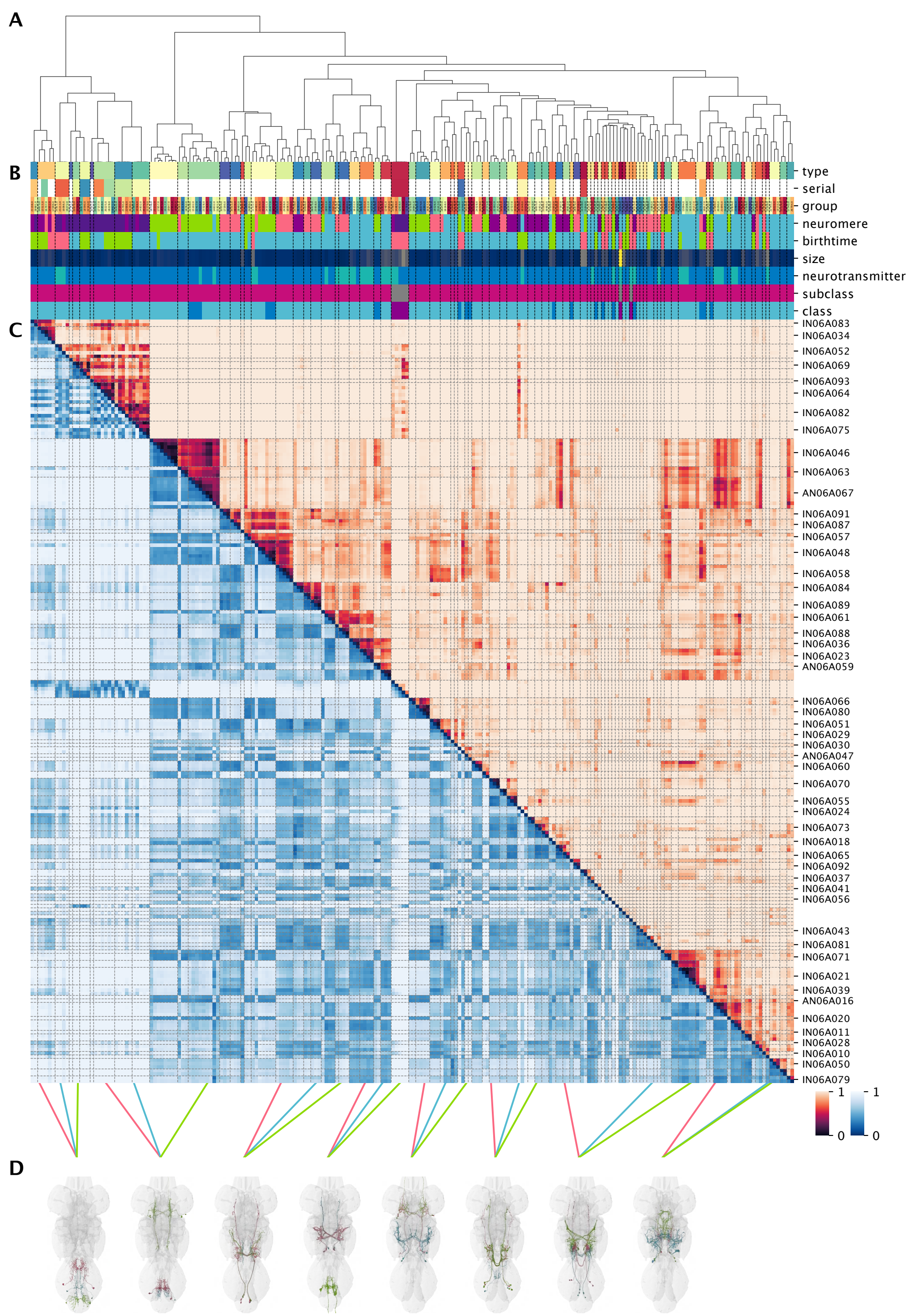
A
B
C
D
type
serial
group
neuromere
birthtime
size
neurotransmitter
subclass
class
IN06A083
IN06A034
IN06A052
IN06A069
IN06A093
IN06A064
IN06A082
IN06A075
IN06A046
IN06A063
AN06A067
IN06A091
IN06A087
IN06A057
IN06A048
IN06A058
IN06A084
IN06A089
IN06A061
IN06A088
IN06A036
IN06A023
AN06A059
IN06A066
IN06A080
IN06A051
IN06A029
IN06A030
AN06A047
IN06A060
IN06A070
IN06A055
IN06A024
IN06A073
IN06A018
IN06A065
IN06A092
IN06A037
IN06A041
IN06A056
IN06A043
IN06A081
IN06A071
IN06A021
IN06A039
AN06A016
IN06A020
IN06A011
IN06A028
IN06A010
IN06A050
IN06A079
1
0
1
0

Hemilineage 06B

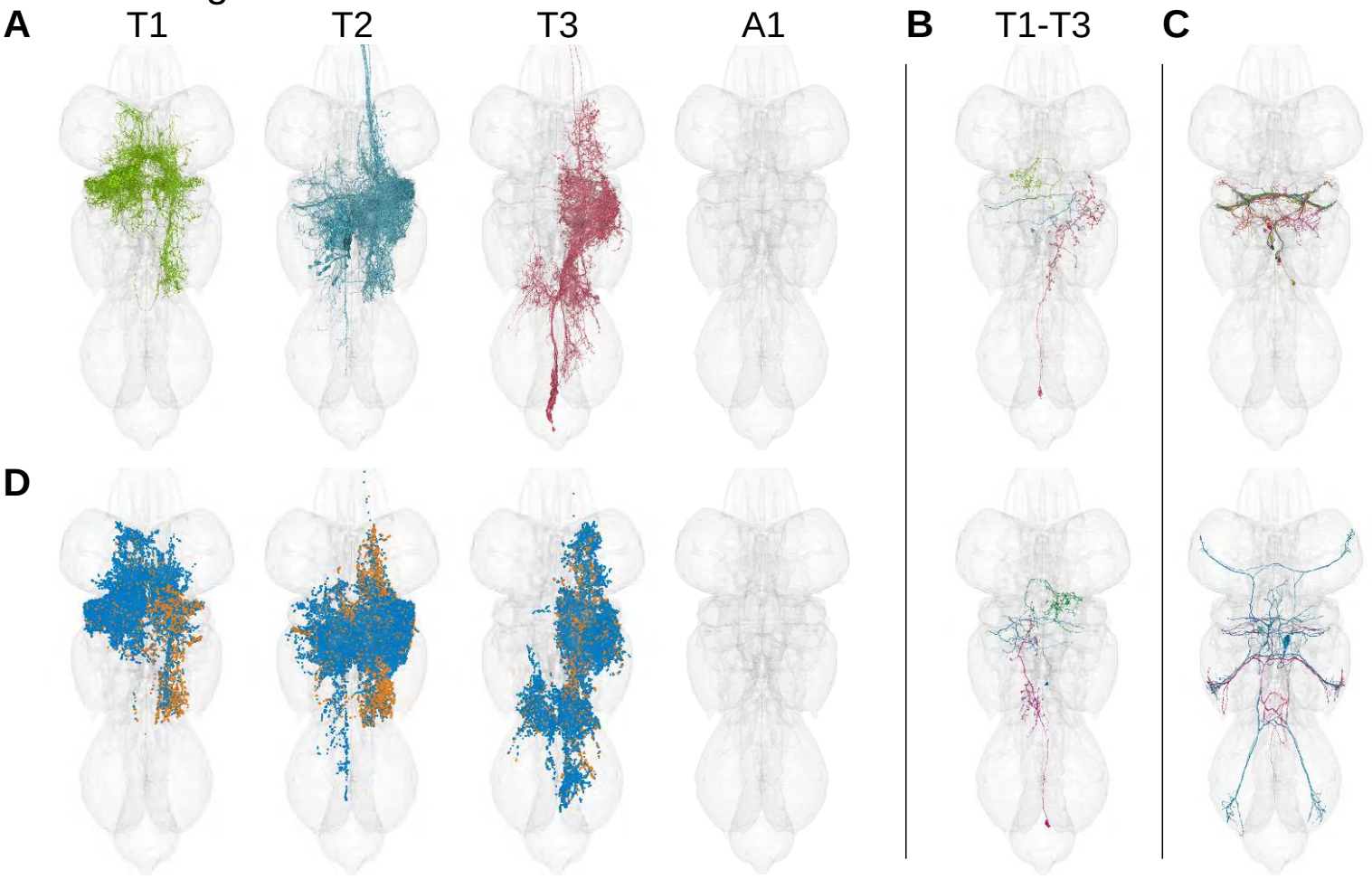

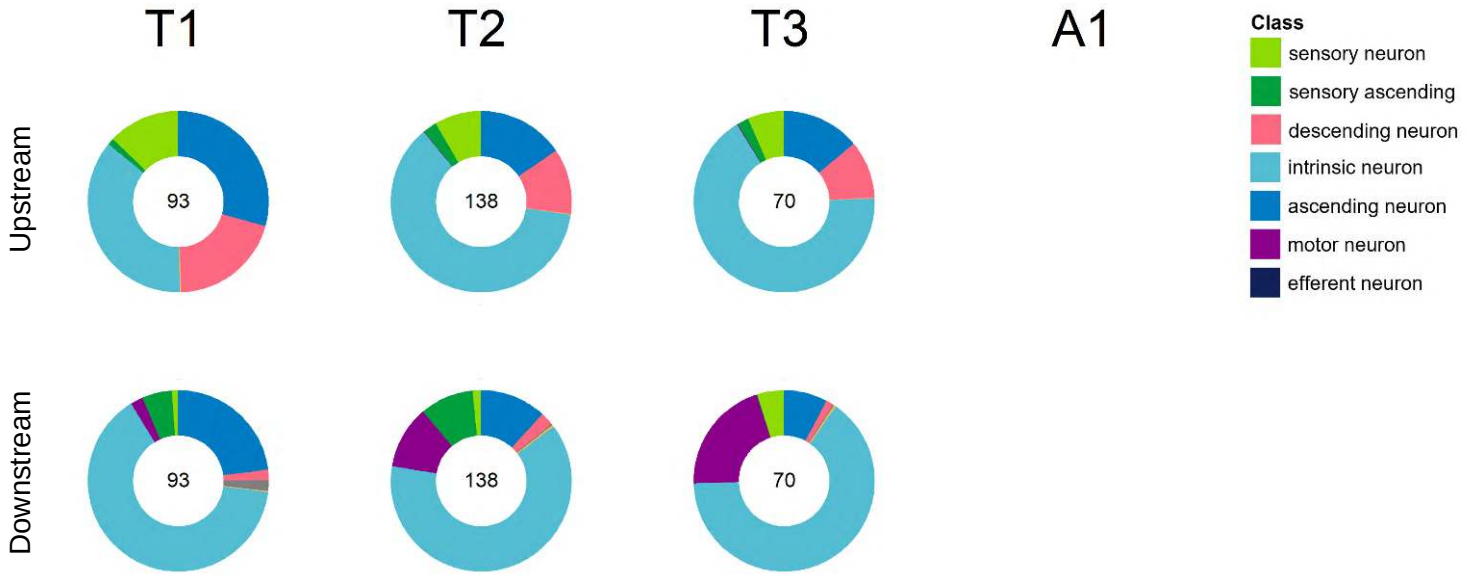

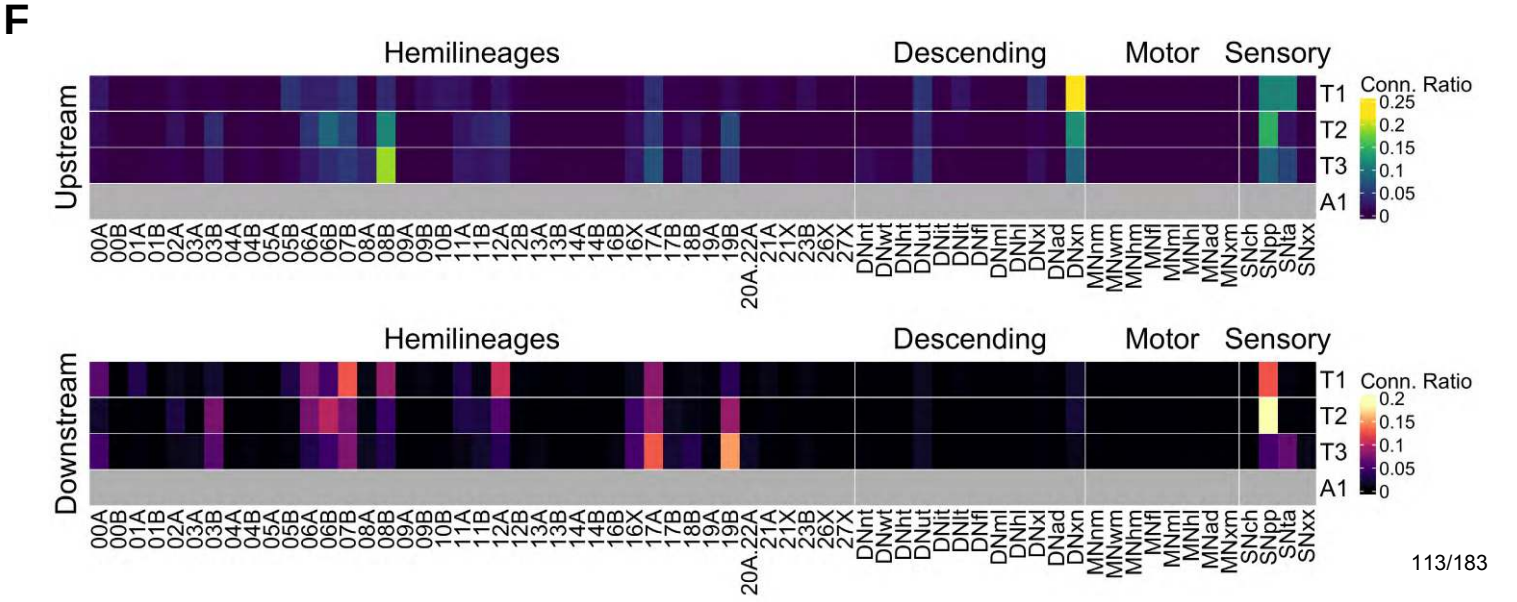

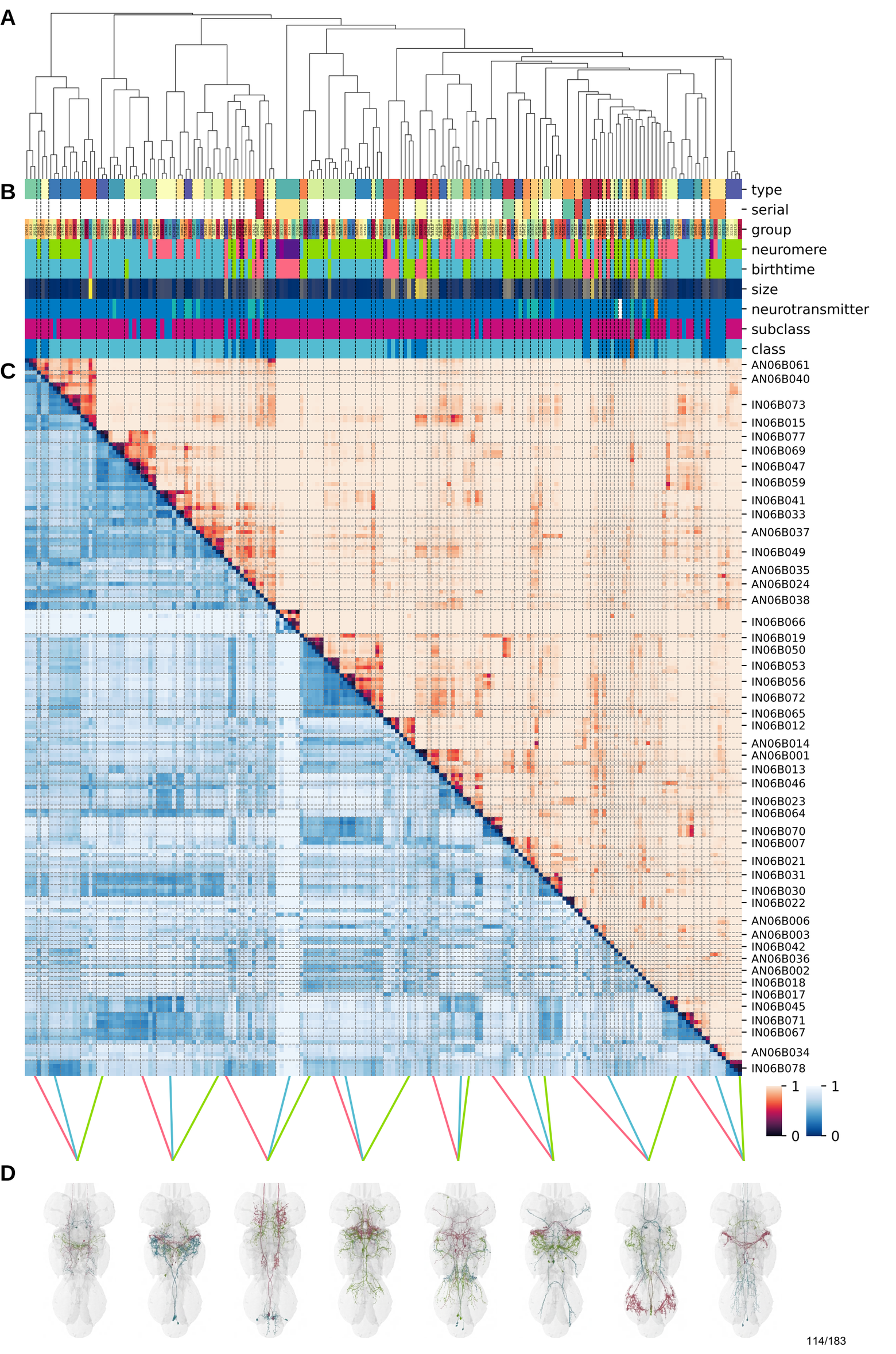
A
B
C
D
type
serial
group
neuromere
birthtime
size
neurotransmitter
subclass
class
AN06B061
AN06B040
IN06B073
IN06B015
IN06B077
IN06B069
IN06B047
IN06B059
IN06B041
IN06B033
AN06B037
IN06B049
AN06B035
AN06B024
AN06B038
IN06B066
IN06B019
IN06B050
IN06B053
IN06B056
IN06B072
IN06B065
IN06B012
AN06B014
AN06B001
IN06B013
IN06B046
IN06B023
IN06B064
IN06B070
IN06B007
IN06B021
IN06B031
IN06B030
IN06B022
AN06B006
AN06B003
IN06B042
AN06B036
AN06B002
IN06B018
IN06B017
IN06B045
IN06B071
IN06B067
AN06B034
IN06B078
1
0
1
0

Hemilineage 07B

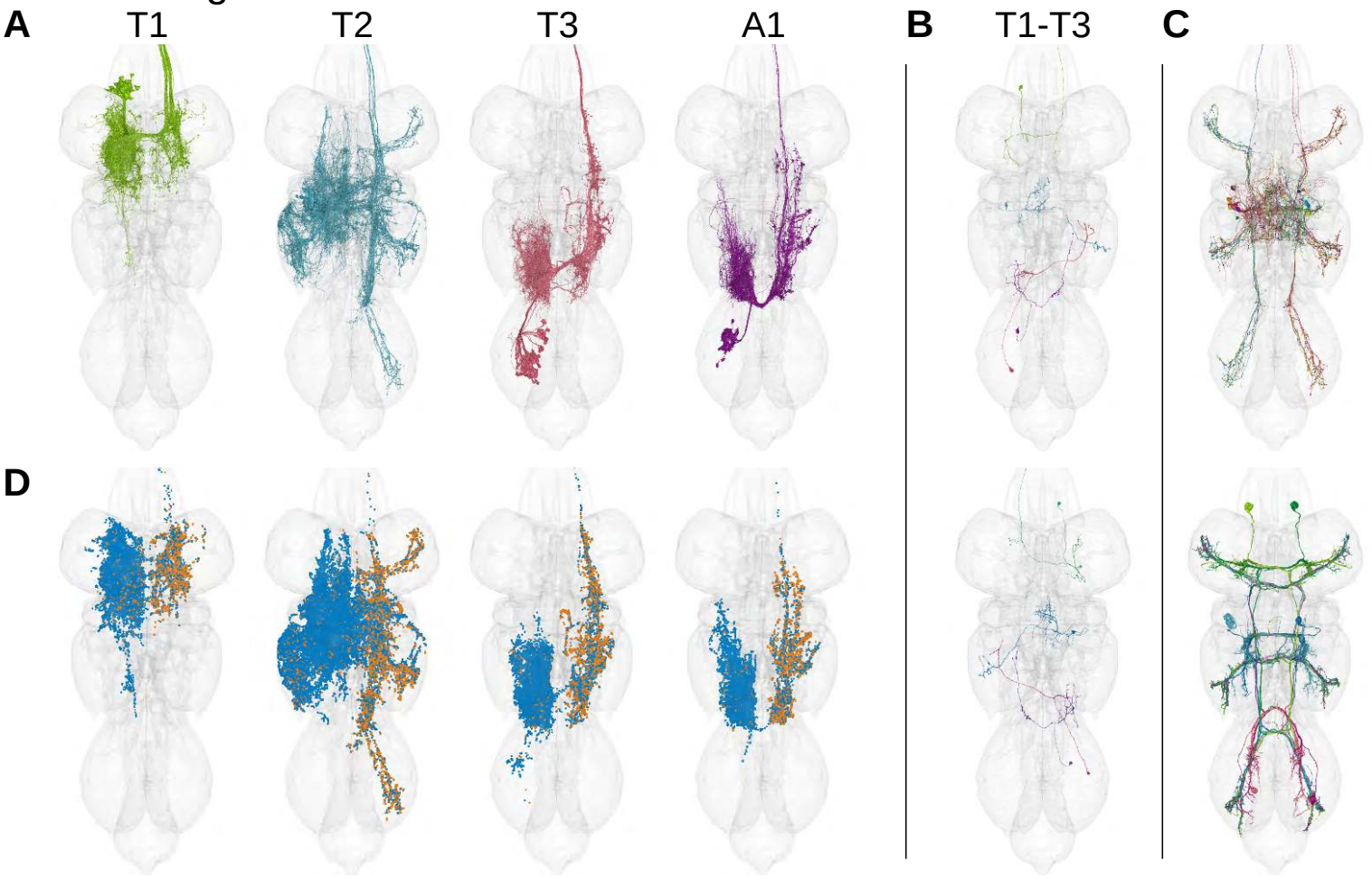

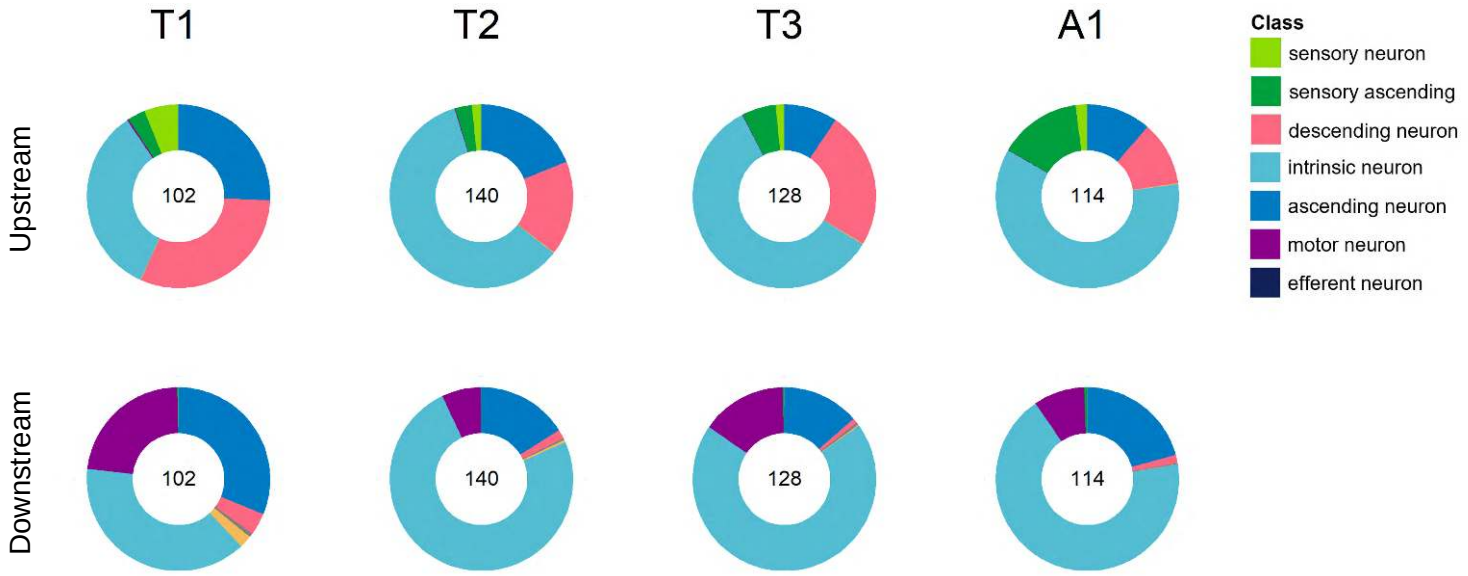

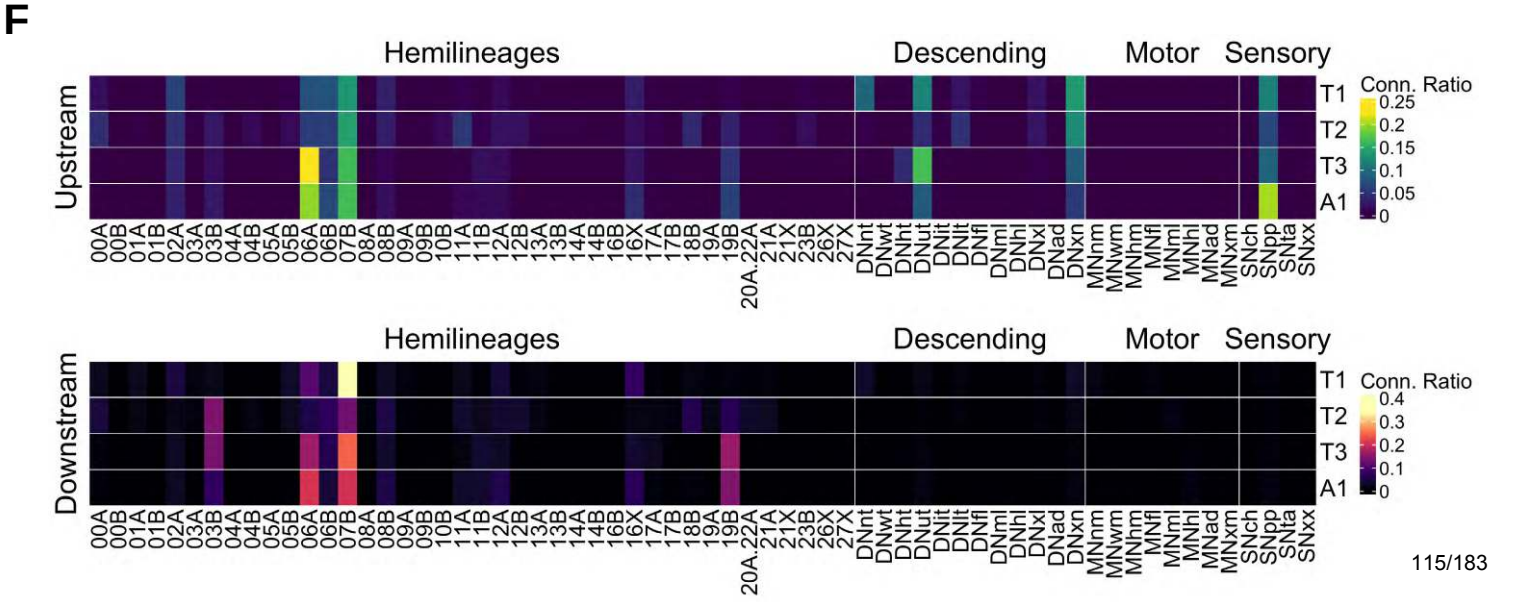

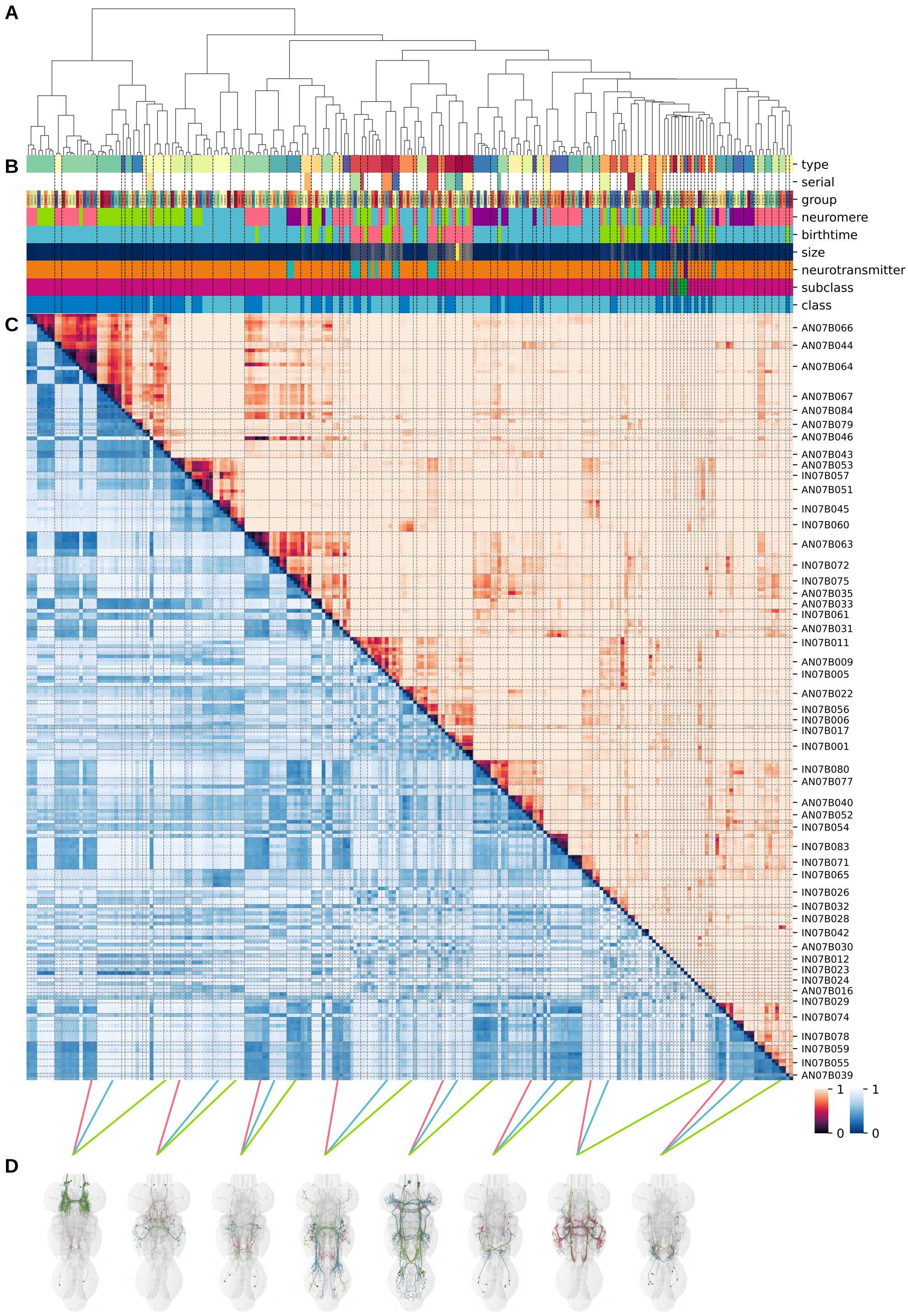
A
B
C
D
type
serial
group
neuromere
birthtime
size
neurotransmitter
subclass
class
AN07B066
AN07B044
AN07B064
AN07B067
AN07B084
AN07B079
AN07B046
AN07B043
AN07B053
IN07B057
AN07B051
IN07B045
IN07B060
AN07B063
IN07B072
IN07B075
AN07B035
AN07B033
IN07B061
AN07B031
IN07B011
AN07B009
IN07B005
AN07B022
IN07B056
IN07B006
IN07B017
IN07B001
IN07B080
AN07B077
AN07B040
AN07B052
IN07B054
IN07B083
IN07B071
IN07B065
IN07B026
IN07B032
IN07B028
IN07B042
AN07B030
IN07B012
IN07B023
IN07B024
AN07B016
IN07B029
IN07B074
IN07B078
IN07B059
IN07B055
AN07B039
1
0
1
0

Hemilineage 08A

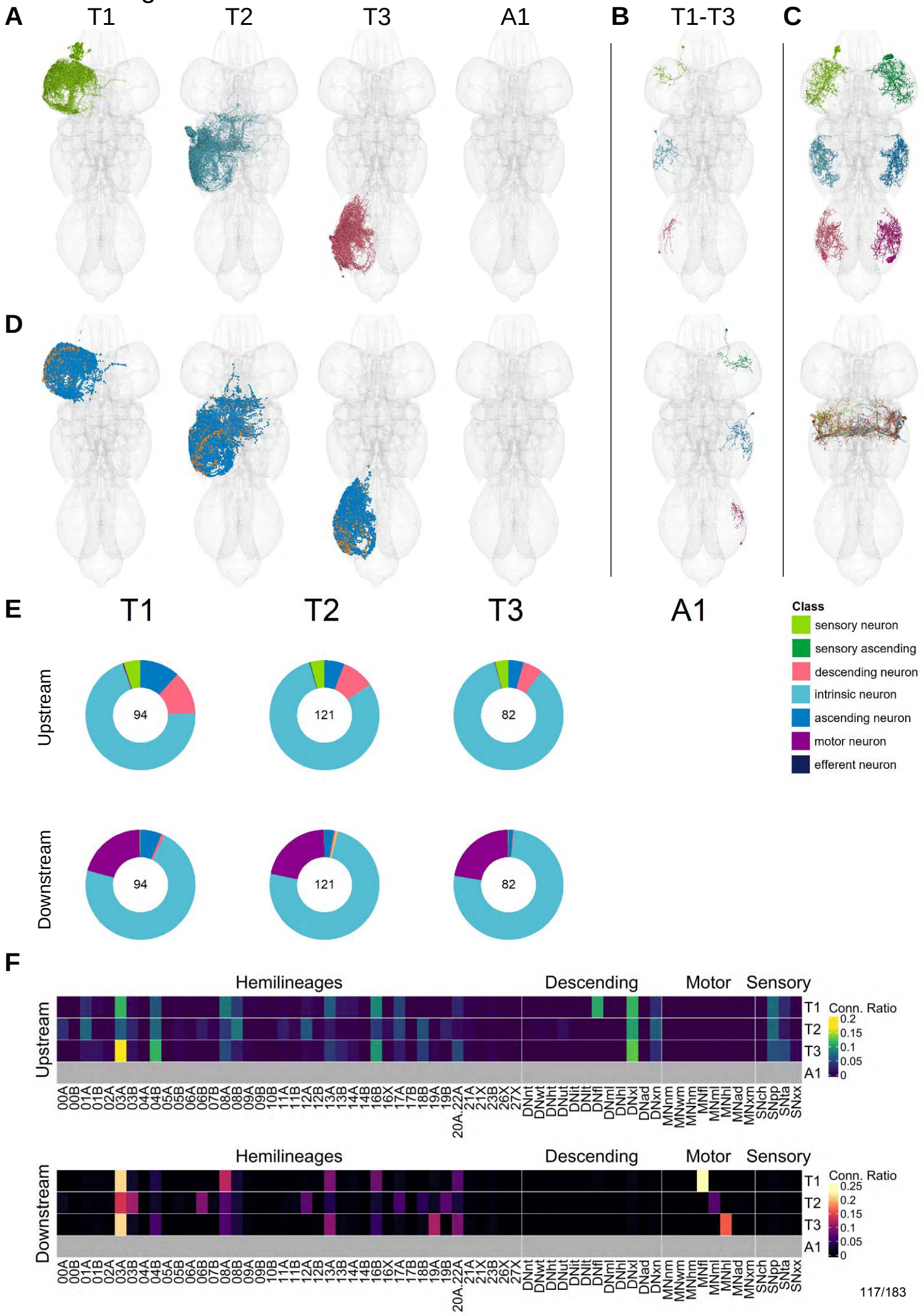

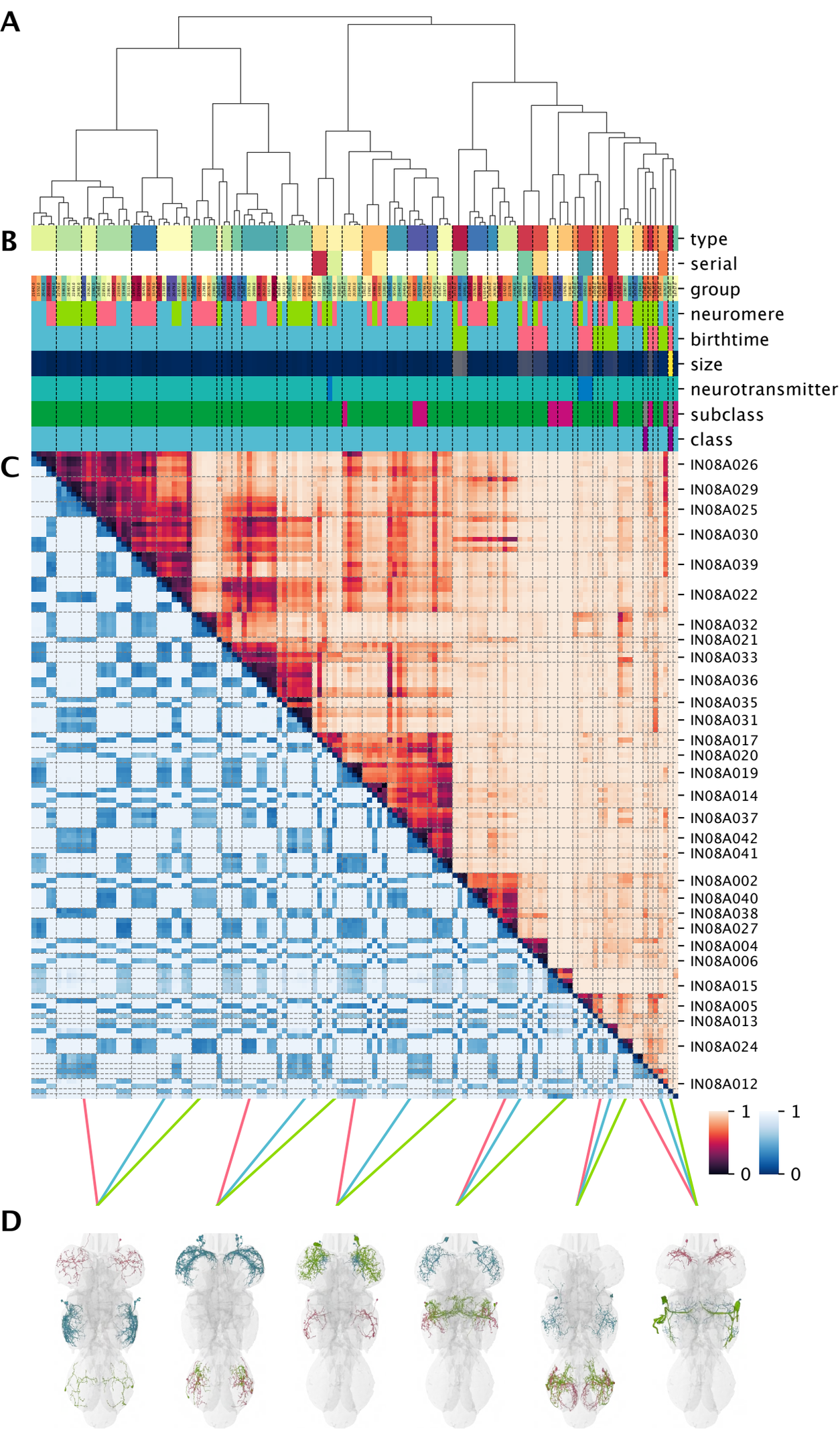
A
B
C
D
type
serial
group
neuromere
birthtime
size
neurotransmitter
subclass
class
IN08A026
IN08A029
IN08A025
IN08A030
IN08A039
IN08A022
IN08A032
IN08A021
IN08A033
IN08A036
IN08A035
IN08A031
IN08A017
IN08A020
IN08A019
IN08A014
IN08A037
IN08A042
IN08A041
IN08A002
IN08A040
IN08A038
IN08A027
IN08A004
IN08A006
IN08A015
IN08A005
IN08A013
IN08A024
IN08A012
1
0
1
0

Hemilineage 08B

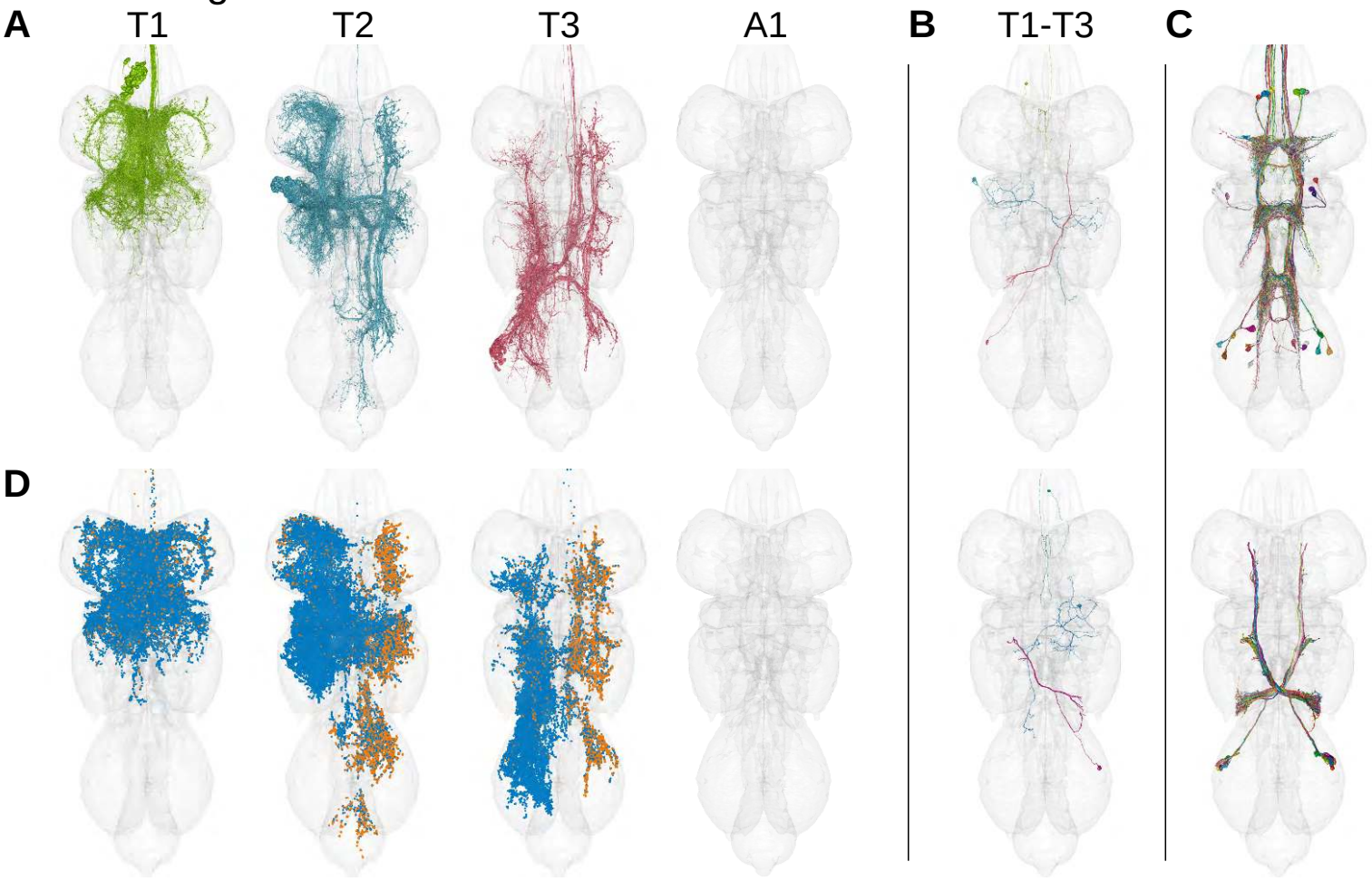

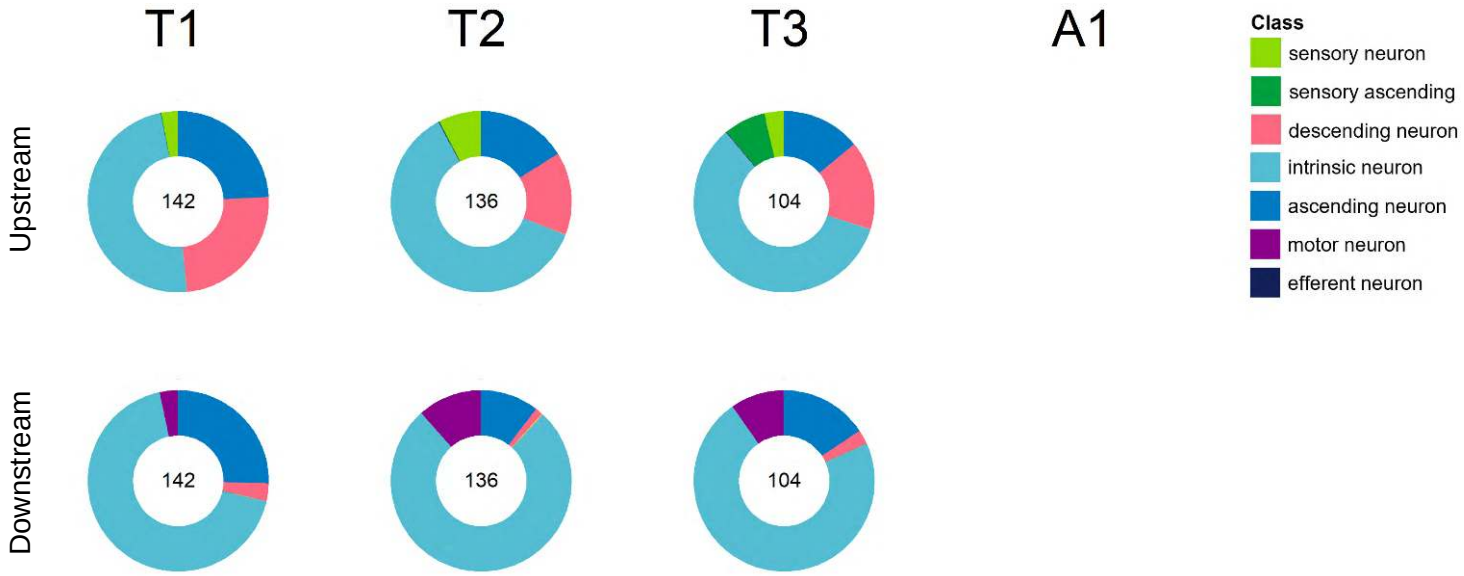

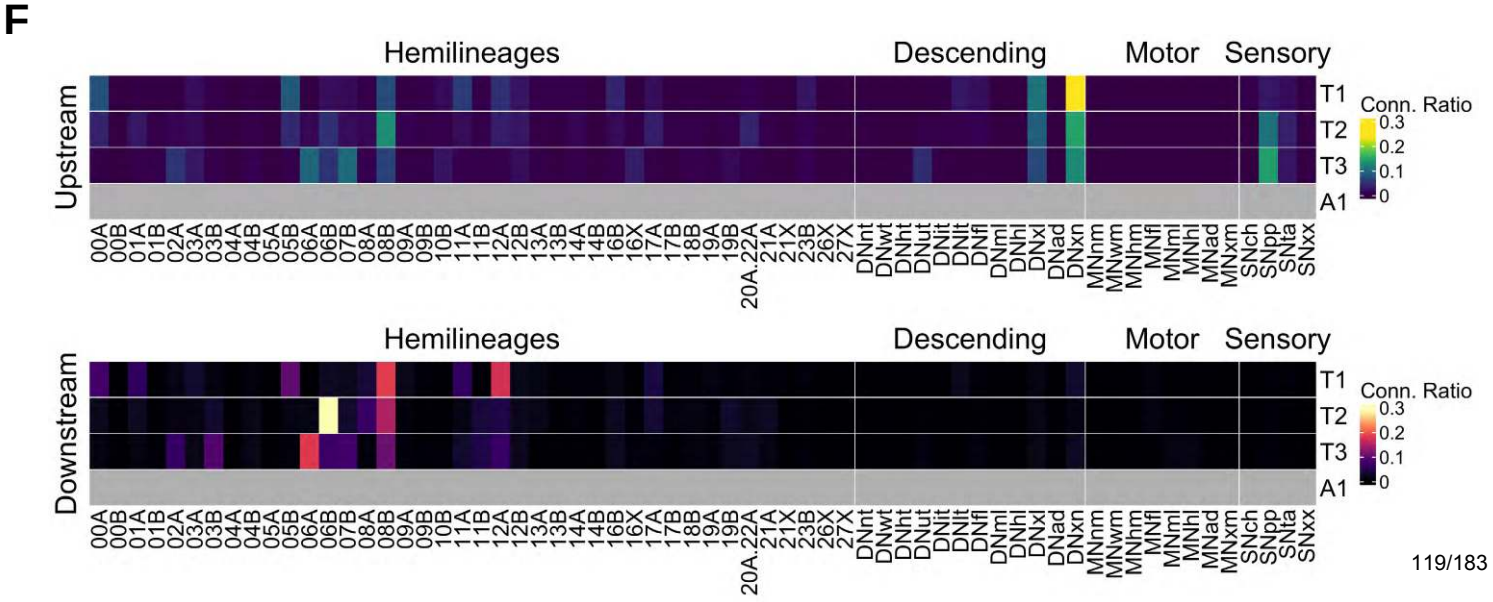

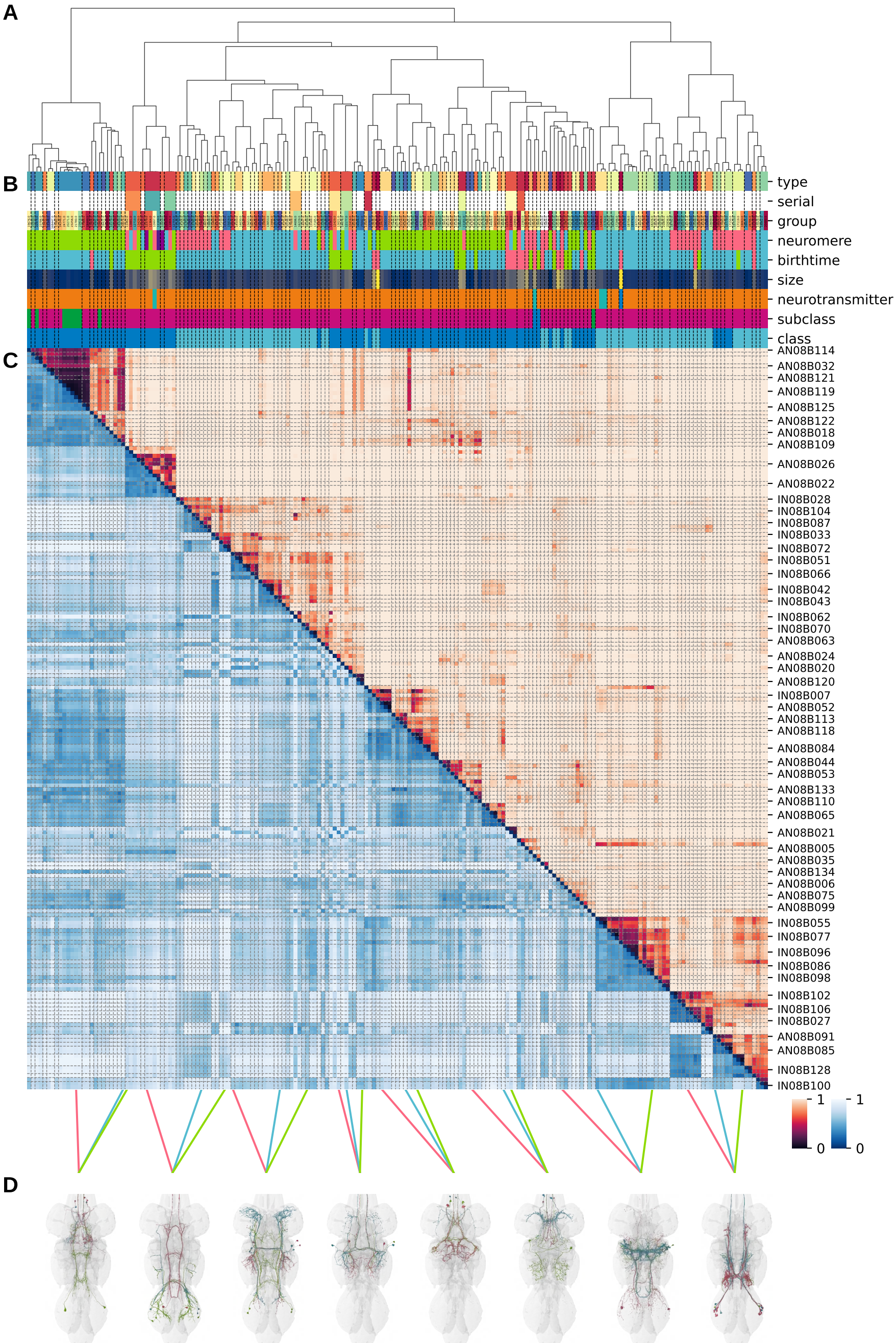
A
B
C
D
type
serial
group
neuromere
birthtime
size
neurotransmitter
subclass
class
AN08B114
AN08B032
AN08B121
AN08B119
AN08B125
AN08B122
AN08B018
AN08B109
AN08B026
AN08B022
IN08B028
IN08B104
IN08B087
IN08B033
IN08B072
IN08B051
IN08B066
IN08B042
IN08B043
IN08B062
IN08B070
AN08B063
AN08B024
AN08B020
AN08B120
IN08B007
AN08B052
AN08B113
AN08B118
AN08B084
AN08B044
AN08B053
AN08B133
AN08B110
AN08B065
AN08B021
AN08B005
AN08B035
AN08B134
AN08B006
AN08B075
AN08B099
IN08B055
IN08B077
IN08B096
IN08B086
IN08B098
IN08B102
IN08B106
IN08B027
AN08B091
AN08B085
IN08B128
IN08B100
1
0
1
0

Hemilineage 09A

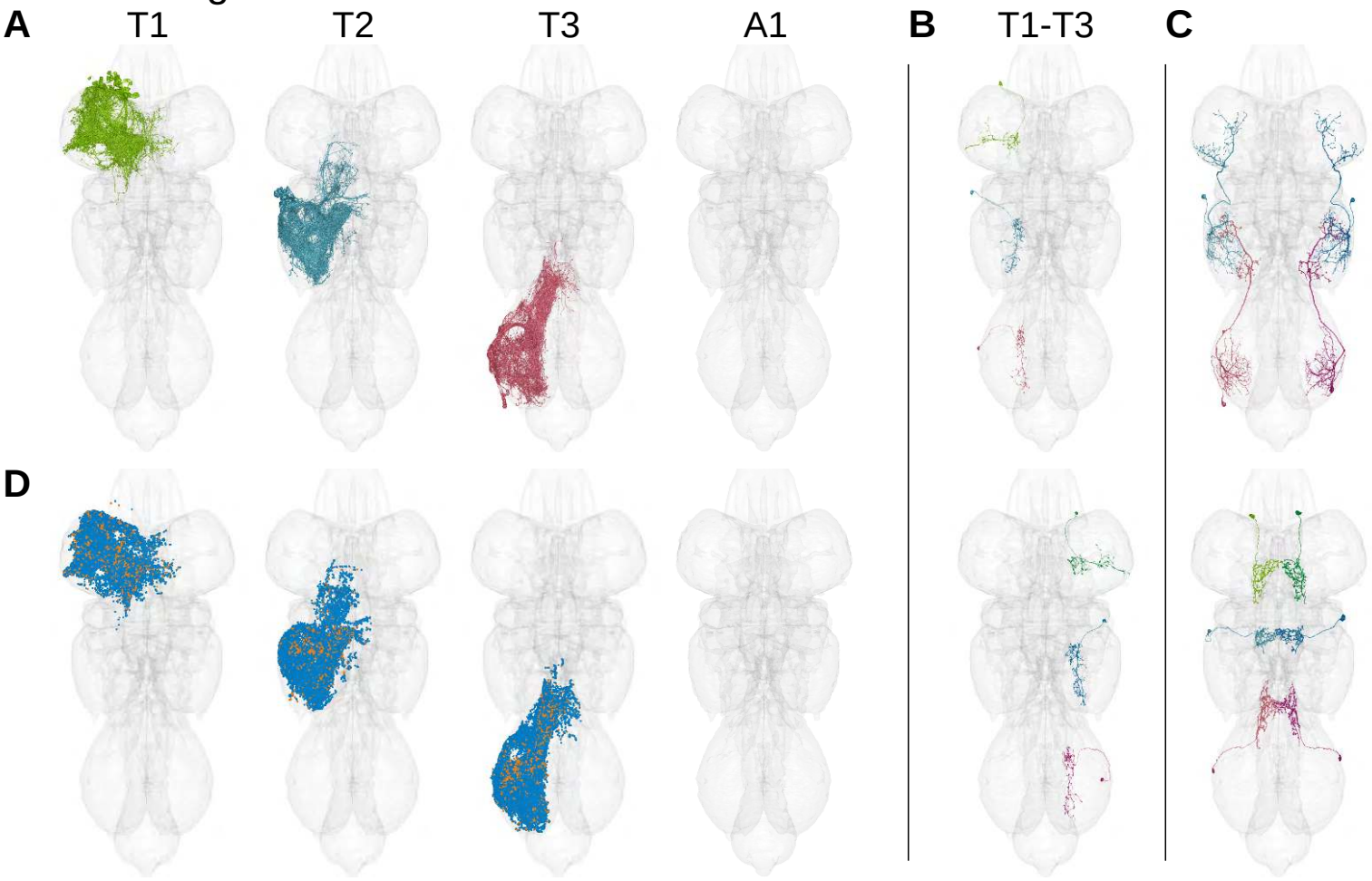

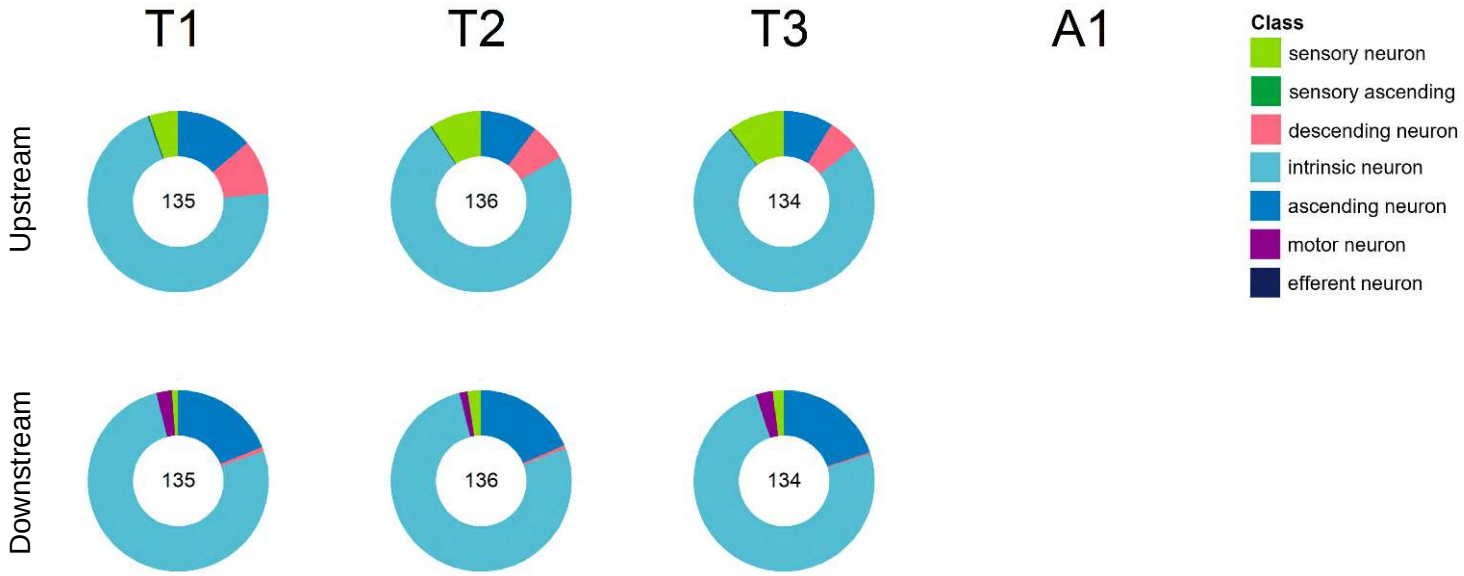

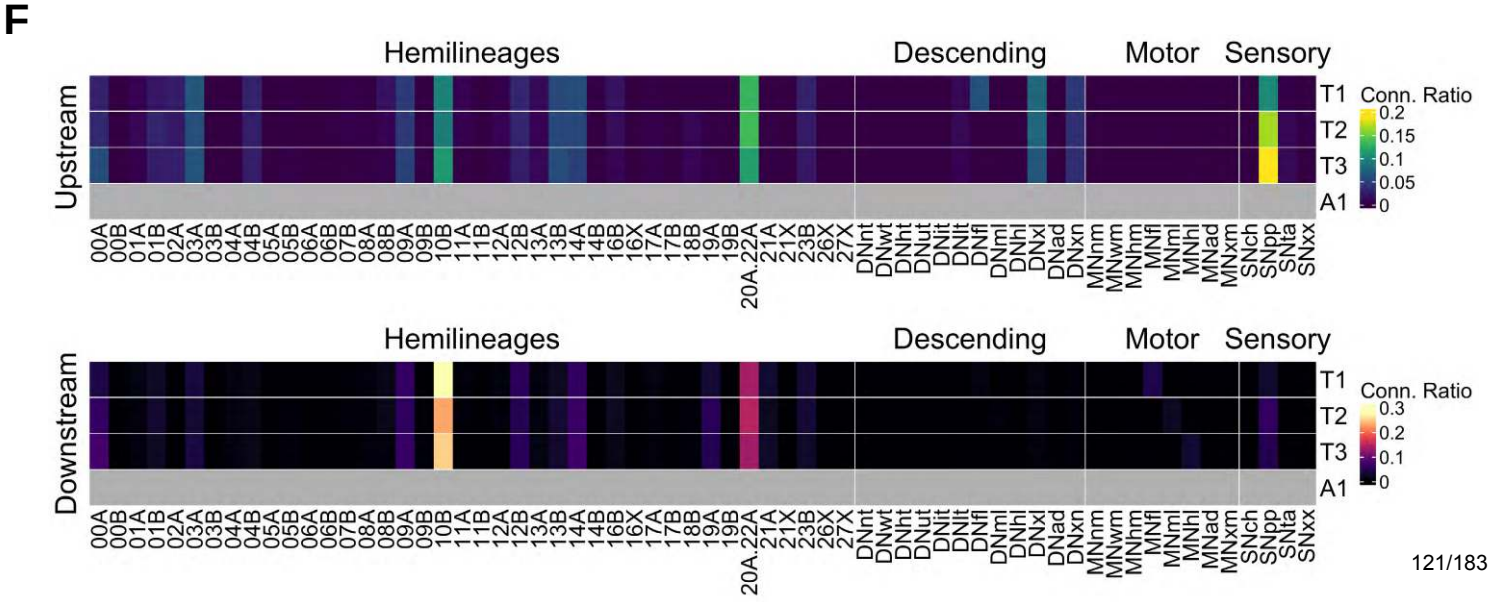

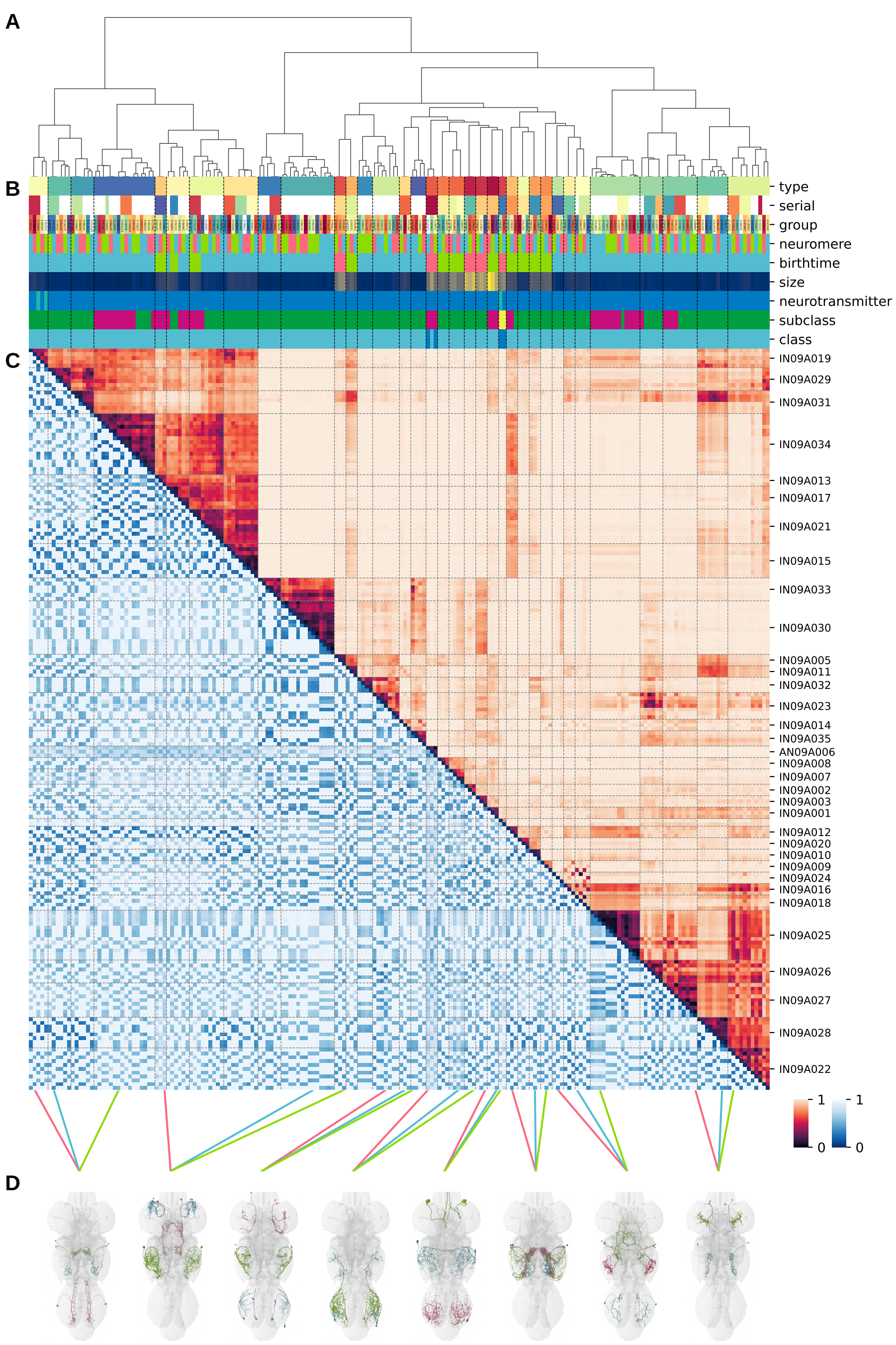
A
B
C
D
type
serial
group
neuromere
birthtime
size
neurotransmitter
subclass
class
IN09A019
IN09A029
IN09A031
IN09A034
IN09A013
IN09A017
IN09A021
IN09A015
IN09A033
IN09A030
IN09A005
IN09A011
IN09A032
IN09A023
IN09A014
IN09A035
AN09A006
IN09A008
IN09A007
IN09A002
IN09A003
IN09A001
IN09A012
IN09A020
IN09A010
IN09A009
IN09A024
IN09A016
IN09A018
IN09A025
IN09A026
IN09A027
IN09A028
IN09A022
1
0
1
0

Hemilineage 09B

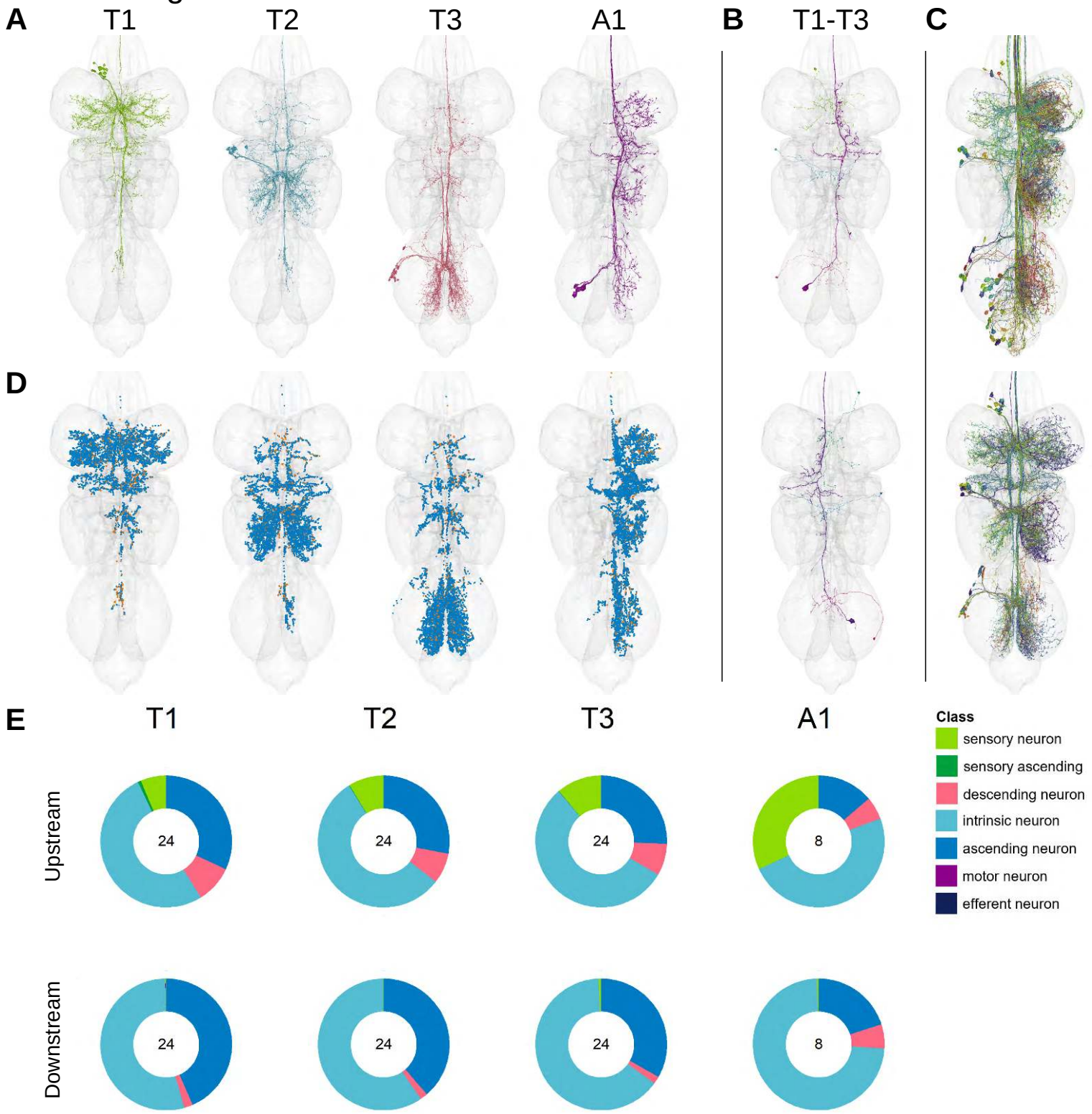

A
B
type
serial
group
neuromere
birthtime
size
neurotransmitter
subclass
class
C
AN09B004
IN09B039
IN09B043
IN09B042
IN09B047
IN09B045
AN09B033
AN09B015
AN09B037
IN09B040
AN09B027
IN09B051
IN09B048
AN09B025
AN09B018
IN09B049
AN09B013
AN09B014
AN09B029
AN09B006
IN09B005
IN09B008
AN09B017
AN09B011
AN09B007
AN09B010
AN09B023
AN09B021
AN09B002
1
0
1
0
D

Hemilineage 10B

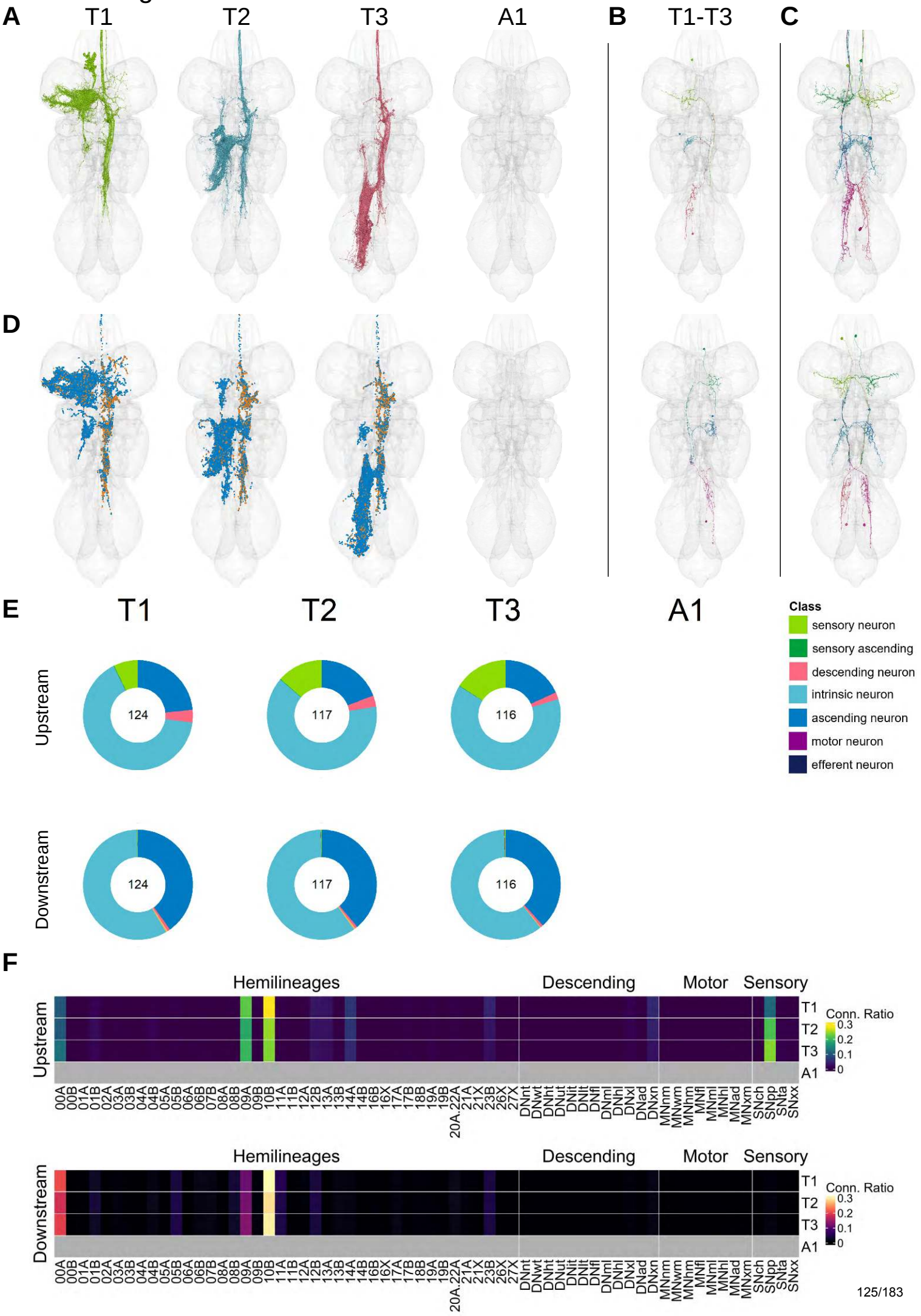

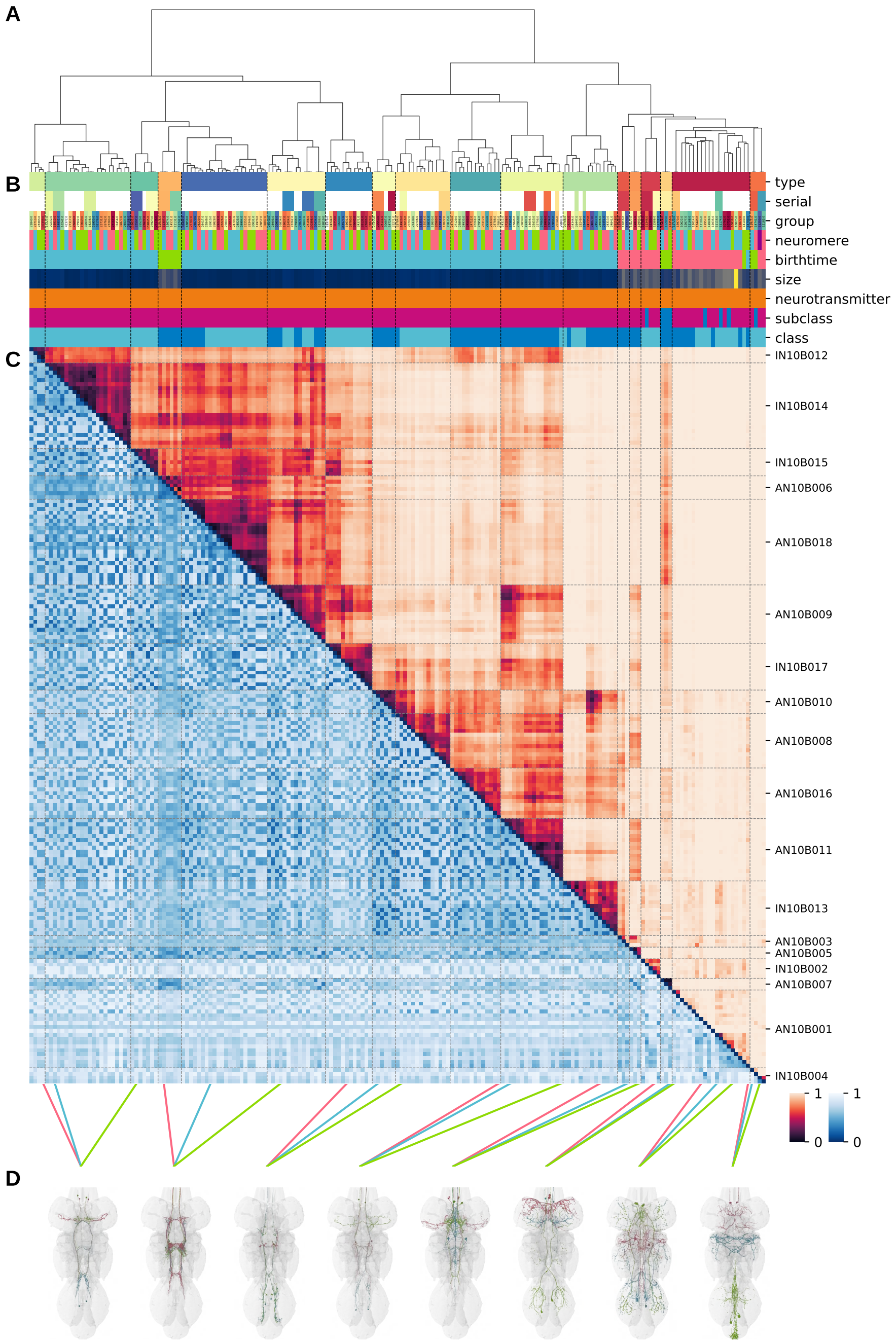
A
B
C
D
type
serial
group
neuromere
birthtime
size
neurotransmitter
subclass
class
IN10B012
IN10B014
IN10B015
AN10B006
AN10B018
AN10B009
IN10B017
AN10B010
AN10B008
AN10B016
AN10B011
IN10B013
AN10B003
AN10B005
IN10B002
AN10B007
AN10B001
IN10B004
1
0
1
0

Hemilineage 11A

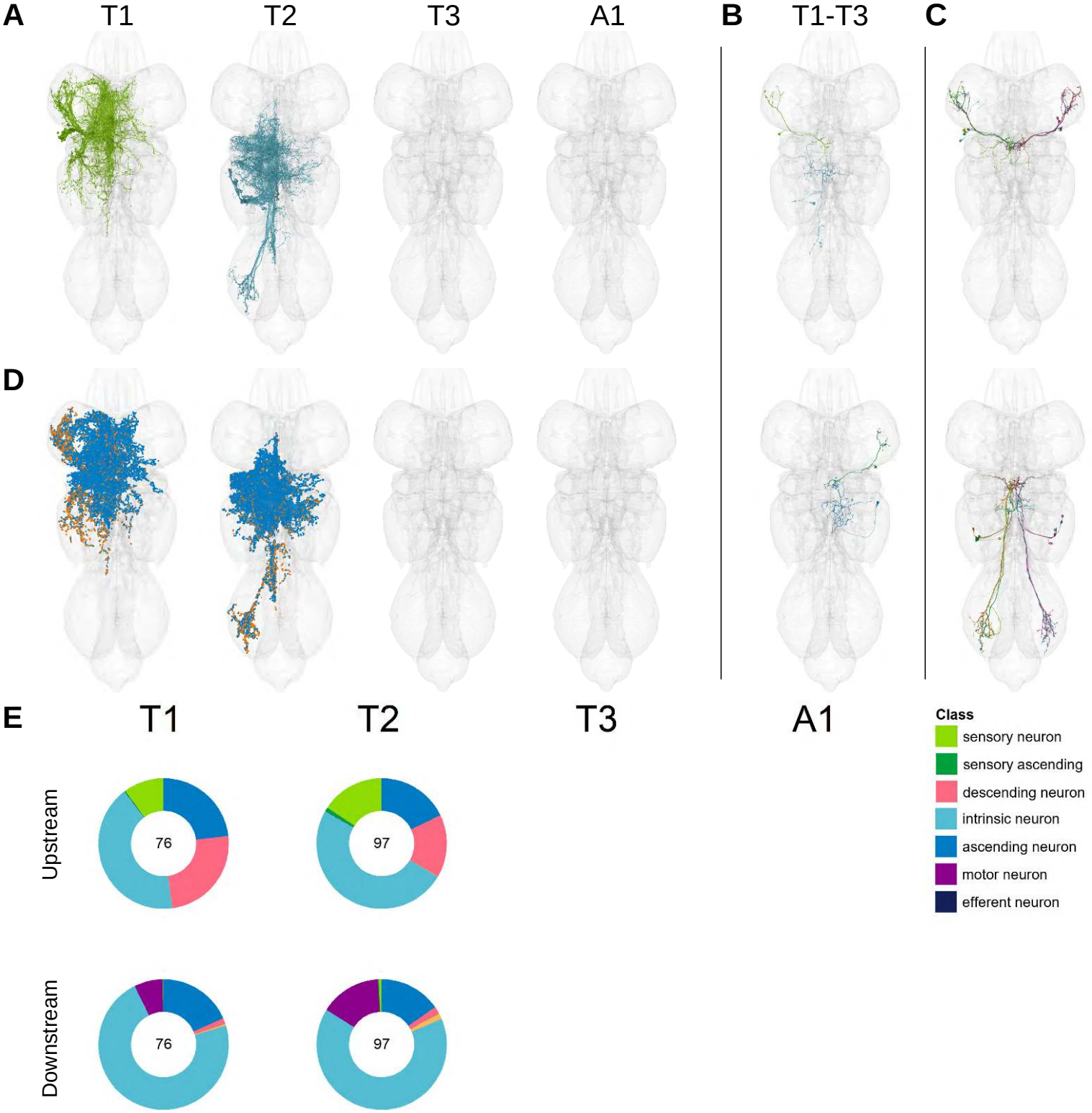

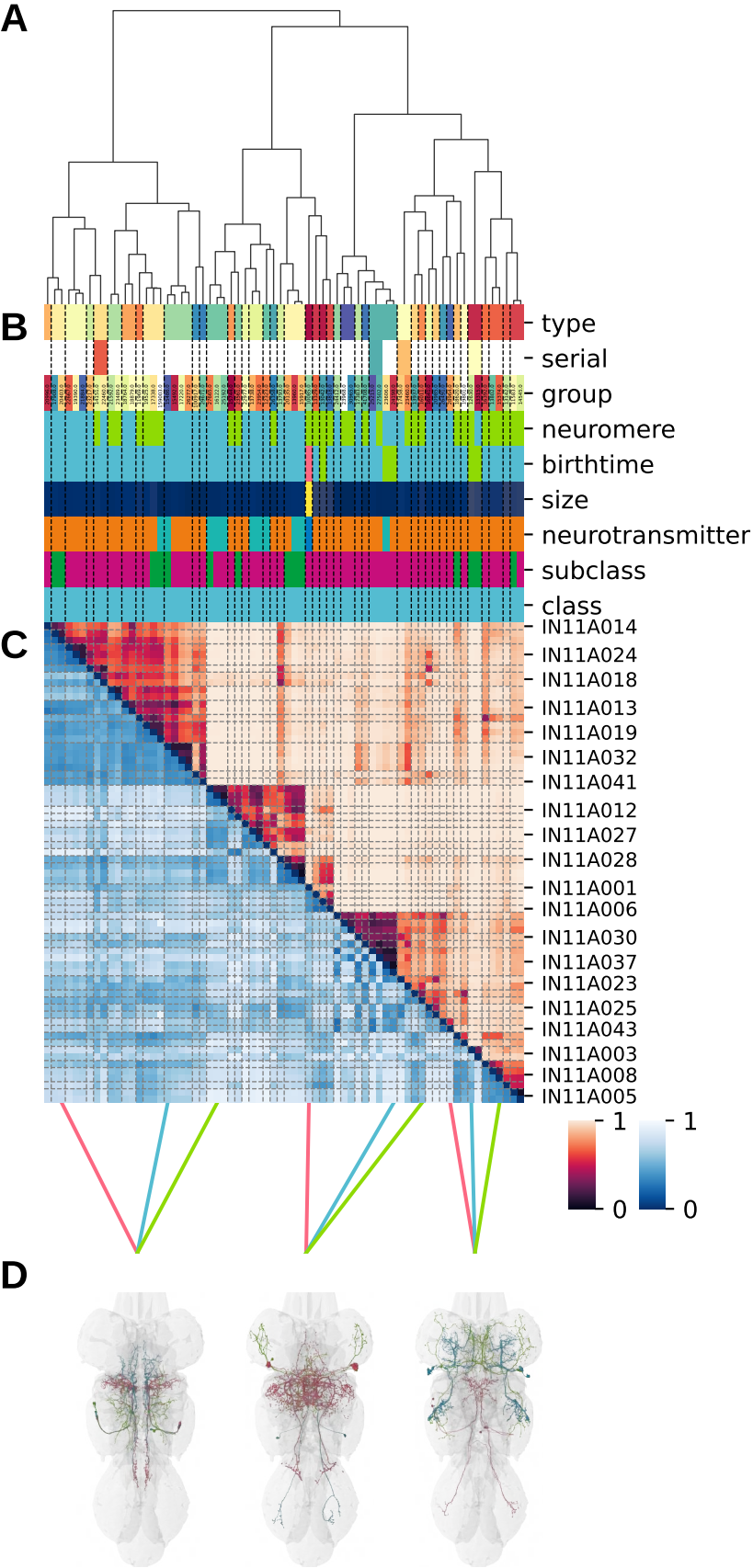
A
B
type
serial
group
neuromere
birthtime
size
neurotransmitter
subclass
class
C
IN11A014
IN11A024
IN11A018
IN11A013
IN11A019
IN11A032
IN11A041
IN11A012
IN11A027
IN11A028
IN11A001
IN11A006
IN11A030
IN11A037
IN11A023
IN11A025
IN11A043
IN11A003
IN11A008
IN11A005
1
0
1
0
D

Hemilineage 11B

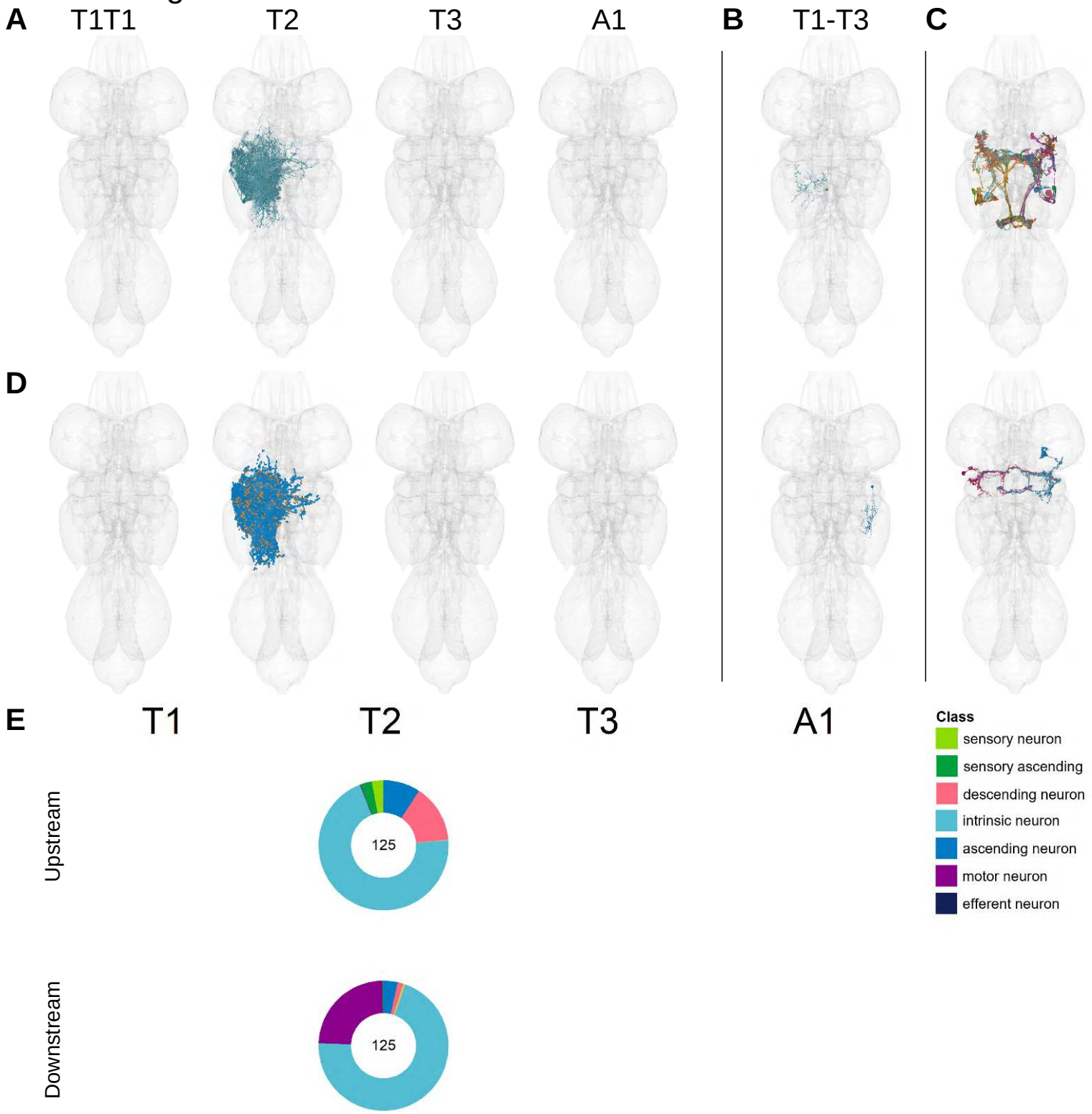

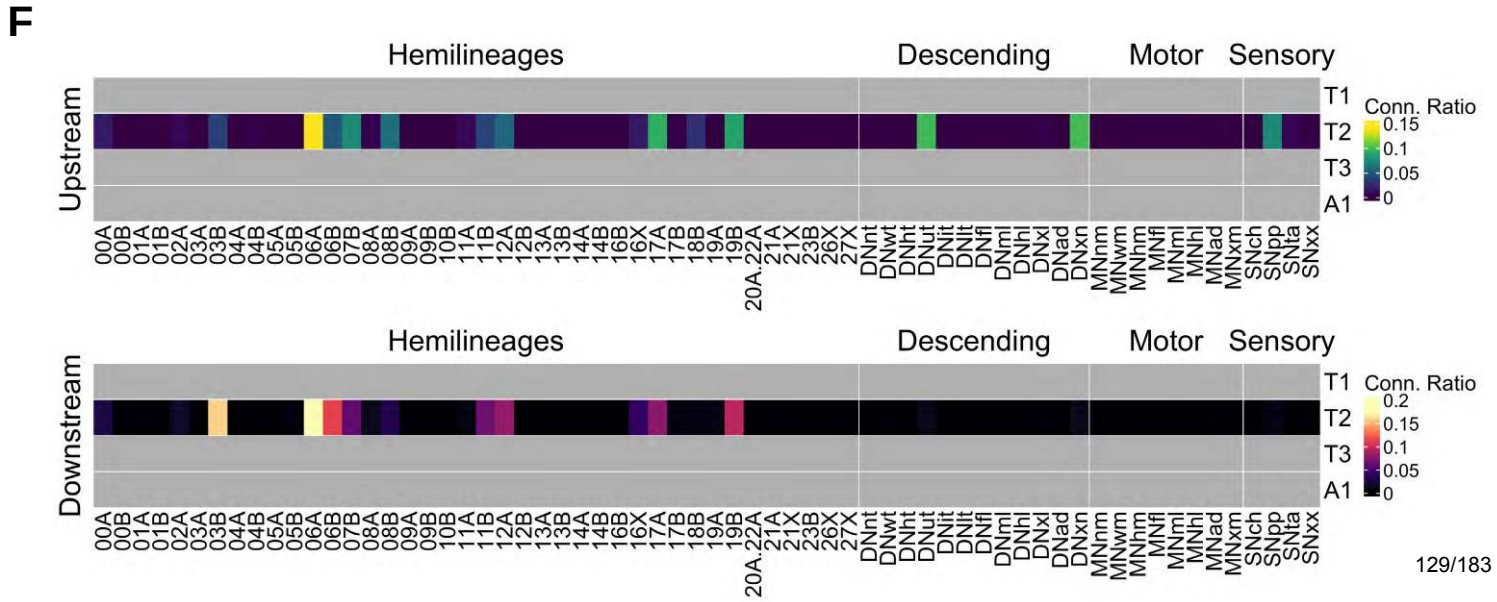

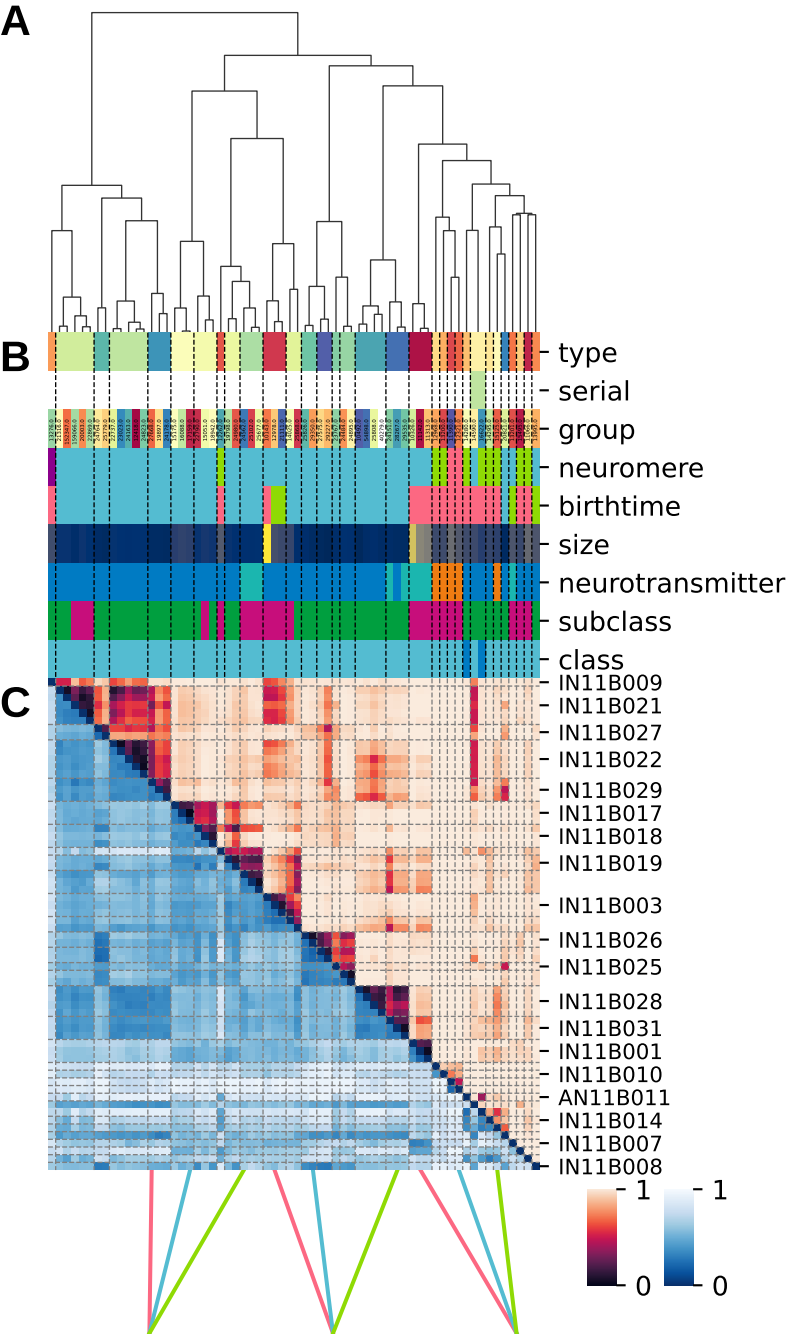
A
B
type
serial
group
neuromere
birthtime
size
neurotransmitter
subclass
class
C
IN11B009
IN11B021
IN11B027
IN11B022
IN11B029
IN11B017
IN11B018
IN11B019
IN11B003
IN11B026
IN11B025
IN11B028
IN11B031
IN11B001
IN11B010
AN11B011
IN11B014
IN11B007
IN11B008
1
0
1
0

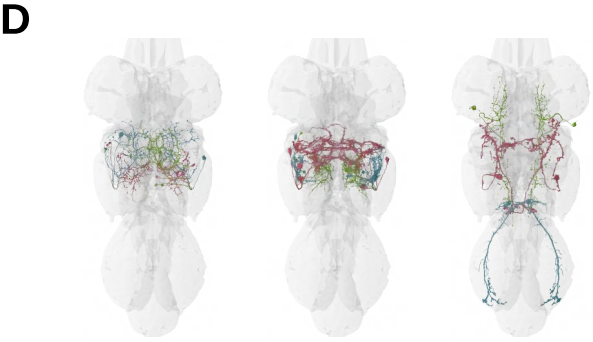
D

Hemilineage 12A

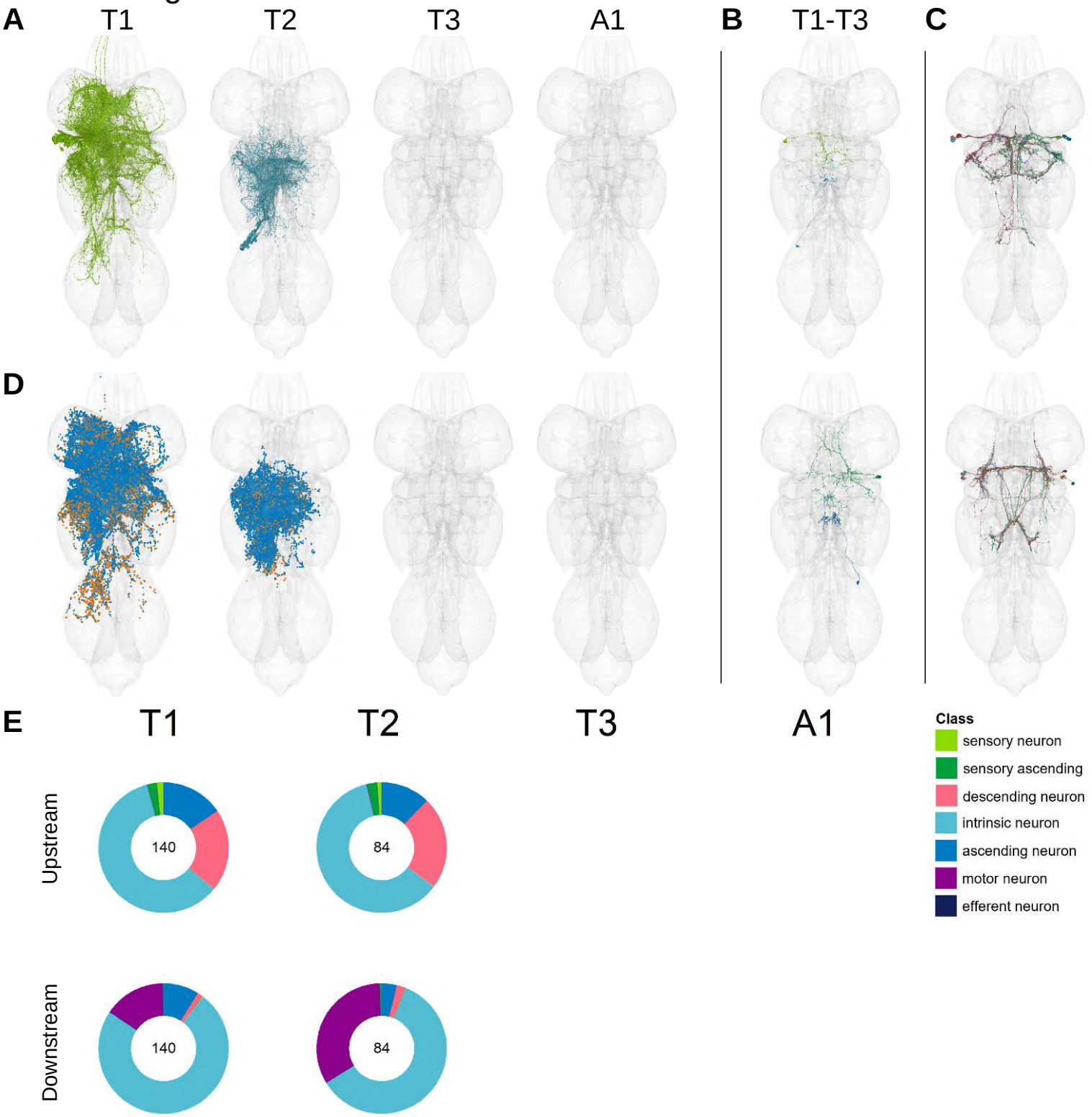

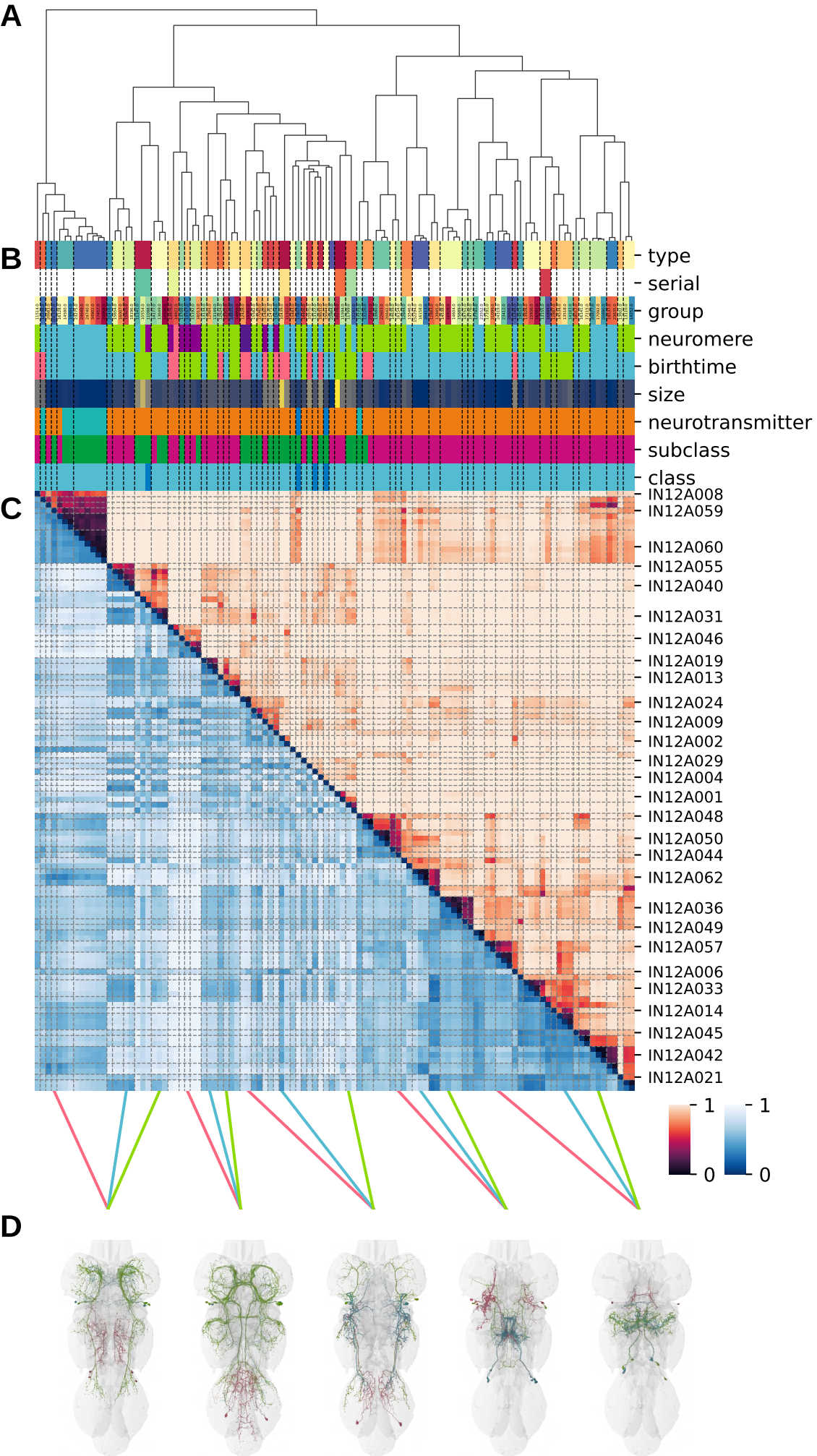
A
B
C
D
type
serial
group
neuromere
birthtime
size
neurotransmitter
subclass
class
IN12A008
IN12A059
IN12A060
IN12A055
IN12A040
IN12A031
IN12A046
IN12A019
IN12A013
IN12A024
IN12A009
IN12A002
IN12A029
IN12A004
IN12A001
IN12A048
IN12A050
IN12A044
IN12A062
IN12A036
IN12A049
IN12A057
IN12A006
IN12A033
IN12A014
IN12A045
IN12A042
IN12A021
1
0
1
0

Hemilineage 12B

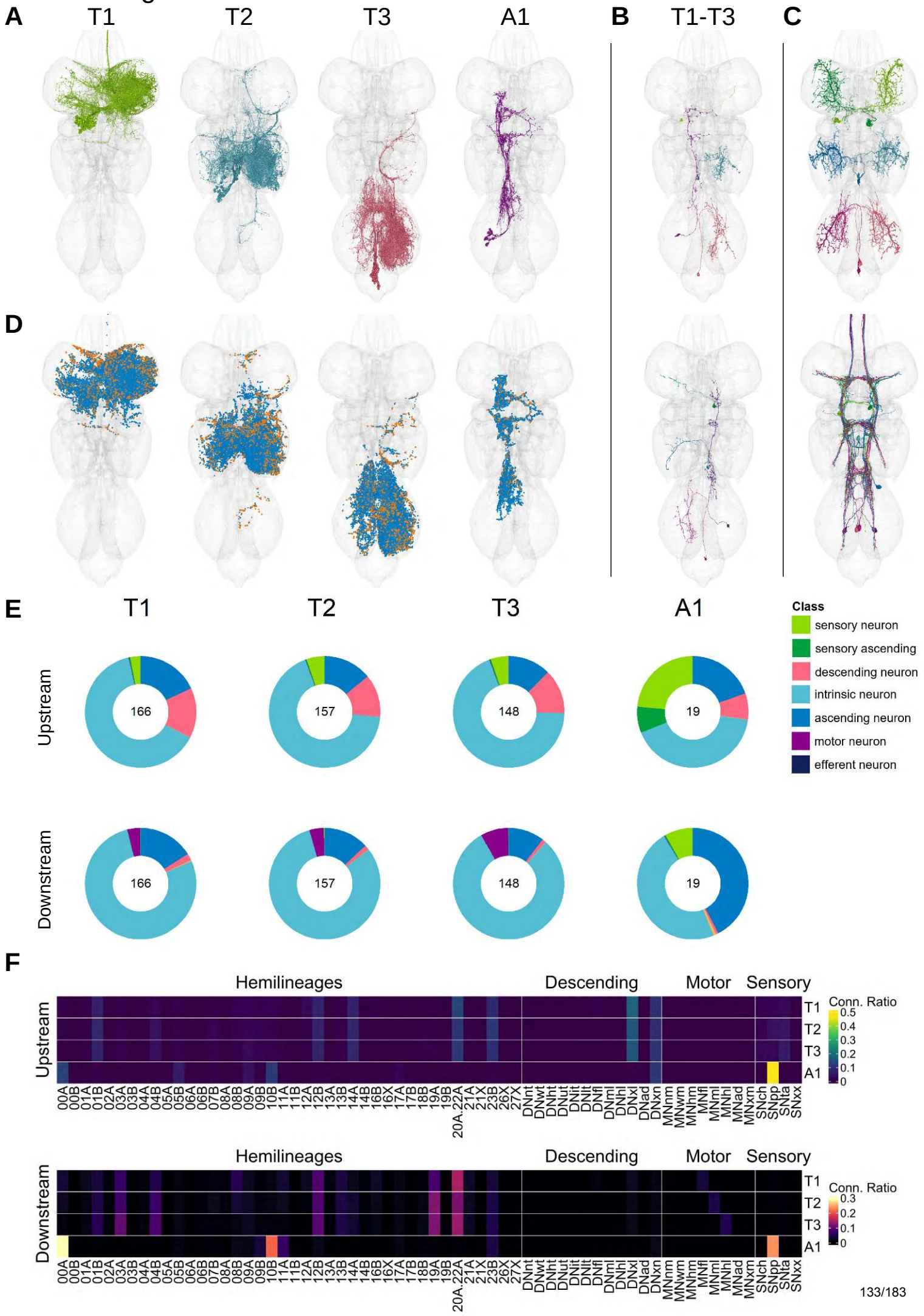

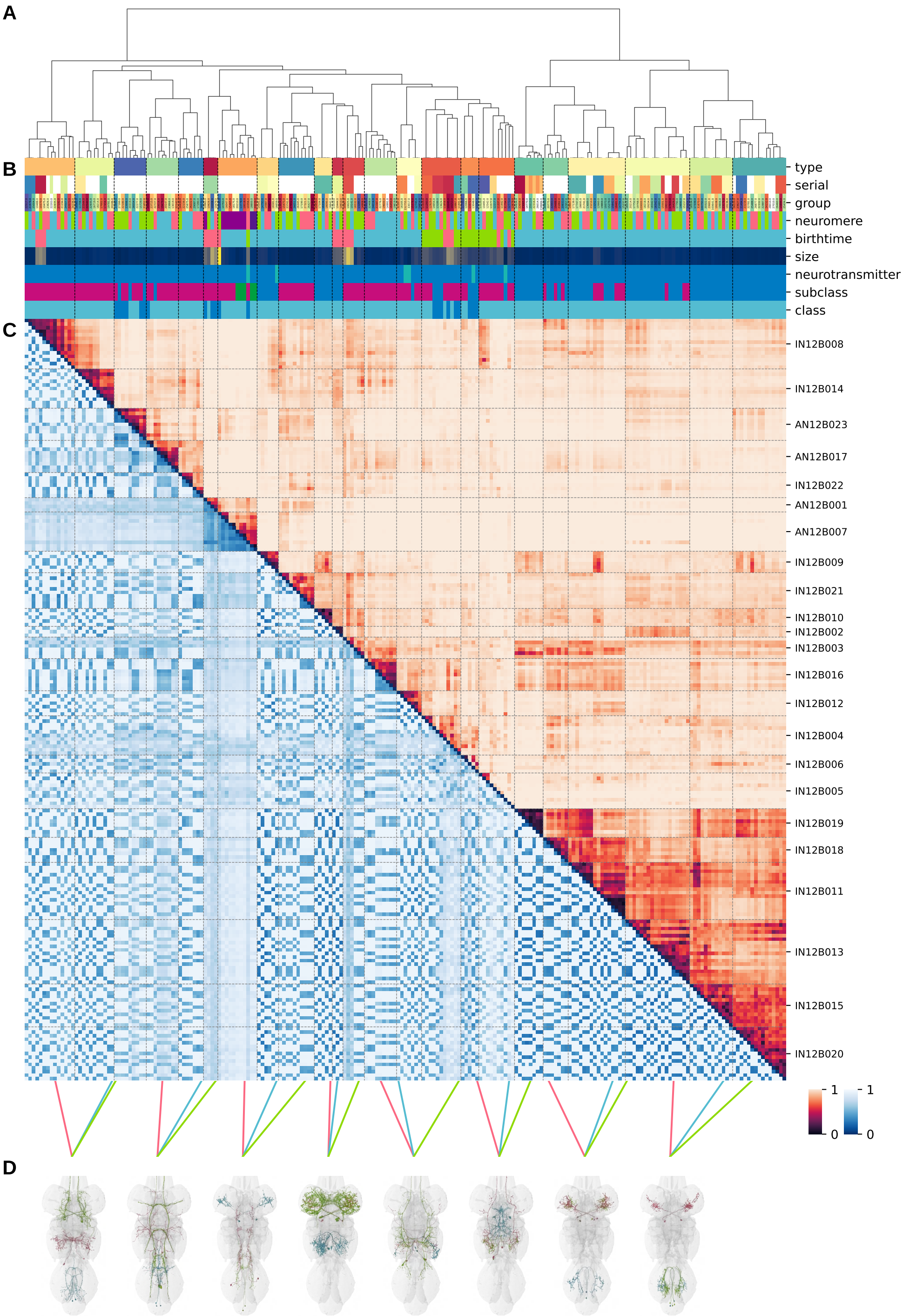
A
B
C
D
type
serial
group
neuromere
birthtime
size
neurotransmitter
subclass
class
IN12B008
IN12B014
AN12B023
AN12B017
IN12B022
AN12B001
AN12B007
IN12B009
IN12B021
IN12B010
IN12B002
IN12B003
IN12B016
IN12B012
IN12B004
IN12B006
IN12B005
IN12B019
IN12B018
IN12B011
IN12B013
IN12B015
IN12B020
1
0
1
0

Hemilineage 13A

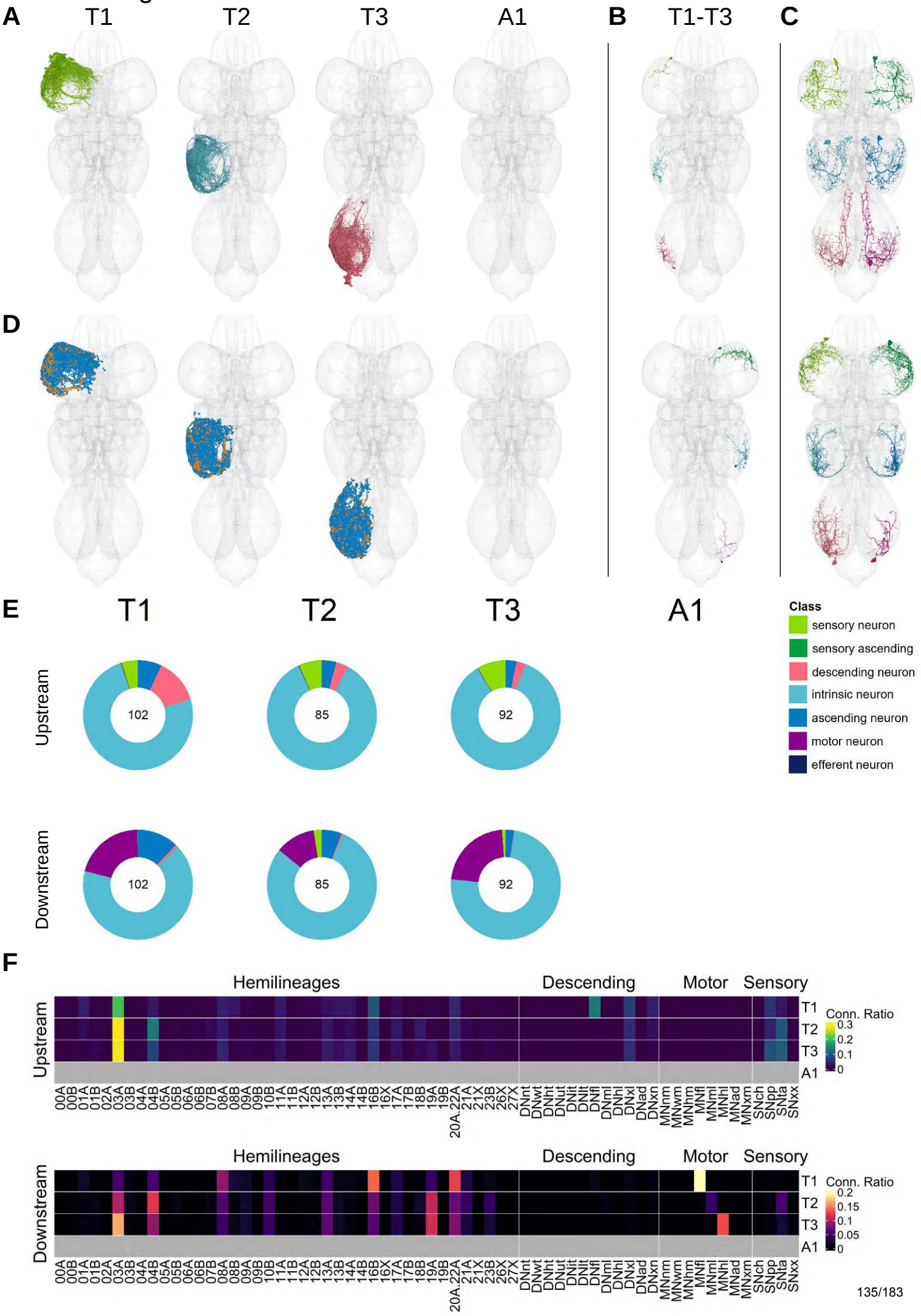

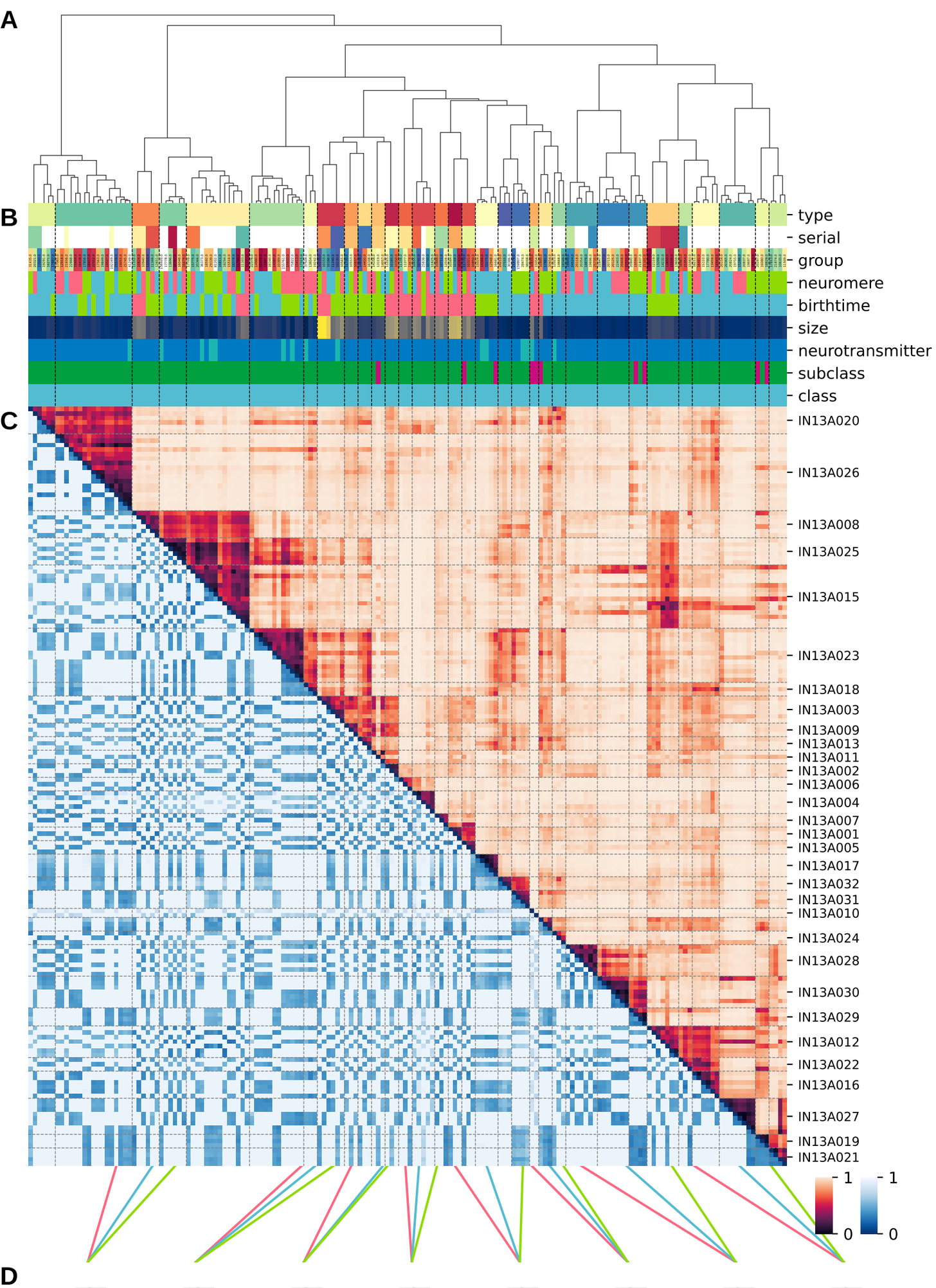
A
B
C
type
serial
group
neuromere
birthtime
size
neurotransmitter
subclass
class
IN13A020
IN13A026
IN13A008
IN13A025
IN13A015
IN13A023
IN13A018
IN13A003
IN13A009
IN13A013
IN13A011
IN13A002
IN13A006
IN13A004
IN13A007
IN13A001
IN13A005
IN13A017
IN13A032
IN13A031
IN13A010
IN13A024
IN13A028
IN13A030
IN13A029
IN13A012
IN13A022
IN13A016
IN13A027
IN13A019
IN13A021
1
0
1
0

D

Hemilineage 13B

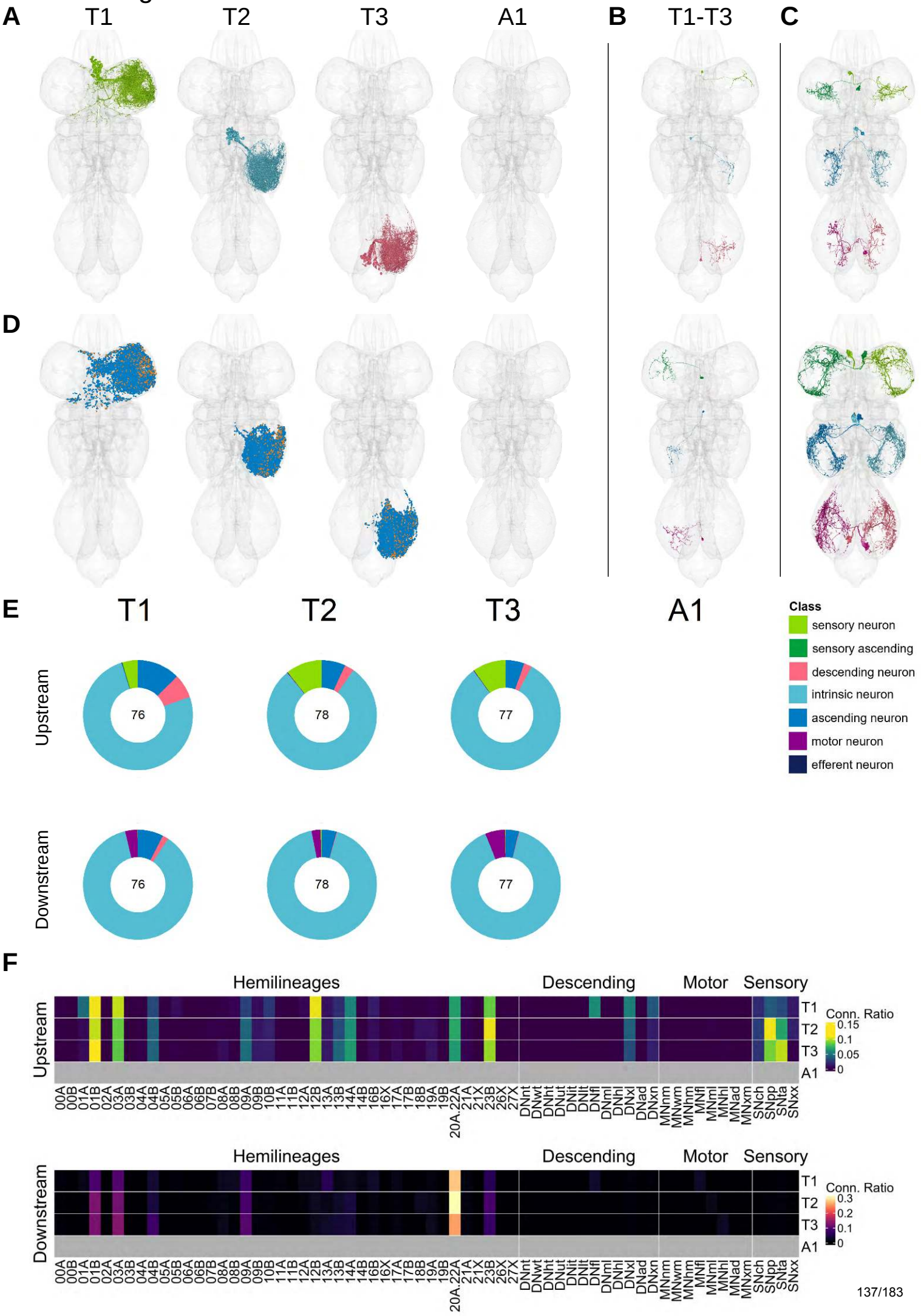

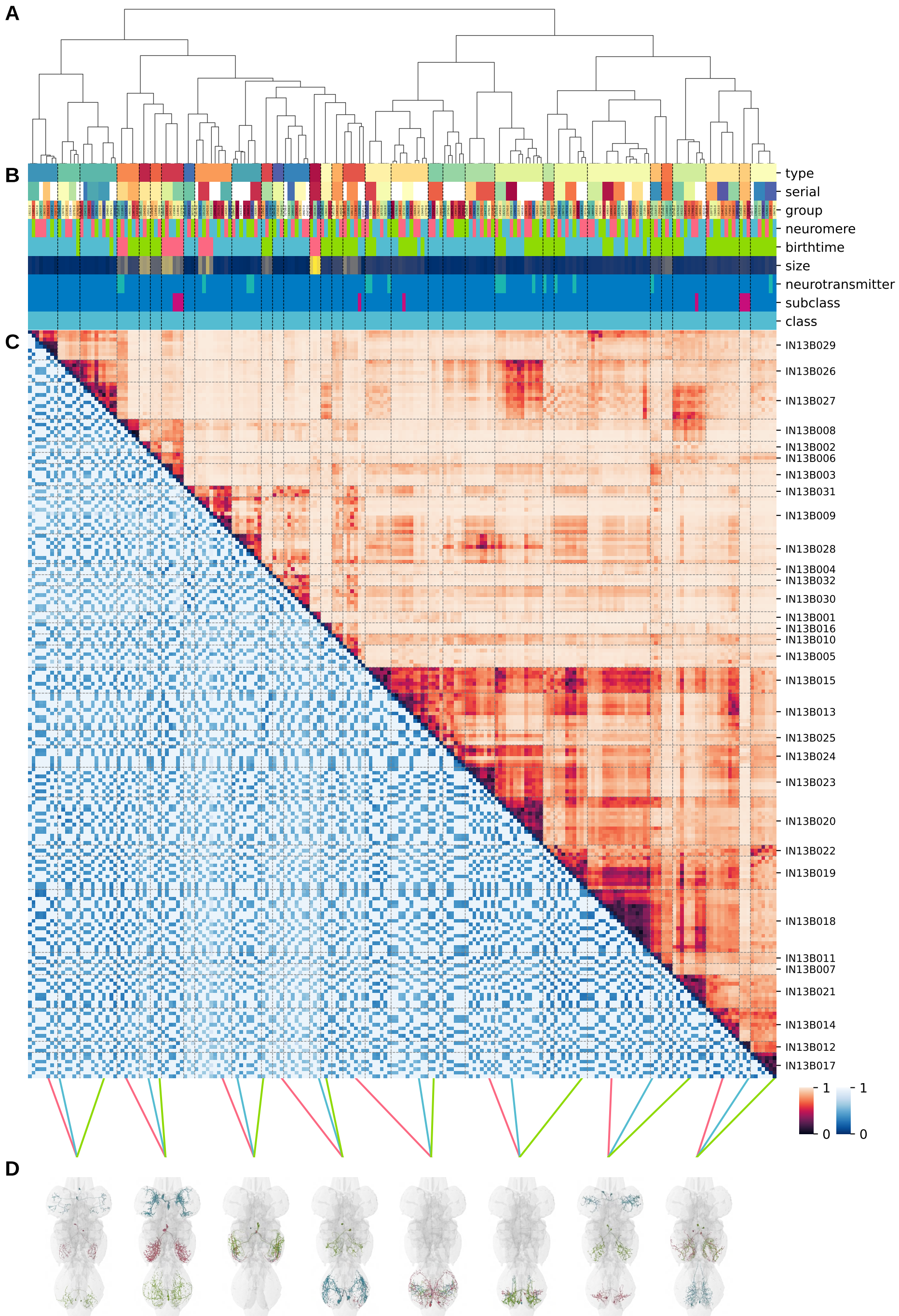
A
B
C
D
type
serial
group
neuromere
birthtime
size
neurotransmitter
subclass
class
IN13B029
IN13B026
IN13B027
IN13B008
IN13B002
IN13B006
IN13B003
IN13B031
IN13B009
IN13B028
IN13B004
IN13B032
IN13B030
IN13B001
IN13B016
IN13B010
IN13B005
IN13B015
IN13B013
IN13B025
IN13B024
IN13B023
IN13B020
IN13B022
IN13B019
IN13B018
IN13B011
IN13B007
IN13B021
IN13B014
IN13B012
IN13B017
1
0
1
0

Hemilineage 14A

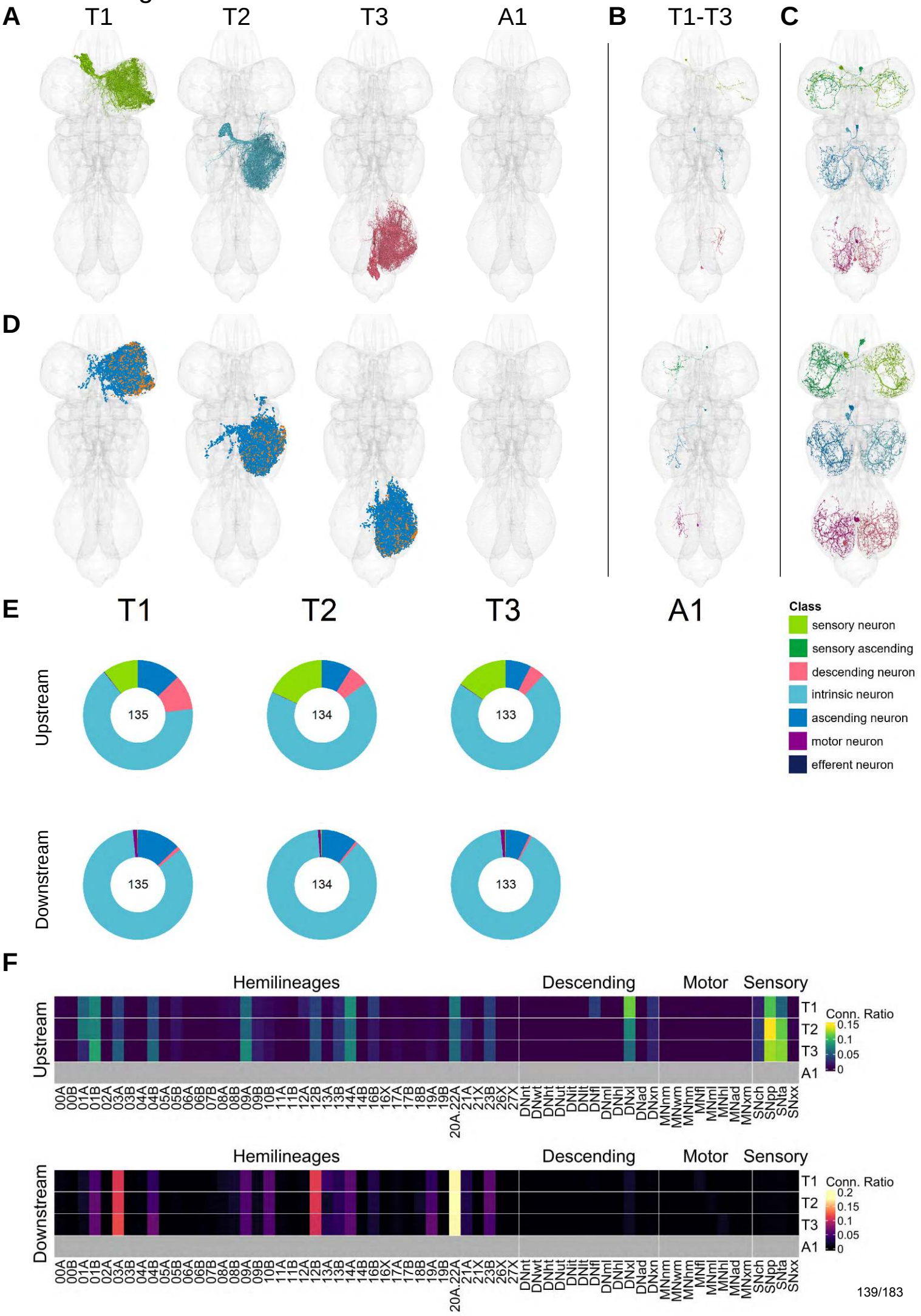

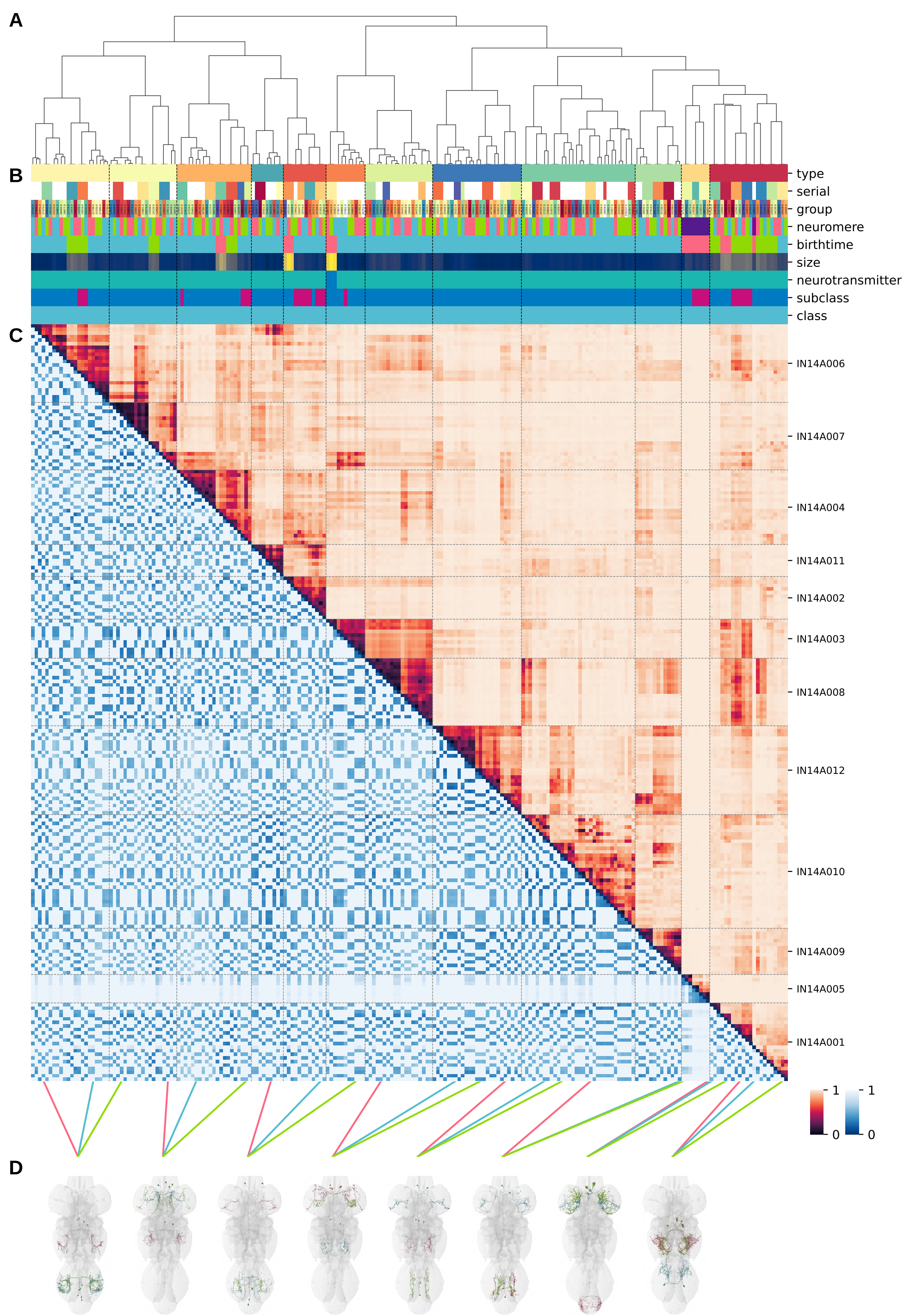
A
B
C
D
type
serial
group
neuromere
birthtime
size
neurotransmitter
subclass
class
IN14A006
IN14A007
IN14A004
IN14A011
IN14A002
IN14A003
IN14A008
IN14A012
IN14A010
IN14A009
IN14A005
IN14A001
1
0
1
0

Hemilineage 15B

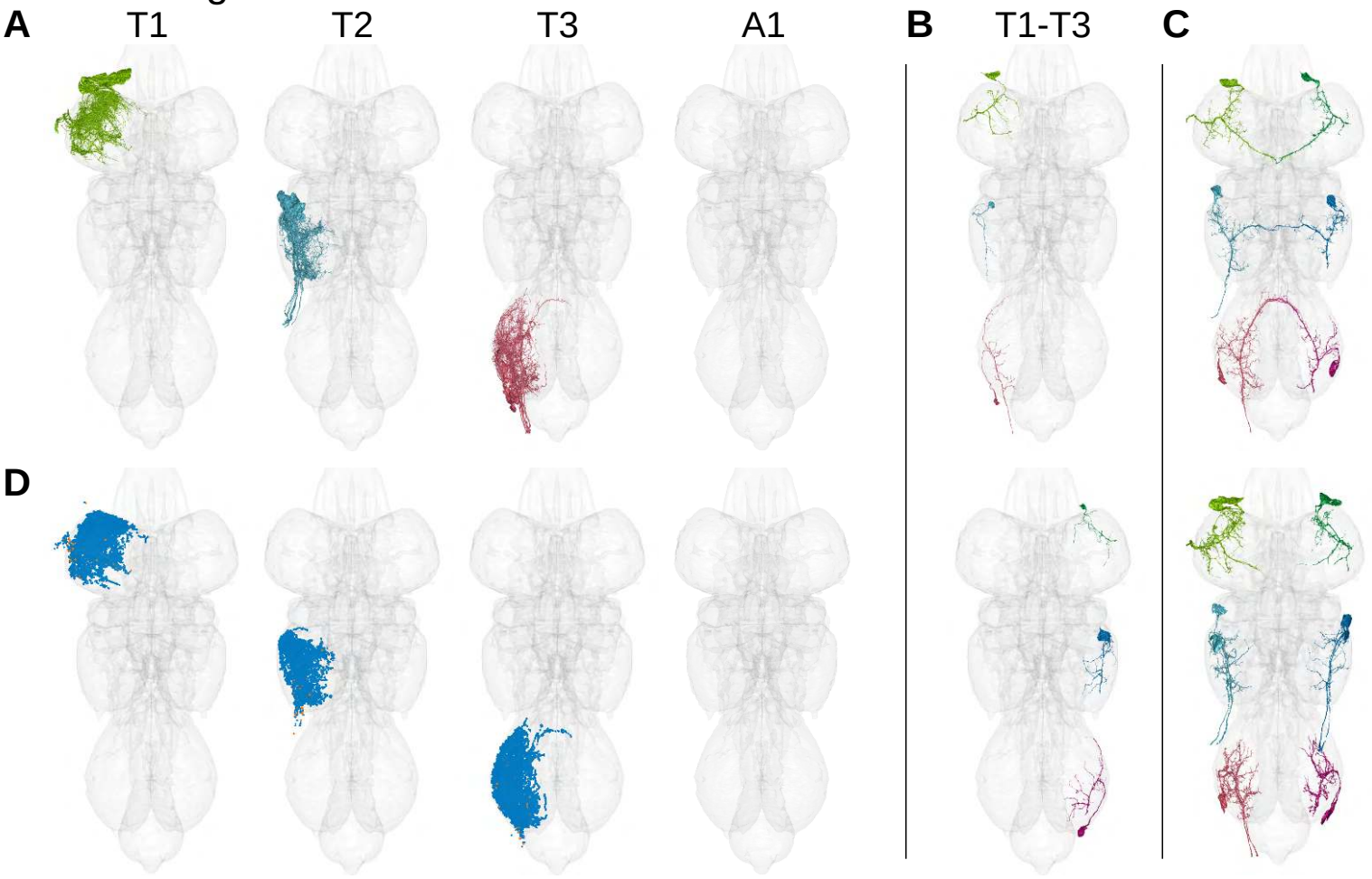

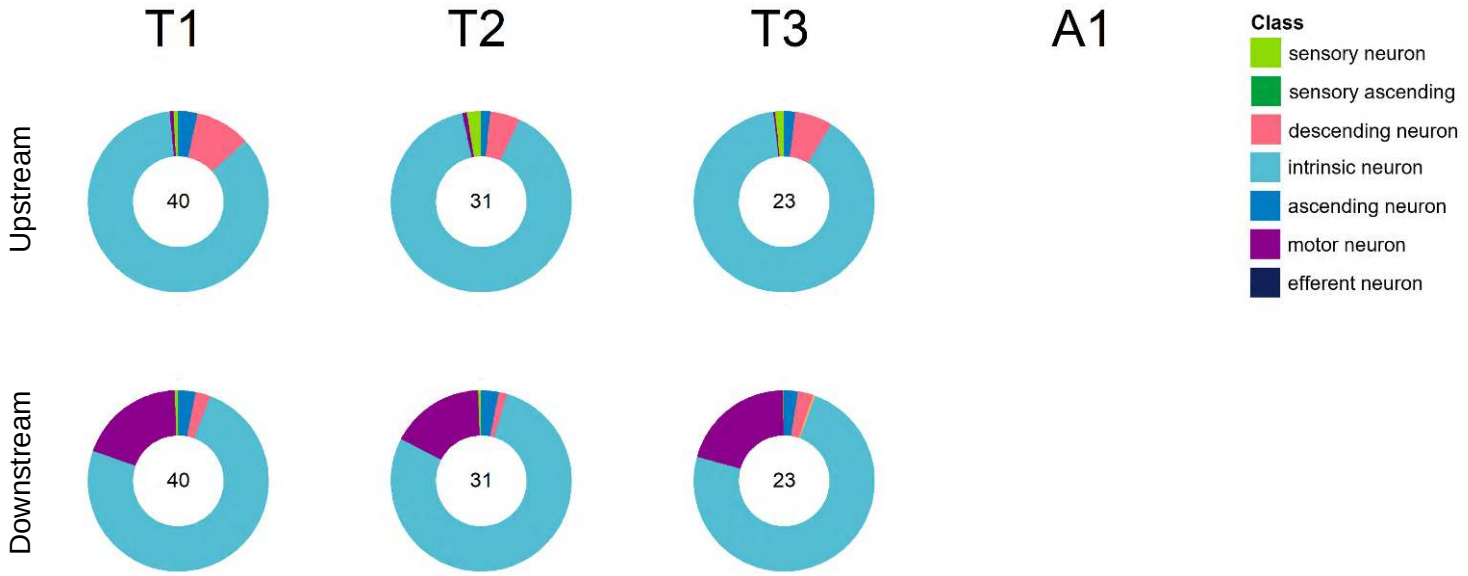

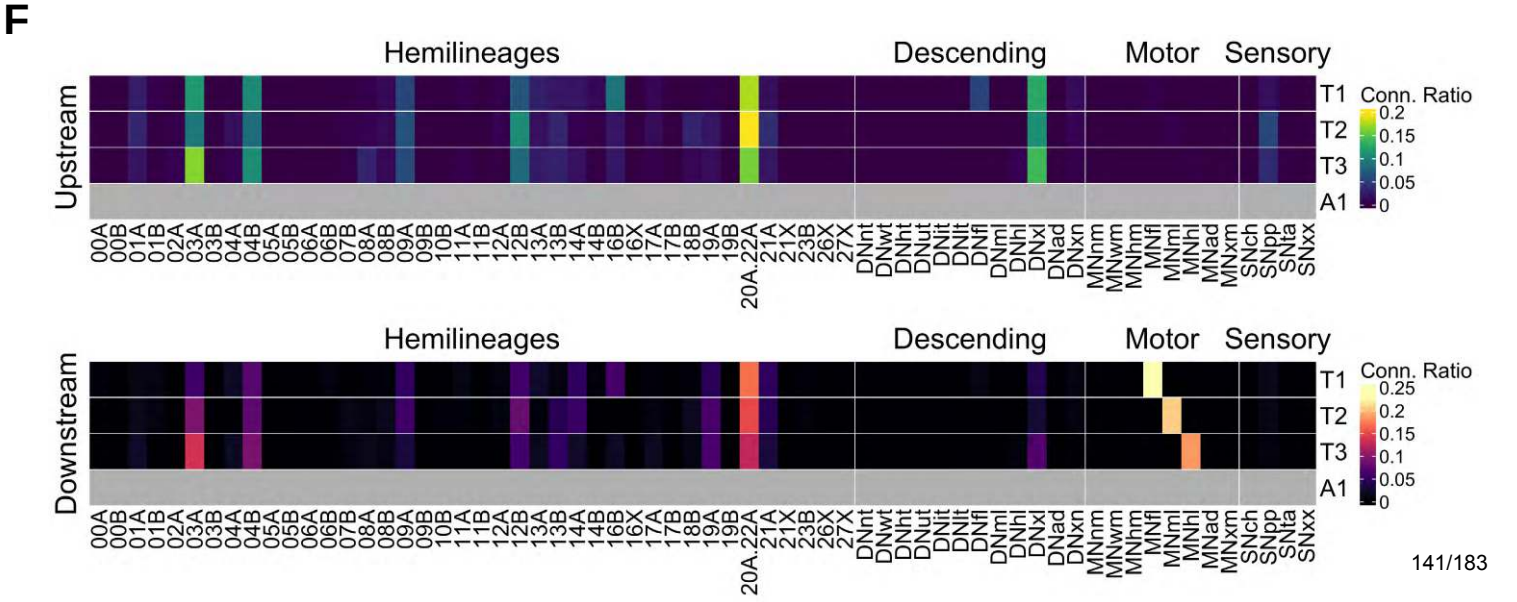

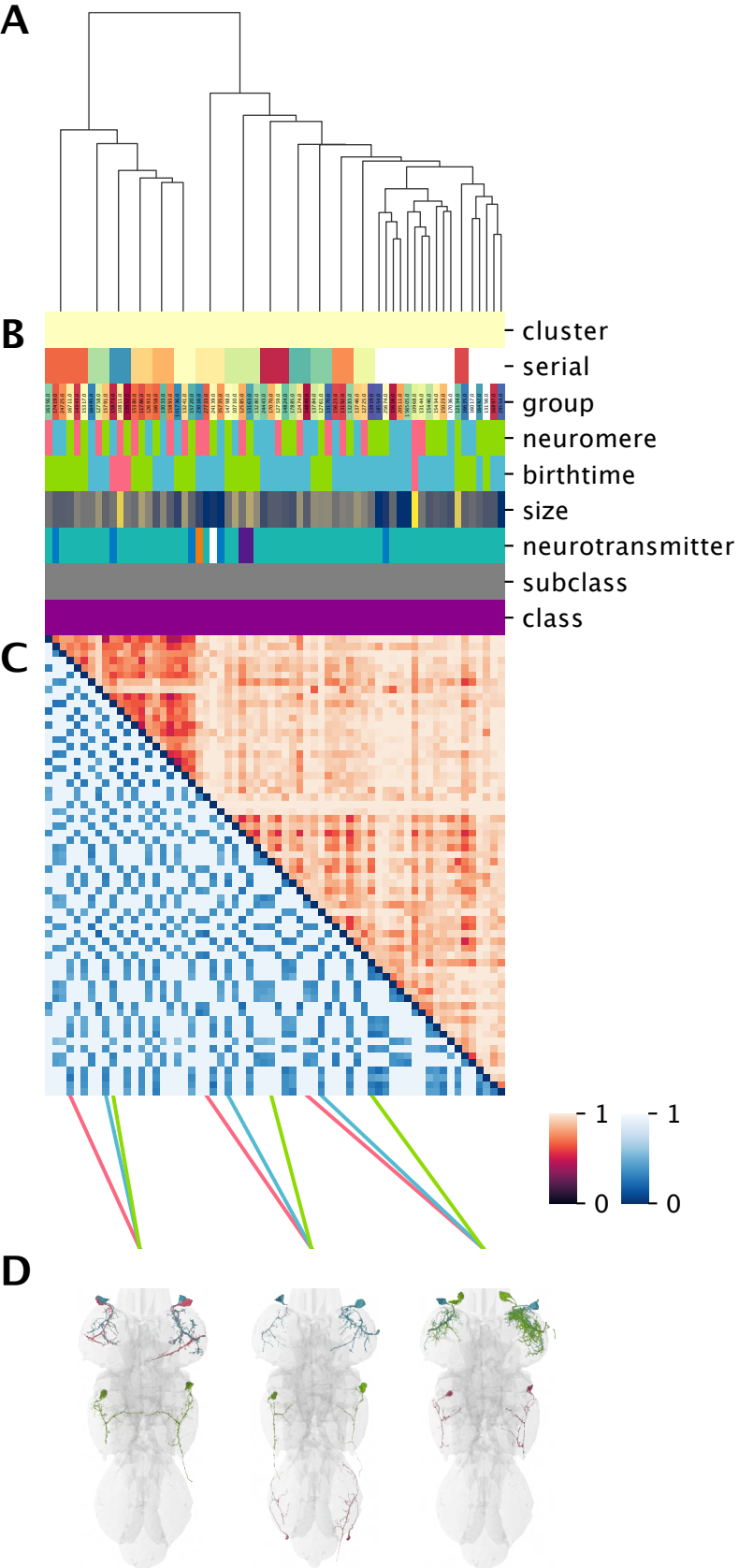
A
B
C
D
cluster
serial
group
neuromere
birthtime
size
neurotransmitter
subclass
class
1
0
1
0

Hemilineage 16B

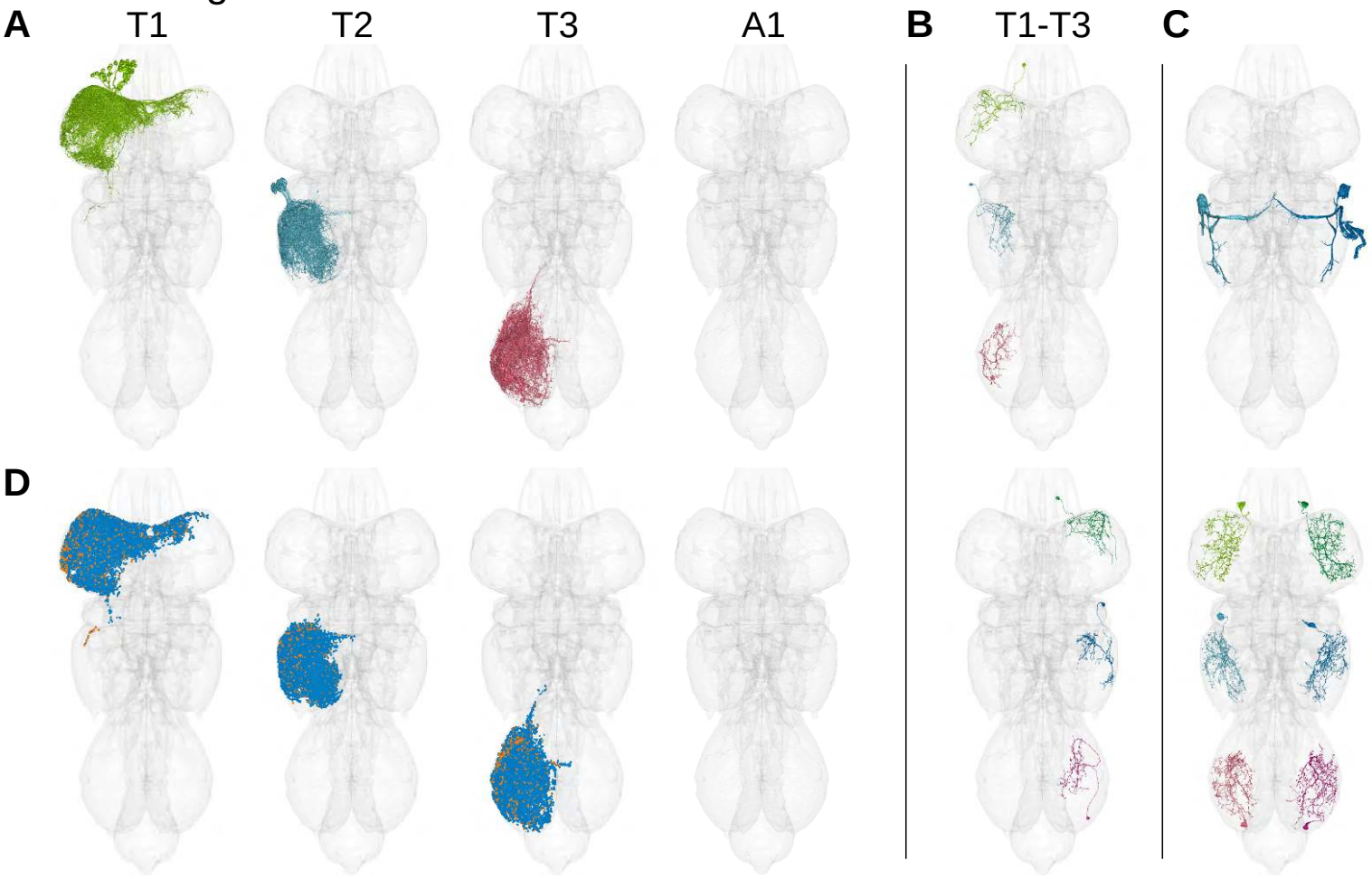

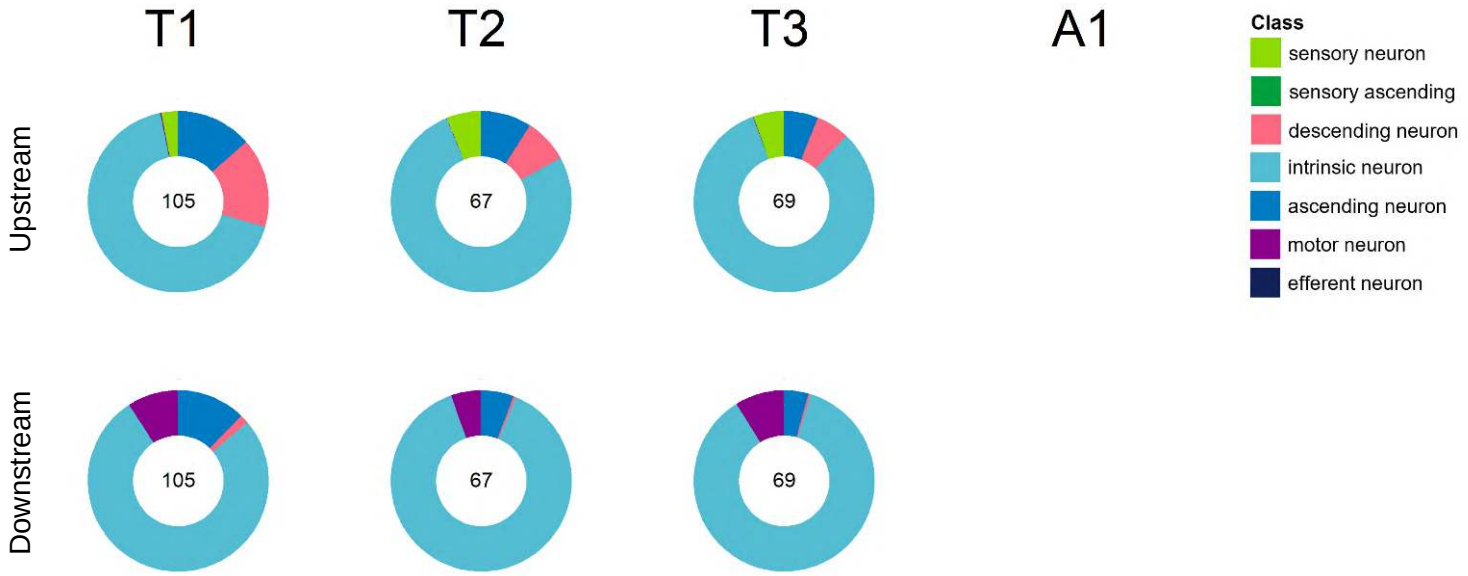

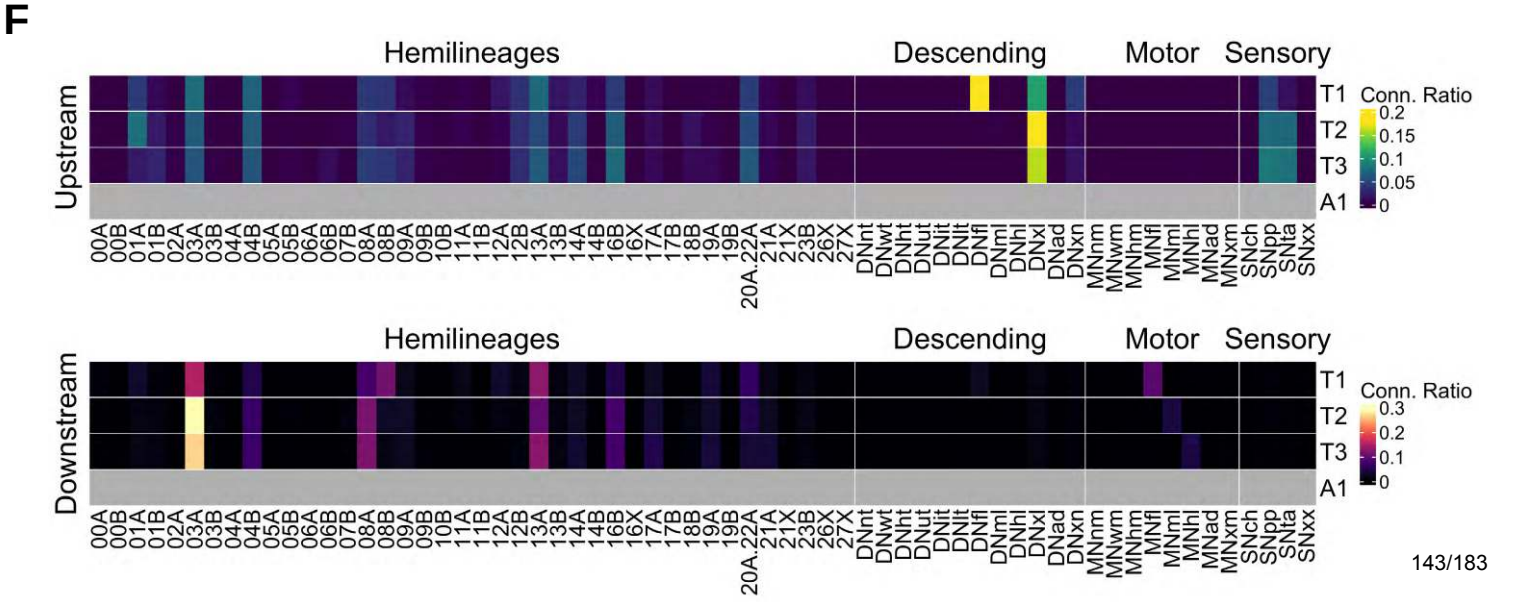

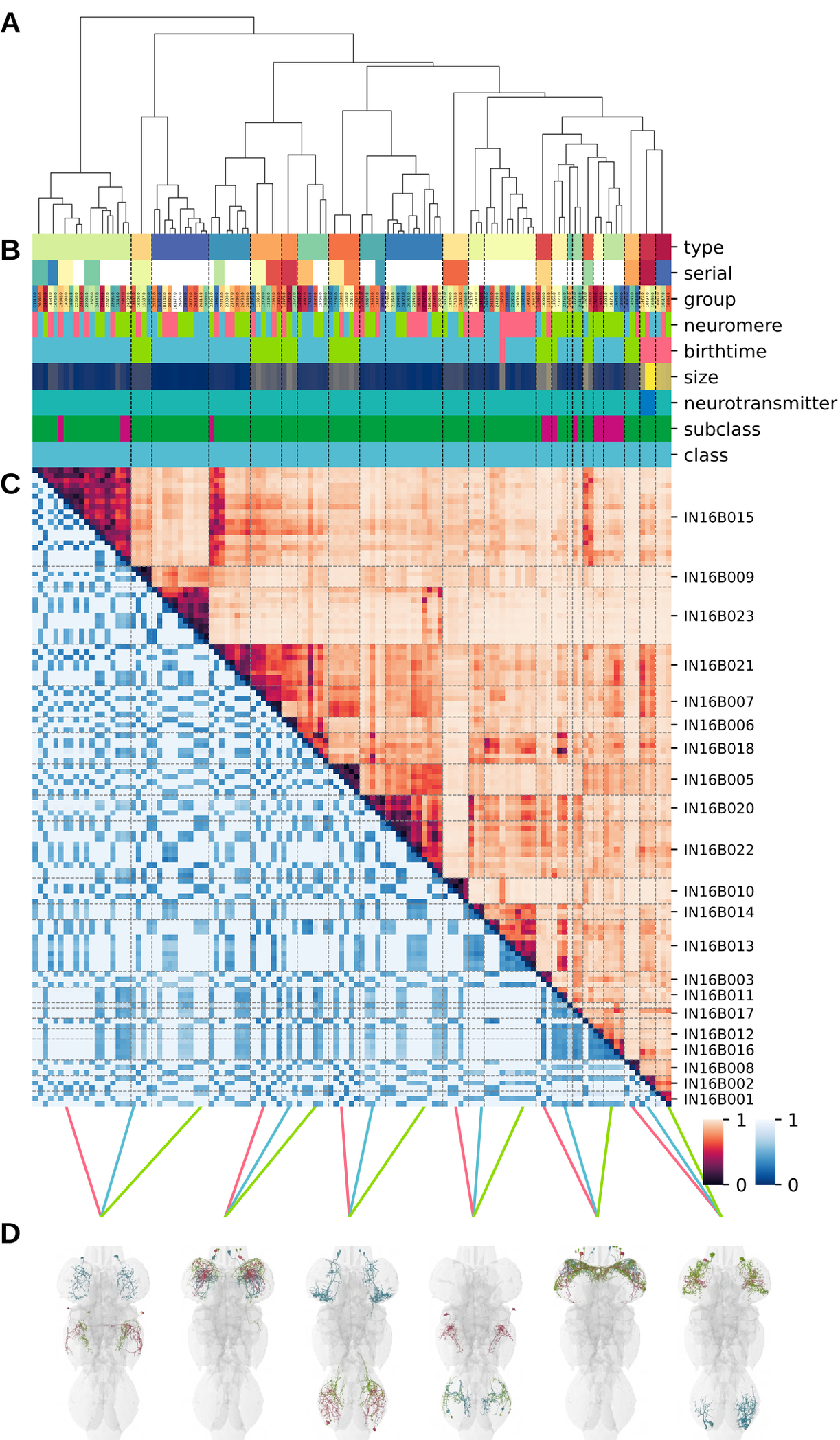
A
B
C
D
type
serial
group
neuromere
birthtime
size
neurotransmitter
subclass
class
IN16B015
IN16B009
IN16B023
IN16B021
IN16B007
IN16B006
IN16B018
IN16B005
IN16B020
IN16B022
IN16B010
IN16B014
IN16B013
IN16B003
IN16B011
IN16B017
IN16B012
IN16B016
IN16B008
IN16B002
IN16B001
1
0
1
0

Hemilineage 16X

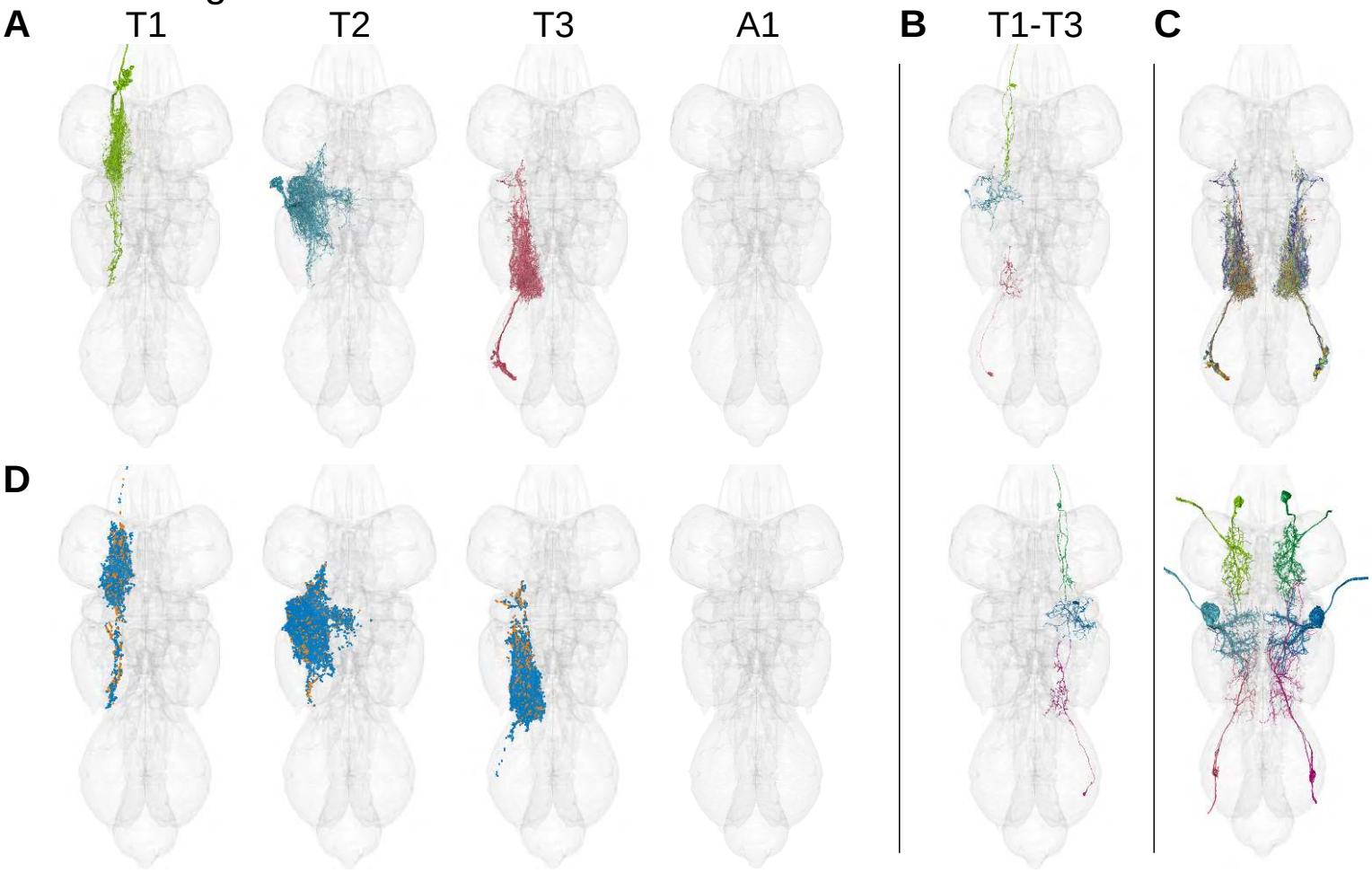

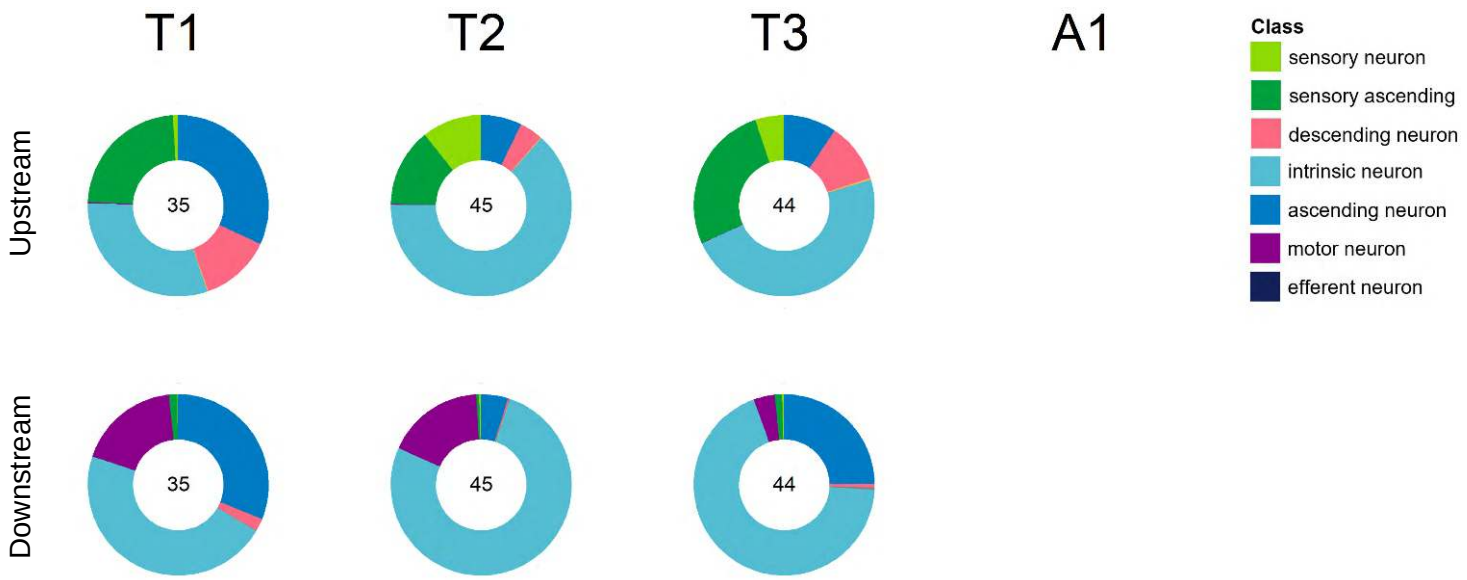

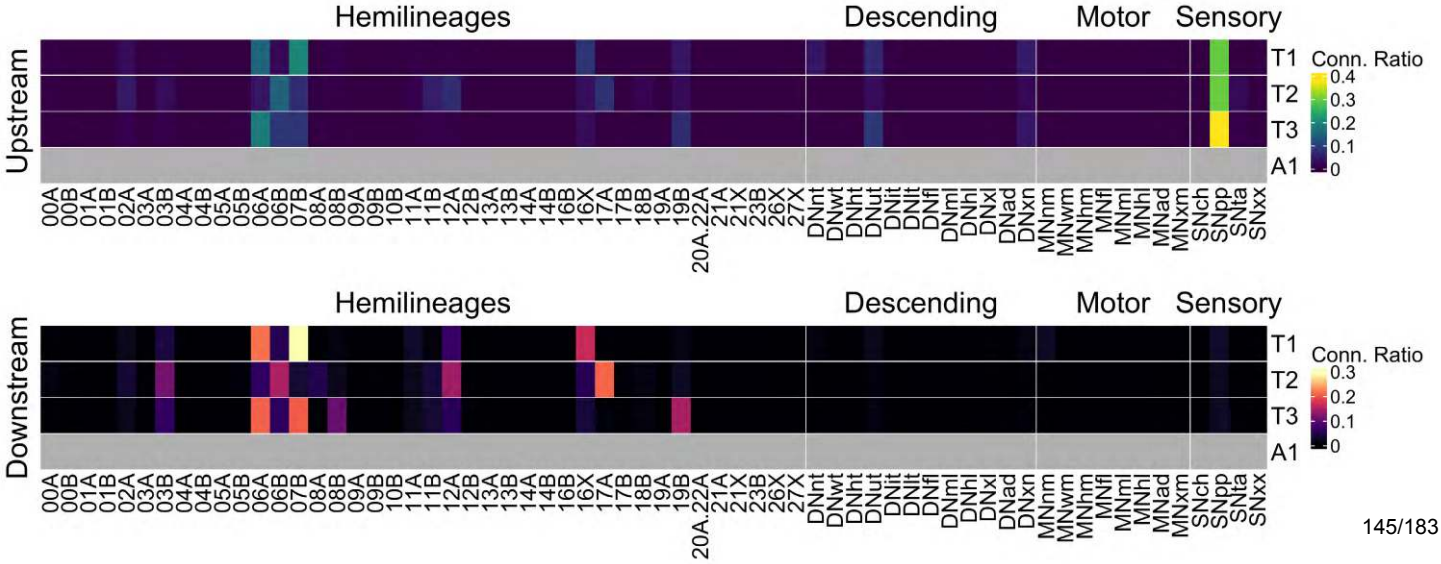

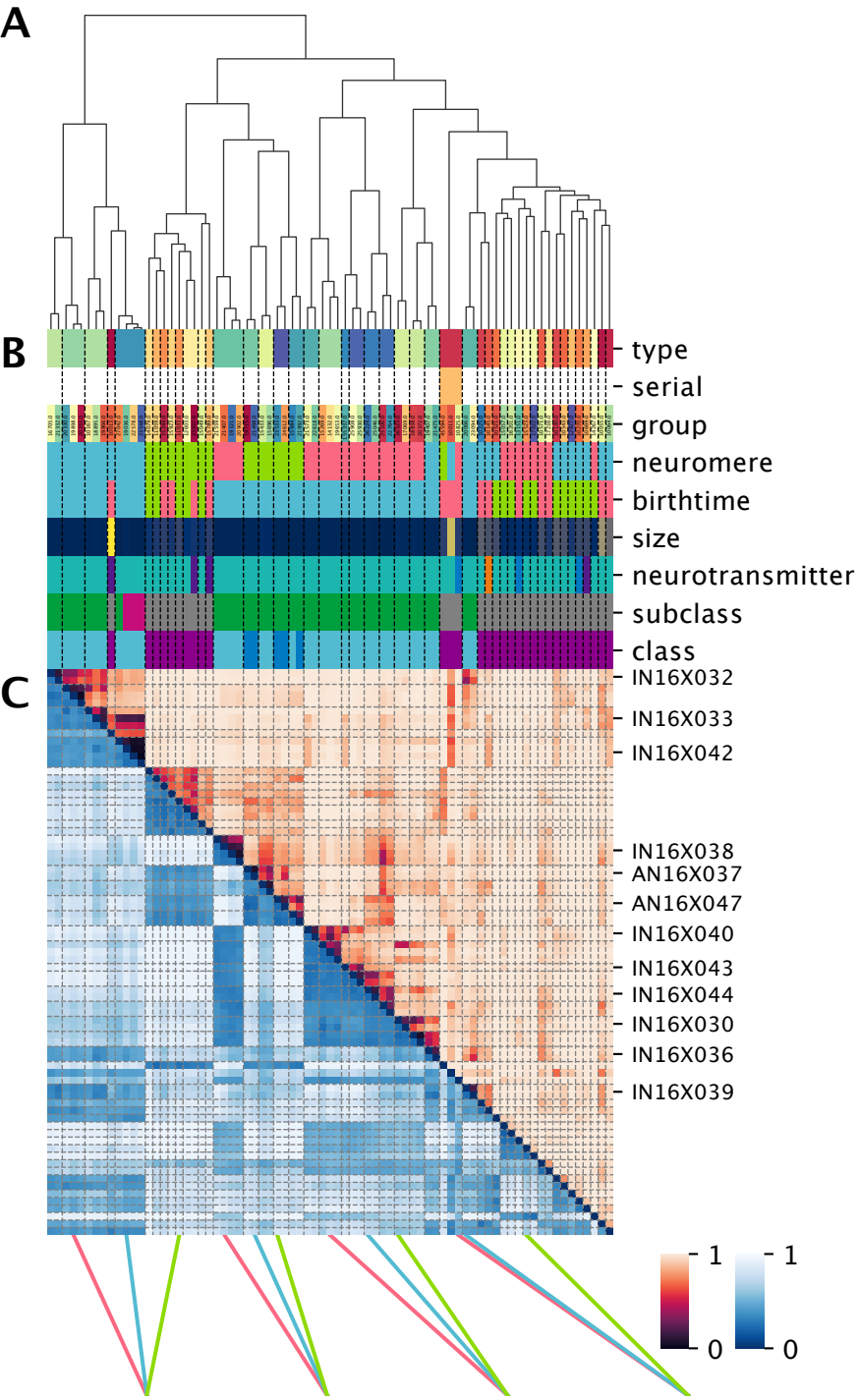
A
B
C
type
serial
group
neuromere
birthtime
size
neurotransmitter
subclass
class
IN16X032
IN16X033
IN16X042
IN16X038
AN16X037
AN16X047
IN16X040
IN16X043
IN16X044
IN16X030
IN16X036
IN16X039
1
0
1
0

D

Hemilineage 17A

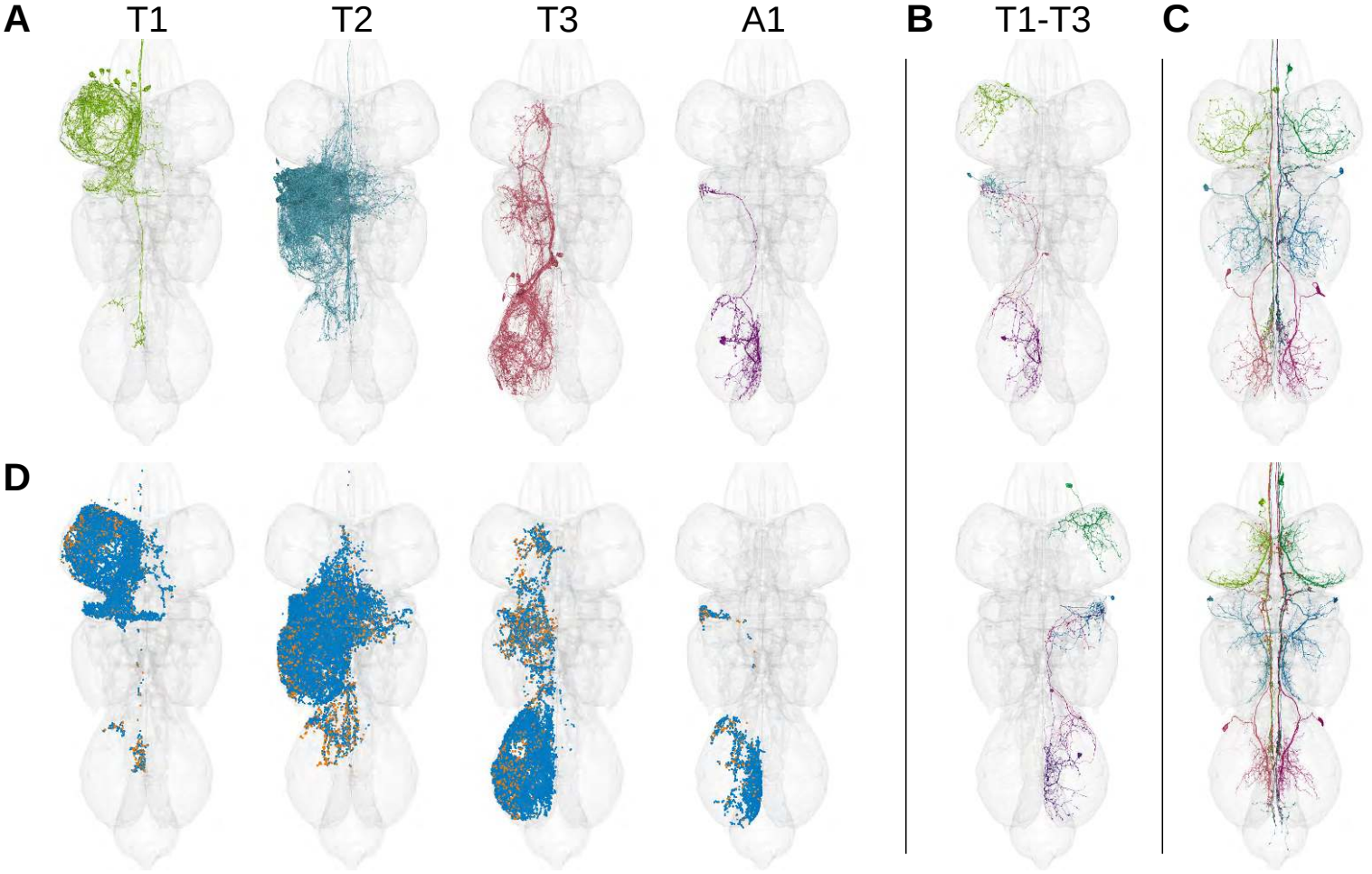

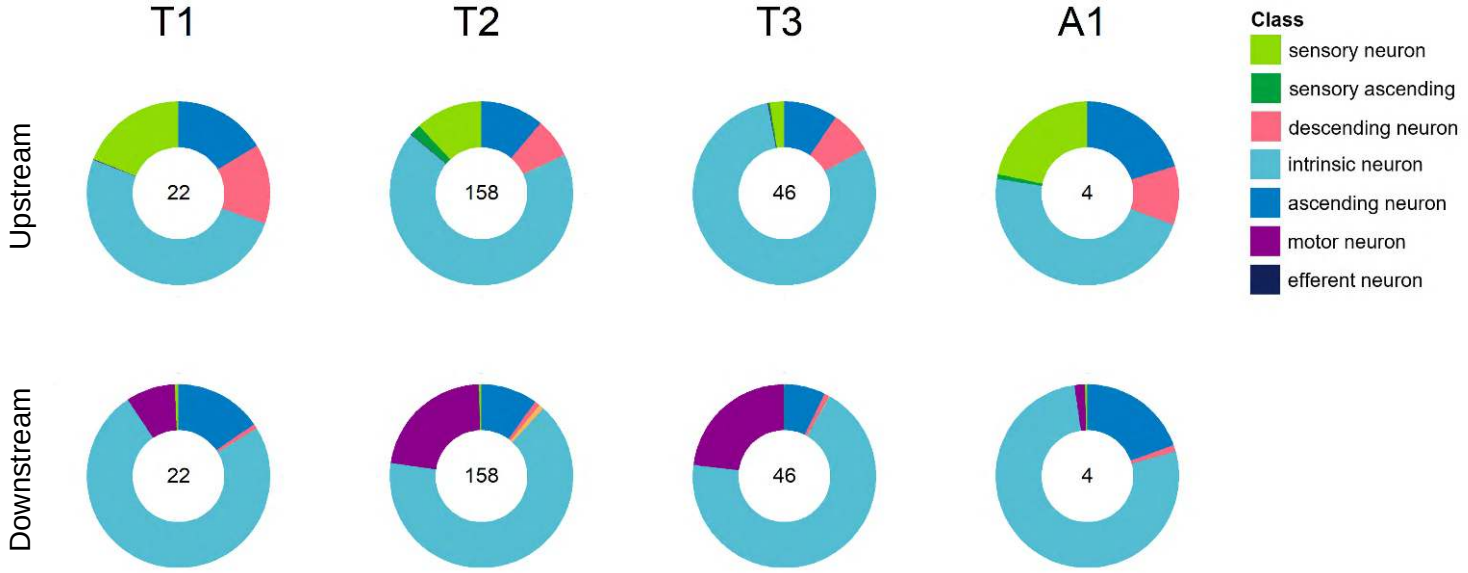

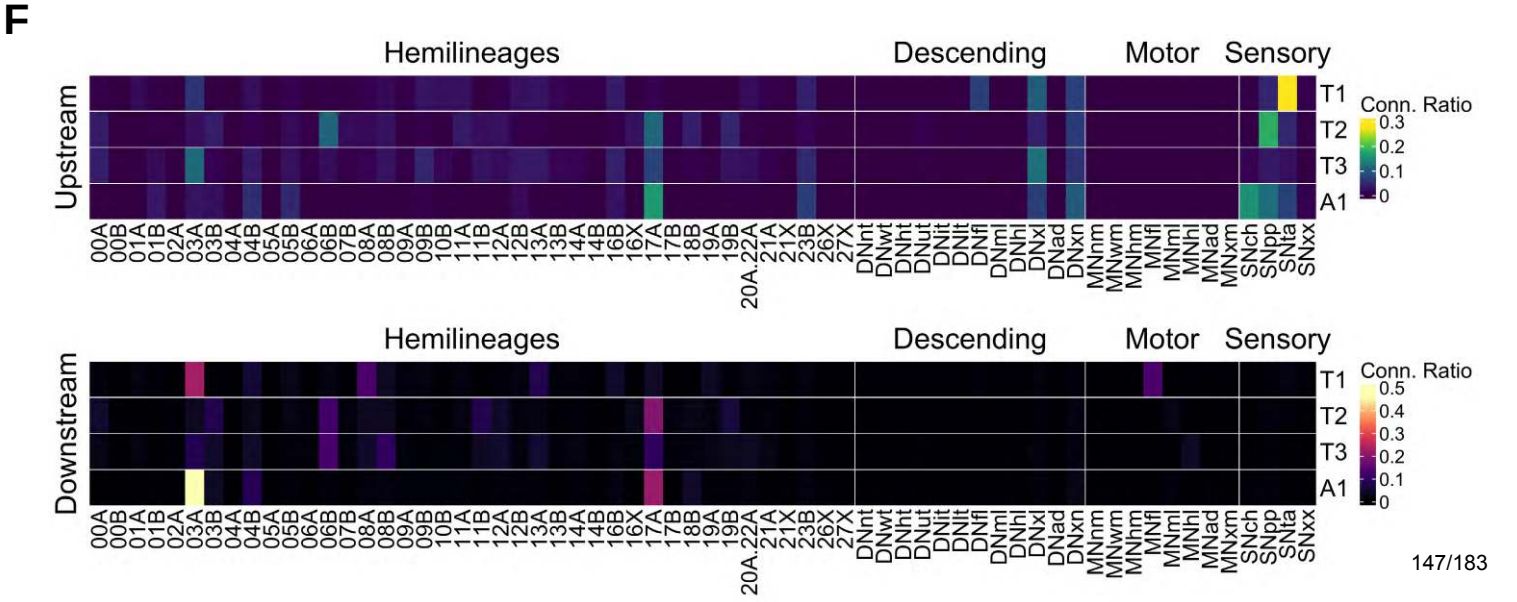

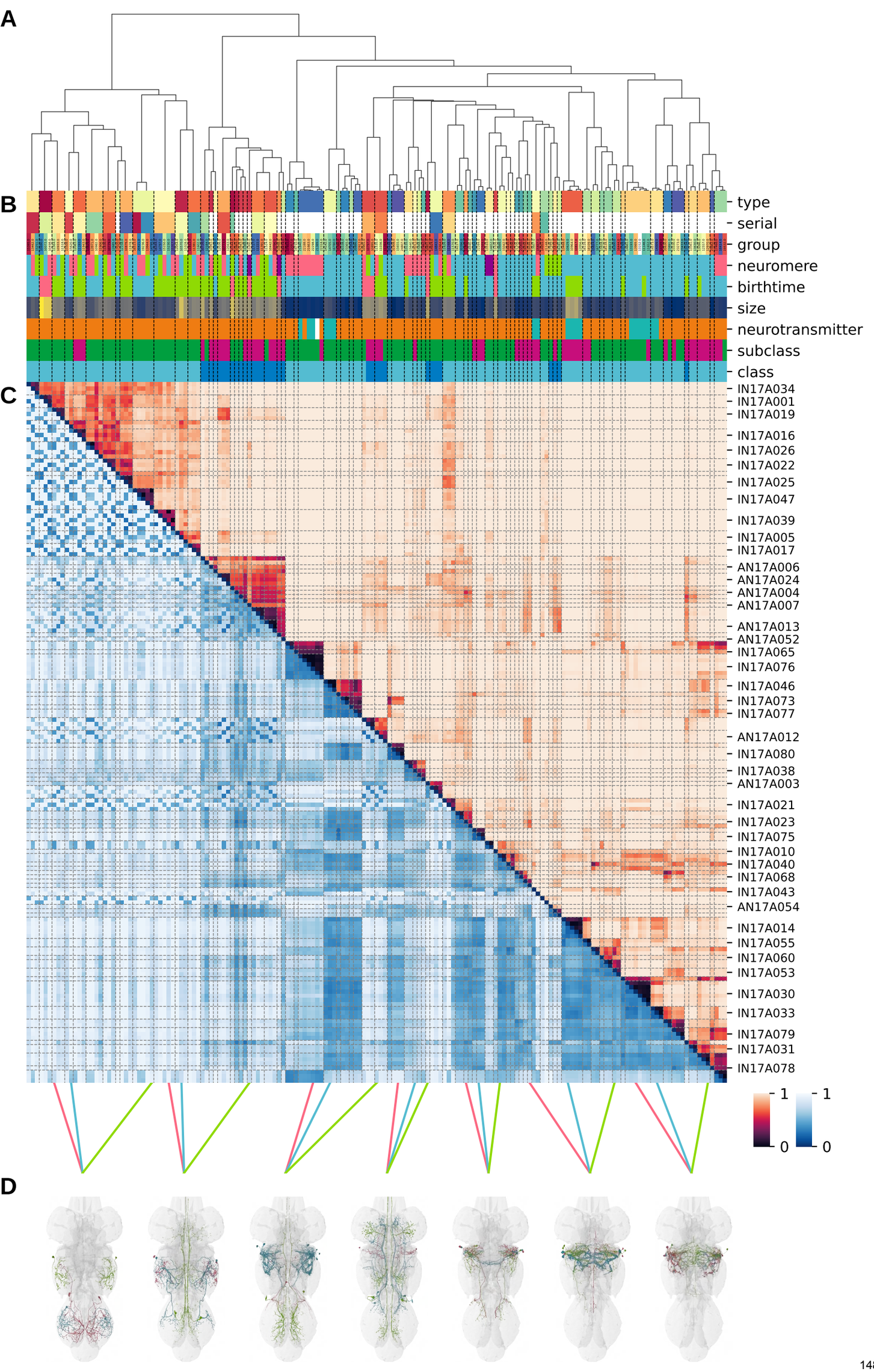
A
B
C
D
type
serial
group
neuromere
birthtime
size
neurotransmitter
subclass
class
IN17A034
IN17A001
IN17A019
IN17A016
IN17A026
IN17A022
IN17A025
IN17A047
IN17A039
IN17A005
IN17A017
AN17A006
AN17A024
AN17A004
AN17A007
AN17A013
AN17A052
IN17A065
IN17A076
IN17A046
IN17A073
IN17A077
AN17A012
IN17A080
IN17A038
AN17A003
IN17A021
IN17A023
IN17A075
IN17A010
IN17A040
IN17A068
IN17A043
AN17A054
IN17A014
IN17A055
IN17A060
IN17A053
IN17A030
IN17A033
IN17A079
IN17A031
IN17A078
1
0
1
0

Hemilineage 18B

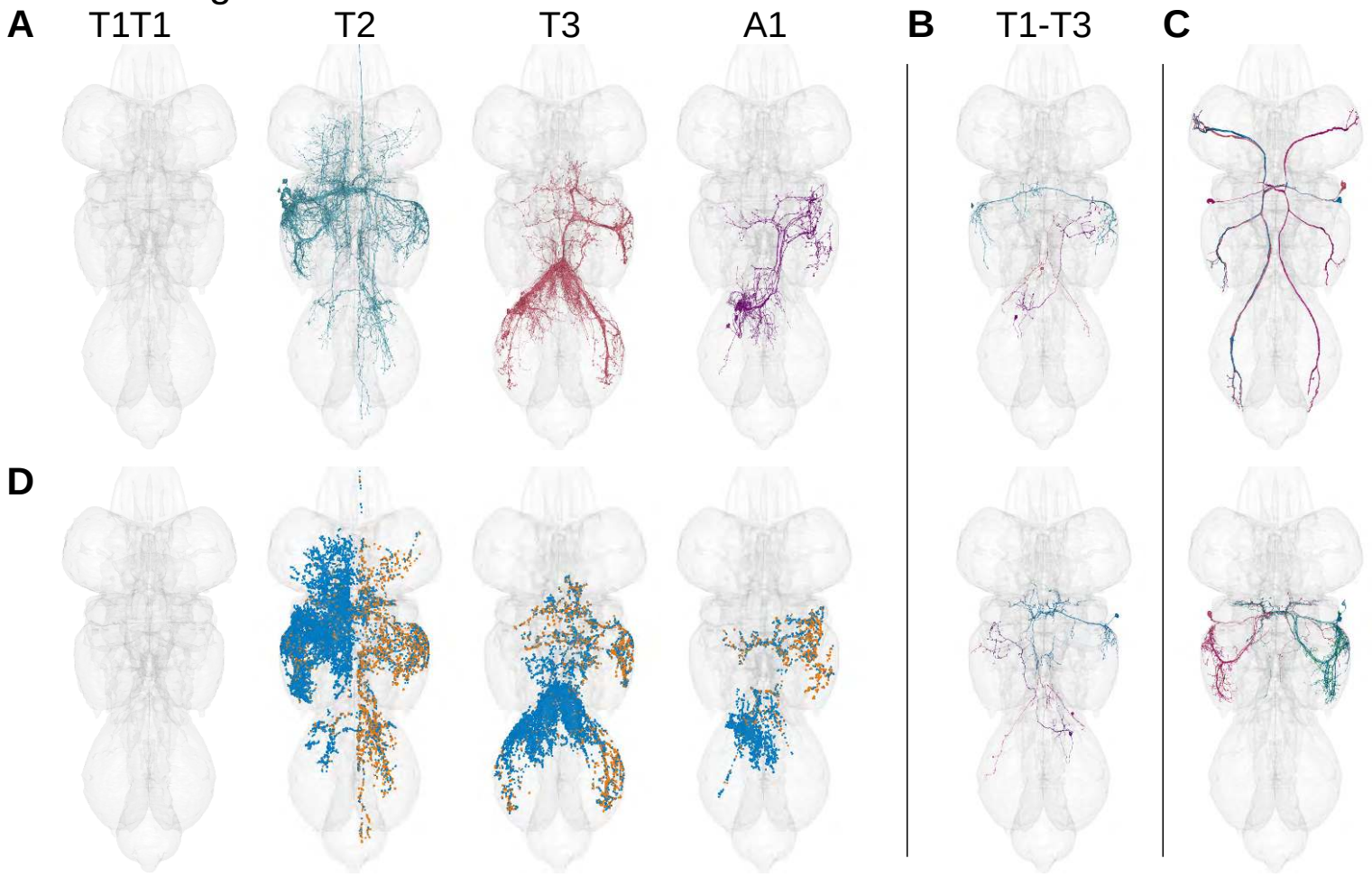

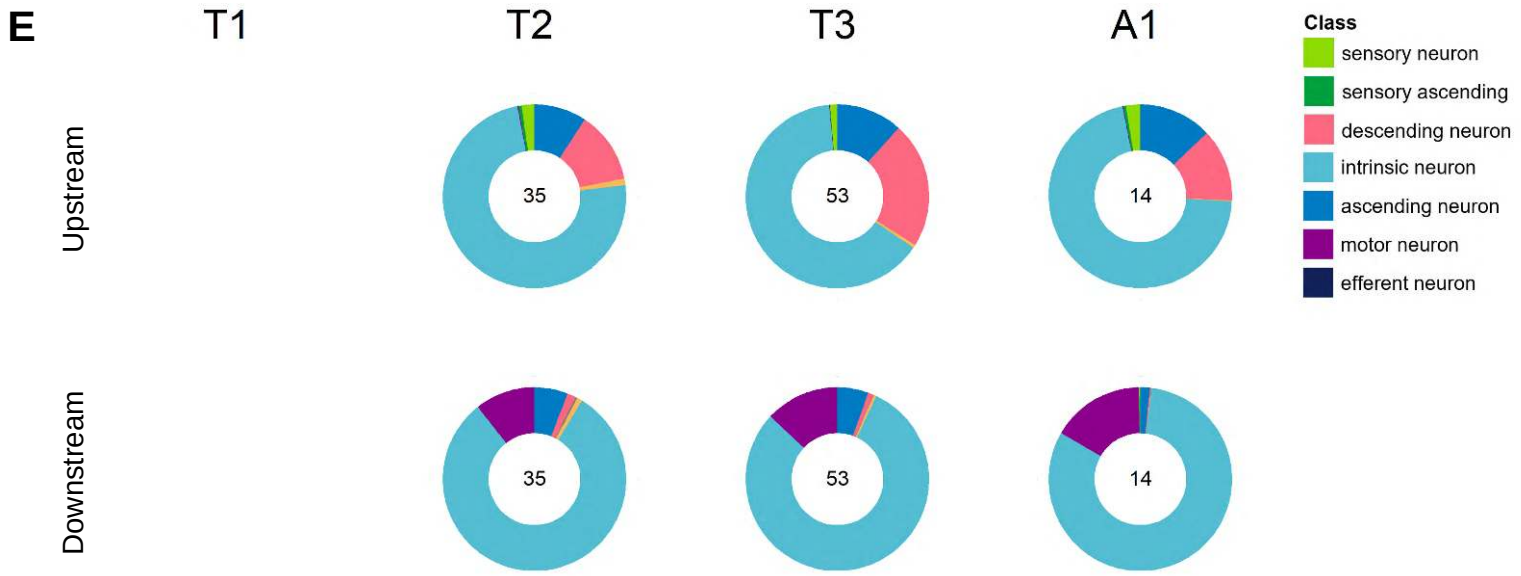

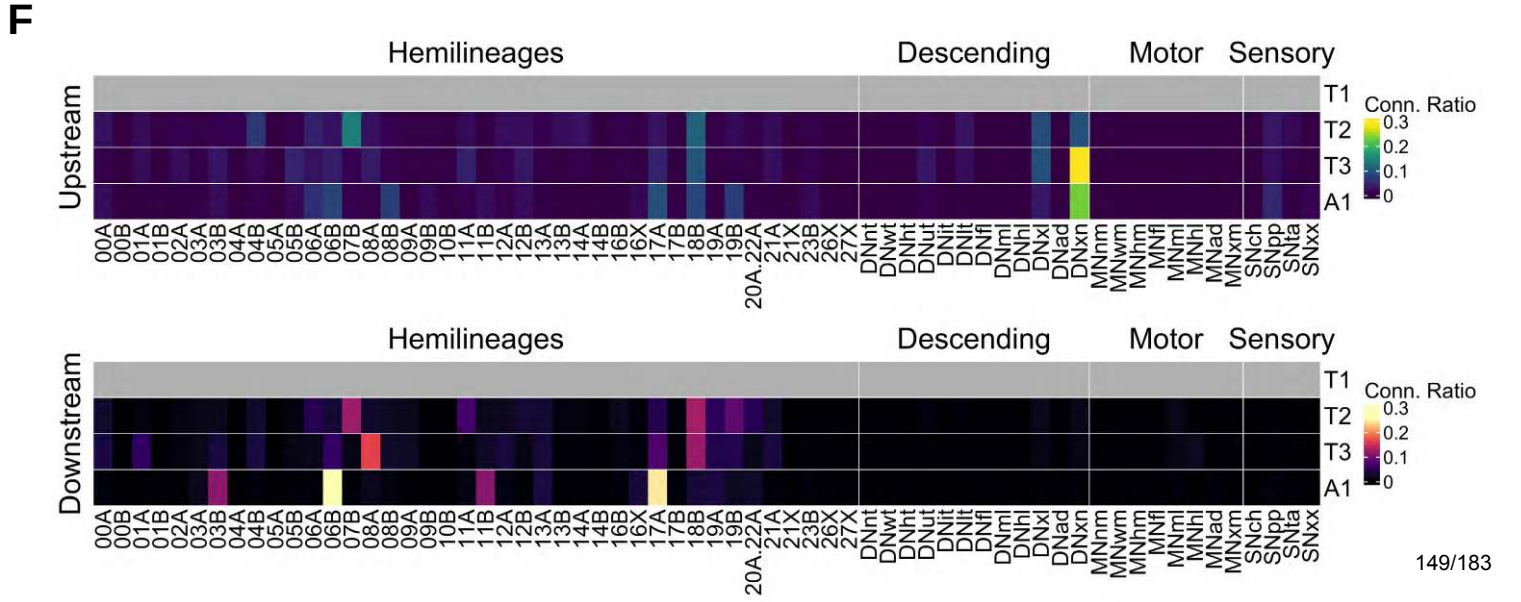

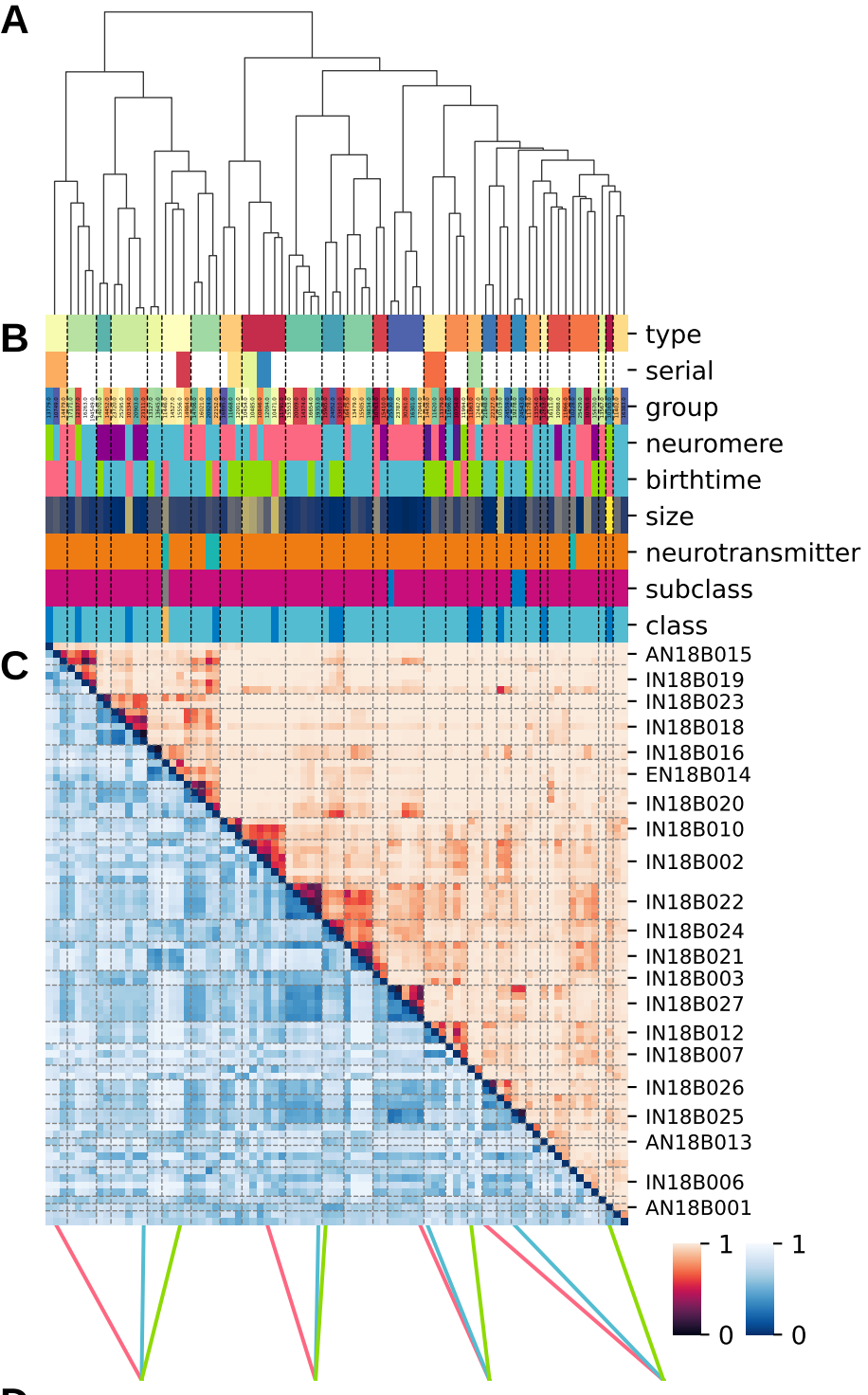
A
B
type
serial
group
neuromere
birthtime
size
neurotransmitter
subclass
class
C
AN18B015
IN18B019
IN18B023
IN18B018
IN18B016
EN18B014
IN18B020
IN18B010
IN18B002
IN18B022
IN18B024
IN18B021
IN18B003
IN18B027
IN18B012
IN18B007
IN18B026
IN18B025
AN18B013
IN18B006
AN18B001
1
0
1
0

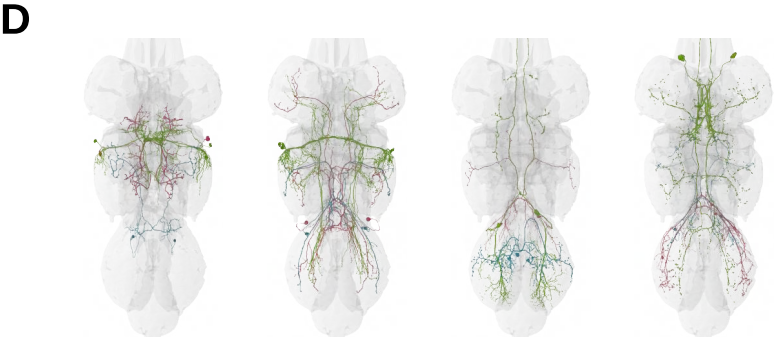
D

Hemilineage 19A

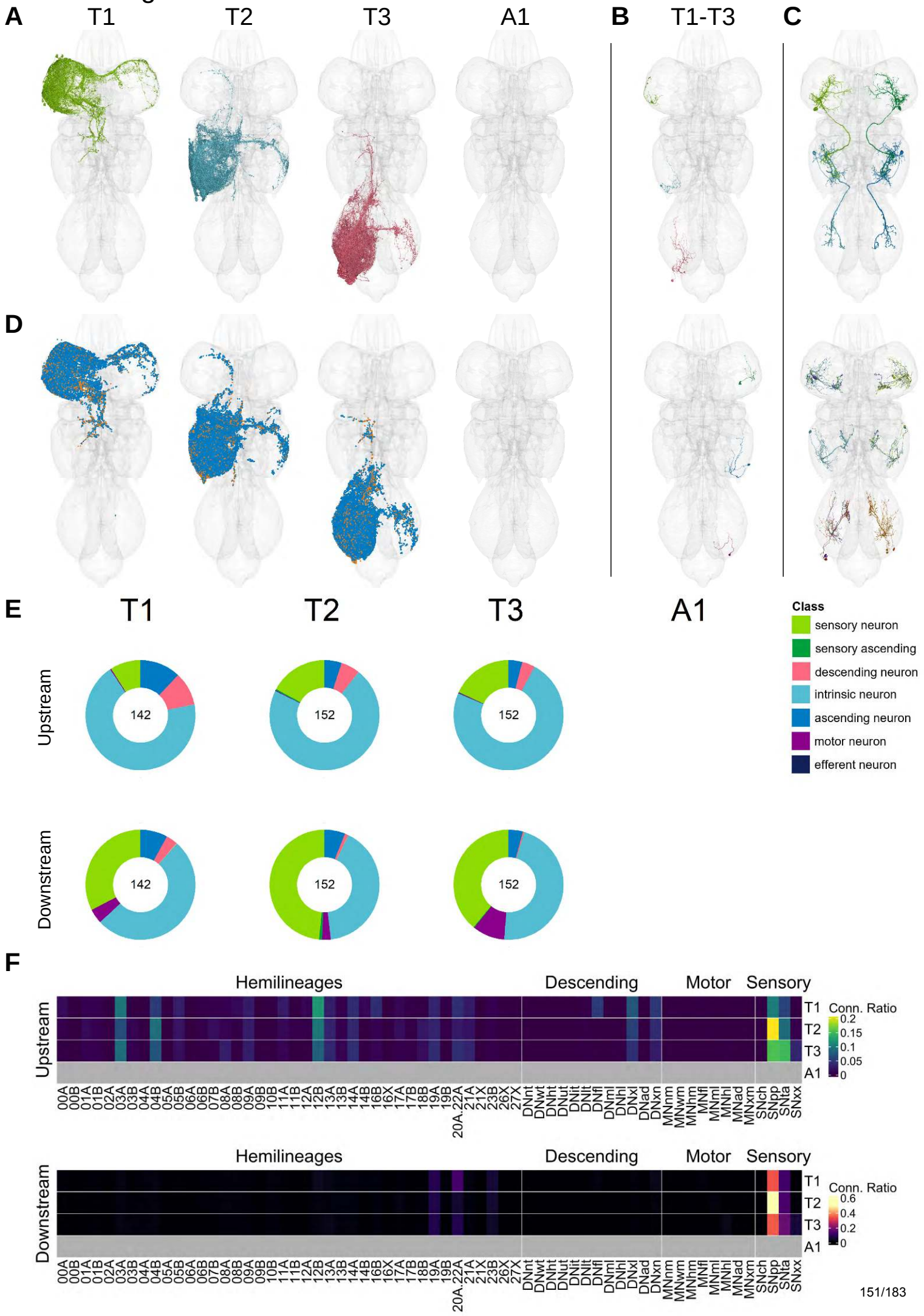

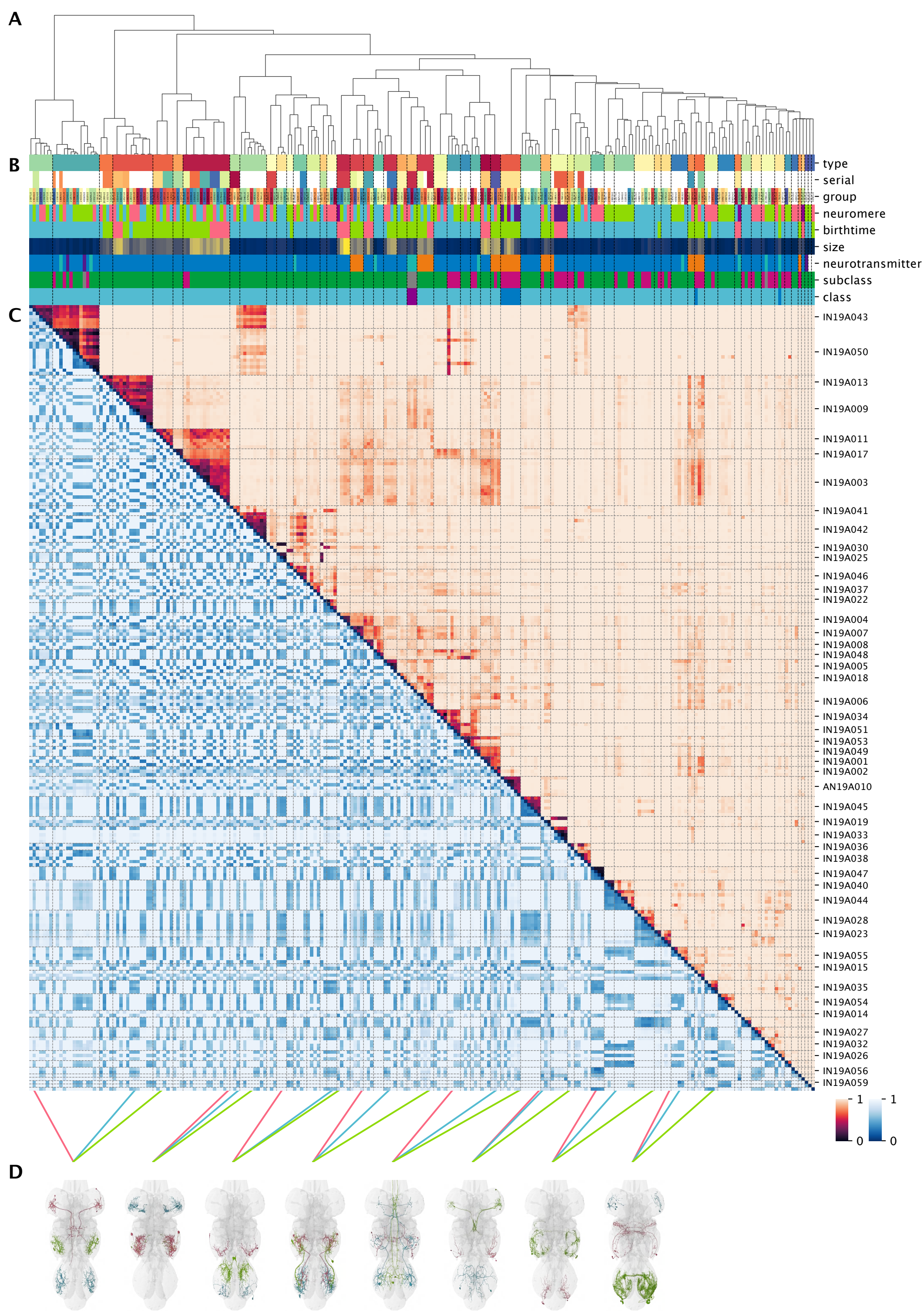
A
B
C
D
type
serial
group
neuromere
birthtime
size
neurotransmitter
subclass
class
IN19A043
IN19A050
IN19A013
IN19A009
IN19A011
IN19A017
IN19A003
IN19A041
IN19A042
IN19A030
IN19A025
IN19A046
IN19A037
IN19A022
IN19A004
IN19A007
IN19A008
IN19A048
IN19A005
IN19A018
IN19A006
IN19A034
IN19A051
IN19A053
IN19A049
IN19A001
IN19A002
AN19A010
IN19A045
IN19A019
IN19A033
IN19A036
IN19A038
IN19A047
IN19A040
IN19A044
IN19A028
IN19A023
IN19A055
IN19A015
IN19A035
IN19A054
IN19A014
IN19A027
IN19A032
IN19A026
IN19A056
IN19A059
1
0
1
0

Hemilineage 19B

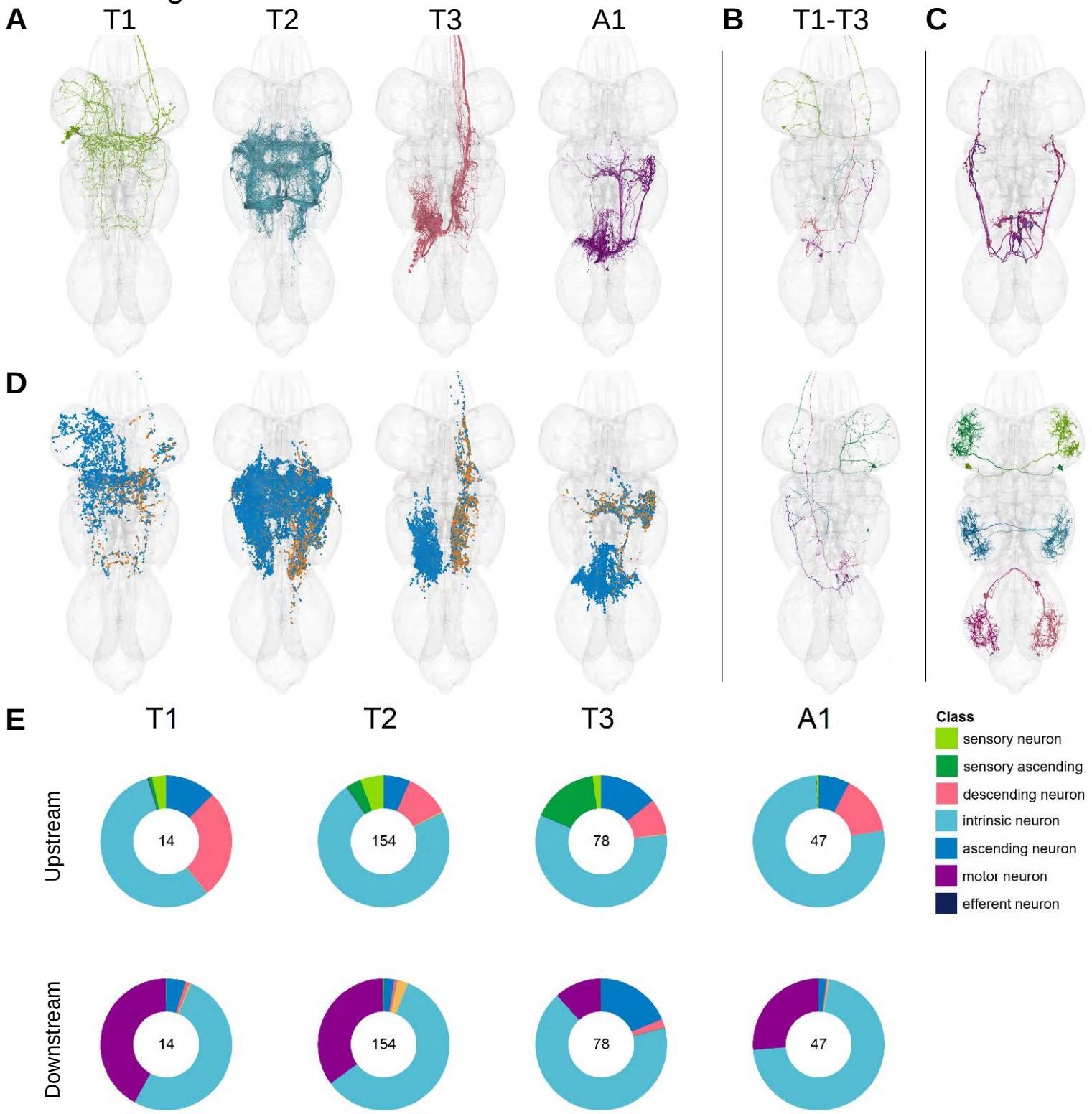

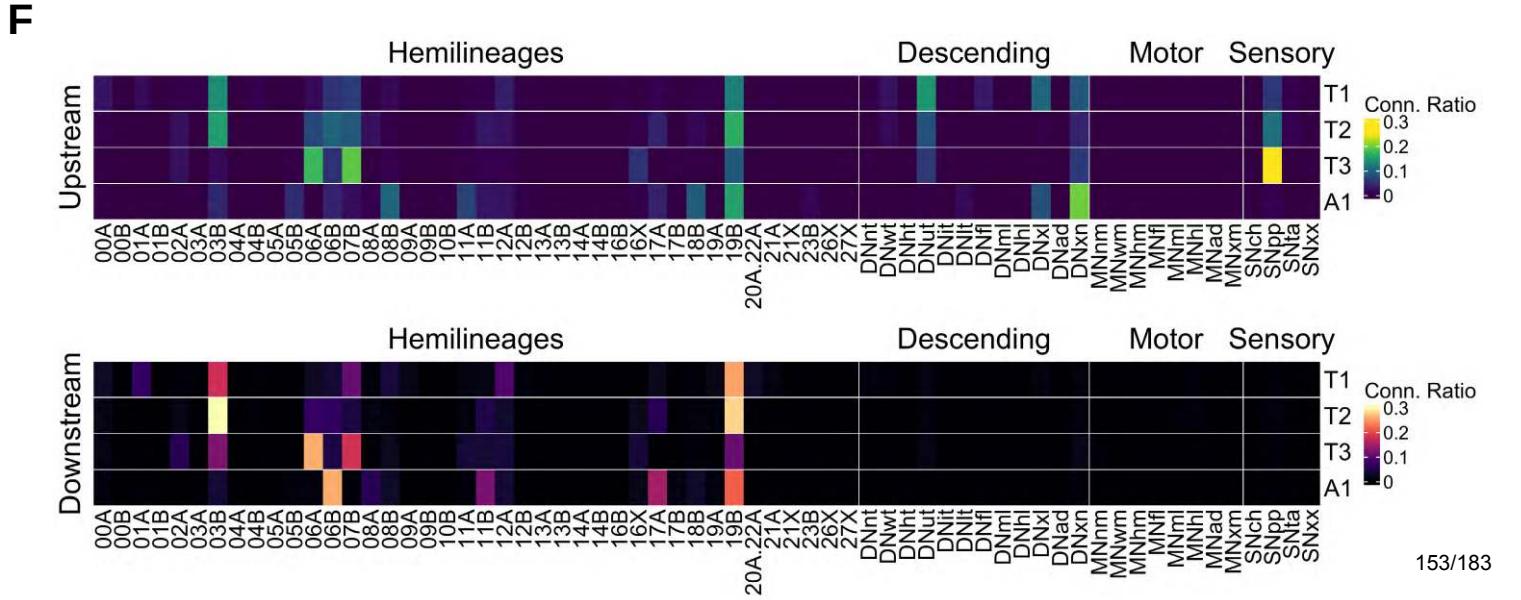

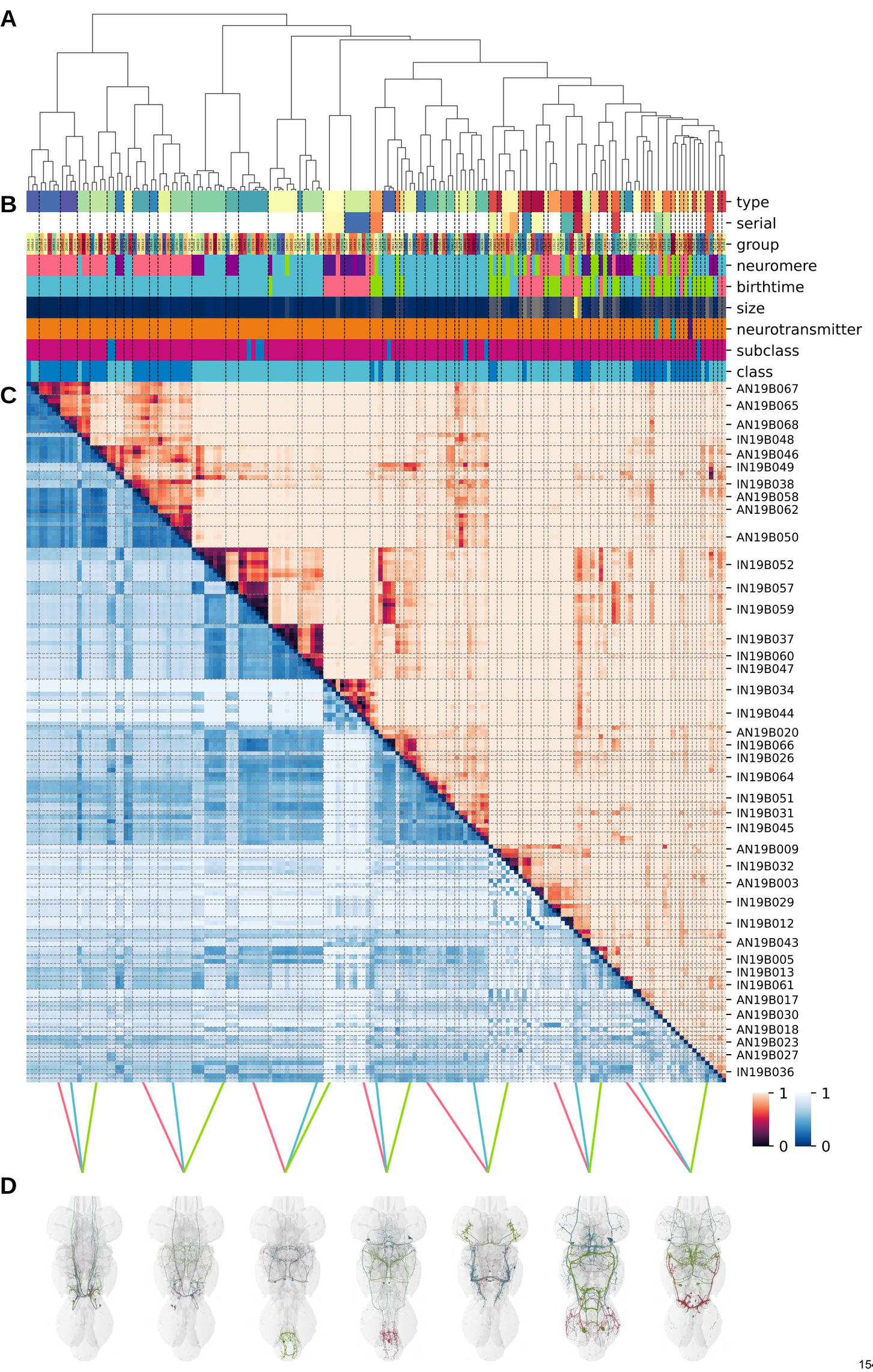
A
B
C
D
type
serial
group
neuromere
birthtime
size
neurotransmitter
subclass
class
AN19B067
AN19B065
AN19B068
IN19B048
AN19B046
IN19B049
IN19B038
AN19B058
AN19B062
AN19B050
IN19B052
IN19B057
IN19B059
IN19B037
IN19B060
IN19B047
IN19B034
IN19B044
AN19B020
IN19B066
IN19B026
IN19B064
IN19B051
IN19B031
IN19B045
AN19B009
IN19B032
AN19B003
IN19B029
IN19B012
AN19B043
IN19B005
IN19B013
IN19B061
AN19B017
AN19B030
AN19B018
AN19B023
AN19B027
IN19B036
1
0
1
0

Hemilineage 20A.22A

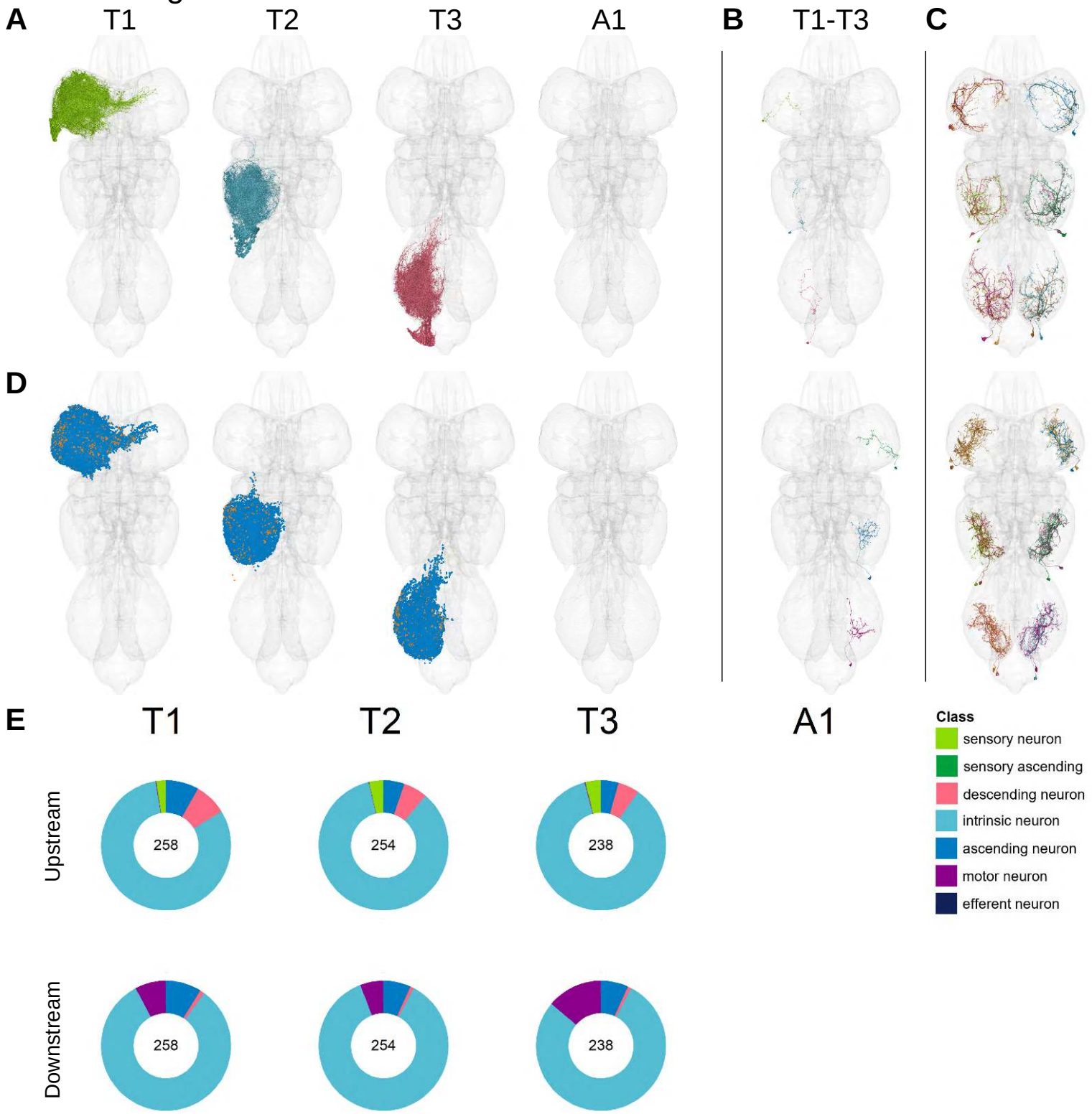

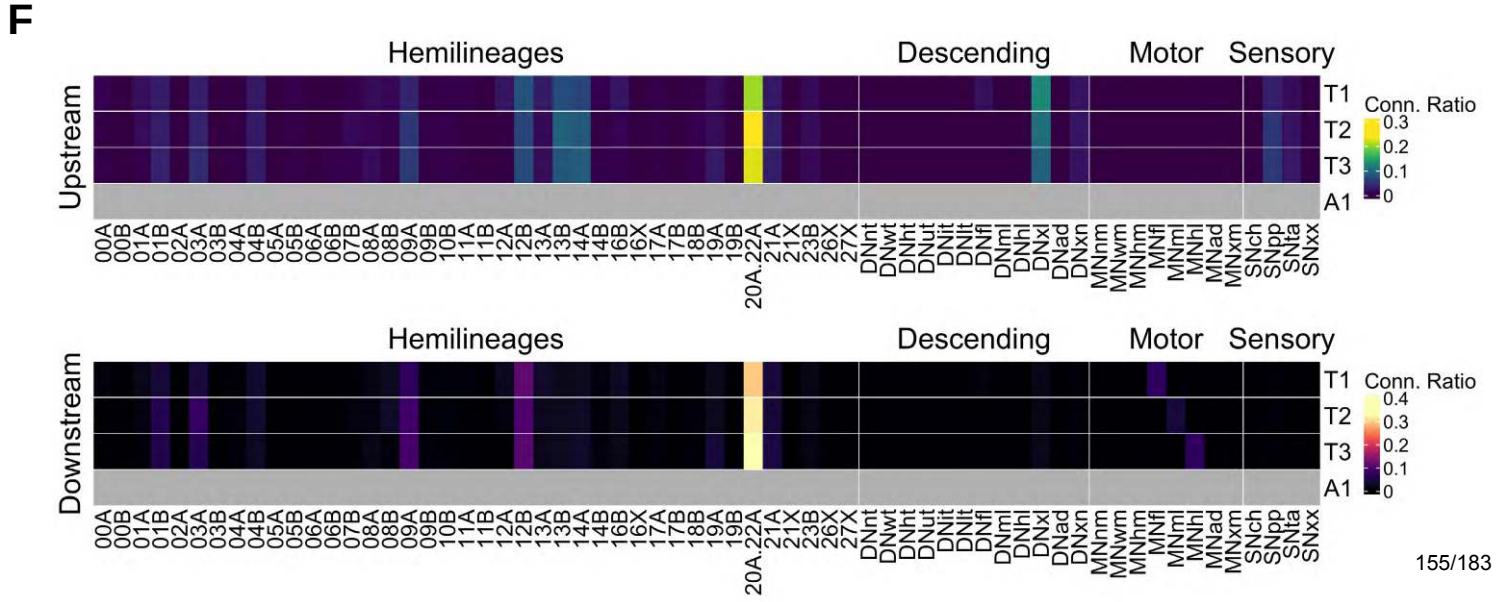

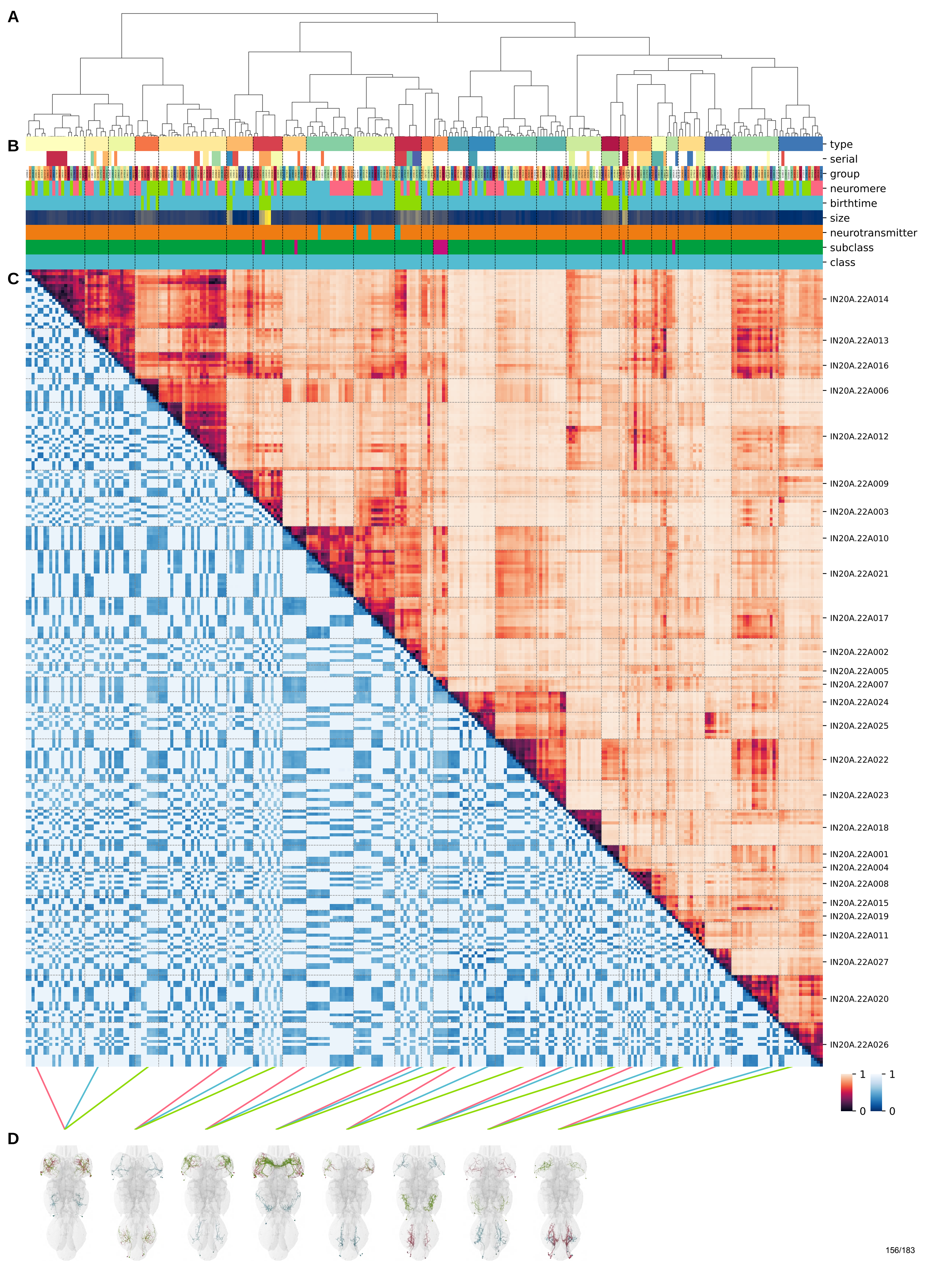
A
B
C
D
type
serial
group
neuromere
birthtime
size
neurotransmitter
subclass
class
IN20A.22A014
IN20A.22A013
IN20A.22A016
IN20A.22A006
IN20A.22A012
IN20A.22A009
IN20A.22A003
IN20A.22A010
IN20A.22A021
IN20A.22A017
IN20A.22A002
IN20A.22A005
IN20A.22A007
IN20A.22A024
IN20A.22A025
IN20A.22A022
IN20A.22A023
IN20A.22A018
IN20A.22A001
IN20A.22A004
IN20A.22A008
IN20A.22A015
IN20A.22A019
IN20A.22A011
IN20A.22A027
IN20A.22A020
IN20A.22A026
1
0
1
0

Hemilineage 21A

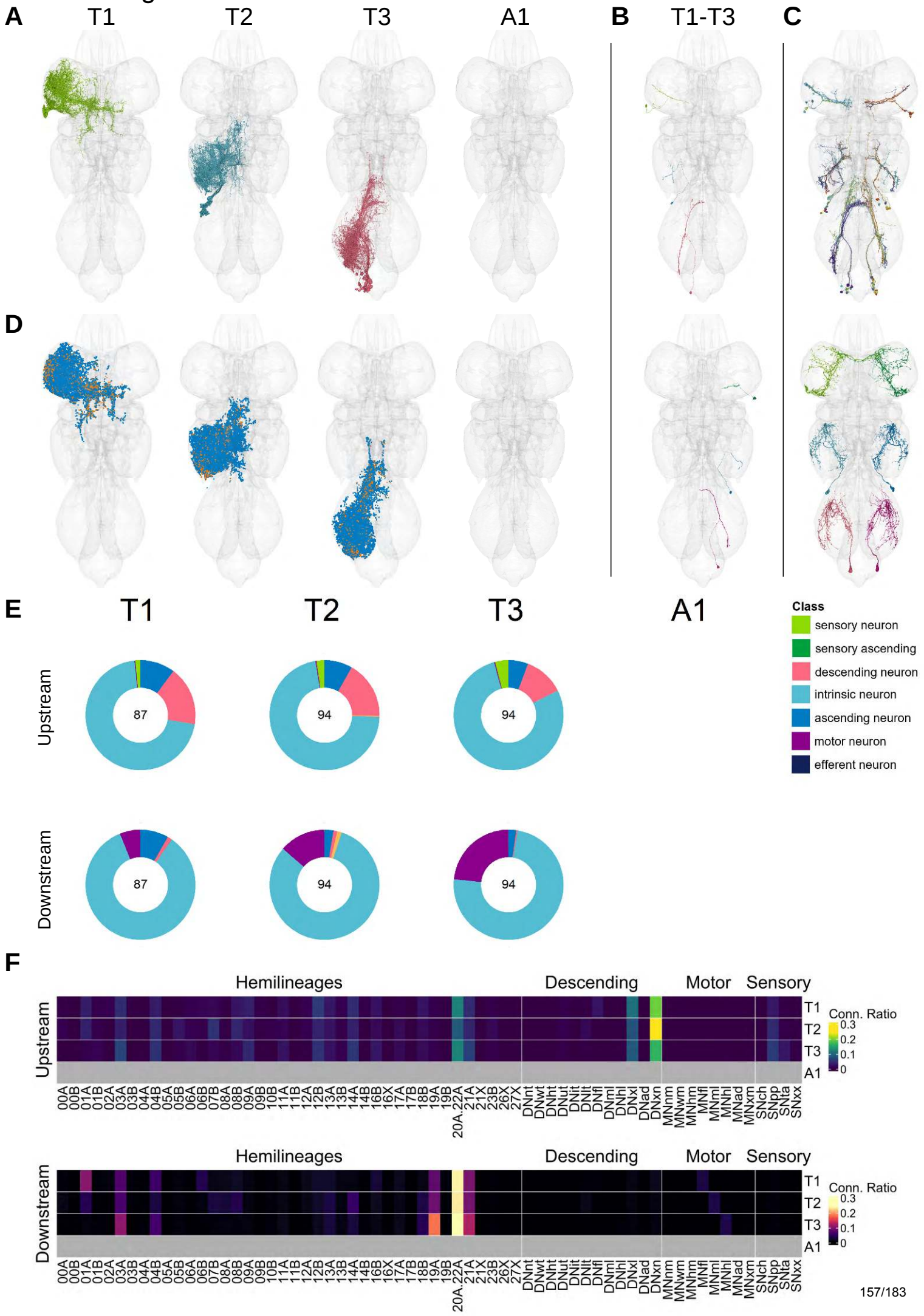

A
B
C
D
type
serial
group
neuromere
birthtime
size
neurotransmitter
subclass
class
IN21A043
IN21A044
IN21A045
IN21A035
IN21A038
IN21A026
IN21A046
IN21A028
IN21A022
IN21A039
IN21A032
IN21A027
IN21A029
IN21A041
IN21A031
IN21A008
IN21A014
IN21A019
IN21A021
IN21A003
IN21A017
IN21A025
IN21A024
IN21A048
IN21A006
IN21A002
IN21A016
IN21A013
IN21A012
IN21A005
IN21A009
IN21A010
IN21A015
IN21A007
IN21A018
IN21A001
IN21A011
IN21A030
IN21A023
IN21A037
IN21A042
IN21A040
IN21A052
IN21A051
1
0
1
0

Hemilineage 23B

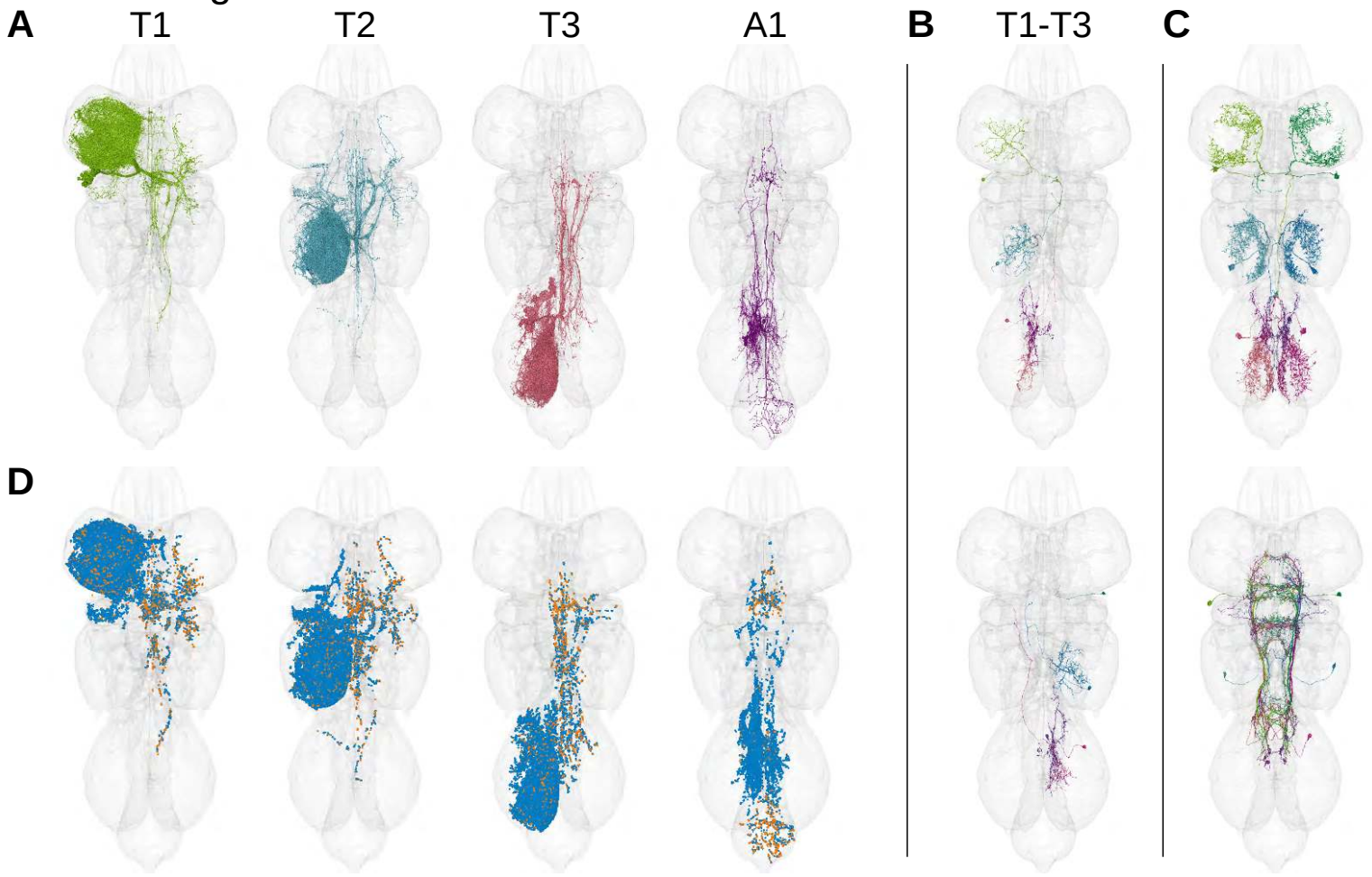

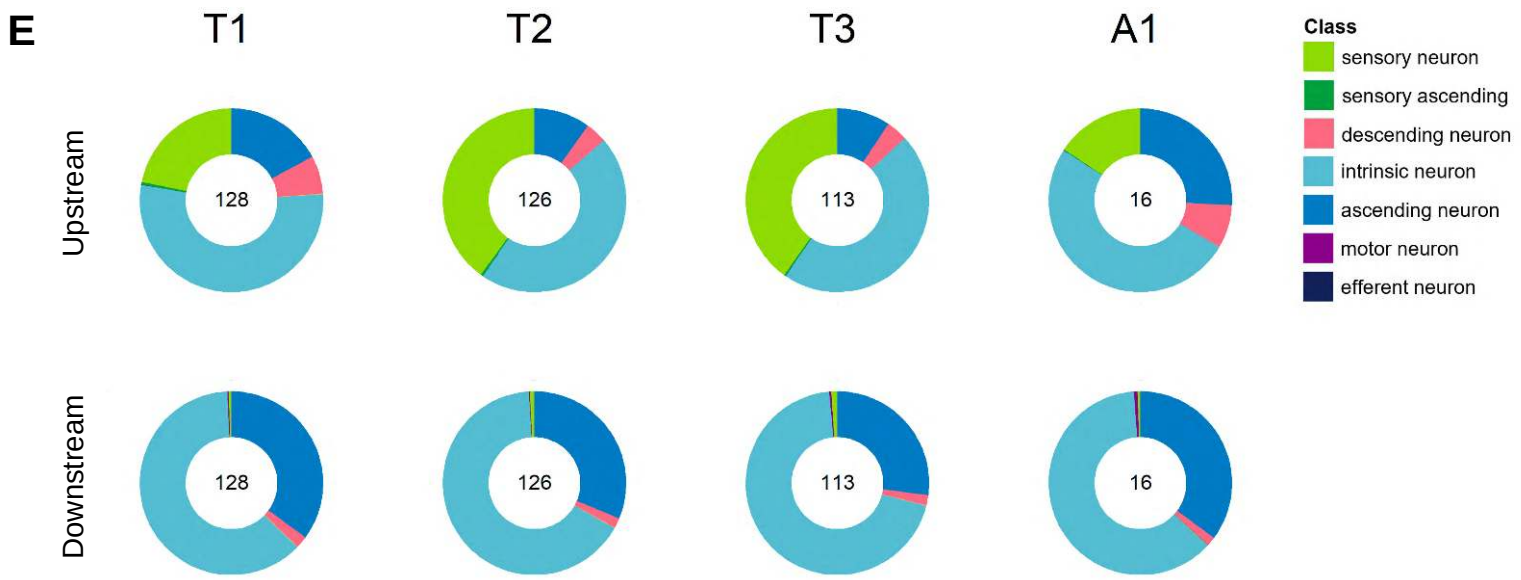

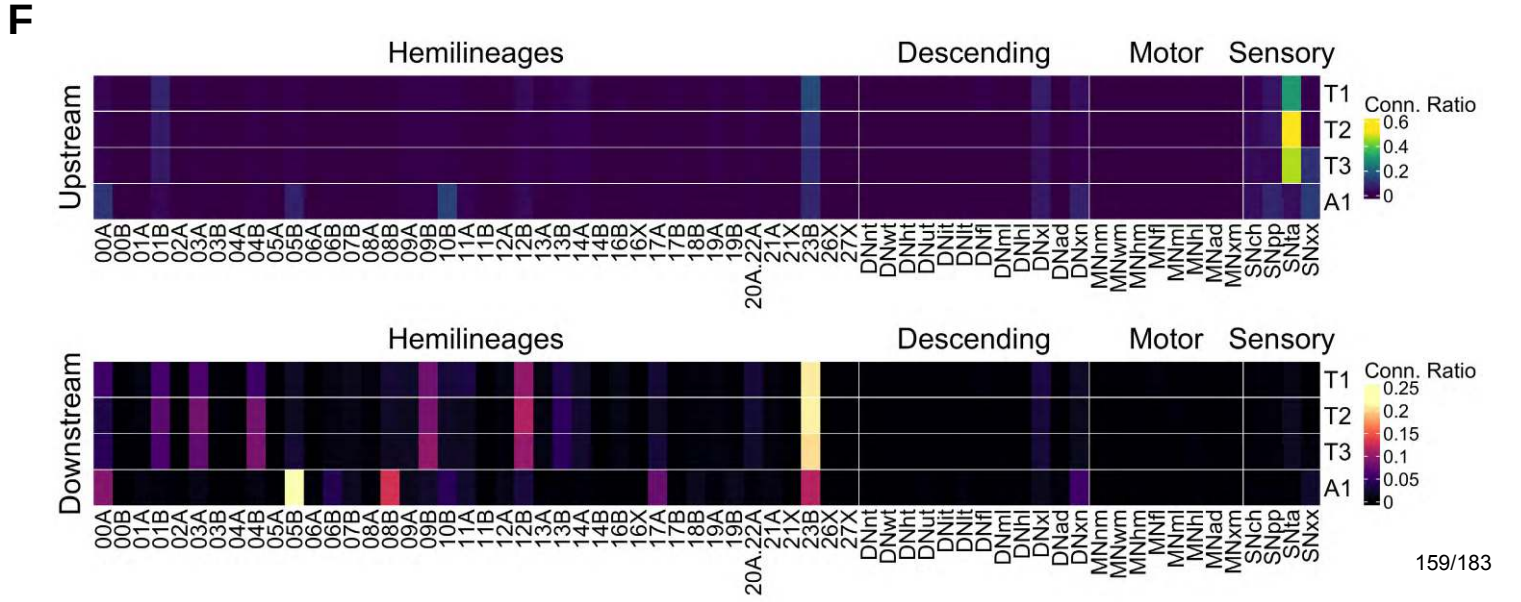

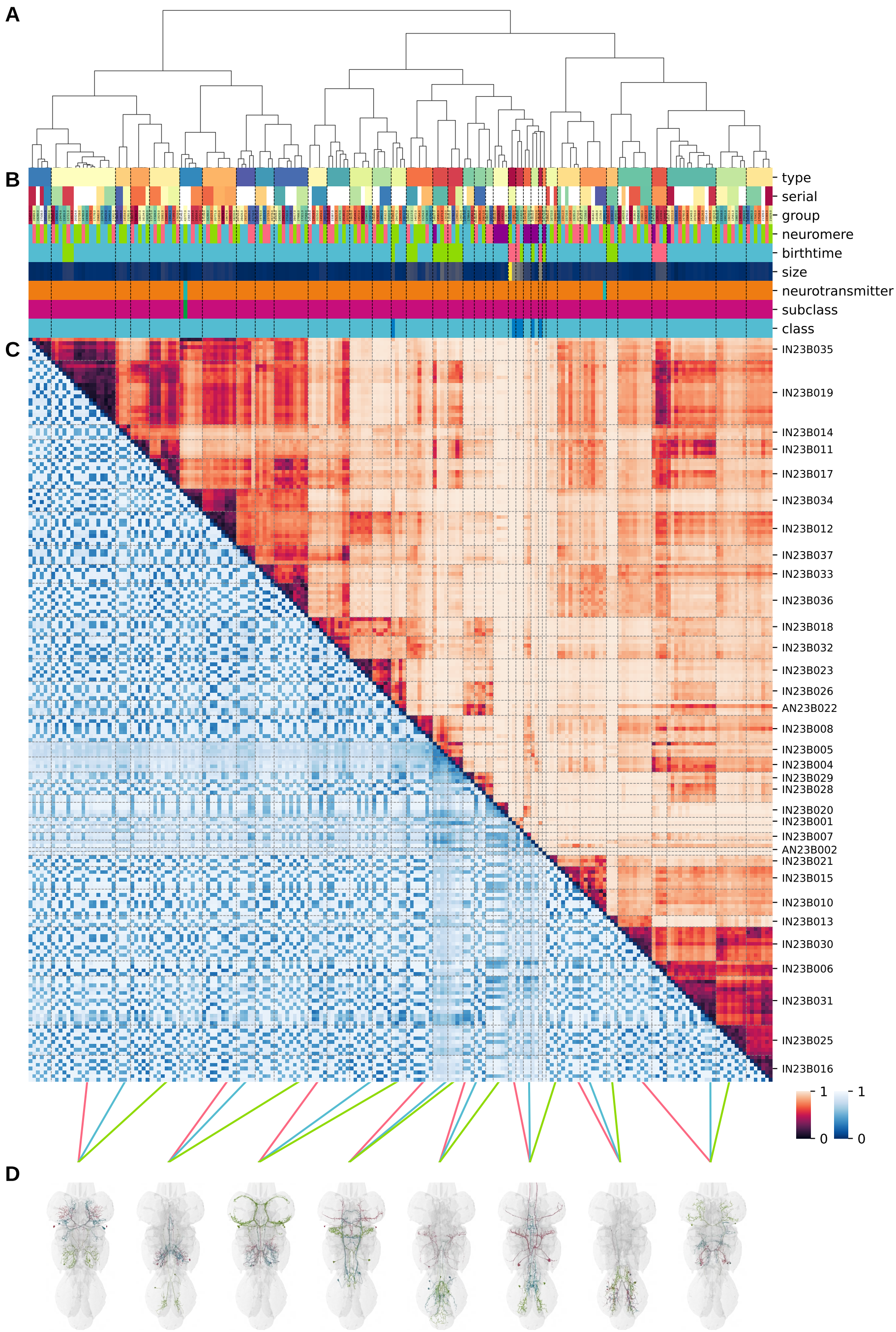
A
B
C
D
type
serial
group
neuromere
birthtime
size
neurotransmitter
subclass
class
IN23B035
IN23B019
IN23B014
IN23B011
IN23B017
IN23B034
IN23B012
IN23B037
IN23B033
IN23B036
IN23B018
IN23B032
IN23B023
IN23B026
AN23B022
IN23B008
IN23B005
IN23B004
IN23B029
IN23B028
IN23B020
IN23B001
IN23B007
AN23B002
IN23B021
IN23B015
IN23B010
IN23B013
IN23B030
IN23B006
IN23B031
IN23B025
IN23B016
1
0
1
0

Hemilineage 24B.25B

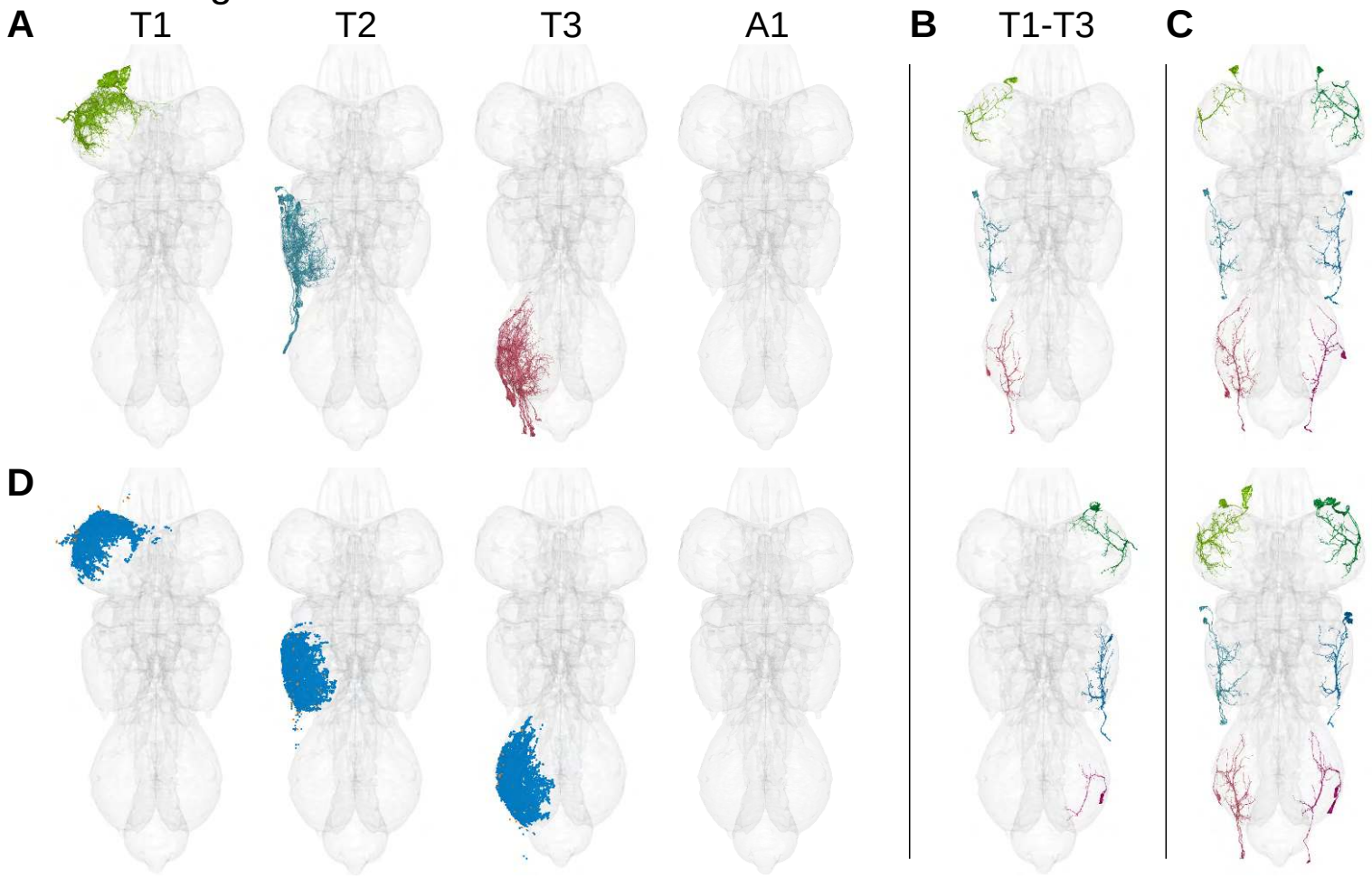

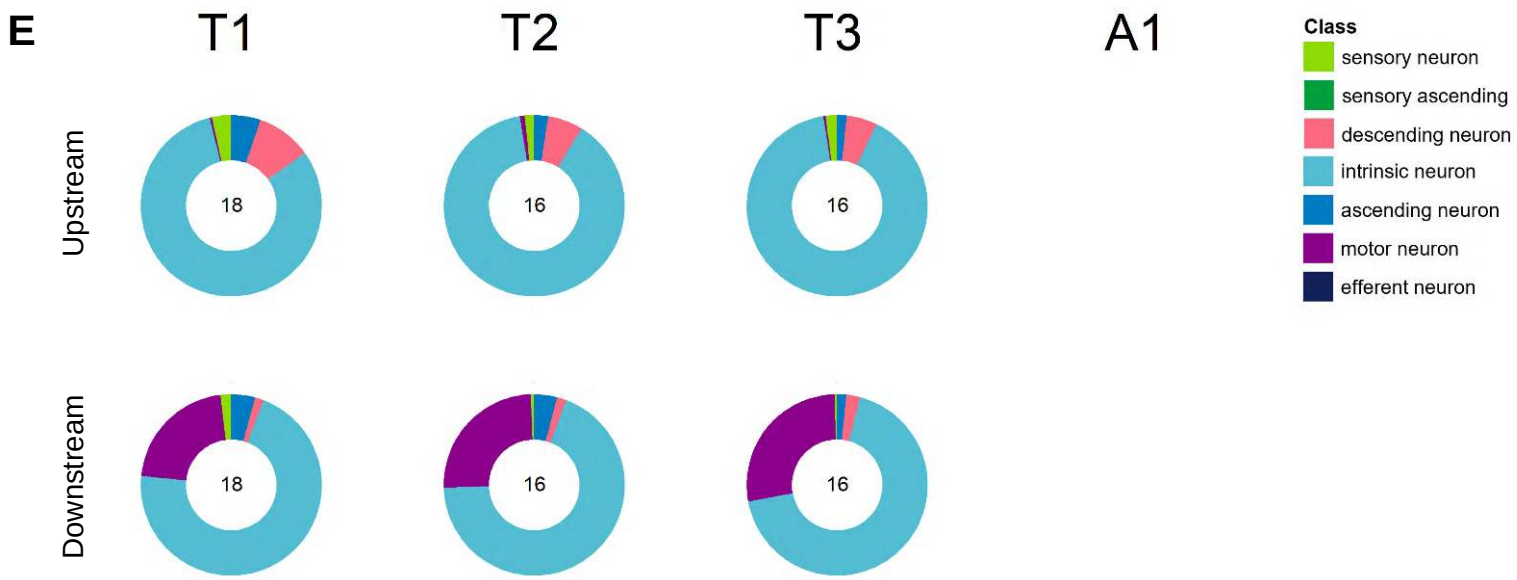

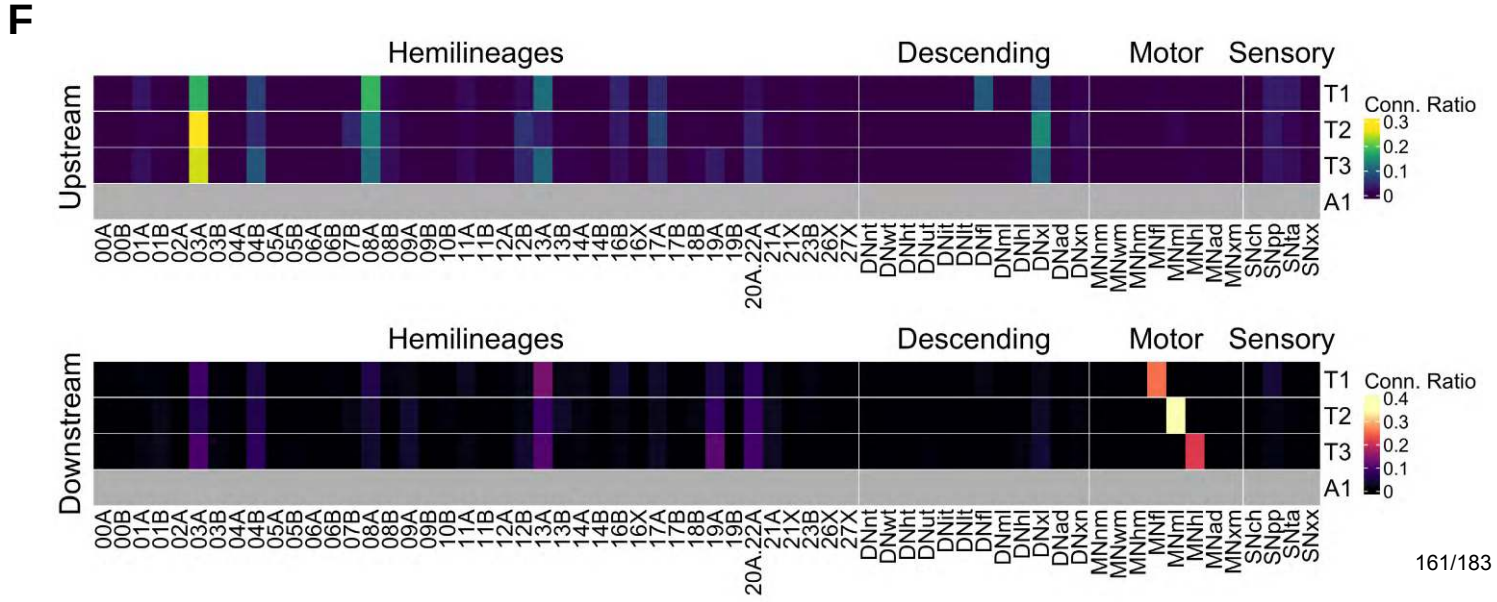

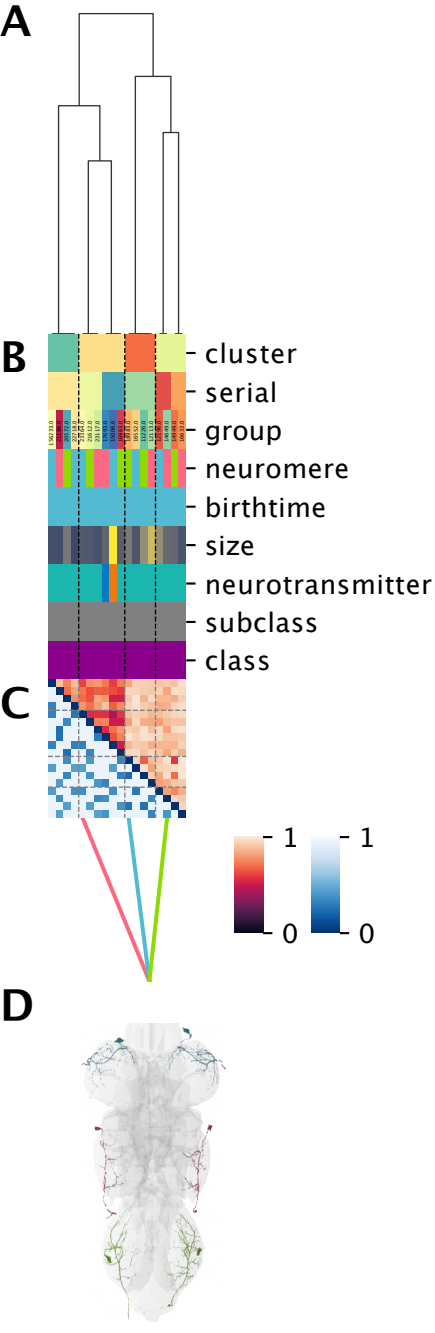
A
B
cluster
serial
group
neuromere
birthtime
size
neurotransmitter
subclass
class
C
1
0
1
0
D

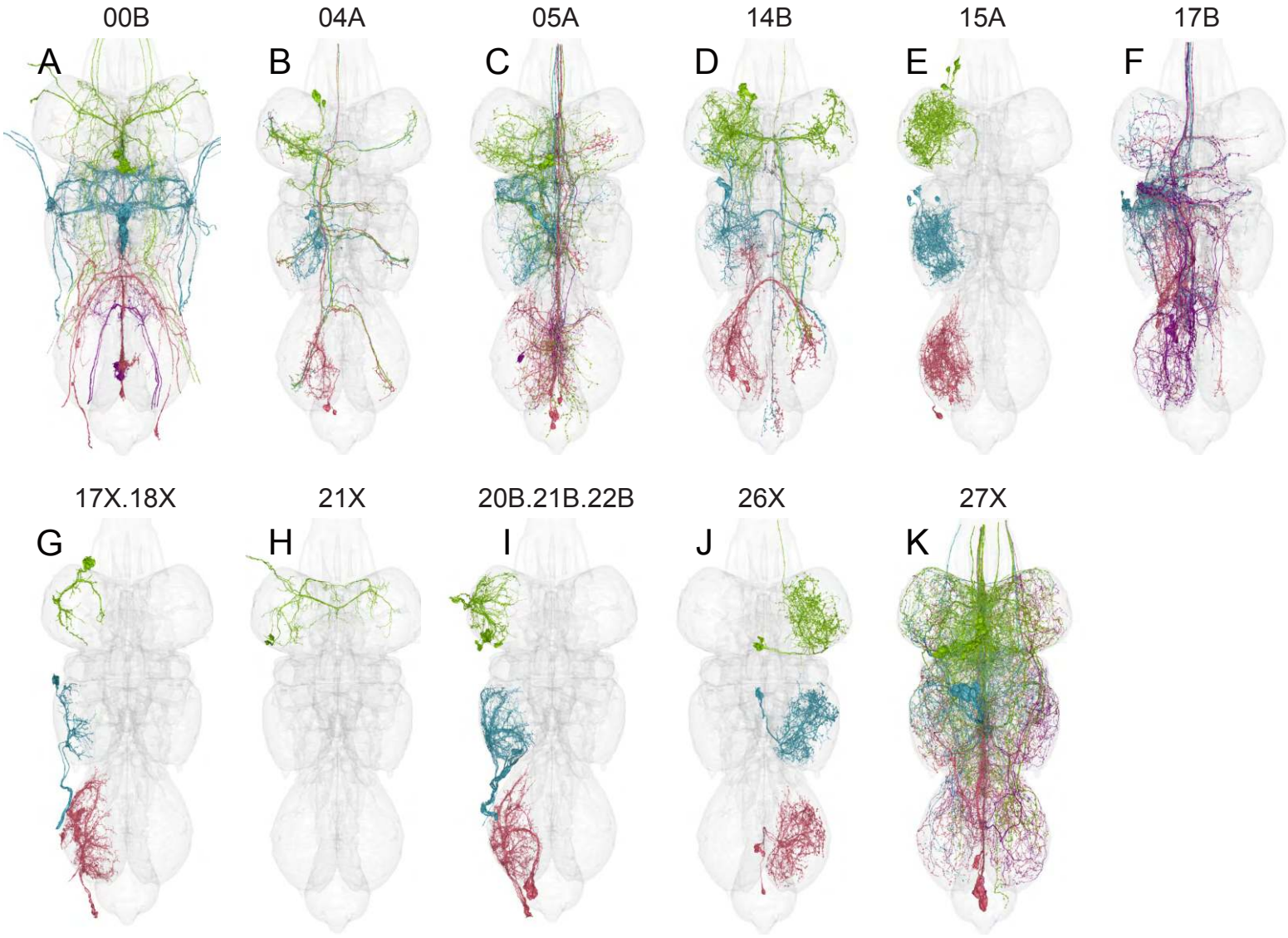
00B
04A
05A
14B
15A
17B
A
B
C
D
E
F
17X.18X
21X
20B.21B.22B
26X
27X
G
H
I
J
K

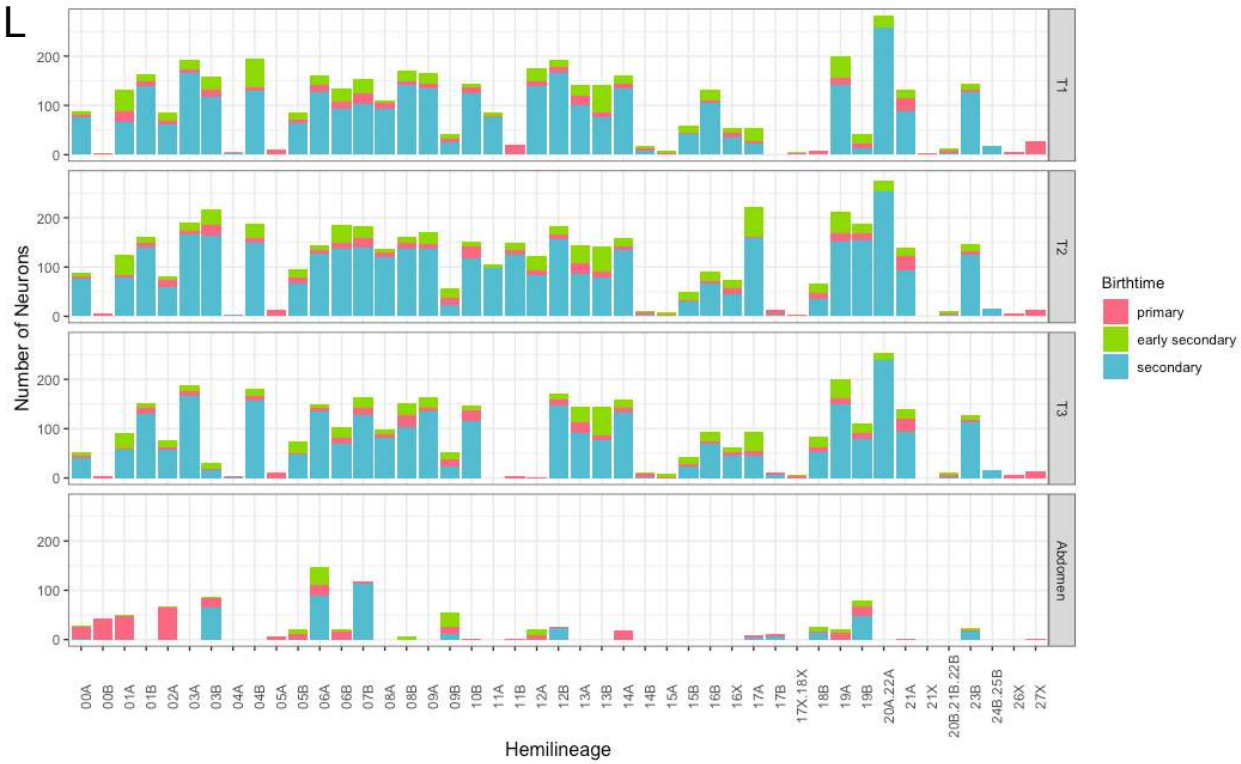
L
Number of Neurons
T1
T2
T3
Abdomen
Birthtime
primary
early secondary
secondary
Hemilineage
00A
00B
01A
01B
02A
03A
03B
04A
04B
05A
05B
06A
06B
07B
08A
08B
09A
09B
10B
11A
11B
12A
12B
13A
13B
14A
14B
15A
15B
16B
16X
17A
17B
17X.18X
18B
19A
19B
20A.22A
21A
21X
20B.21B.22B
23B
24B.25B
26X
27X

Synaptic Organisation of Primary T2 Neurons

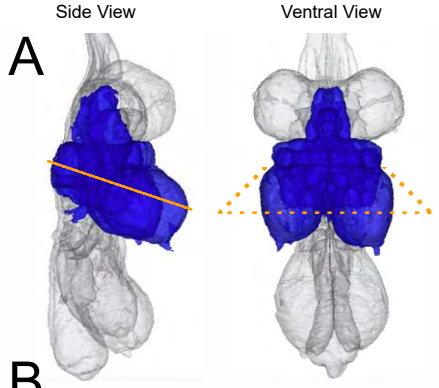

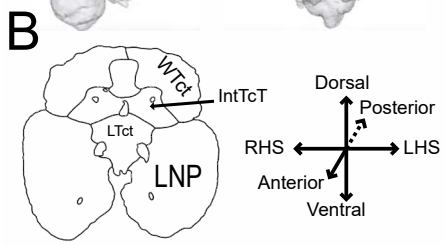

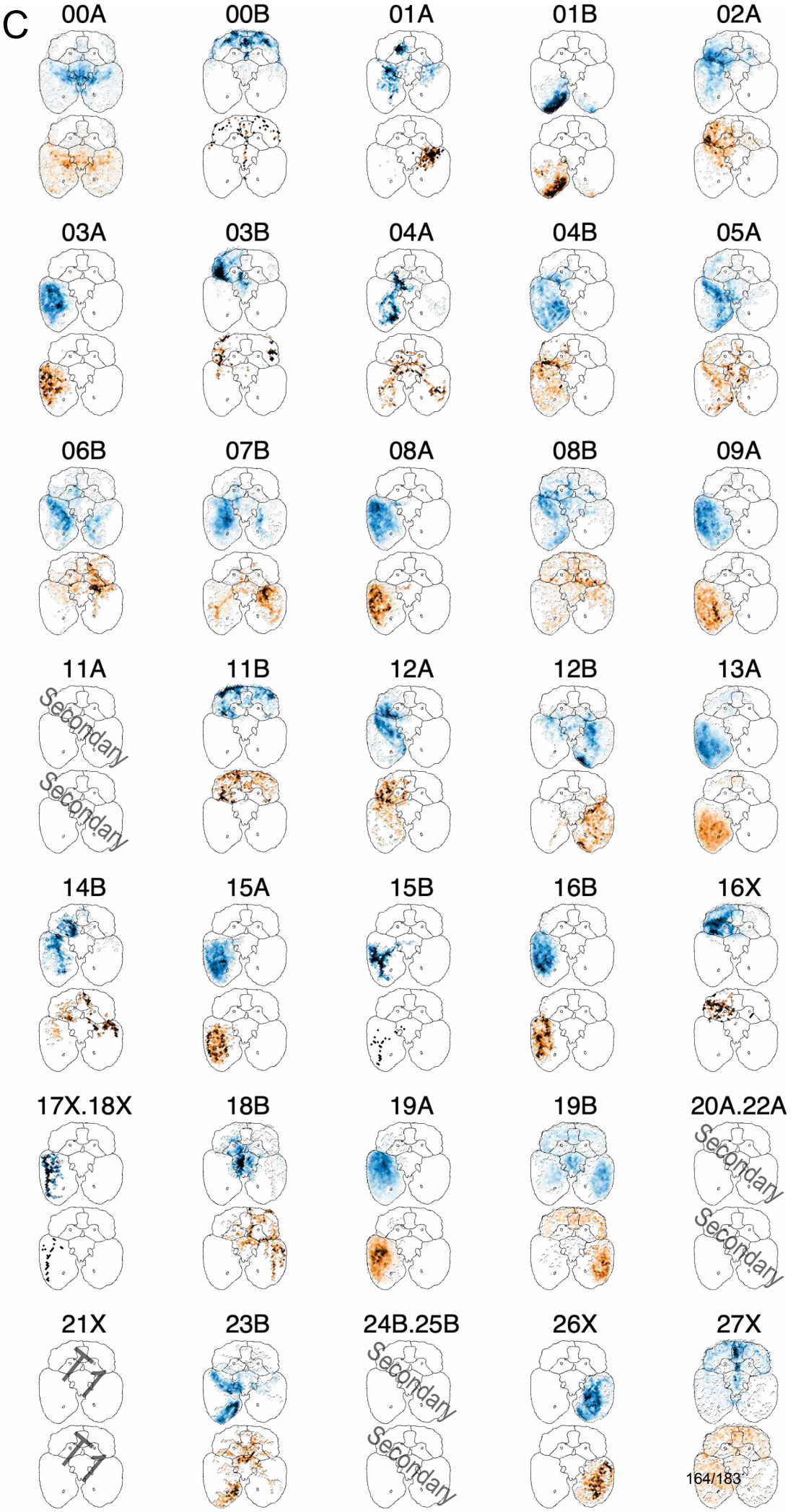

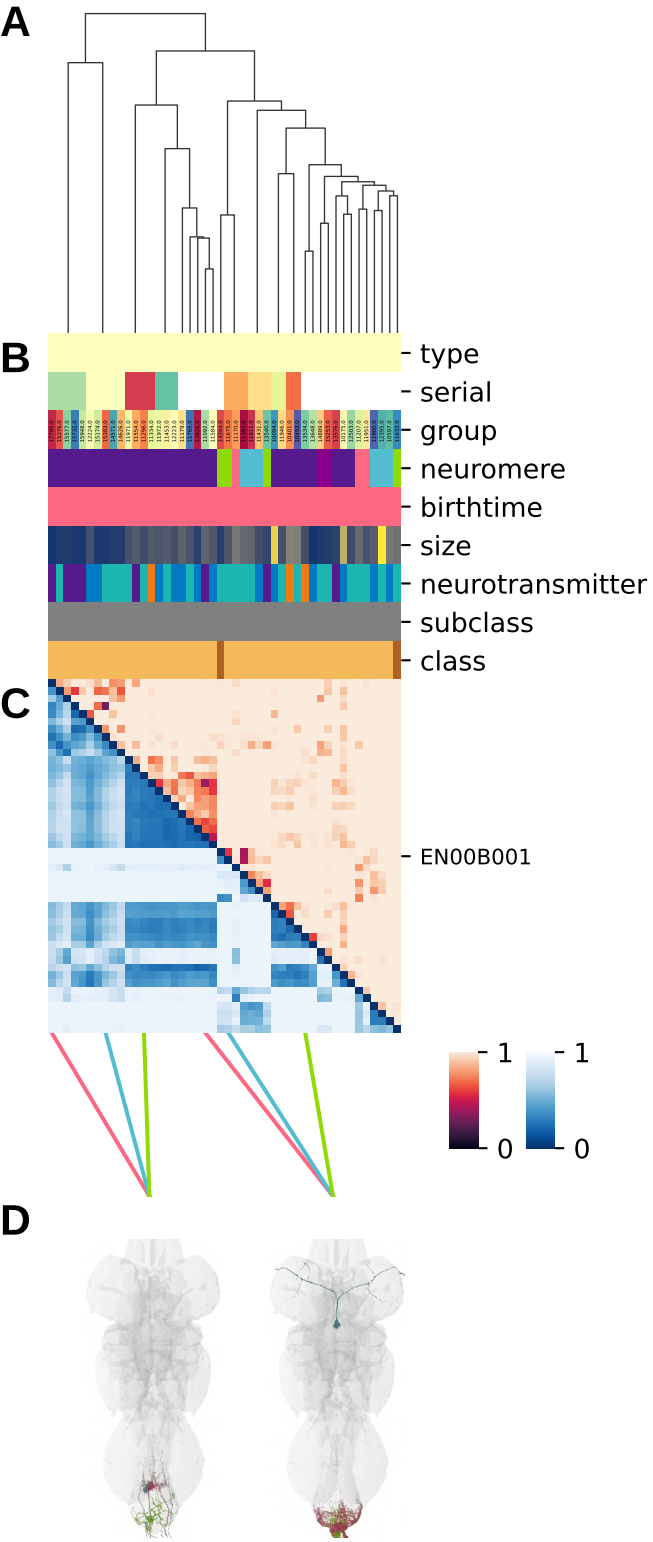
A
B
type
serial
group
neuromere
birthtime
size
neurotransmitter
subclass
class
C
EN00B001
1
0
1
0
D

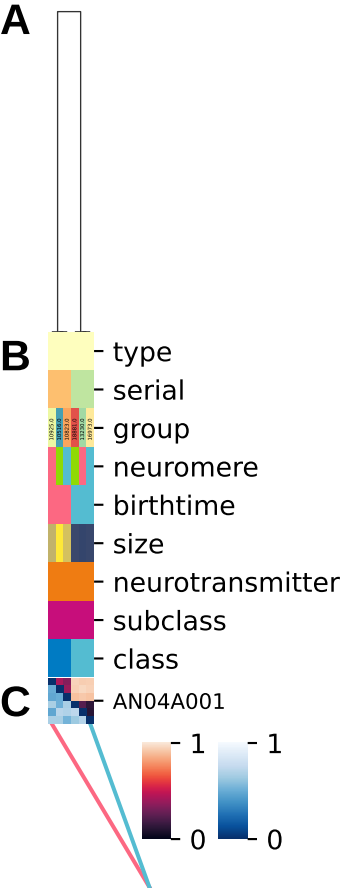
A
B
type
serial
group
neuromere
birthtime
size
neurotransmitter
subclass
class
C
AN04A001
1
0
1
0

D

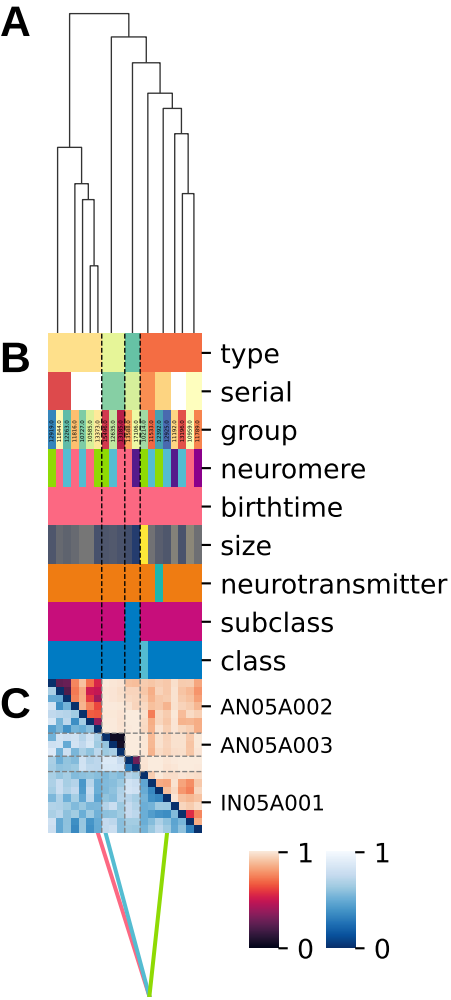
A
B
C
type
serial
group
neuromere
birthtime
size
neurotransmitter
subclass
class
AN05A002
AN05A003
IN05A001
1
0
1
0

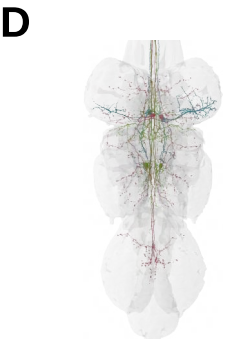
D

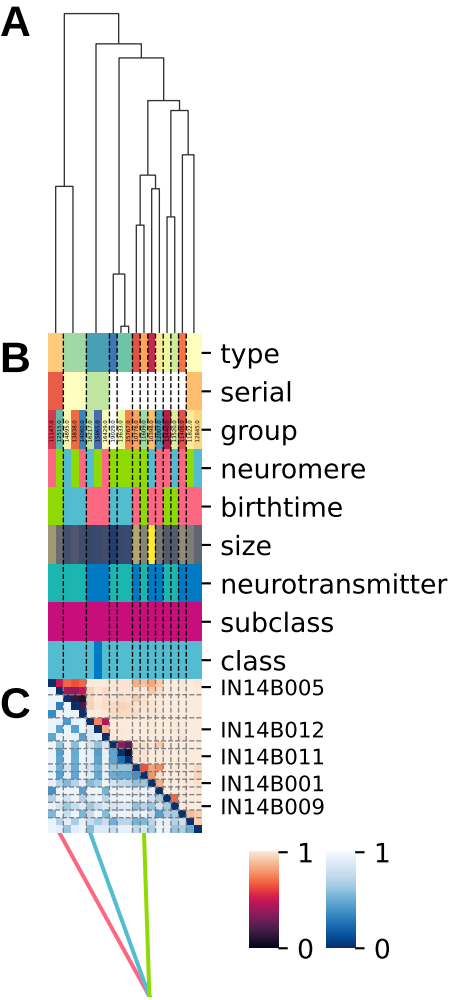
A
B
C
type
serial
group
neuromere
birthtime
size
neurotransmitter
subclass
class
IN14B005
IN14B012
IN14B011
IN14B001
IN14B009
1
0
1
0

D

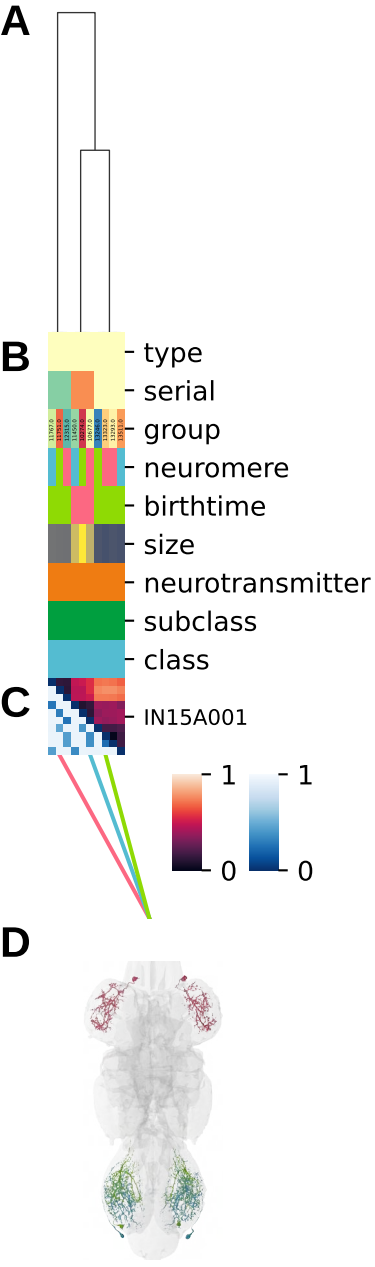
A
B
type
serial
group
neuromere
birthtime
size
neurotransmitter
subclass
class
C
IN15A001
1
0
1
0
D

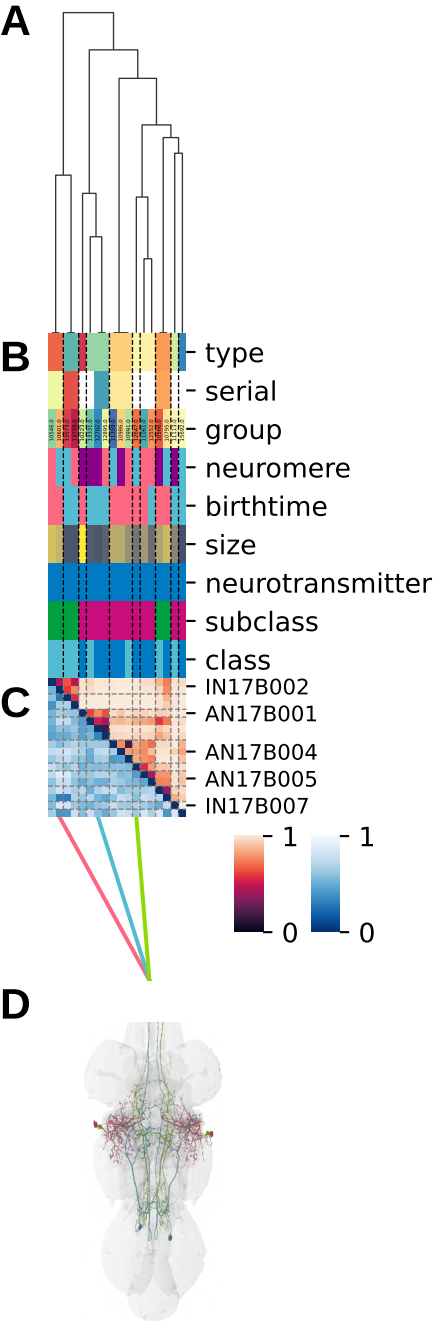
A
B
type
serial
group
neuromere
birthtime
size
neurotransmitter
subclass
class
C
IN17B002
AN17B001
AN17B004
AN17B005
IN17B007
1
0
1
0
D

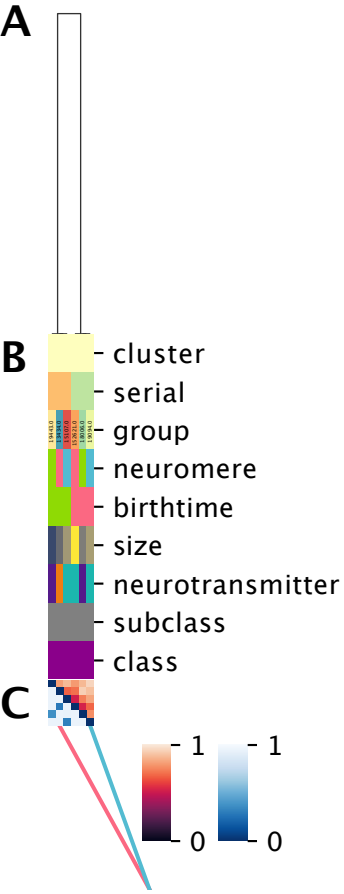
A
B
cluster
serial
group
neuromere
birthtime
size
neurotransmitter
subclass
class
C
1
0
1
0

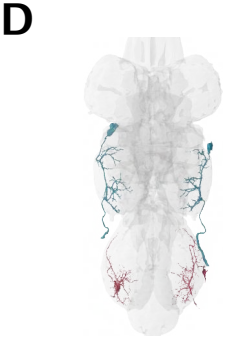
D

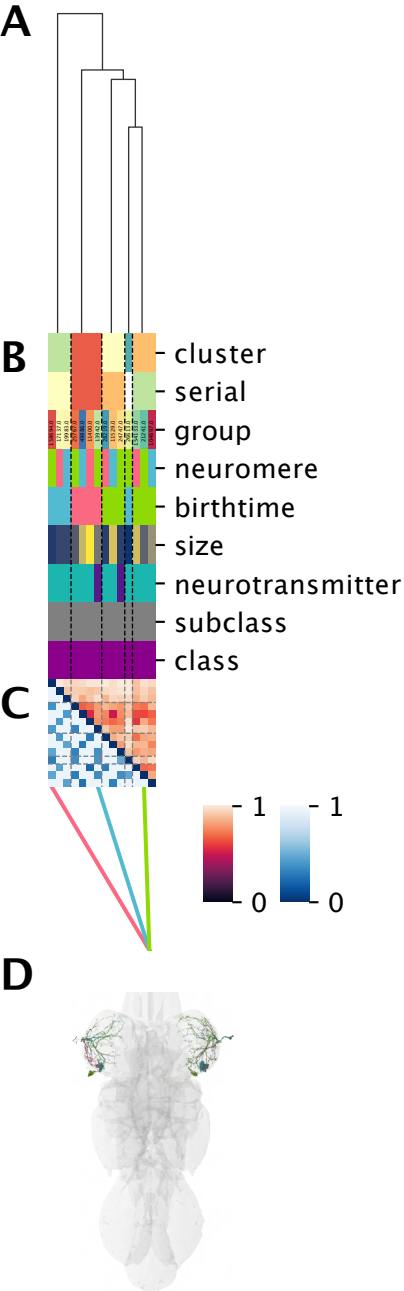
A
B
cluster
serial
group
neuromere
birthtime
size
neurotransmitter
subclass
class
C
1
0
1
0
D

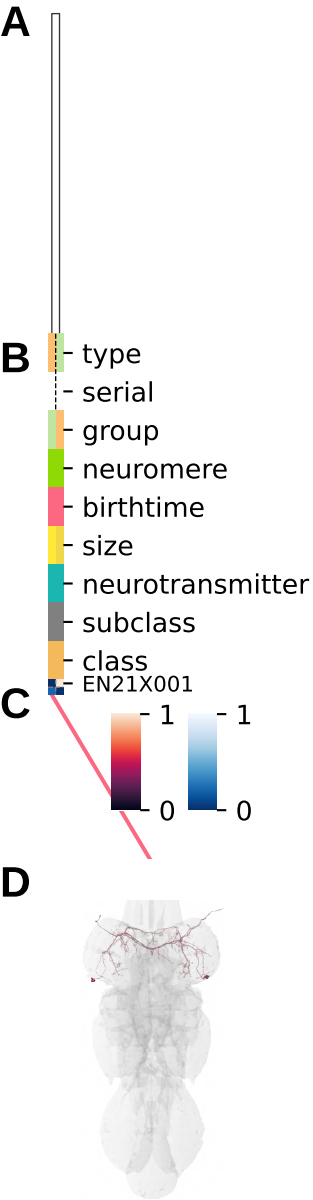
A
B
type
serial
group
neuromere
birthtime
size
neurotransmitter
subclass
class
EN21X001
C
1
0
1
0
D

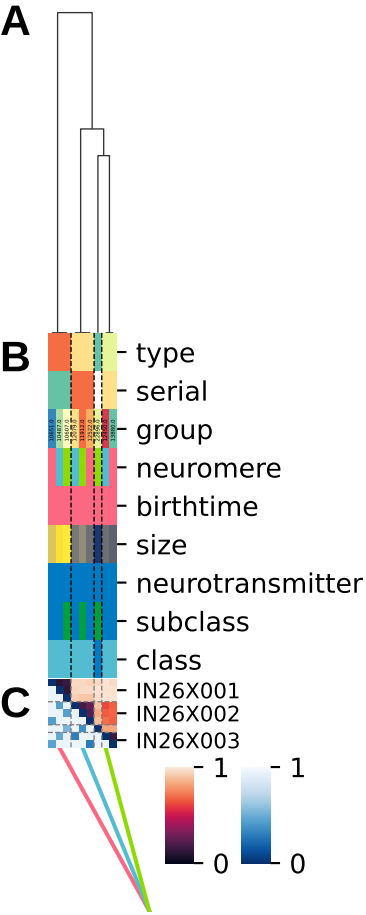
A
B
type
serial
group
neuromere
birthtime
size
neurotransmitter
subclass
class
C
IN26X001
IN26X002
IN26X003
1
0
1
0

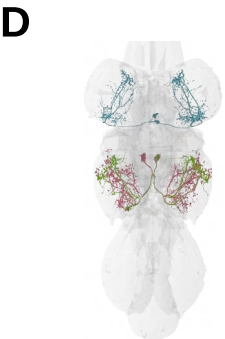
D

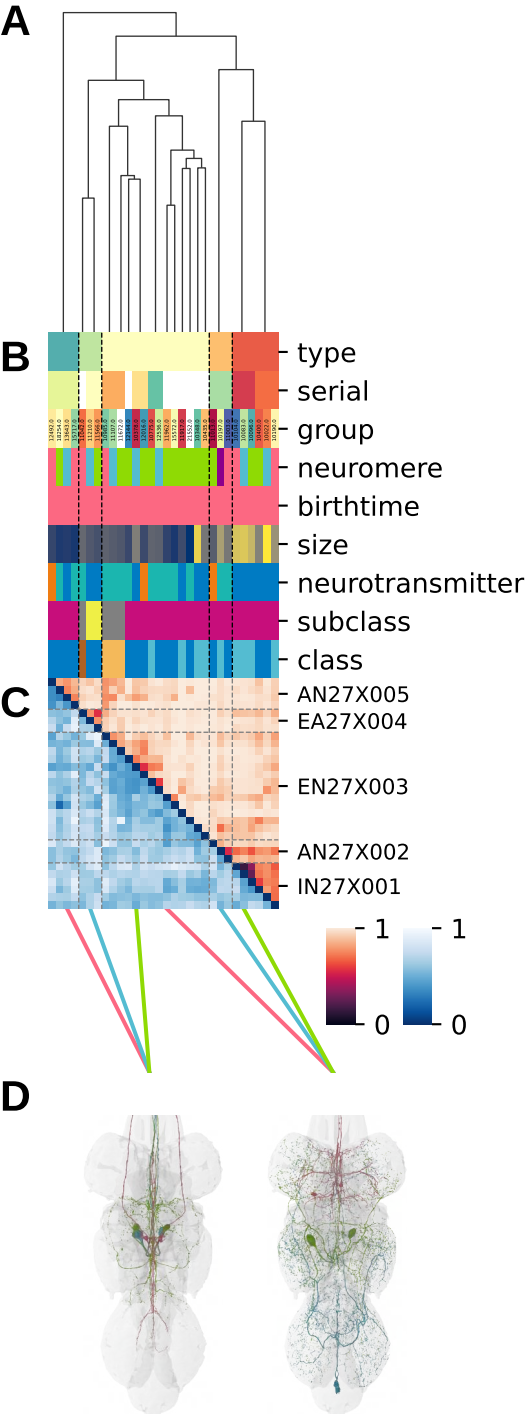
A
B
type
serial
group
neuromere
birthtime
size
neurotransmitter
subclass
class
C
AN27X005
EA27X004
EN27X003
AN27X002
IN27X001
1
0
1
0
D

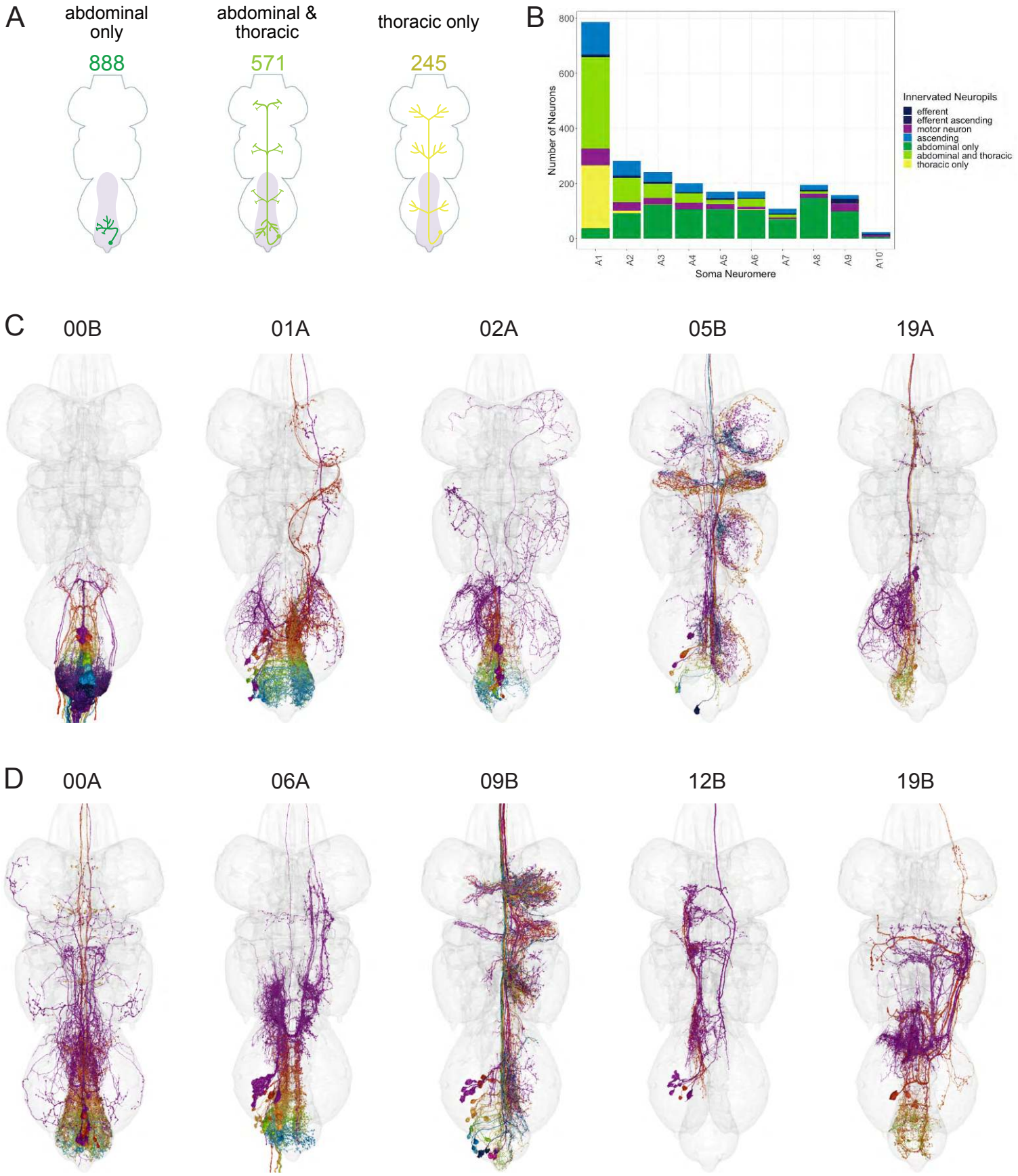
A
abdominal only
888
abdominal & thoracic
571
thoracic only
245
B
Number of Neurons
800
600
400
200
0
A1
A2
A3
A4
A5
A6
A7
A8
A9
A10
Soma Neuromere
Innervated Neuropils
efferent
efferent ascending
motor neuron
ascending
abdominal only
abdominal and thoracic
thoracic only
C
00B
01A
02A
05B
19A
D
00A
06A
09B
12B
19B

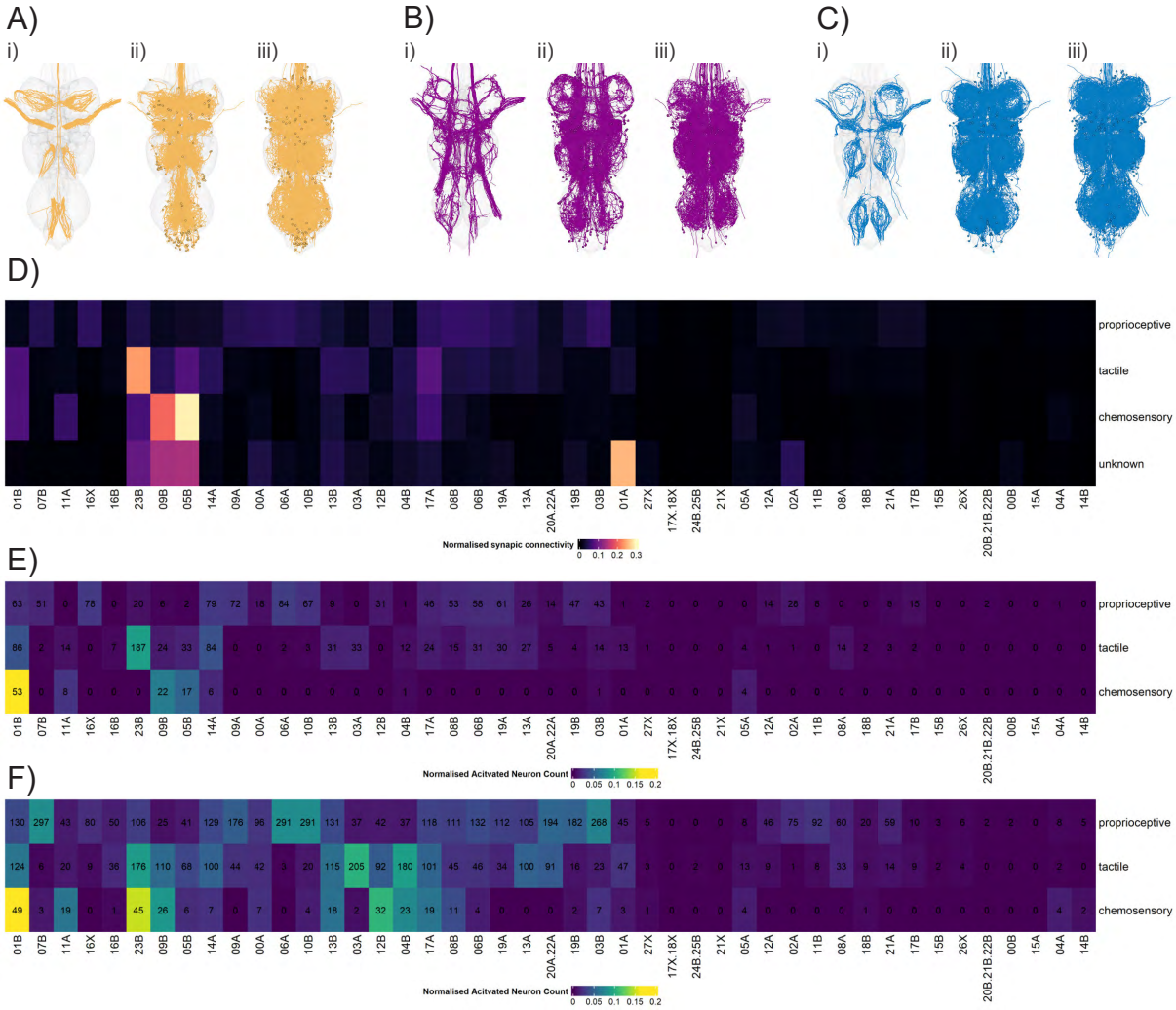
A)
i)
ii)
iii)
B)
i)
ii)
iii)
C)
i)
ii)
iii)
D)
propriocepive
tactile
chemosensory
unknown
01B 07B 11A 16X 16B 23B 09B 05B 14A 09A 00A 06A 10B 13B 03A 12B 04B 17A 08B 06B 19A 13A 20A.22A 19B 03B 01A 27X 17X.18X 24B.25B 21X 05A 12A 02A 11B 08A 18B 21A 17B 15B 26X 20B.21B.22B 00B 15A 04A 14B
Normalised synapic connectivity
0 0.1 0.2 0.3
E)
propriocepive
tactile
chemosensory
01B 07B 11A 16X 16B 23B 09B 05B 14A 09A 00A 06A 10B 13B 03A 12B 04B 17A 08B 06B 19A 13A 20A.22A 19B 03B 01A 27X 17X.18X 24B.25B 21X 05A 12A 02A 11B 08A 18B 21A 17B 15B 26X 20B.21B.22B 00B 15A 04A 14B
Normalised Acitvated Neuron Count
0 0.05 0.1 0.15 0.2
F)
propriocepive
tactile
chemosensory
01B 07B 11A 16X 16B 23B 09B 05B 14A 09A 00A 06A 10B 13B 03A 12B 04B 17A 08B 06B 19A 13A 20A.22A 19B 03B 01A 27X 17X.18X 24B.25B 21X 05A 12A 02A 11B 08A 18B 21A 17B 15B 26X 20B.21B.22B 00B 15A 04A 14B
Normalised Acitvated Neuron Count
0 0.05 0.1 0.15 0.2

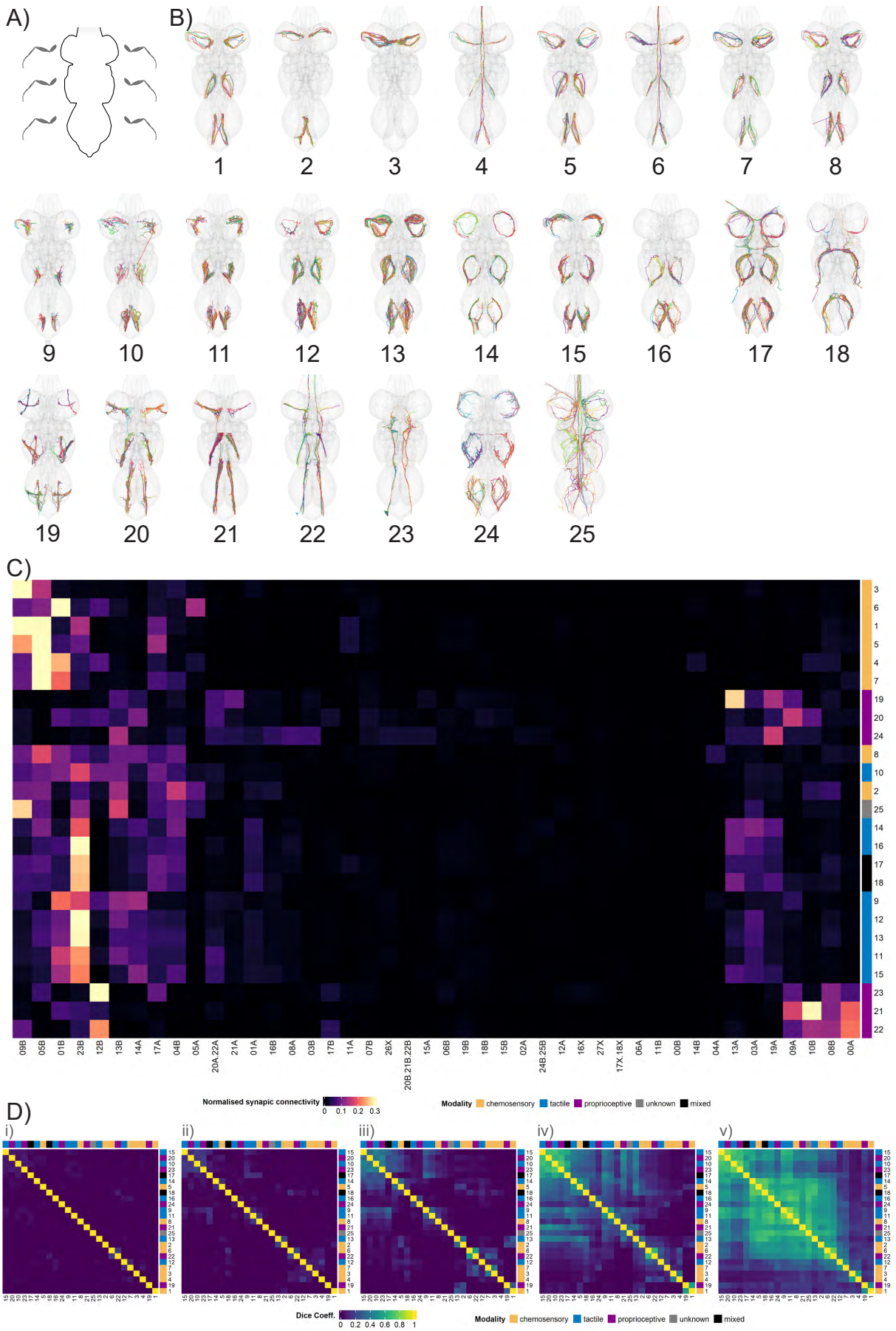
A)
B)
1
2
3
4
5
6
7
8
9
10
11
12
13
14
15
16
17
18
19
20
21
22
23
24
25
C)
09B
05B
01B
23B
12B
13B
14A
17A
04B
05A
20A.22A
21A
01A
16B
08A
03B
17B
11A
07B
26X
20B.21B.22B
15A
06B
19B
18B
15B
02A
24B.25B
12A
16X
27X
17X.18X
06A
11B
00B
14B
04A
13A
03A
19A
09A
10B
08B
00A
Normalised synapic connectivity
0 0.1 0.2 0.3
Modality chemosensory tactile proprioceptive unknown mixed
D)
i)
ii)
iii)
iv)
v)
Dice Coeff.
0 0.2 0.4 0.6 0.8 1
Modality chemosensory tactile proprioceptive unknown mixed

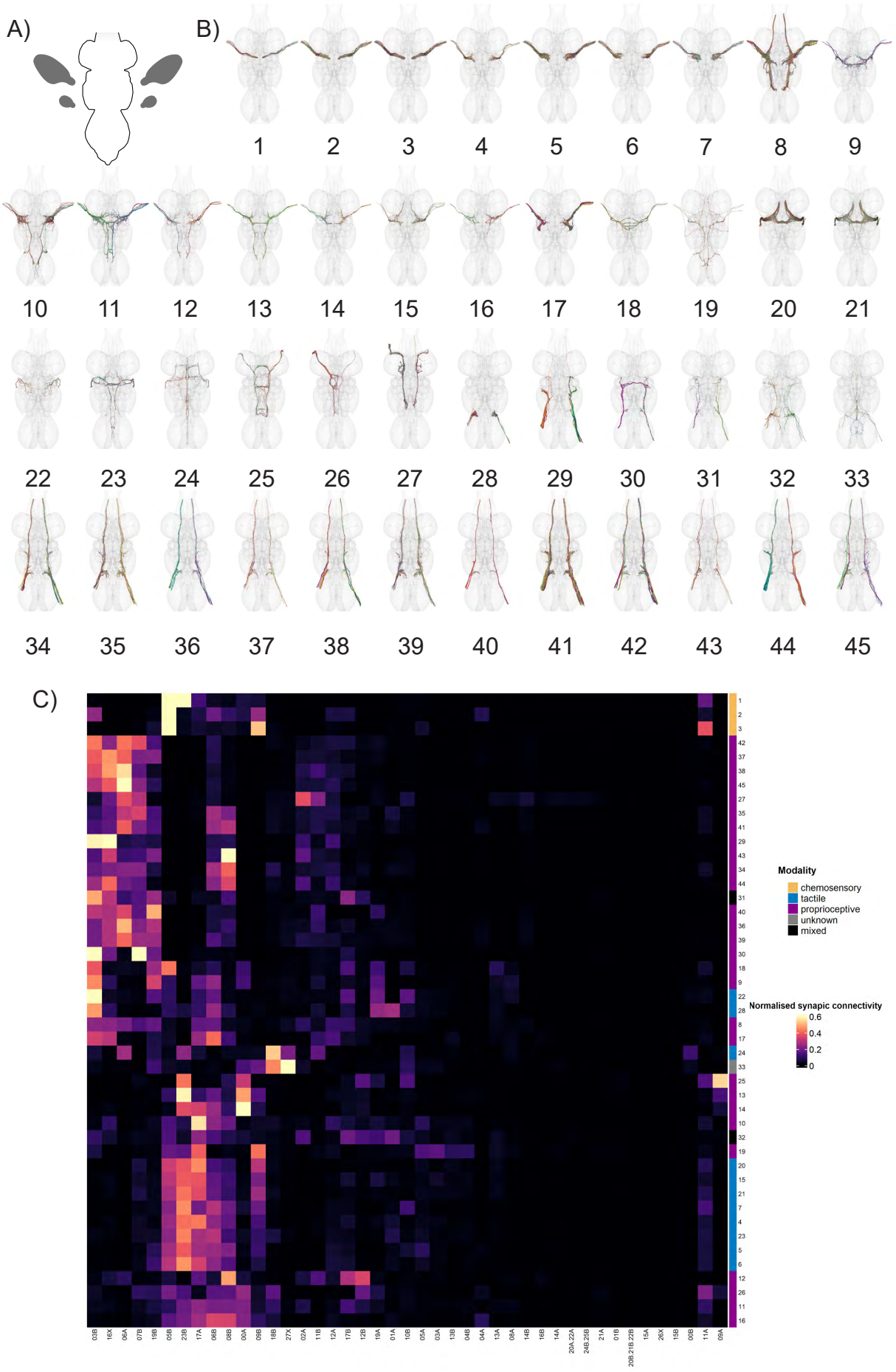
A)
B)
1
2
3
4
5
6
7
8
9
10
11
12
13
14
15
16
17
18
19
20
21
22
23
24
25
26
27
28
29
30
31
32
33
34
35
36
37
38
39
40
41
42
43
44
45
C)
Modality
chemosensory
tactile
proprioceptive
unknown
mixed
Normalised synapic connectivity
0.6
0.4
0.2
0

A

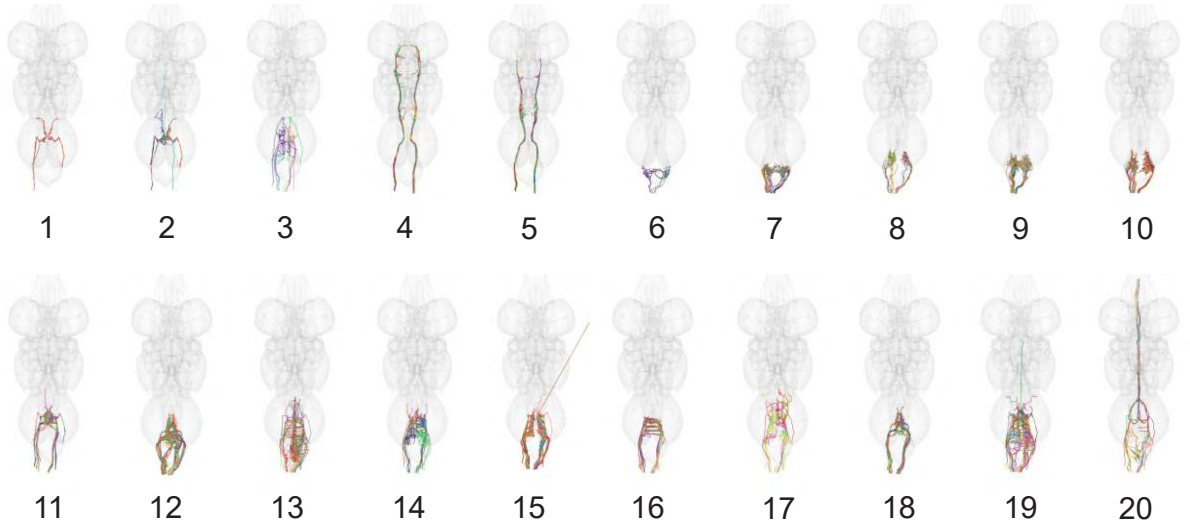
1
2
3
4
5
6
7
8
9
10
11
12
13
14
15
16
17
18
19
20

B

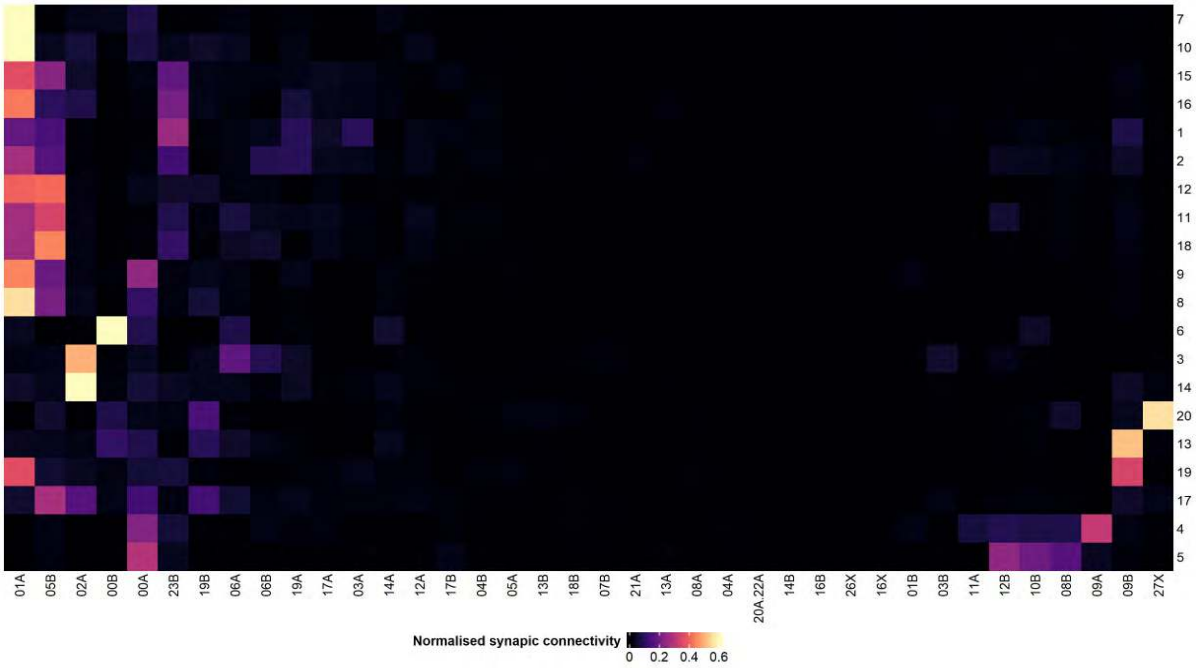
7
10
15
16
1
2
12
11
18
9
8
6
3
14
20
13
19
17
4
5
01A
05B
02A
00B
00A
23B
19B
06A
06B
19A
17A
03A
14A
12A
17B
04B
05A
13B
18B
07B
21A
13A
08A
04A
20A,22A
14B
16B
26X
16X
01B
03B
11A
12B
10B
08B
09A
09B
27X
Normalised synapic connectivity
0
0.2
0.4
0.6

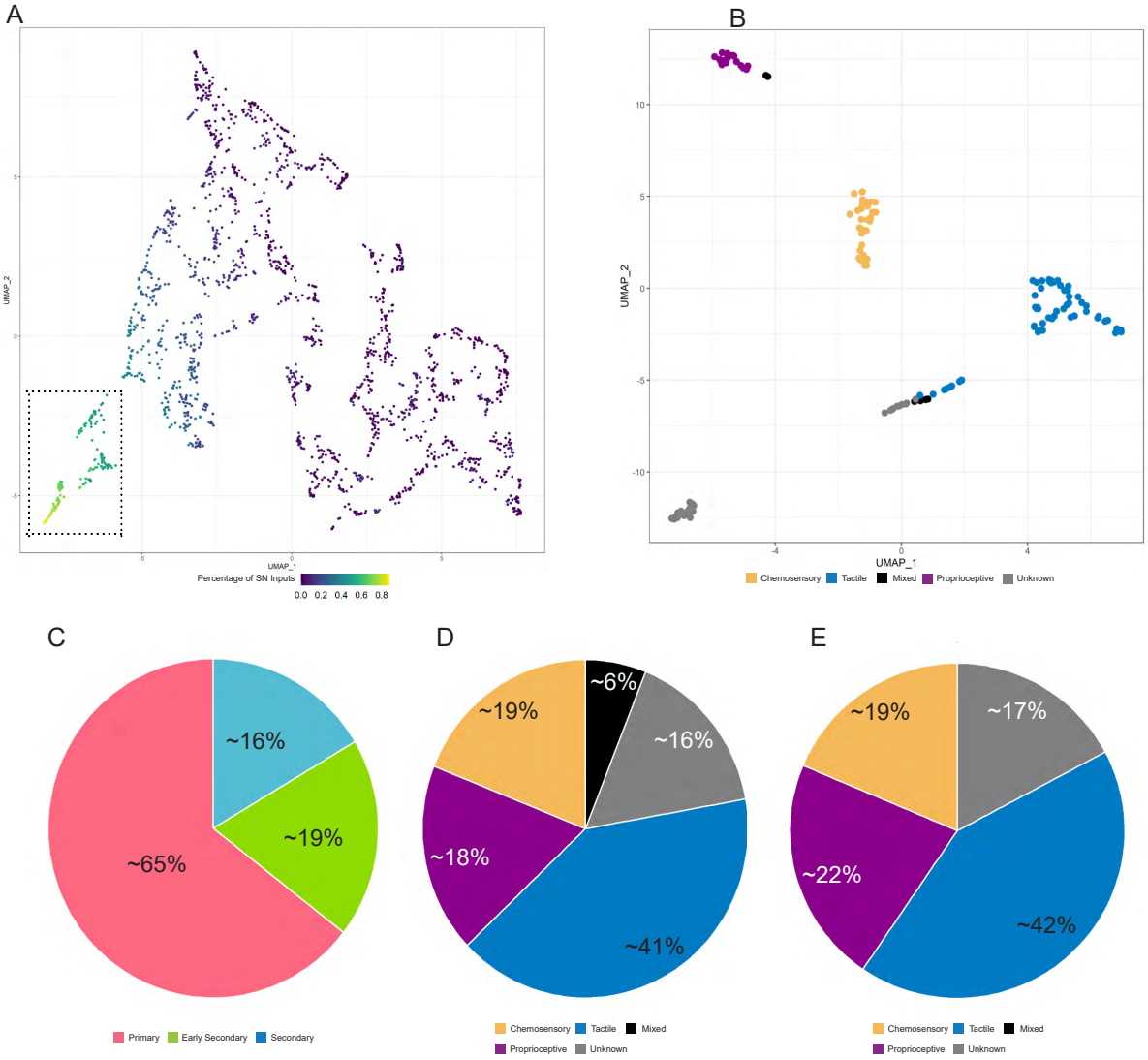
A
UMAP_2
UMAP_1
Percentage of SN Inputs
0.0 0.2 0.4 0.6 0.8
B
UMAP_2
UMAP_1
Chemosensory Tactile Mixed Proprioceptive Unknown
C
~16%
~19%
~65%
Primary Early Secondary Secondary
D
~6%
~19%
~16%
~18%
~41%
Chemosensory Tactile Mixed
Proprioceptive Unknown
E
~19%
~17%
~22%
~42%
Chemosensory Tactile Mixed
Proprioceptive Unknown

A. Hemilineage to hemilineage local connectivity (T2 only)

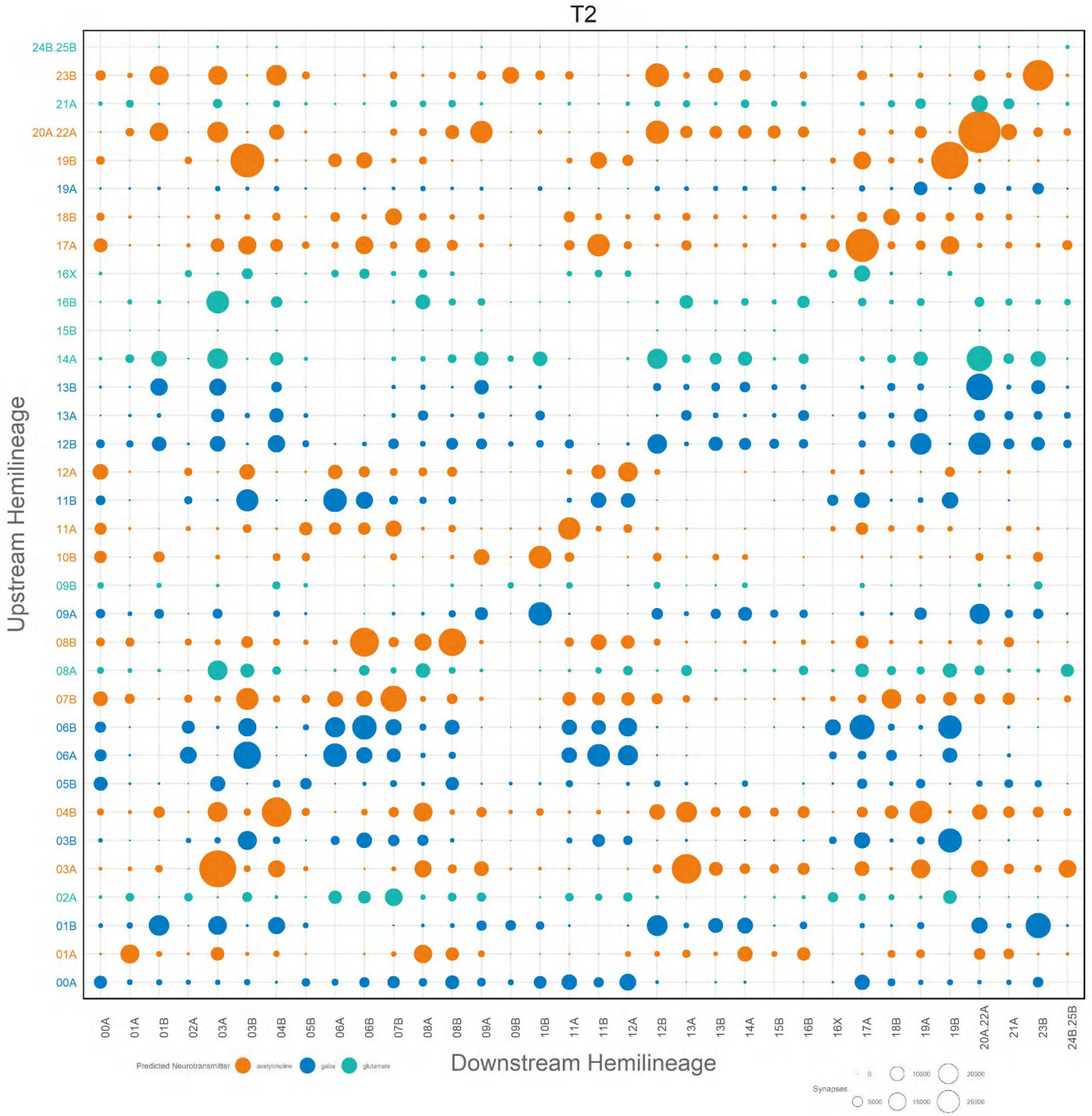

B. Schematic of top upstream partners for hemilineage to hemilineage local connectivity (T2 only)

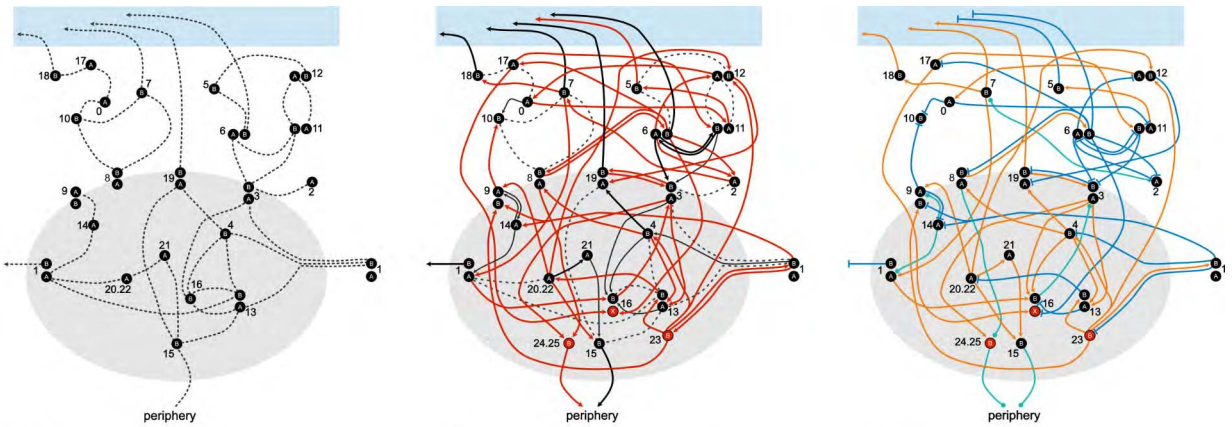

key

- Initial contacts of neurite bundles in late larva as reported in Truman, Schuppe, Shepherd & Williams (2004)

key

- confirmed strong edge
- confirmed edge
- previously included hemilineage
- missing/weak edge
- new strong edge
- additional hemilineage

key

- acetylcholine
- gaba
- glutamate
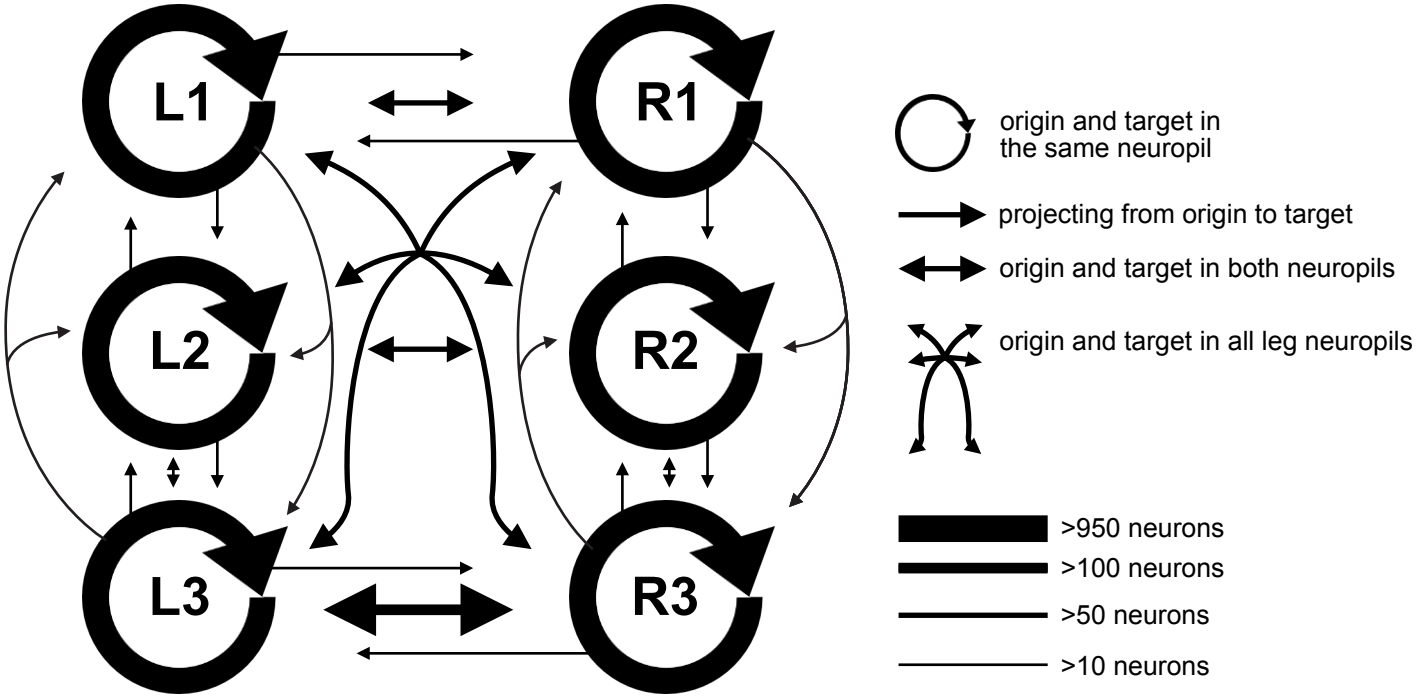
Intrinsic neurons dedicated to the six leg neuropils